

Metocean desktop study (preliminary research)

Contractor: Smart Sea OÜ

Client: Environmental Investment Centre

Version 1

Table of contents

Conclusions.....	4
Kokkuvõte	7
1. Background and general description of metocean conditions	10
2. Data sources and methods.....	13
3. Results.....	16
3.1. Wind conditions	16
3.1.1. Average wind conditions	18
3.1.2. Extreme wind conditions	43
3.1.3. Characteristic wind profiles.....	82
3.1.4. Spatial variation of wind speed across the ELWIND site	83
3.1.5. Qualitive assessment of effect of other wind farms under development in the Baltic Sea 88	
3.2. Wave conditions	90
3.2.1. Average conditions	91
3.2.2. Extreme wave conditions.....	117
3.2.3. Spatial variations	138
3.3. Current conditions	140
3.3.1. Normal conditions	140
3.3.2. Extreme conditions	193
3.3.3. Spatial variations	195
3.4. Sea level.....	200
3.4.1. Normal conditions	200
3.4.2. Extreme conditions	201
3.4.3. Spatial variations	203
3.4.4. Assessment of long-term sea level rise	203
3.5. Ice conditions	204
3.5.1. Ice thickness for specified return periods.....	204
3.5.2. Risk of current or wind induced ice floe	205
3.5.3. Frequency of ice concentration.....	206
3.5.4. Ridged ice	208
3.5.5. Spatial variations	209
3.6. Other parameters	212
4. Results of joint probability analysis	220
4.1. Wind and waves.....	221

4.2.	Current and waves	227
4.3.	Current and wind	228
4.4.	Water level and wind	229
4.5.	Water level and current	231
5.	Identified uncertainties or knowledge gaps.....	232
6.	References	235

Conclusions

This work aimed to describe meteorological and oceanographic conditions in the ELWIND wind farm development site in the west of the Sõrve peninsula in Saaremaa Island.

Annual and monthly wind roses show the dominance of southwesterly winds as well known for the Baltic Sea area. The secondary peak of occurrence of moderate and strong winds is from a northerly and northwesterly direction. Strong southwesterlies are more common in autumn and winter period while winds are generally weaker in spring and autumn. There is a 30-40% increase in wind speed from the 10 m level to 950 hPa level (approximately 500 m elevation) depending on the season. Wind gust speeds have been up to 35 m/s in the nearby coastal stations according to 20 years of data. However, the maximum 10-minute and gust wind speed could be even higher in the ELWIND site compared to coastal stations as wind tends to be stronger further offshore compared to near coastline conditions. Wind conditions in the ELWIND are not currently under the impact of other wind farms, but when one of the neighboring farms is constructed, the wind speed will be reduced from northerly, northwesterly and westerly directions.

Typically for the Baltic Sea, there are no permanent currents in the ELWIND area. The temporal variability of currents is high and related to the wind forcing and its variability. In the southern side of the ELWIND area, the long-term mean current is parallel to the Sõrve peninsula to the north. In the northern part of the ELWIND area, the long-term mean current turns to the west. This pattern is encouraged by southwesterly winds and prevails more in autumn and winter due to supporting wind regime. The current reverses in the case of winds from the northerly sector. There is probably a two-layer current structure during the presence of the seasonal thermocline (April-October) while the flow is one-layer when the thermocline does not exist or is deeper than the sea depth in the area (November-March). The current speed is quite low in the area and likely does not exceed 1 m/s and even currents with speed above 0.5 m/s are rare.

Sea level variability is quite low in the area. The amplitude of daily sea level (maximum minus minimum of daily sea level) was less than 2 m for the 30-year period.

There is strong interannual variability of ice coverage and its properties in the ELWIND area. Ice coverage does not occur every winter in the area. The maximum spatially averaged daily ice thickness within the ELWIND area has been 15 cm in the period from 1994-2023 while the overall maximum thickness has been 40 cm in the same period. The 50-year (1980-2022)

maximum drift ice thickness has been ca 50 cm in the area. The latter period included several very severe winters in the 1980s. Ice coverage has decreased in recent decades, and the decreasing trend is expected to continue also in the future, but occasionally winters with severe ice conditions with ice thickness of 50 cm still could occur in the ELWIND area. The average length of ice cover is less than one month during ice season and most ice is in the form of drifting ice. Thus, ice floe will occur in the ELWIND area, although it happens less than half of winters.

The spatial mean ice concentration ≥ 0.9 within the ELWIND area occurred only in three consecutive winters (2009/2010, 2010/2011, and 2011/2012) in the years 1994-2023. The average duration of that high (≥ 0.9) concentration was one week in these three winters. The occurrence of winters when the spatial mean ice concentration was ≥ 0.5 and ≥ 0.1 was 28% and 42%. The occurrence of deformed ice is rather low in the ELWIND area due to the overall small presence of ice in the area. However, during severe winters considerable ridged ice could occur in the area.

The spatial distributions of ice properties reveal coastal-offshore gradients. There are more severe ice conditions in the coastal area of Saaremaa Island. The drifting ice that appears occasionally in the ELWIND area most likely originates from the coastal area.

The main force generating waves, currents, and sea level variations in the Baltic Sea is coming from wind. Therefore, joint occurrence of strong wind and active hydrodynamic processes is expected. Other factors such as morphology, air pressure variability, thermohaline gradients, etc. contribute to the variability as well. There is a clear tendency that higher significant wave height occurs when wind is stronger. High waves occur primarily with wind from the southwest and also with northwesterly winds. Stronger currents co-occur with stronger wind. Higher sea level is associated with the southwesterly winds. There is a multiscale temporal impact of wind on the sea level variability, i.e. not only the instantaneous and synoptic scale wind determine the sea level height, but also for instance long-term wind forcing regulates water exchange between Baltic and North Sea and thereby overall water volume and sea level in the Baltic Sea. Anyhow, the sea level amplitude is quite low in the ELWIND area.

Several knowledge gaps and uncertainties were detected and are described in more detail in the chapter 5. The wind field is generally well described but offshore wind conditions, especially the events of strong and extremely strong wind are not well enough described. Likewise, the vertical structure of the wind profile requires additional high-resolution data. To fully

understand the offshore conditions one should measure wind speed and direction and their vertical distribution in the ELWIND area.

The used wave product generally performs well, but it slightly underestimates the highest waves in extreme storms. Also, the present study did not describe the wave spectrum characteristics. To fill the latter gap and to capture the highest waves in extreme conditions wave measurements should be conducted in the ELWIND area.

The current velocities might be underestimated and there are likely uncertainties in resolving the vertical structure of currents in the present study. Targeted high-resolution modeling, which is validated with in-situ current profiling measurements should be conducted in the ELWIND area to provide the current structure data with necessary detail.

The sea level variability is well described in the current study. The only shortcoming is the long time step (1 day) of the used product.

The used sea ice product likely quite well represents the conditions as validation with observations has shown good results. However, ice conditions could be challenging to predict in the future as there is very high interannual variability.

Water column properties (temperature, salinity) are probably quite well described in the current study for engineering purposes, but for the environmental impact assessment studies high-resolution modeling, which is validated by measurements in the ELWIND area, must be applied.

The annual cycles of air pressure, air temperature, and relative humidity are probably well described in the current document.

Kokkuvõte

Selle töö eesmärk oli kirjeldada meteoroloogilisi ja okeanograafilisi tingimusi ELWINDi tuulepargi arenduspiirkonnas, mis asub Sõrve poolsaarest läänes. Piirkonnas on kõige sagedasemad edelatuuled. Edelatuulte järel on mõõdukate ja tugevate tuulte sekundaarne esinemismaksimum põhja- ja loodesuunast. Tugevad edelatuuled on sagedasemad sügis- ja talveperioodil, samas kui kevadel ja sügisel on nende tuulte esinemine tagasihoidlikum ja tuul on ka üldiselt nõrgem. Tuule kiirus suureneb 10 m kõrguselt 950 hPa tasemele (umbes 500 m kõrgusele) sõltuvalt aastaajast 30-40%. Tuuleilide kiirus on lähirannikul ulatunud kuni 35 m/s. ELWINDi alal võib tõenäoliselt esineda ka tugevamaid iile. ELWINDi ala tuuleolud ei ole praegu teiste tuuleparkide mõju all, kuid kui mõni naabruses asuv park ehitatakse, siis tuule kiirus põhja-, loode- ja läänekaarte tuulte puhul väheneb.

Läänemerele tüüpiliselt ei ole ELWINDi piirkonnas püsivaid hoovusi. Hoovuste lühiajaline varieeruvus on kõrge ja seotud tuule muutlikkusega. ELWINDi piirkonna lõunapoolses osas on pikaajaline keskmine hoovus paralleelne Sõrve poolsaarega, põhja suunas. ELWINDi piirkonna põhjaosas pöördub pikaajaline keskmine hoovus läände. Sellist hoovusmuustrit toetavad edelatuuled ja see on sügis- ja talveperioodil valdav tänu kõrgemale edelatuulte korduvusele. Hoovus pöördub põhjakaarte tuulte korral, st. sellisel juhul on voolamine piki rannikut lõunasse. Tõenäoliselt on termokliini (aprill-oktoober) olemasolu ajal piirkonnas kahekihiline hoovuste struktuur. Voolamine on ühekihiline, kui termokliin ei eksisteeri või on sügavam kui mere sügavus piirkonnas (november-märts). Hoovuse kiirus piirkonnas on üsna väike ja tõenäoliselt ei ületa 1 m/s ning ka hoovused kiirusega üle 0,5 m/s on haruldased. Veetaseme varieeruvus piirkonnas on tagasihoidlik ja 30 aasta amplituud on alla 2 m.

ELWINDi piirkonnas on jääkate tugev aastatevaheline varieeruvus. Jääkate ei esine piirkonnas igal talvel. ELWINDi alal on perioodil 1994-2023 ruumis keskmistatud jää paksus olnud maksimaalselt 15 cm, samas mõnes ruumipunktis ELWINDi alal on olnud samal perioodil jää paksus vähemalt ühel päeval ka 40 cm. 50-aastane (1980-2022) maksimaalne triivjää paksus on olnud piirkonnas ligikaudu 50 cm. Jääkate esinemine on viimastel aastakümnetel vähenenud ja vähenemise trendi eeldatakse jätkuvat ka tulevikus (Luomaranta et al., 2014), kuid aeg-ajalt võivad ELWINDi piirkonnas ka tulevikus esineda karmid talved, sh. 50 cm paksuse jääga.

Jääkatte keskmine kestus on alla ühe kuu ja enamasti esineb see triivjää kujul. ELWINDi piirkonnas esines aastatel 1994-2023 ruumiline keskmine jää kontsentratsioon ≥ 0.9 ainult kolmel järjestikusel talvel (2009/2010, 2010/2011 ja 2011/2012). Nende kolme talve kõrge (≥ 0.9) jää kontsentratsiooniga olukorra keskmine kestus oli üks nädal. Talvede esinemine, kui ruumiline keskmine jää kontsentratsioon oli ≥ 0.5 ja ≥ 0.1 oli vastavalt 28% ja 42%. Rüsijää esinemine on ELWINDi alal tagasihoidlik, kuid karmidel talvedel võib rüsijääd piirkonnas leiduda. Jäätingimustes on piirkonnas Saaremaa ranniku- ja avamerevaheline gradient. Rannikualadel on jäätingimused karmimad. Triivjää, mis aeg-ajalt ELWINDi piirkonnas esineb, pärineb tõenäoliselt Saaremaa rannikualadelt.

Läänemere lainete, hoovuste ja merepinna taseme varieeruvuse käivitaja on peamiselt tuul, mistõttu tuule tugevnedes võib eeldada ka hüdrodünaamiliste protsesside aktiveerumist, kuigi viimast mõjutavad ka muud tegurid. Tuule kiiruse ja suuna ning laine kõrguse vahel on selge seos. Kõrged lained esinevad peamiselt edela- ja loodetuultega.

Tuule tugevnedes kasvab hoovuskiirus ja edelatuuled põhjustavad veetaseme tõusu. Tuule mõju veetasemele esineb erinevates ajamastaapides. Pikaajalised tuuleolud mõjutavad merepinna üldist taset Läänemeres läbi veevahetuse reguleerimise Läänemere ja Põhjamere vahel. Sünoptilist mastaapi (tundidest nädalani) tuule mõju põhjustab Läänemeres veepinna kaldeid ja võnkumisi, mis avalduvad ka ELWINDi alal.

Tuvastati mitmed teadmiste puudujäägid ja määramatused, mis on kirjeldatud üksikasjalikumalt peatükis 5. Tuuleväli on üldiselt hästi kirjeldatud, kuid avamere tuuleolud, eriti tugevate tuulte sündmused, ei ole piisavalt hästi kirjeldatud. Samuti vajab tuuleprofiili vertikaalne struktuur täiendavaid kõrge lahutusega andmeid. Avamere tingimuste täielikuks mõistmiseks tuleks mõõta tuule kiirust ja suunda ning nende vertikaalset jaotust ELWINDi piirkonnas. Lainetuse iseloomustamiseks kasutatud mudelprodukt toimib üldiselt hästi, kuid see tõenäoliselt alahindab veidi kõrgeimaid laineid äärmuslikes tormides. Samuti ei kirjeldanud praegune uuring lainetuse spektrit. Viimase lünga täitmiseks ja äärmuslikes tingimustes kõrgeimate lainete kirjeldamiseks tuleks ELWINDi piirkonnas läbi viia lainemõõtmised.

Praeguses uuringus kasutatud mudelandmete tuginedes võivad hoovuse kiirused olla alahinnatud. Kõrgema lahutusega andmestikku vajaks hoovuse vertikaalse struktuuri kirjeldamine. Keskkonnamõju hindamise uuringute jaoks tuleks ELWINDi piirkonnas läbi viia kõrge lahutusega modelleerimine, mis on valideeritud in-situ mõõdetud hoovuste profiilide andmestikuga.

Merepinna taseme varieeruvus on tõenäoliselt praeguses uuringus hästi kirjeldatud. Ainus puudus on kasutatud mudelprodukti pikk keskmistamise aken (1 päev).

Kasutatud merejää produkt esindab tõenäoliselt üsna hästi ELWINDi ala tingimusi, kuna valideerimine on näidanud häid tulemusi. Samas jäätingimusi on keeruline ennustada, kuna aastatevaheline muutlikkus on väga kõrge.

1. Background and general description of met-ocean conditions

This work aims to describe the meteorological and oceanographic conditions in the ELWIND wind farm development site. The current study relies on the existing data and model products. No targeted modeling or measurement activities were done in the frame of the present study. The used data sources and methods are described in Chapter 2, which is followed by the description of wind, wave, current, ice, and other parameters in the ELWIND area in chapters 3 and 4. The identified knowledge gaps and uncertainties are presented in the chapter 5.

The study area is located in the eastern part of the central sub-basin (Baltic Proper) of the Baltic Sea. It is located west from the Sõrve peninsula of Saaremaa Island (Fig. 1.1). The L-shaped wind farm development area is located at the coastal slope with sea depths ranging from < 20 m in the southeastern part to > 40 m in the northwestern part. The area is covered by land from east and north, but open from other directions. The distance to the nearest shore at the Sõrve peninsula is approximately 12 km.

Wind regime in the area is typical for the Baltic Sea area with the highest occurrence of winds from a southwesterly direction. The higher occurrence of southwesterly winds is connected to the stronger airflow from the Open Atlantic and is correlated to a positive NAO index (Lehmann et al., 2002). The wind is influenced by the topography of the area and as a result winds along the axis of the Baltic Proper prevail in the area (Soomere and Keevallik, 2001). Especially moderate and stronger winds occur more frequently from a south-westerly direction. The secondary peak of occurrence of moderate and strong winds is from a northerly sector (Soomere and Keevallik, 2001). The mean wind speed is higher in autumn and winter period and lower in spring and summer. Likewise, the storminess is higher in the two former seasons and lower in spring and summer. This seasonality is reflected also in the anisotropy of the directional distribution of winds, especially the directional distribution of moderate and strong winds. The occurrence of strong south-westerlies is particularly high in the autumn and winter periods. The mean wind speed in the Vilsandi meteorostation (located on the Island of Vilsandi, north of the study area) was 6.4 m/s in 1977-1991 (Soomere and Keevallik, 2001). The mean wind speed from the southwesterly direction during the same period was 8.0 m/s. The maximum 10-minute

wind speed in the same period has been 25 m/s during a storm from the southwesterly direction (Soomere and Keevallik, 2001).

The offshore wind profile is typically characterized by a logarithmic or power law distribution, where wind speed increases rapidly within the surface layer (the lowest tens of meters of the atmosphere) and then only gradually increases throughout the remainder of the Ekman layer, which generally extends up to 0.1–1 km in height. However, in coastal areas, the vertical structure could be more complicated, e.g. negative gradients under certain meteorological and hydrological conditions might occur (Barthelmie et al., 2007). Partly negative shear in a wind speed profile can lead to a local wind maximum in the profile (low-level jet), or a local wind minimum in the profile (low-level minimum) (Hallgren et al., 2020).

The wave conditions in Baltic Sea depend on the direction and speed of the wind, the fetch, and the depth. Since the fetch in the Baltic Sea (compared to the open ocean) is short, waves reach saturation relatively quickly, and wave energy decreases rapidly when the wind subsides. The average significant wave height at the mouth of the Gulf of Finland and in the open Baltic Sea exceeds 1 meter. The maximum significant wave height in the open Baltic Sea can exceed 8 meters.

The primary driver of currents in the Baltic Sea is wind, but density gradients also contribute. Wind generates currents through the shear stress on the sea surface. This results in water level gradients, which in turn create currents. In the development area on the eastern coast of the Baltic proper, south-westerly winds cause higher water levels, resulting in a geostrophic current along the coast towards the north while winds from the northerly sector cause a reversal of the current (Liblik et al., 2022). Depending on stratification, the Baltic Sea can exhibit one-, two-, or three-layer current structure (Suhhova et al., 2018). Currents transport water masses with different properties, as well as pollution, such as nutrients, oil, or debris from human activities. Average current speeds are around 10 cm/s in the Eastern Baltic Sea (Liblik et al., 2022; Suhhova et al., 2018).

Wintertime ice coverage has decreased in the Baltic Sea in recent decades and this decreasing trend is expected to continue also in the future (Luomaranta et al., 2014). According to data from 1980 to 2022, ice coverage does not occur in the wind farm development area during more than half of the winters (Tikanmäki et al., 2025) and on average the duration of ice coverage is less than one month in the area.

Sea level variability is quite low in the area. The role of tides in the sea level variability is marginal in the Baltic Sea. The main causes for the sea level variability are wind-driven convergence and divergence, long waves, and seiches. The amplitude of sea level variability is less than +/- 1 meter from the long-term mean. Since the area is not next to the coast and there is an open boundary, Irbe Strait, where the converged water could flow from the Baltic Proper to the Gulf of Riga, extreme high-water levels do not occur in the development area.

The vertical structure of the water column in the Baltic Sea is complex and influenced by several factors. The structure is affected by heat exchange with the atmosphere, freshwater inflows, advection, and vertical mixing (Leppäranta and Myrberg, 2009). Stratification is strongest during the warm period when a thermocline is present. Temperature could rise over 20 °C in the surface layer during summers. Below the thermocline is a saltier and colder intermediate layer, which forms in winter. Beneath the intermediate layer, at a depth of about 50-70 meters, is the halocline, a salinity gradient that separates the intermediate layer from the deep layer. The deep layer is saltier and usually slightly warmer than the intermediate layer. In autumn, the thermocline weakens and moves deeper. In winter, the water column mixes from the surface to the halocline, and the surface water temperature drops < 5 °C. The water beneath the halocline is oxygen-depleted. The water could be hypoxic or even anoxic, i.e. H₂S could form there. This water could under favorable hydrodynamic conditions move upwards to the depths of 40-50 m, but not to the surface (Liblik et al., 2022).

The water of the Baltic Sea is brackish. The upper layer salinity in the Baltic Proper is in the order of 6-8 g/kg. The deep layer water is considerably saltier. Below the halocline, in the Gotland Deep, salinity could be up to 14 g/kg.

2. Data sources and methods

Hourly 10 m level wind velocities, air pressure and air temperature data (product name: *ERA5 hourly data on single levels from 1940 to present*) and wind velocities at 1000 hPa, 975 hPa, 950 hPa (*ERA5 hourly data on pressure levels from 1940 to present*) of ERA5 reanalysis data (Hersbach et al., 2020) from 1994 to 2023 were used in the analysis. Except for the spatial distribution description, the time-series data from the cell near the ELWIND area was used in the analysis (see Fig. 2.1 for the location of the cell center). ERA5 data was complemented by 10-minute average wind direction and speed data and wind gust speed data from Sõrve and Vilsandi meteorostations, operated by Estonian Environment Agency. Likewise, air pressure, relative humidity, and air temperature data were used from the two meteorostations. ERA5 product performs reasonably well in offshore conditions (Cheynet et al., 2025) and is generally accepted for wind farm studies (Jourdi er, 2020; Olauson, 2018), but it likely underestimates strong wind speed events offshore (Gandoin and Garza, 2024). Likewise, it likely does not fully capture the vertical velocity structure of the wind profile (Hallgren et al., 2020). However, these biases could be reduced by completing local lidar measurements and further validation and correction of a model data (Gandoin and Garza, 2024). Coastal wind observations at Sõrve and Vilsandi are generally acceptable to describe wind conditions at sea, although Vilsandi station is impacted by nearby obstacles from some directions (Žukova, 2009).

Hourly wave data from 1994 to 2023 was acquired from the Copernicus Marine Service (<https://marine.copernicus.eu/>) product *Baltic Sea Wave Hindcast* (BALTICSEA_MULTIIYEAR_WAV_003_015). Except for the spatial distribution, the time-series data from the cell in the ELWIND area was used in the analysis (see Fig. 2.1 for the location of the cell center). Significant wave height, wave period (mean wave period from variance spectral density second frequency moment), and wave propagation direction (the direction wave is coming from) were used as wave climate describing parameters. The product performs well as shown by validation with remote sensing and in-situ measurements (Björkqvist et al., 2024; Björkqvist et al., 2020; Tallinna Tehnikaülikool, 2021).

Daily current velocity components, salinity, temperature, and density (derived from salinity and temperature) from 22 levels (from sea surface down to near-bottom layer at 36 m depth) from 1994 to 2023 from Copernicus Marine Service product *Baltic Sea Physics Reanalysis*

(BALTICSEA_MULTIIYEAR_PHY_003_011) were used in the study. The sea temperature is presented as potential temperature, salinity as Absolute Salinity, and density as potential density anomaly to a reference pressure of 0 dbar. Likewise, sea level data were used in the data analysis from the same product. Except for the spatial distribution of currents and sea level, the time-series data from the cell in the ELWIND area was used in the analysis (see Fig. 2.1 for the location of the cell center). The sea level data is presented as an anomaly from the mean of 1994-2023 period in the location of the time series. Hourly data of current velocity components from the Copernicus Marine Service *Baltic Sea Physics Analysis and Forecast* (BALTICSEA_ANALYSIS AND FORECAST_PHY_003_006) from the year 2023 were also used. Daily maximum current speed from hourly data was compared with the daily mean current speed and the mean offset between the two was derived and applied to the daily data when the return periods of current speeds were estimated. The results of the two products are acceptable (<https://documentation.marine.copernicus.eu/QUID/CMEMS-BAL-QUID-003-011.pdf>, <https://documentation.marine.copernicus.eu/QUID/CMEMS-BAL-QUID-003-006.pdf>; accessed 23.04.2025), but uncertainties in some parameters (e.g. currents) are quite high (Tallinna Tehnikaülikool, 2021).

Daily sea ice concentration and sea ice thickness data were acquired from Copernicus Marine Service product *Baltic Sea ice concentration, extent, and classification time series* (SEAICE_BAL_PHY_L4_MY_011_019). The spatial average of parameters within the ELWIND area for each day was calculated and the analysis relied on this time-series. Validation with observations has shown good results (<https://documentation.marine.copernicus.eu/QUID/CMEMS-SEAICE-QUID-011-004-011-019.pdf>, accessed 23.04.2025).

It has to be noted that for wind and waves the direction shows where wind and waves are coming from while the current direction shows the direction in which water is moving. Thus, for instance, SW wind and NE current are exactly to the same direction. In the plots of ice parameters years represent the start year of the ice season (winter), i.e. for instance 2009 indicates winter 2009/2010.

The Generalized Extreme Value (GEV) distribution was used to estimate the return periods of wind speed; wave height and period; current speed; and high and low sea level.

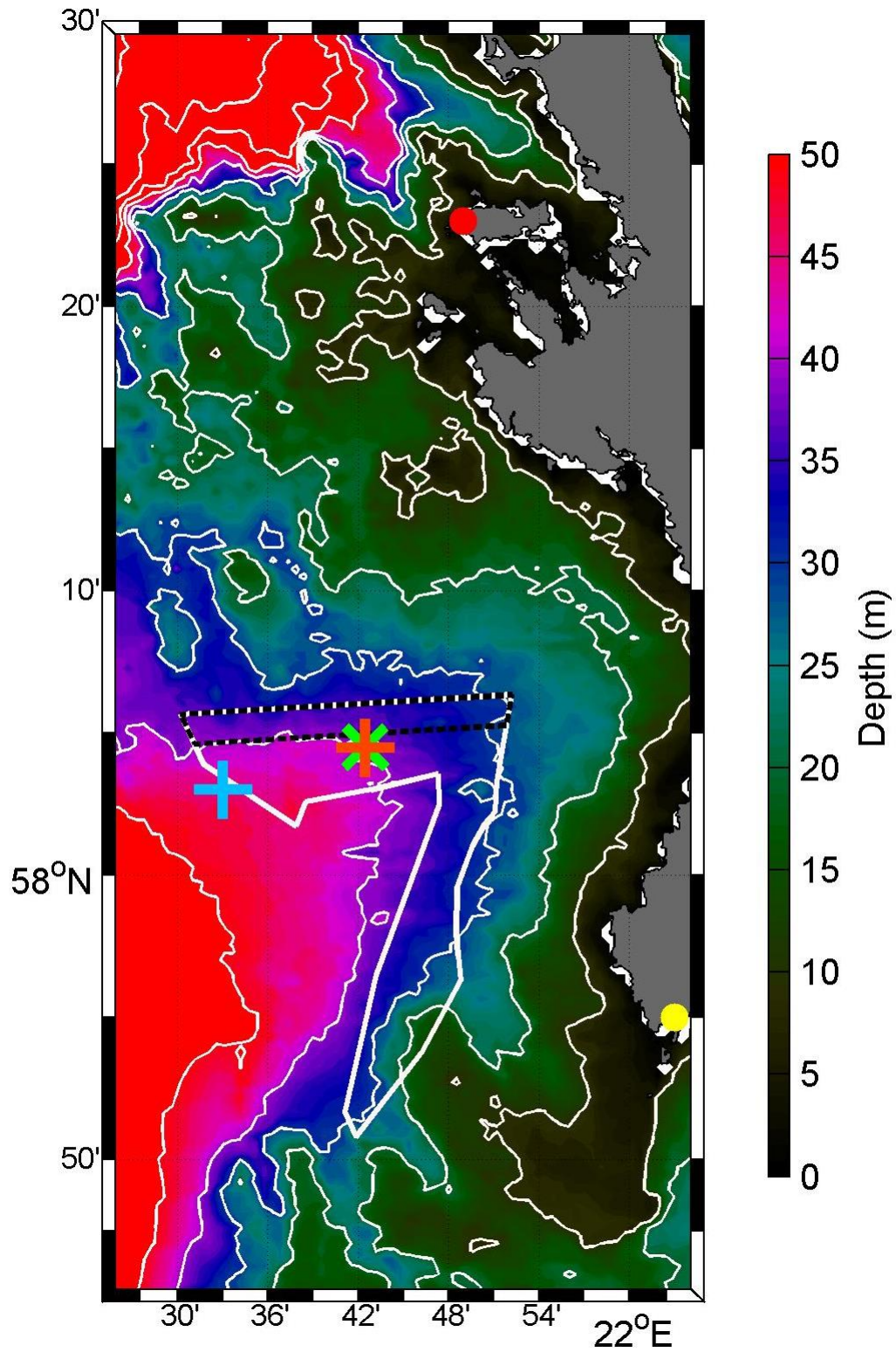


Fig. 2.1. Study area. Sea depths are shown with color scale, white line shows the ELWIND area and the black dashed area is the buffer zone. ERA5, *Baltic Sea Physics Reanalysis*, and *Baltic Sea Wave Hindcast* time-series data extraction locations are shown with blue, green and orange crosses, respectively. Vilsandi meteorostation is shown with the red dot and Sörve meteorostation with the yellow dot.

3. Results

3.1. Wind conditions

Annual and monthly wind roses (Figs. 3.1.1.1-3.1.1.13) show the dominance of southwesterly winds as well known for the Baltic Sea area. The secondary peak of occurrence of moderate and strong winds is from a northerly and northwesterly direction. Strong southwesterlies are more common in autumn and winter period while winds are generally weaker in spring and autumn (Figs. 3.1.1.14-3.1.1.26). The vertical structure of wind speed shows the same seasonality as near boundary wind statistics, i.e. weaker winds through the profile occur in spring and summer and stronger winds in autumn and winter (Fig. 3.1.3.1). There is a 30-40% increase in wind speed from the 10 m level to 950 hPa level (approximately 500 m) depending on the season (Fig. 3.1.3.1).

Similar anisotropic tendency as in average wind conditions are also seen in the return periods (Figs. 3.1.2.1-3.1.2.39). The winds from westerly, northerly and southerly directions have much higher speeds in the same return periods compared to easterly winds. A comparison of ERA5 data with coastal stations reveals that ERA5 underestimates strong wind speeds. The 10-minute average wind speed in meteostations is higher than in hourly averages of ERA5 for the same return periods. Latter is not the case for all wind directions, as probably effects of local obstacles and friction of land likely slow down the airflow there. Wind gust speeds could be up to 35 m/s in the coastal stations according to 20 years of data. However, likely the maximum wind speed could be even higher in the ELWIND site compared to coastal stations as wind tends to be stronger further offshore compared to near the coastline (Fig. 3.1.4.1.). Moreover, the maximum wind gust speed in Estonia, recorded in the Gulf of Riga in the 1967 November storm, has been 48 m/s (Suursaar et al., 2007).

The parameters of Weibull distribution (table 3.1.1) also suggest that wind speed is likely higher in the offshore area. The scale parameter of Weibull distribution is higher in ERA5 data compared to the meteostations, which is the indication of generally stronger winds offshore. However, the shape parameter for ERA5 is larger compared to meteostations, which means that wind speed variability (including occurrence of extremes) is lower in ERA5 data compared to the data from meteostations. Likely, at least partly latter is related to the spatial and temporal averaging of ERA 5, which reduces strong wind speeds in offshore areas. Thus, likely strong events in offshore areas are more common and with higher magnitude than the ERA5 reveals.

Table 3.1.1. Weibull distribution parameters for wind speed. Parameters for ERA5 1-hour, Vilsandi 10-minute, and Sõrve 10-minute wind speed data are given. Estimates from Keevallik et al. (2007) and Soomere (2001) relying on Vilsandi meteorological station data are given for comparison.

	ERA5 (1994- 2023)	Vilsandi (1994- 2023)	Sõrve (1994- 2023)	Vilsandi by Soomere (1976-1991)	Vilsandi by Keevallik et al 10 min (2004-2005)	Vilsandi by Keevallik et al. 3 h (2004- 2005)
Shape	8.35	6.37	6.67	7.24	6.46	6.44
Scale	2.38	1.96	1.87	2.05	1.87	1.94

Wind conditions in the ELWIND are not currently under the impact of other wind farms, but when one of the neighboring farms is constructed, the wind speed will be reduced from some directions as described in subchapter 3.1.5.

3.1.1. Average wind conditions

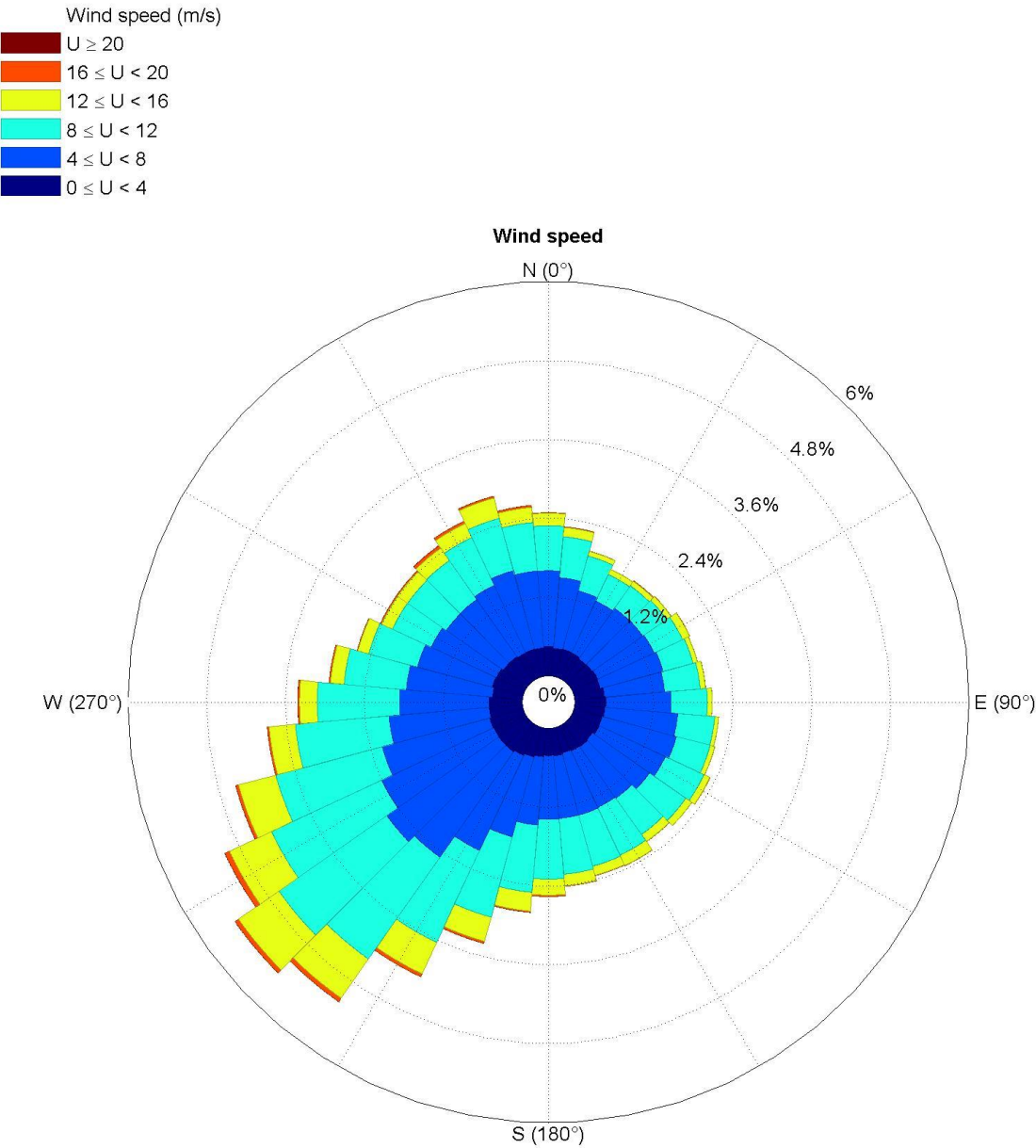


Fig. 3.1.1.1. Windrose for the year-round data based on ERA5 data.

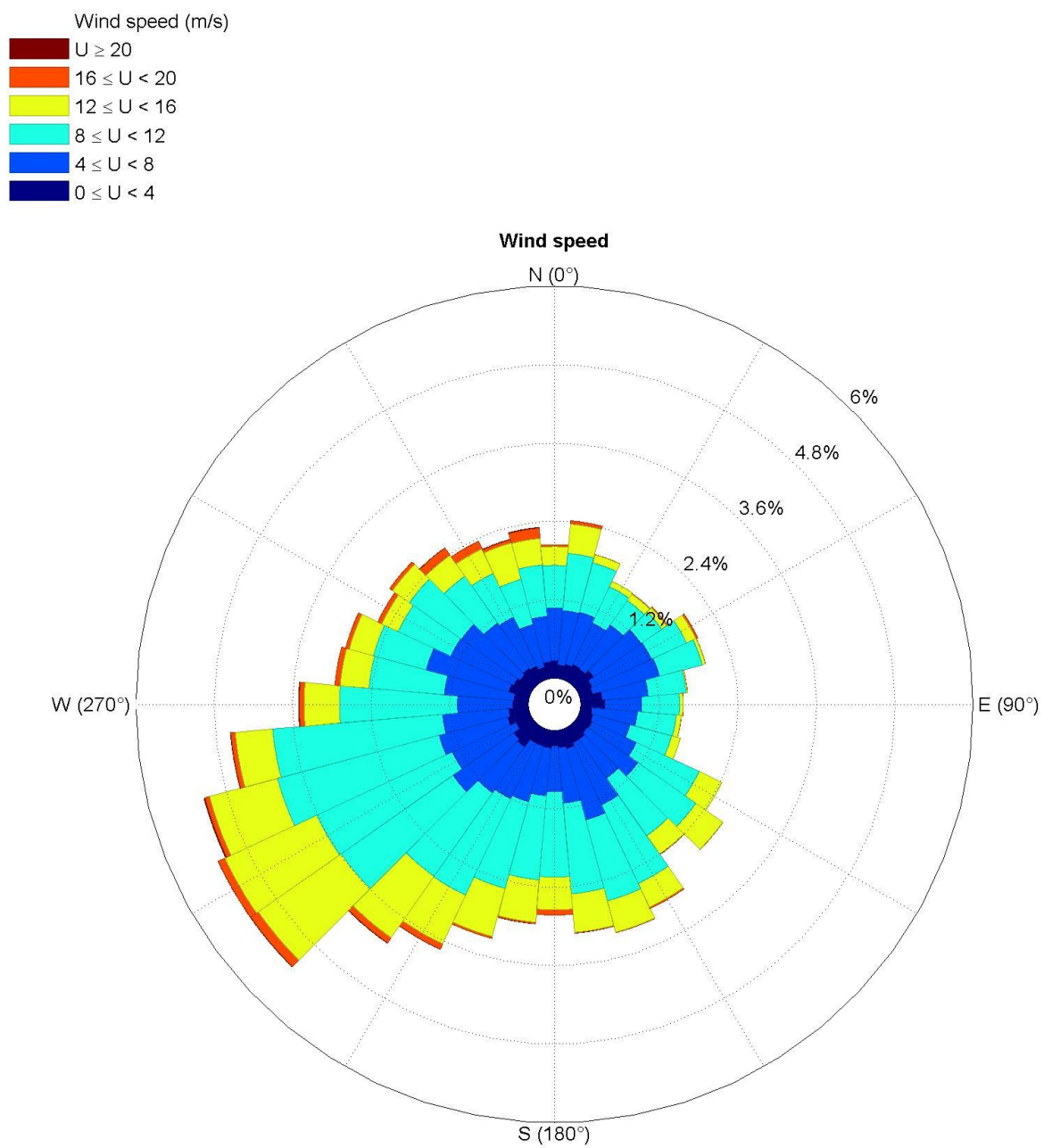


Fig. 3.1.1.2. Windrose for January based on ERA5 data.

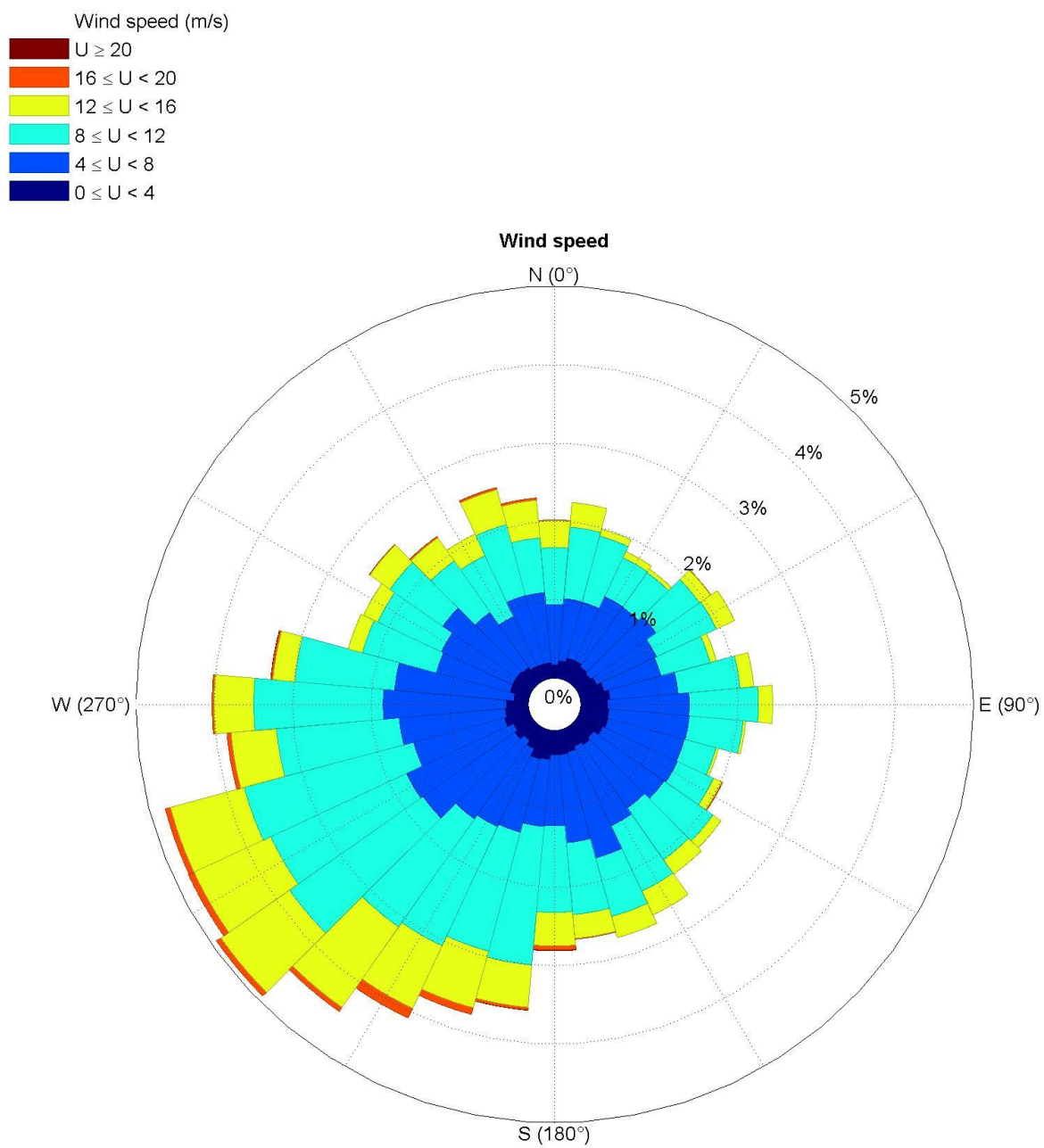


Fig. 3.1.1.3. Windrose for February based on ERA5 data.

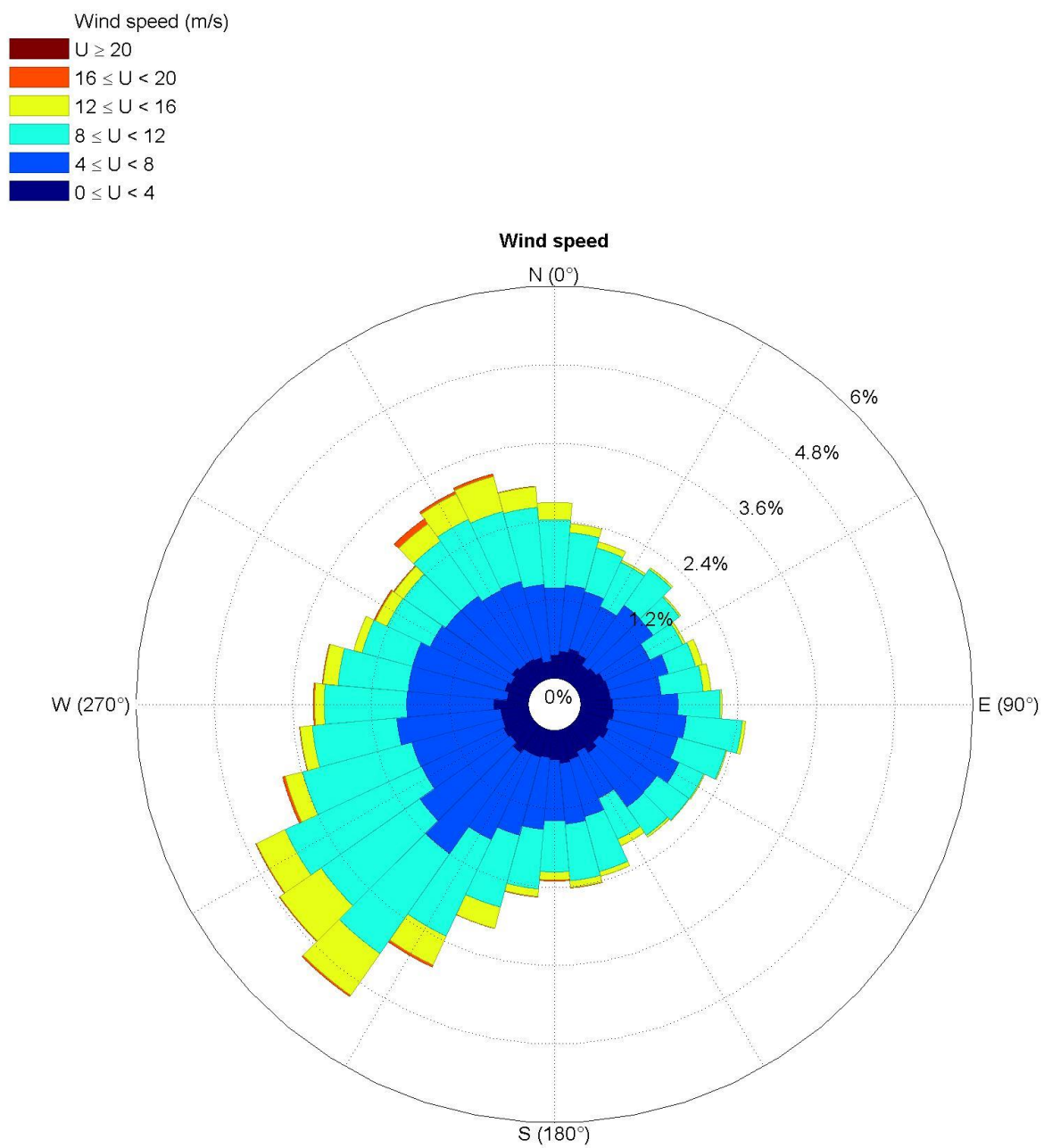


Fig. 3.1.1.4. Windrose for March based on ERA5 data.

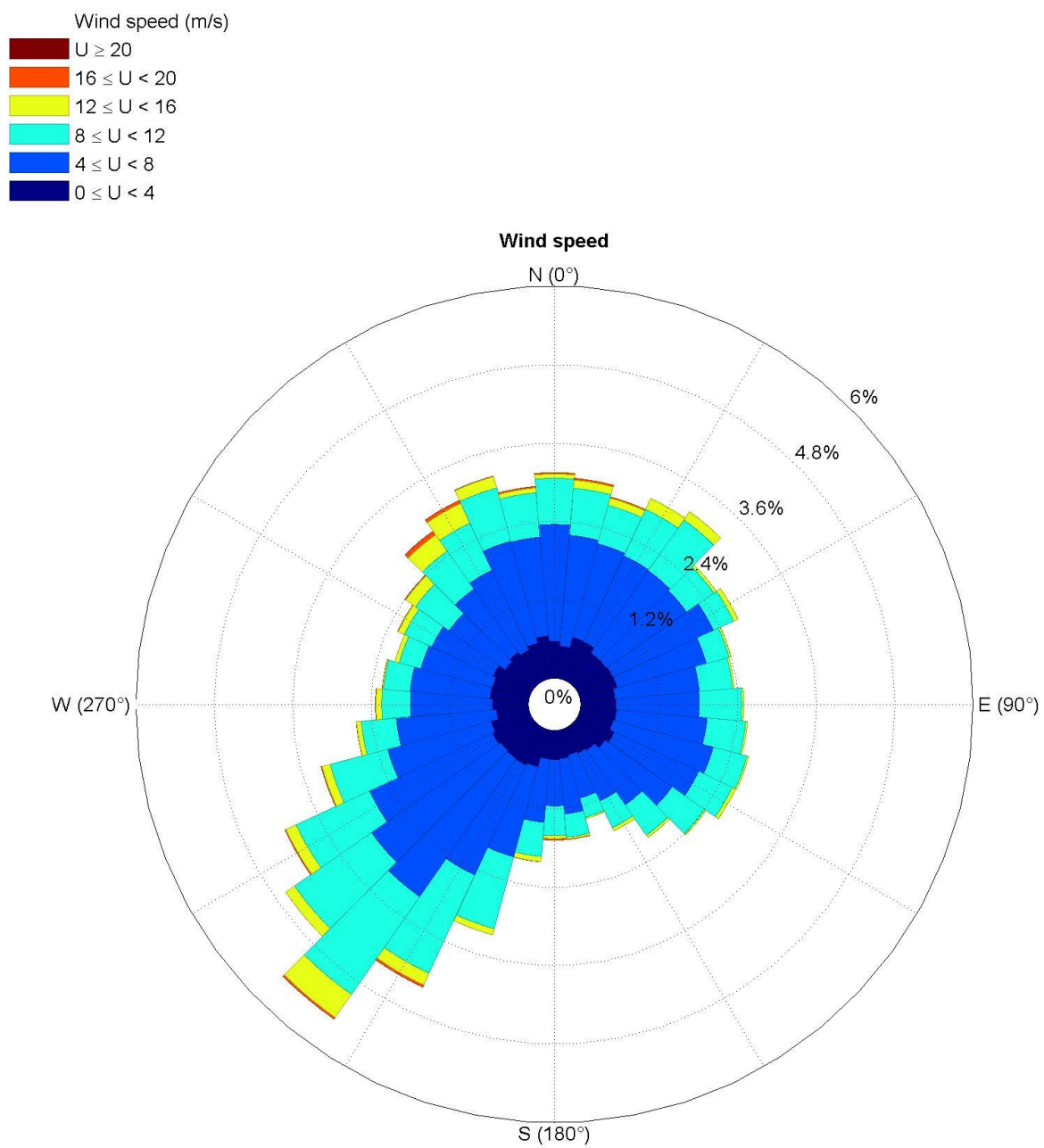


Fig. 3.1.1.5. Windrose for April based on ERA5 data.

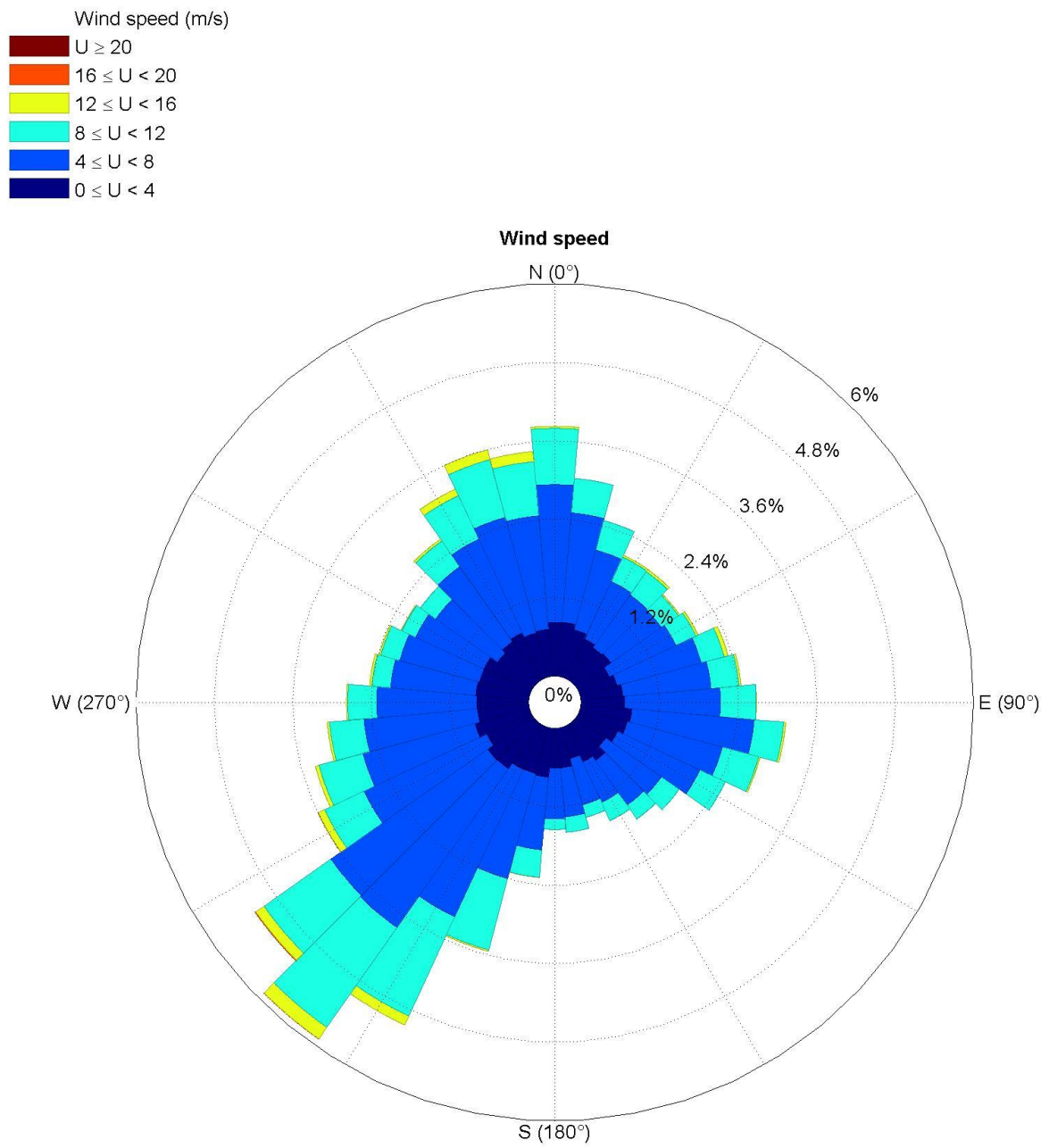


Fig. 3.1.1.6. Windrose for May based on ERA5 data.

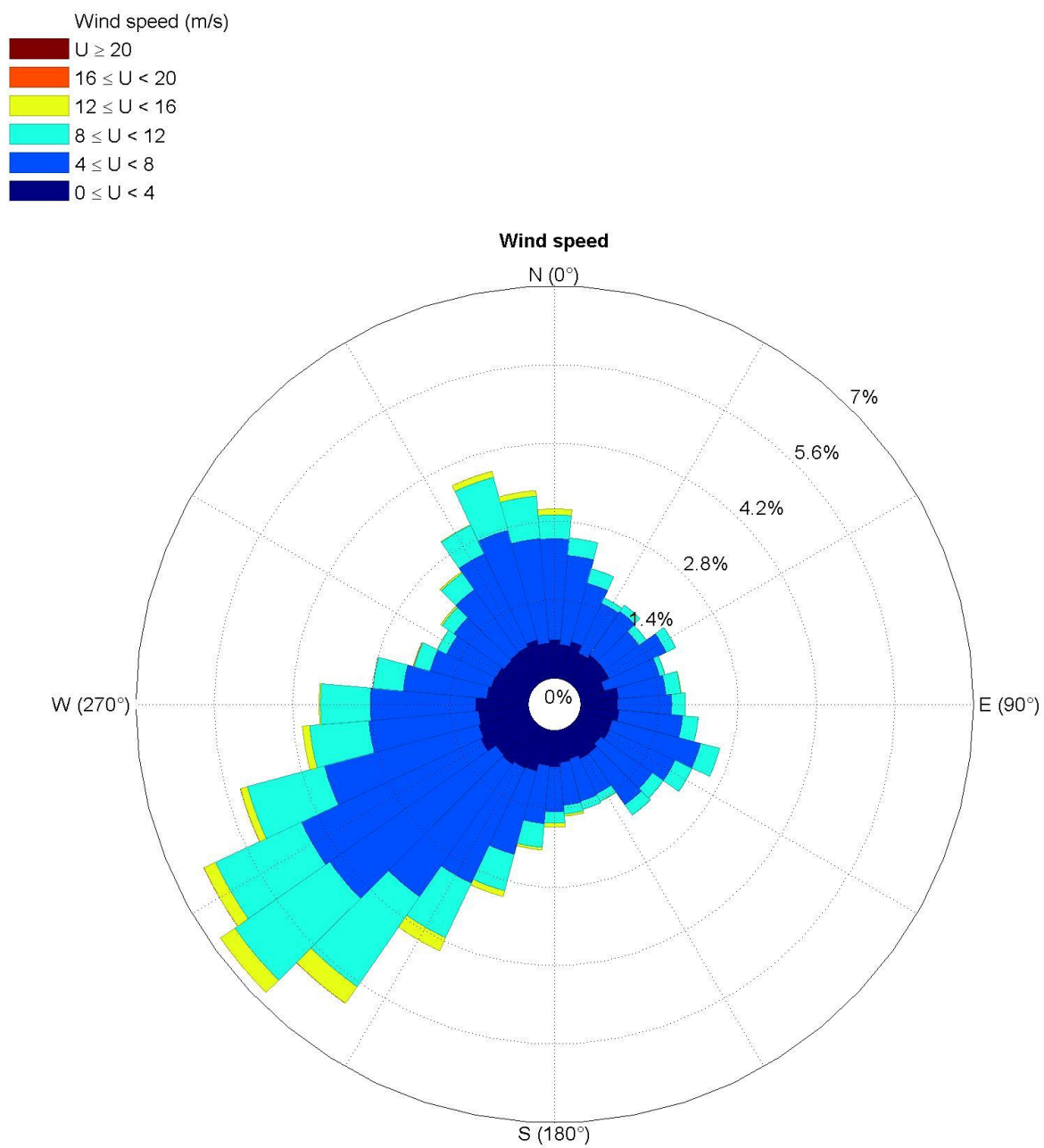


Fig. 3.1.1.8. Windrose for July based on ERA5 data.

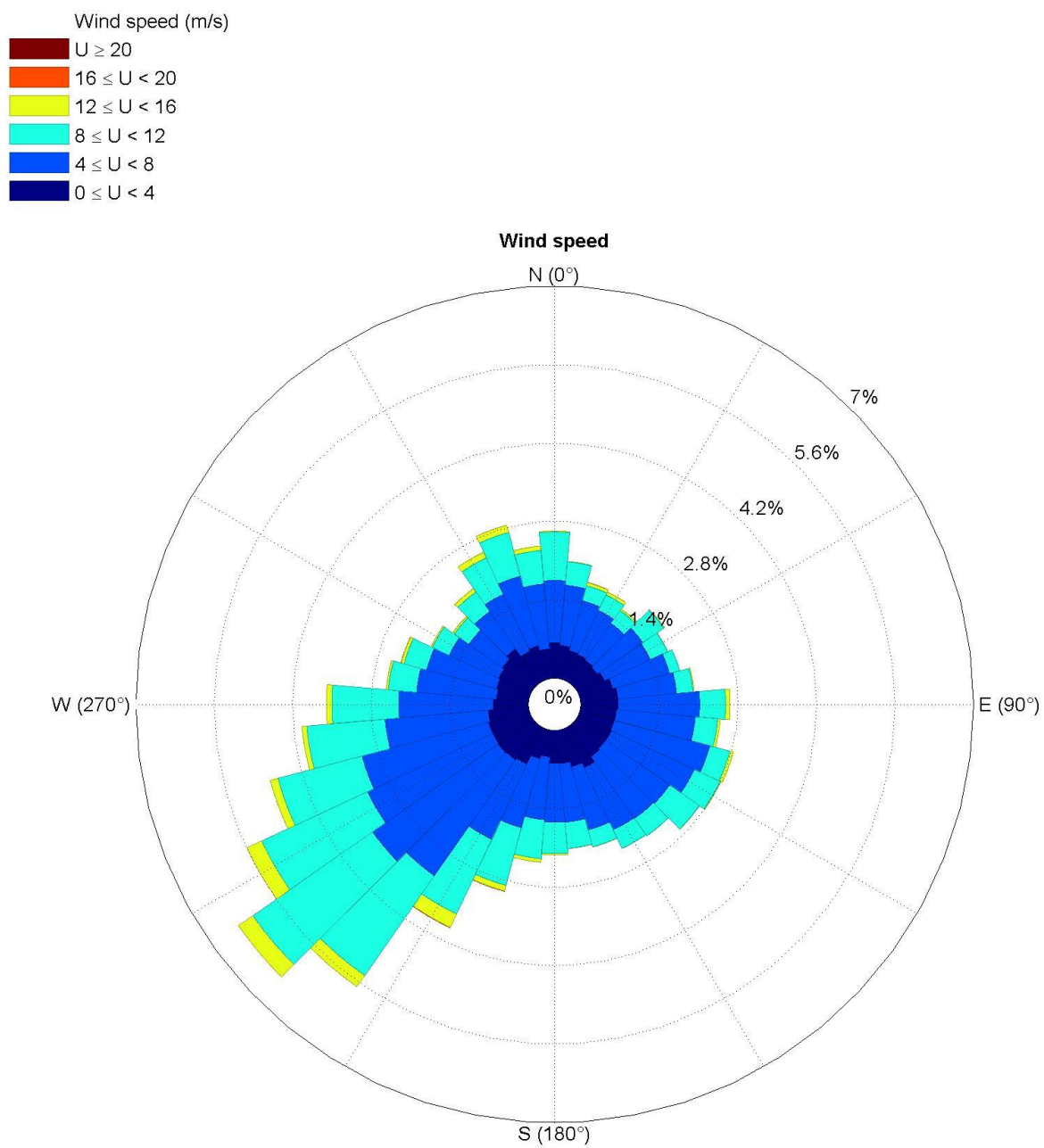


Fig. 3.1.1.9. Windrose for August based on ERA5 data.

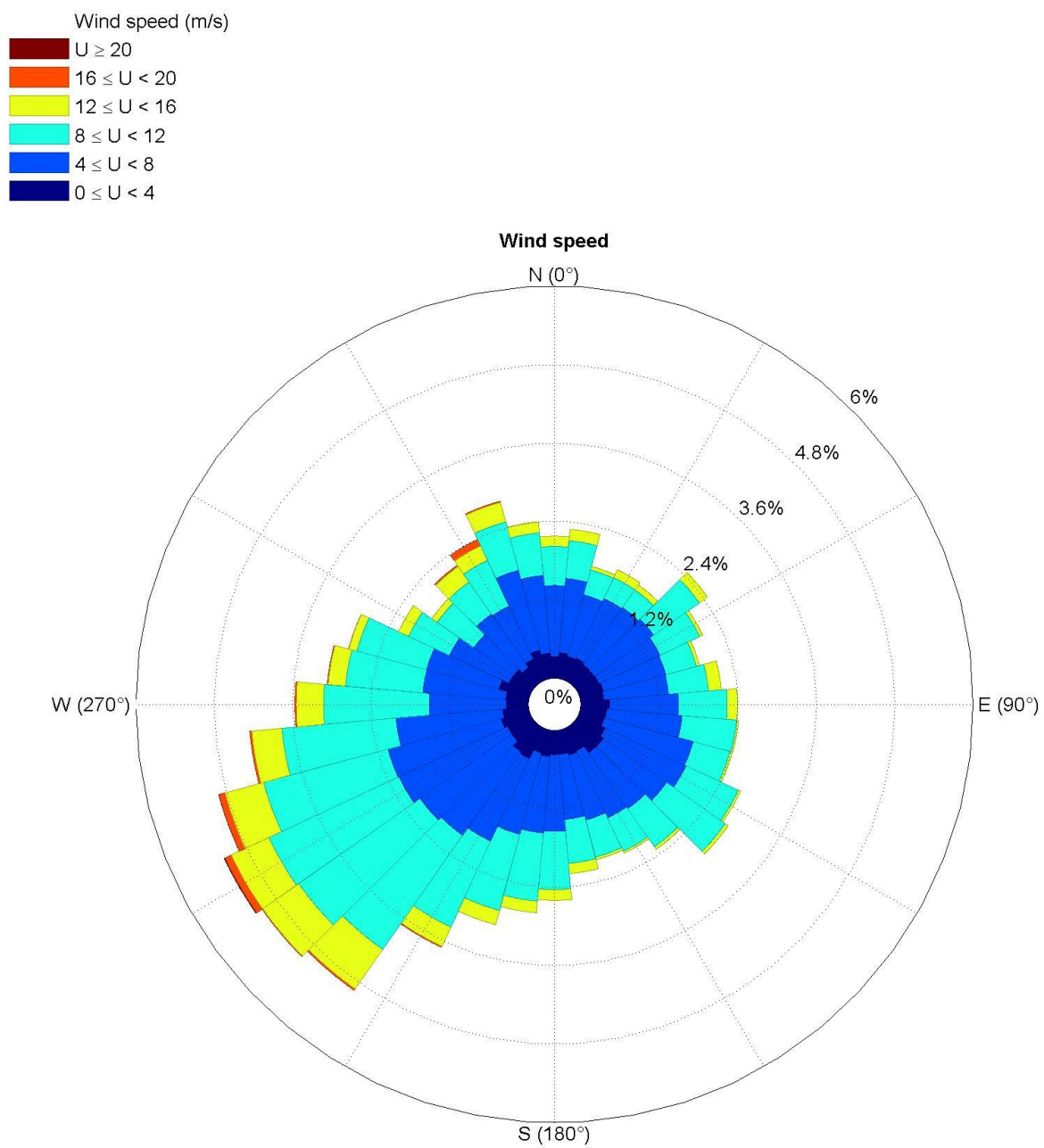


Fig. 3.1.1.10. Windrose for September based on ERA5 data.

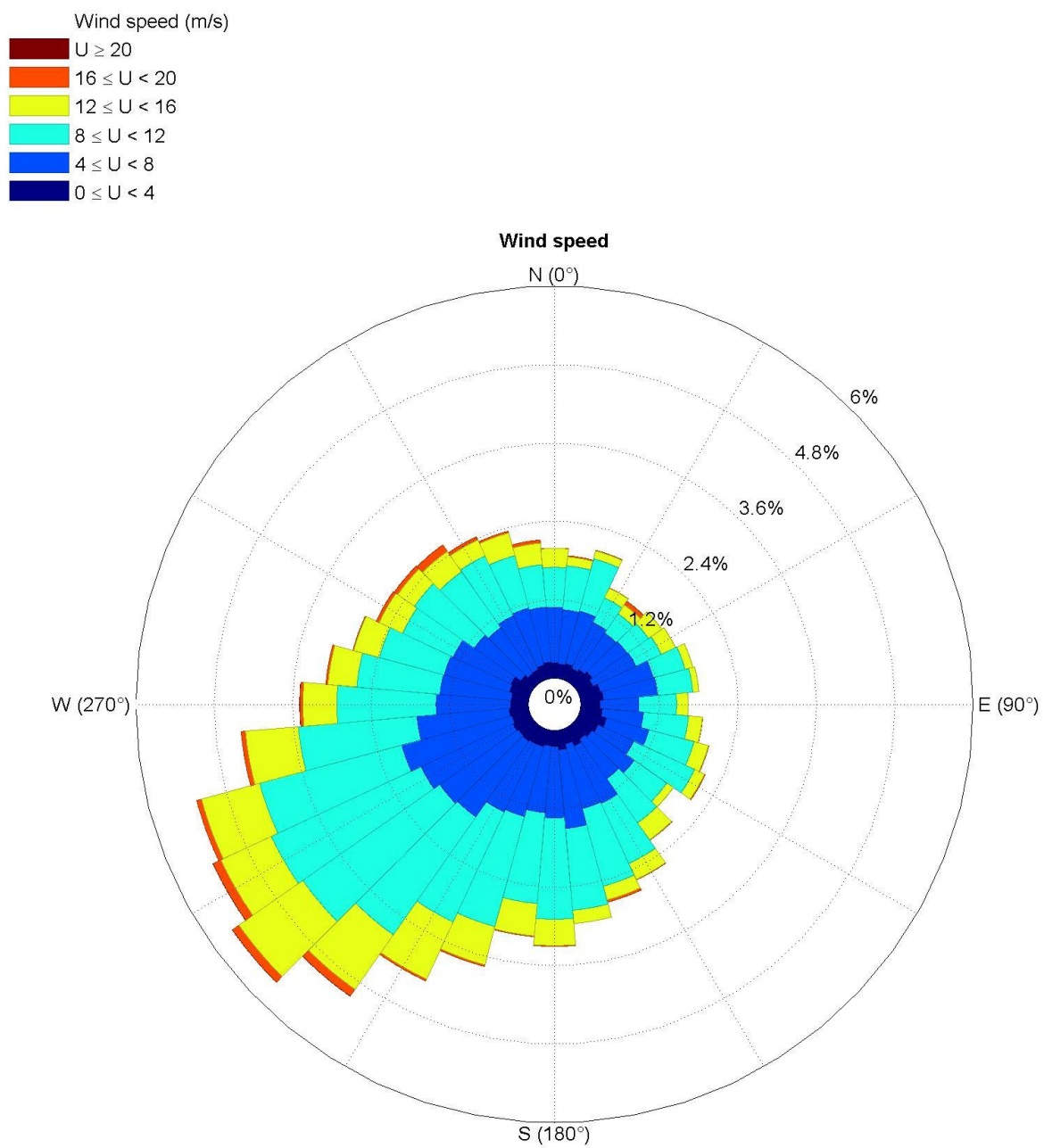


Fig. 3.1.1.11. Windrose for October based on ERA5 data.

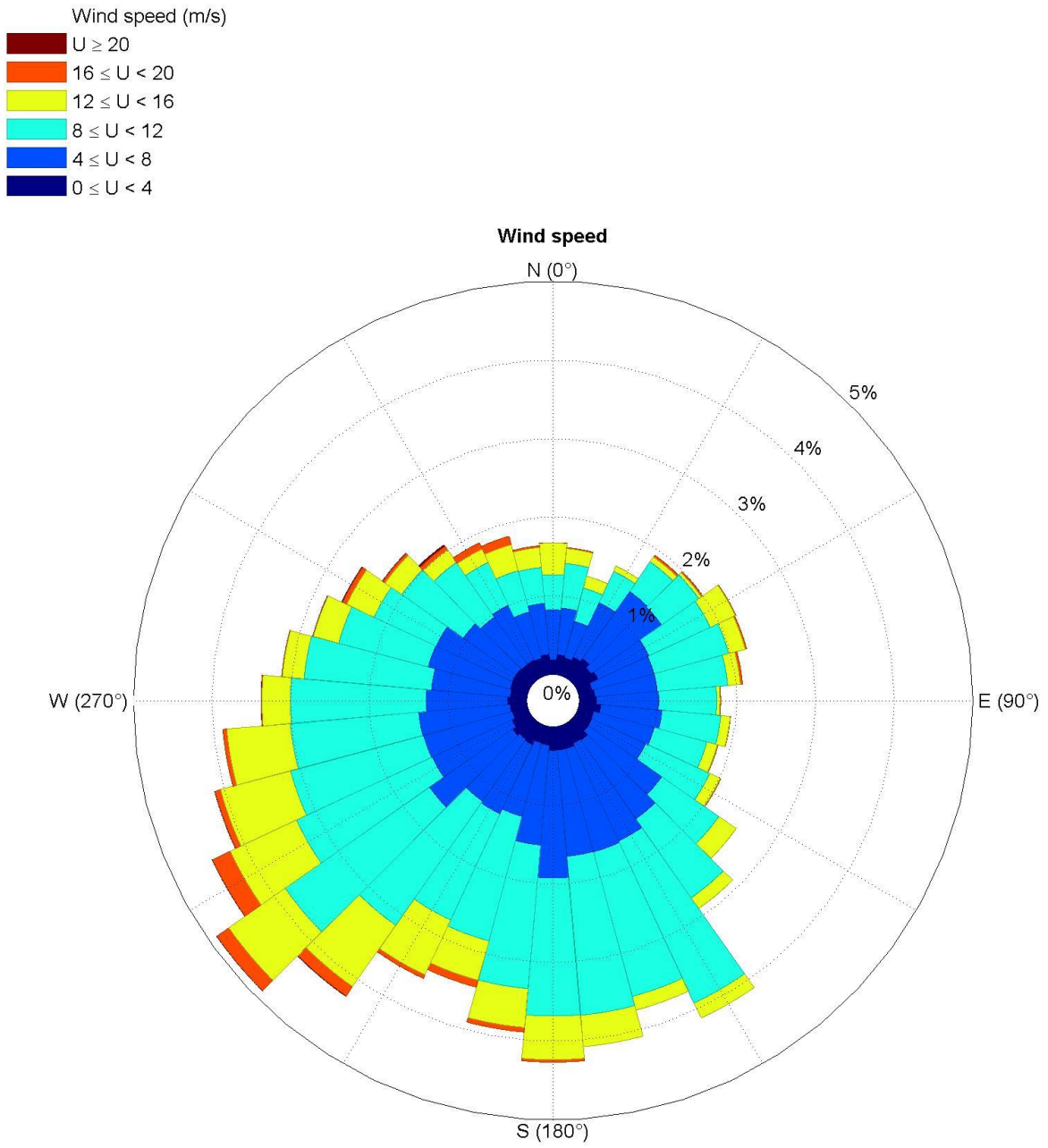


Fig. 3.1.1.12. Windrose for November based on ERA5 data.

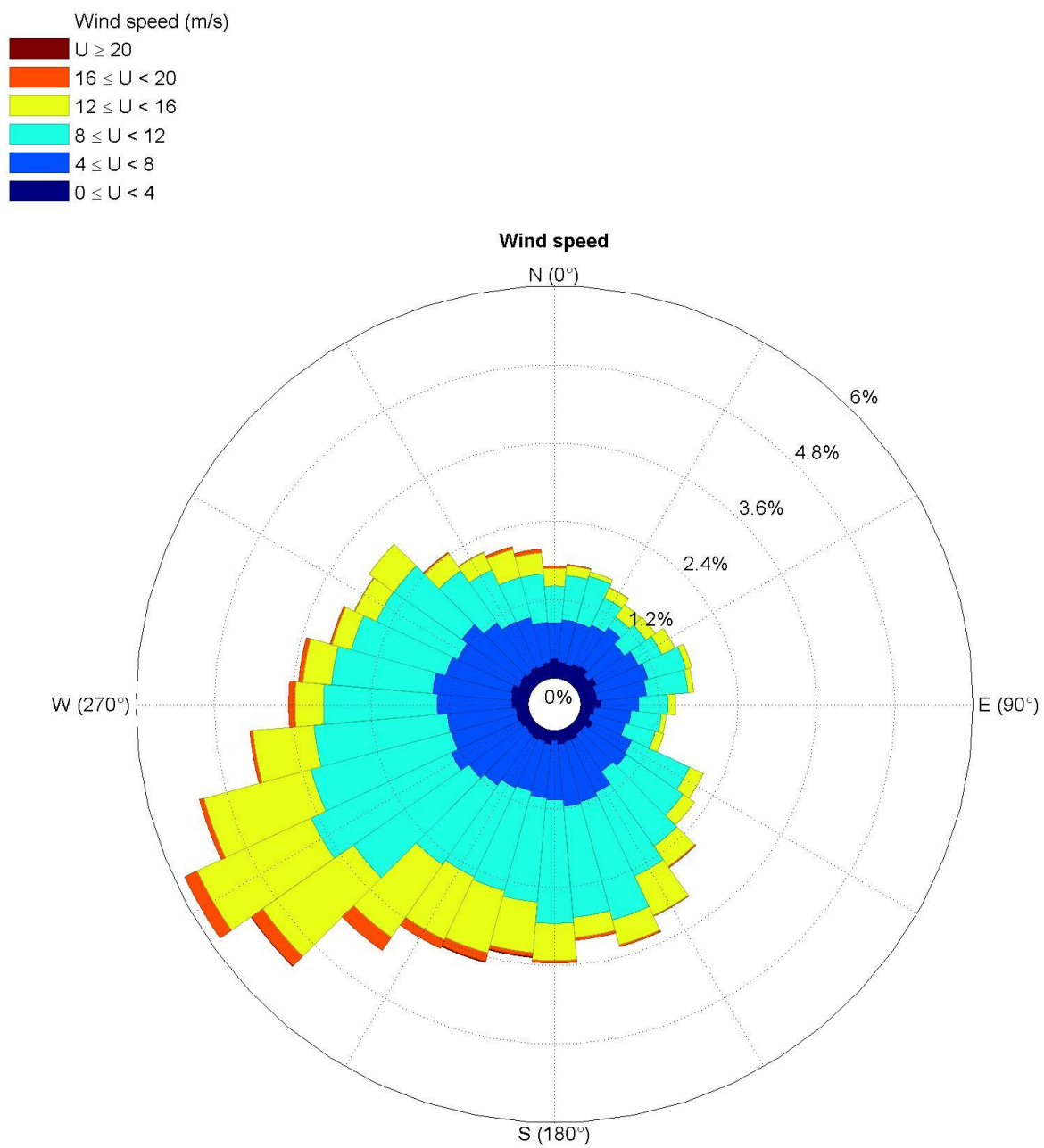


Fig. 3.1.1.13. Windrose for December based on ERA5 data.

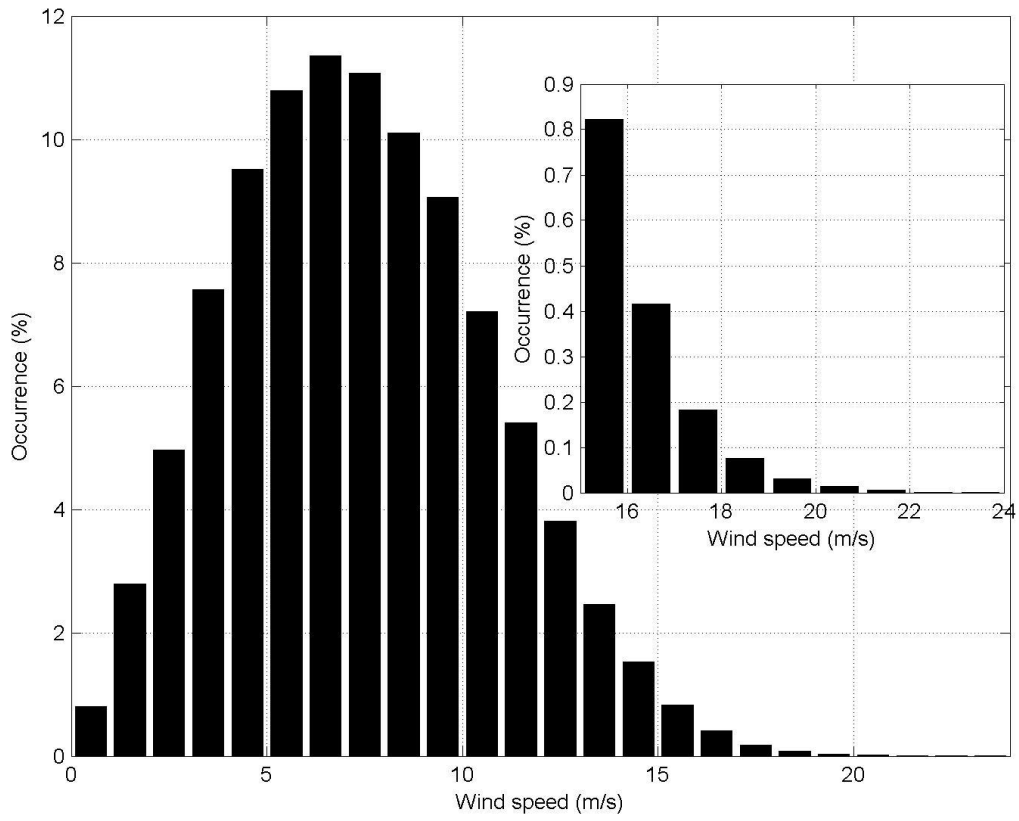


Fig. 3.1.1.14. Annual occurrence of wind speed based on ERA5 data

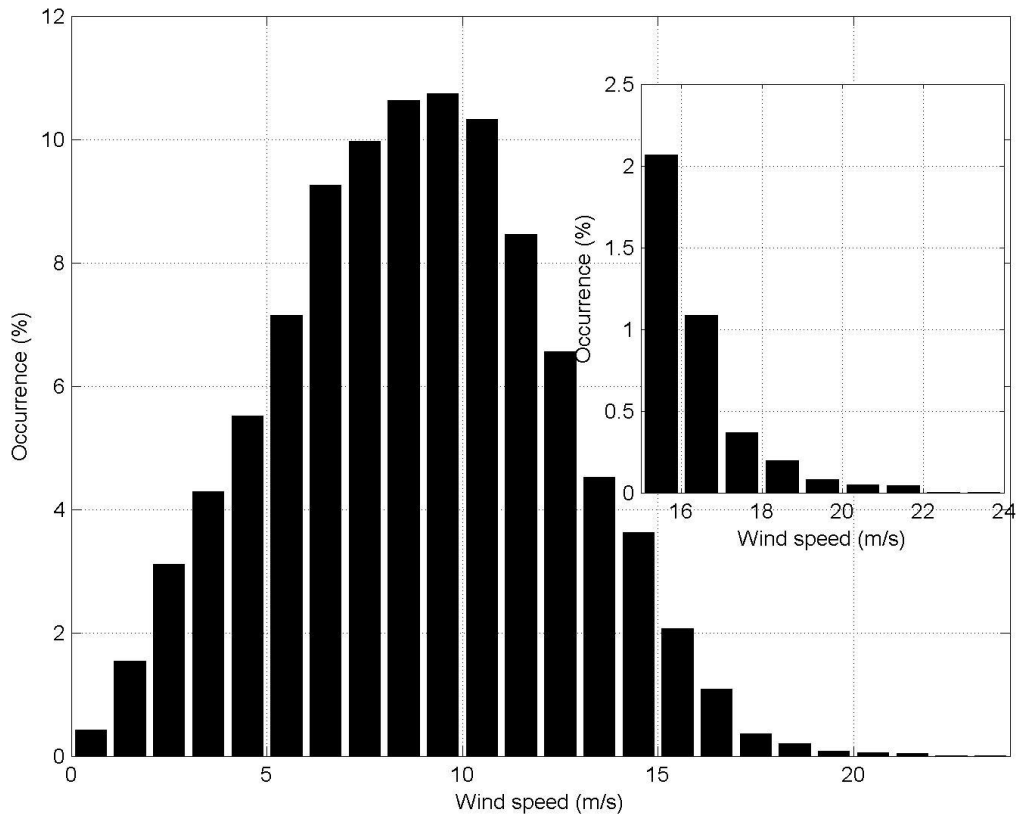


Fig. 3.1.1.15. Occurrence of wind speed in January based on ERA5 data

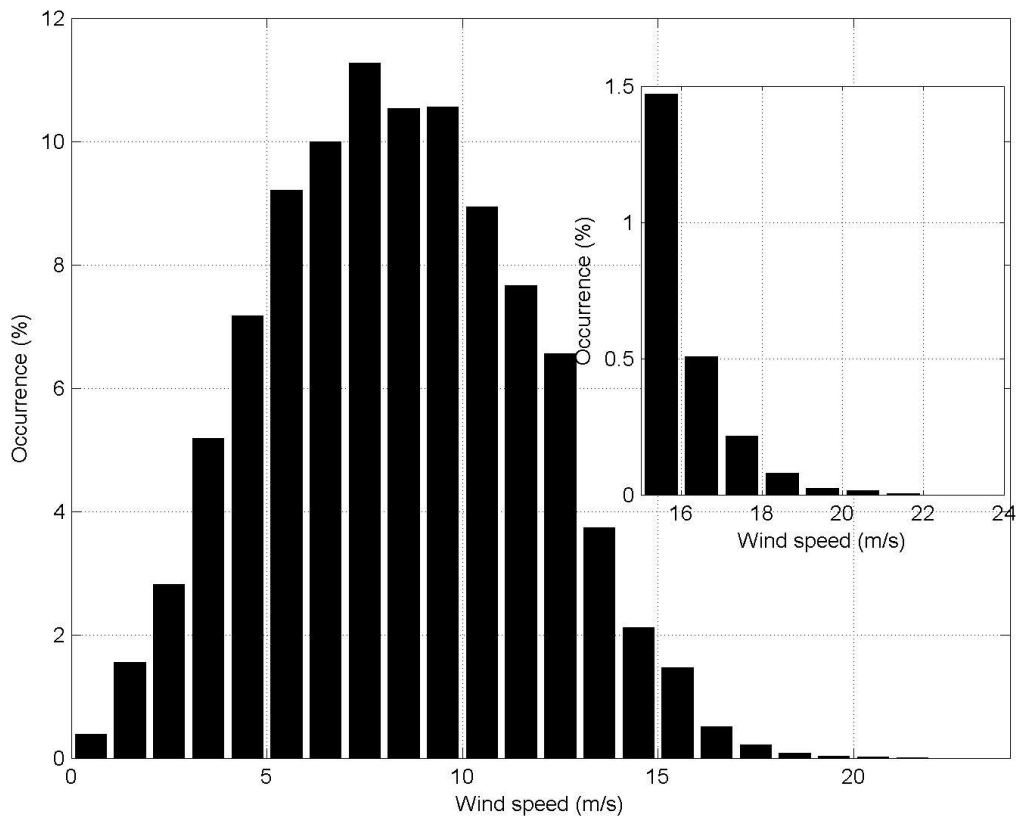


Fig. 3.1.1.16. Occurrence of wind speed in February based on ERA5 data

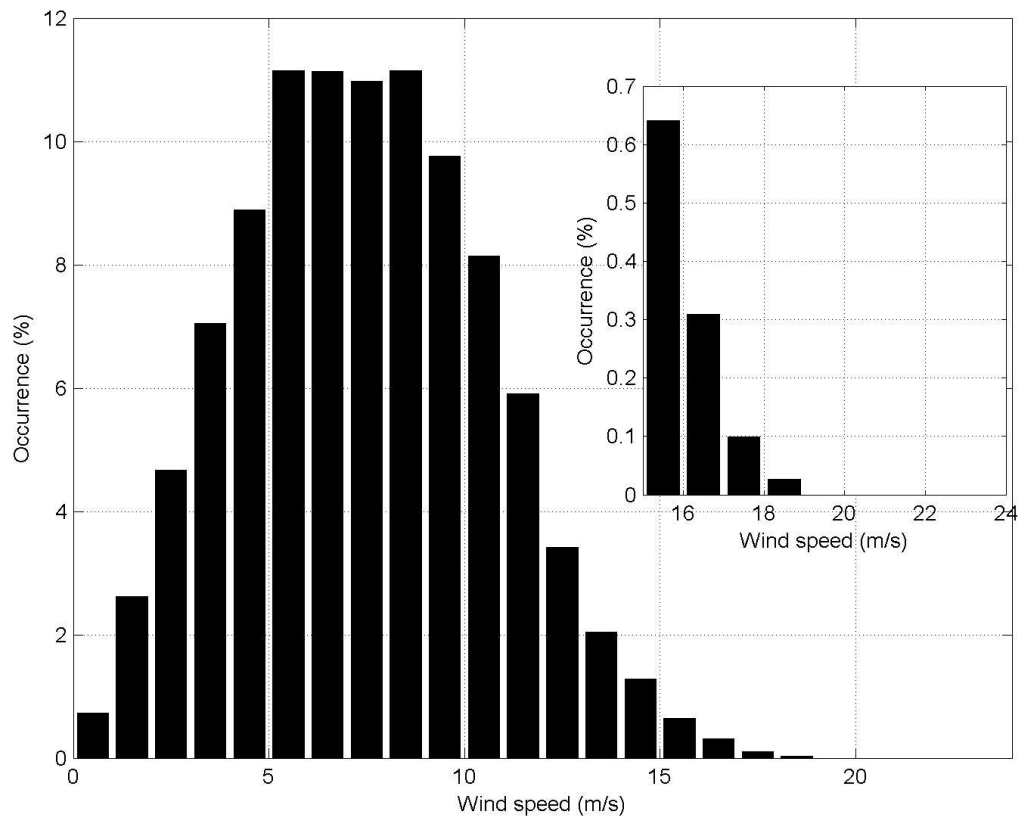


Fig. 3.1.1.17. Occurrence of wind speed in March based on ERA5 data

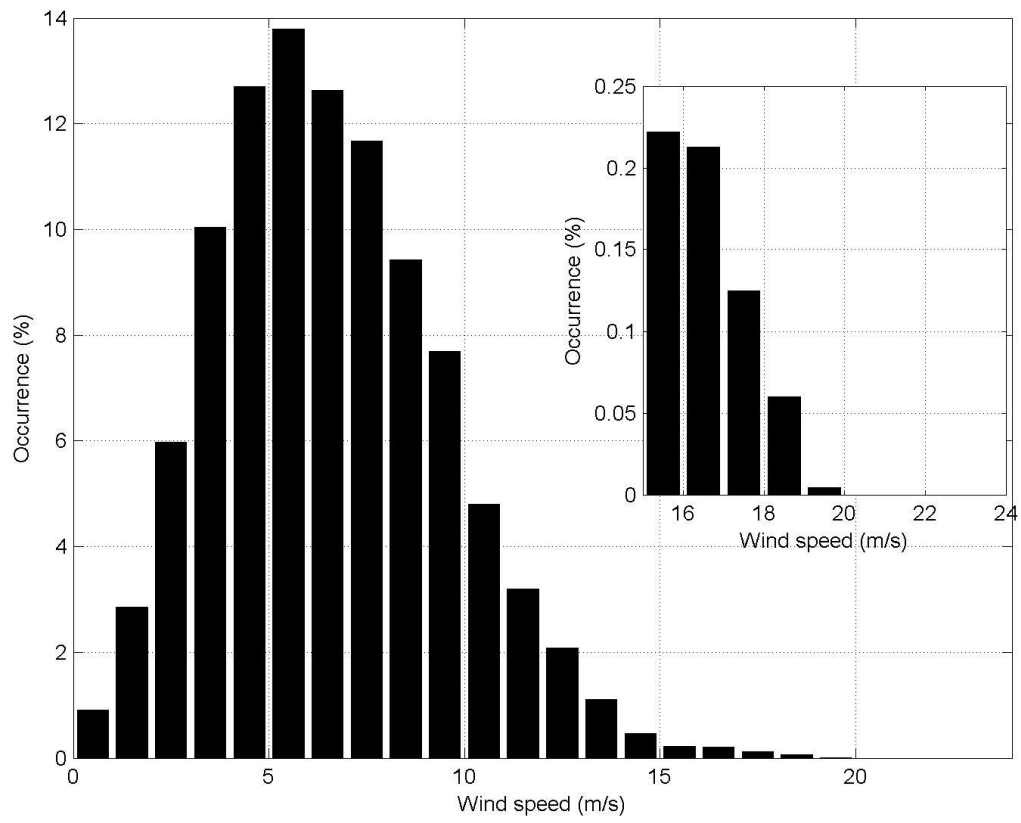


Fig. 3.1.1.18. Occurrence of wind speed in April based on ERA5 data

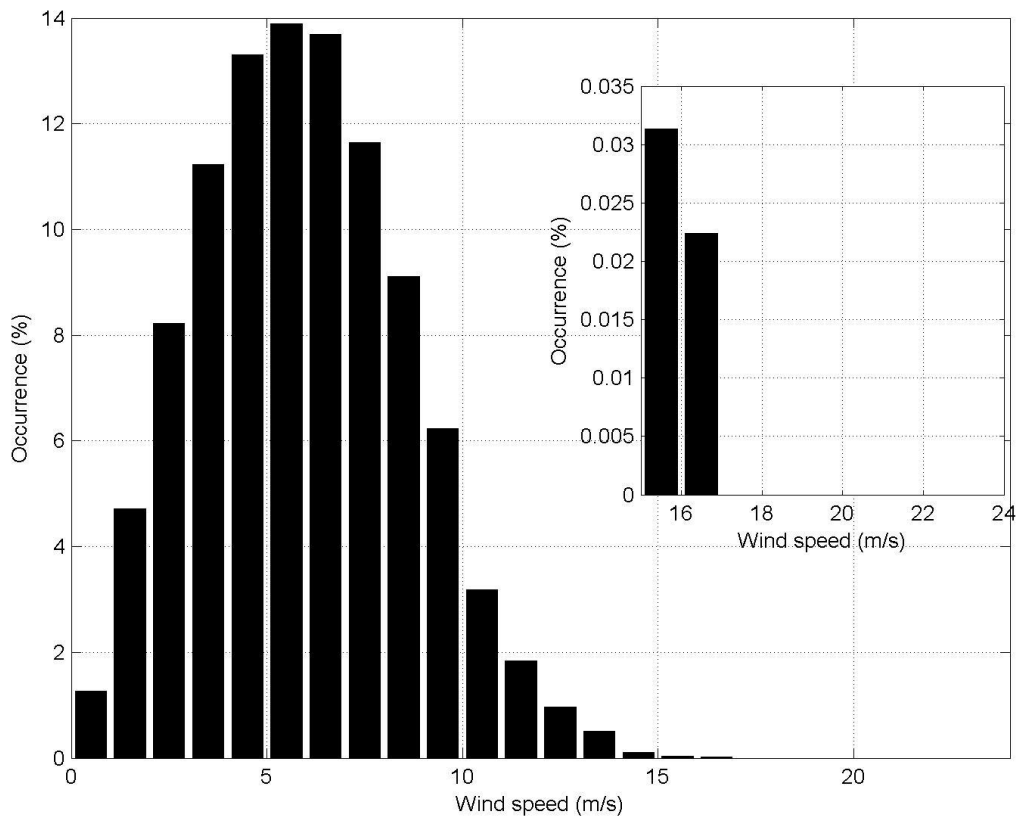


Fig. 3.1.1.19. Occurrence of wind speed in May based on ERA5 data

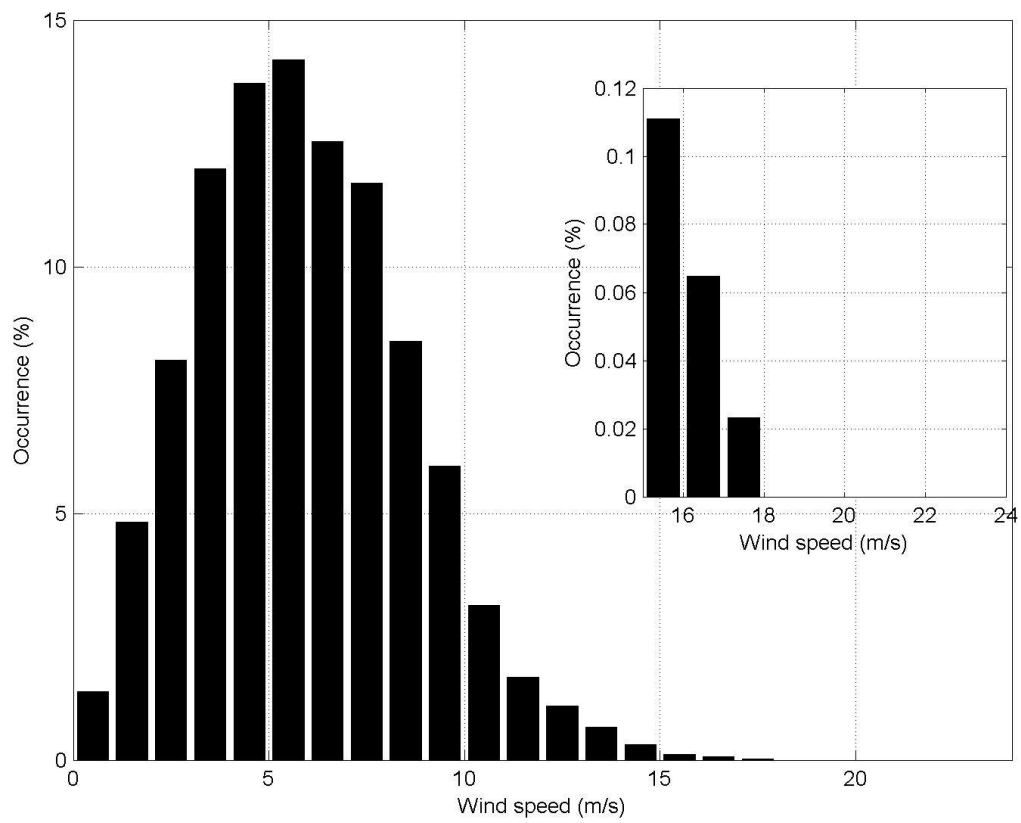


Fig. 3.1.1.20. Occurrence of wind speed in June based on ERA5 data

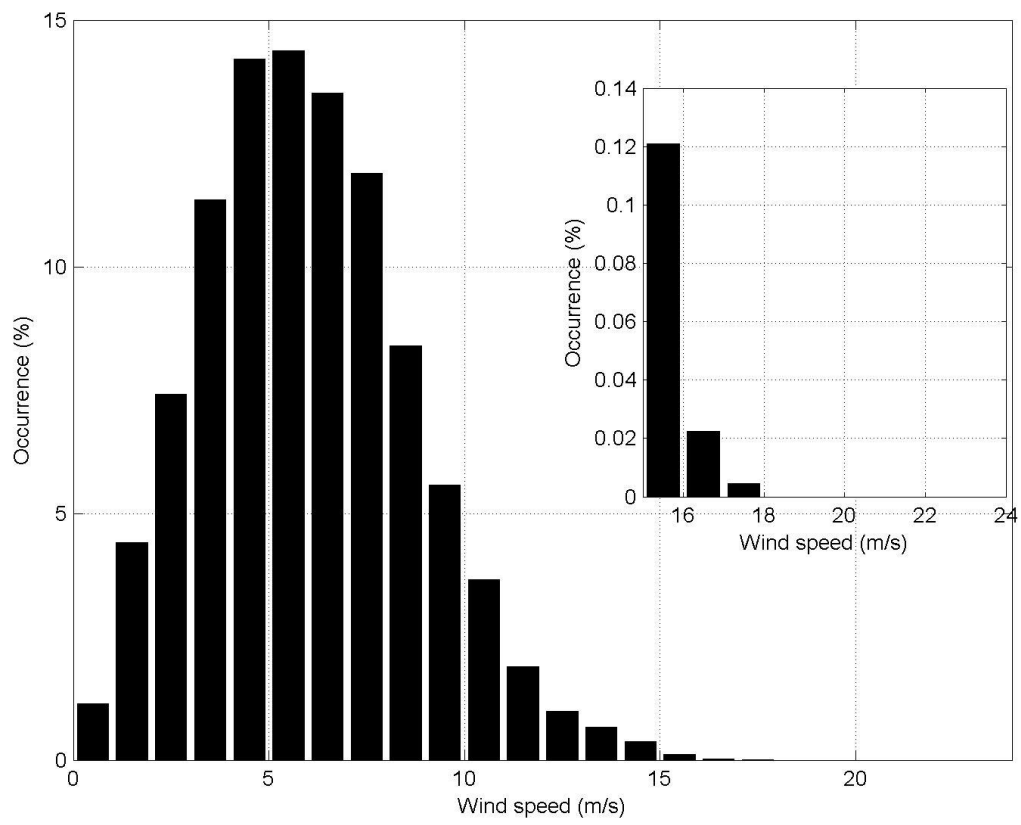


Fig. 3.1.1.21. Occurrence of wind speed in July based on ERA5 data

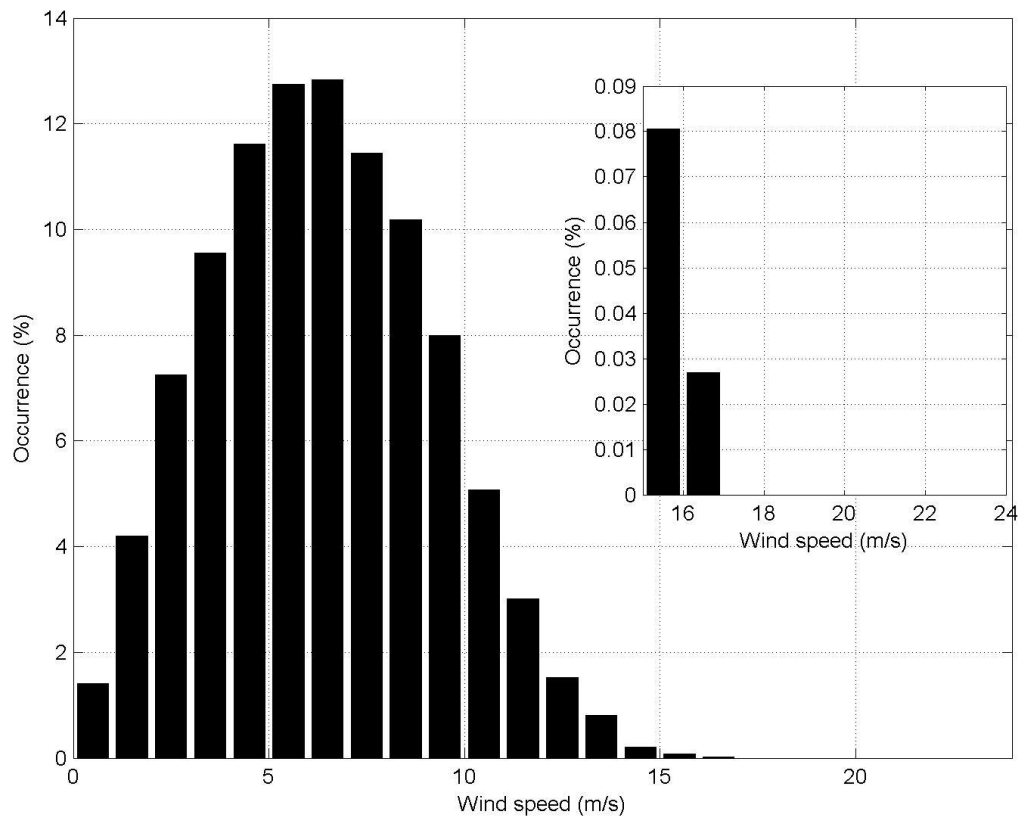


Fig. 3.1.1.22. Occurrence of wind speed in August based on ERA5 data

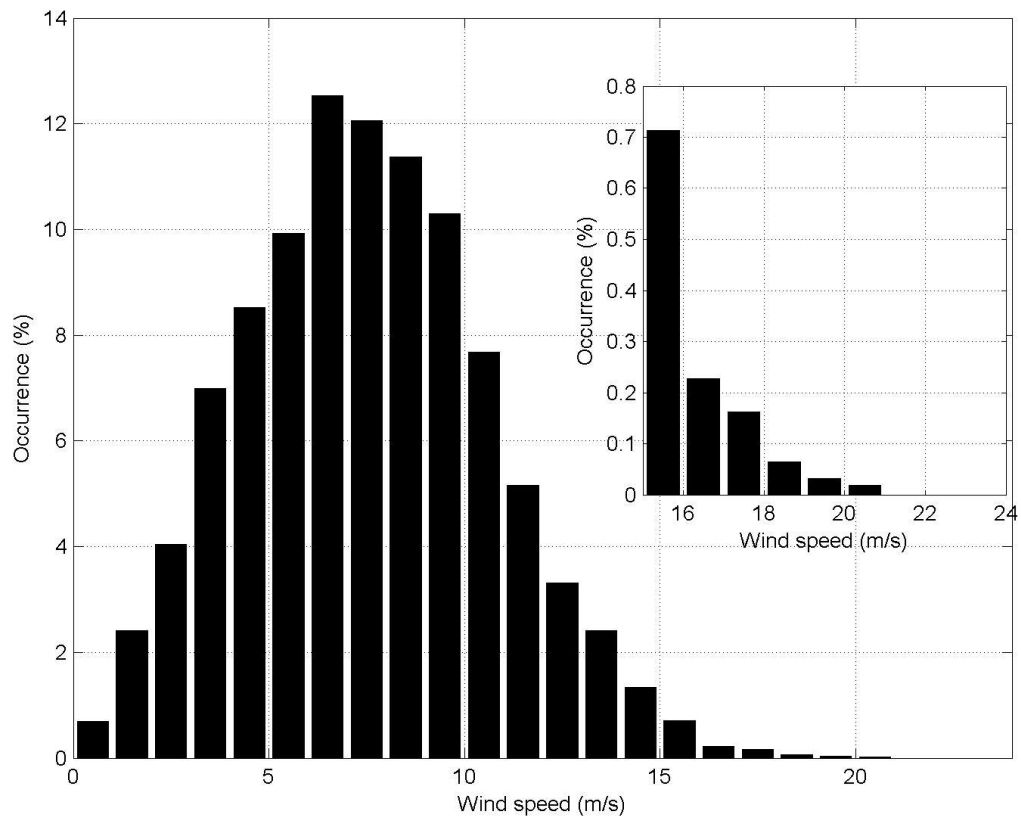


Fig. 3.1.1.23. Occurrence of wind speed in September based on ERA5 data

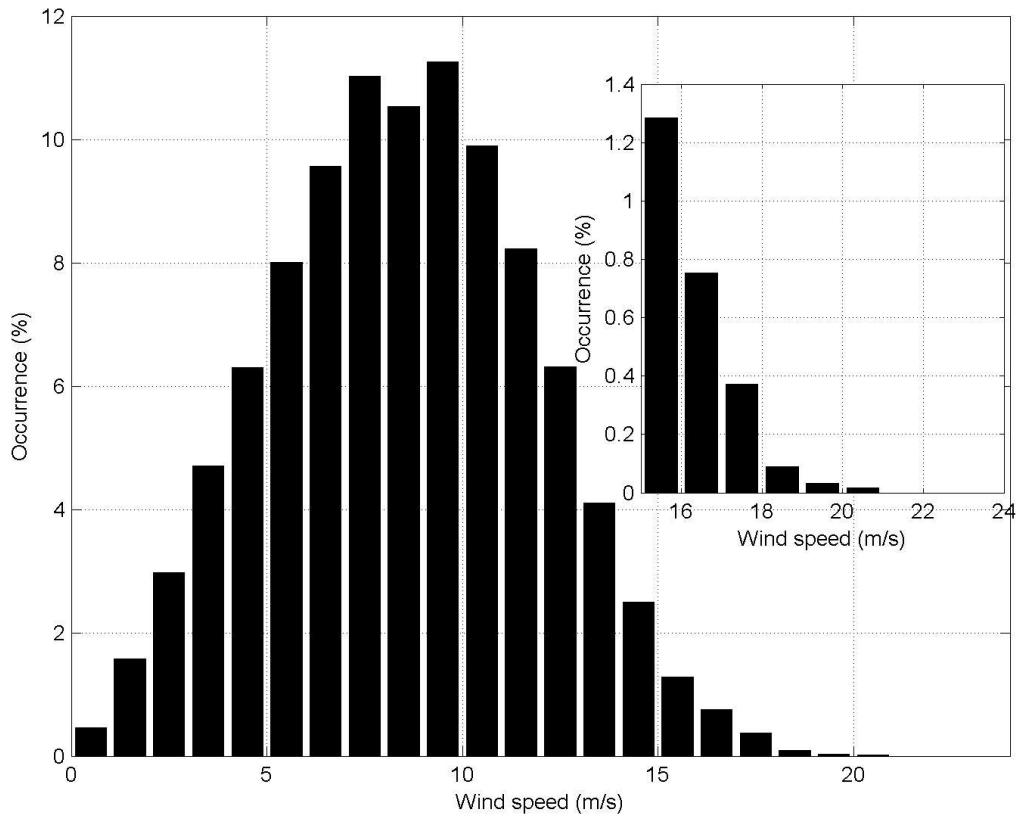


Fig. 3.1.1.24. Occurrence of wind speed in October based on ERA5 data

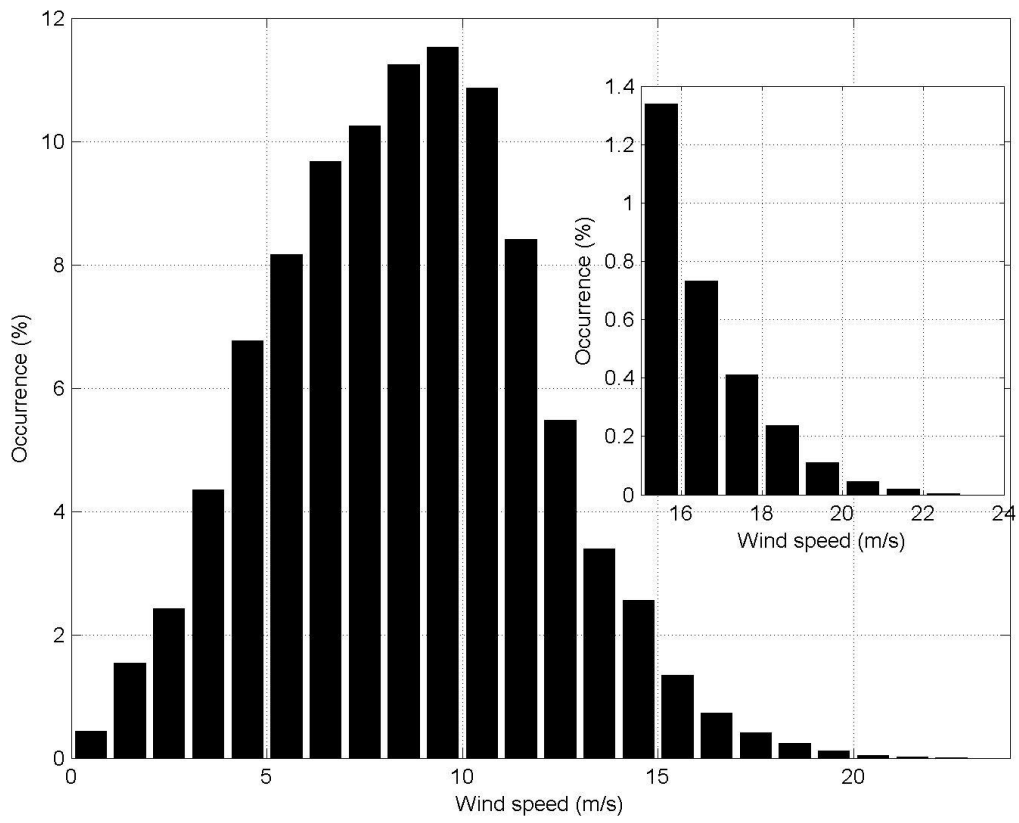


Fig. 3.1.1.25. Occurrence of wind speed in November based on ERA5 data

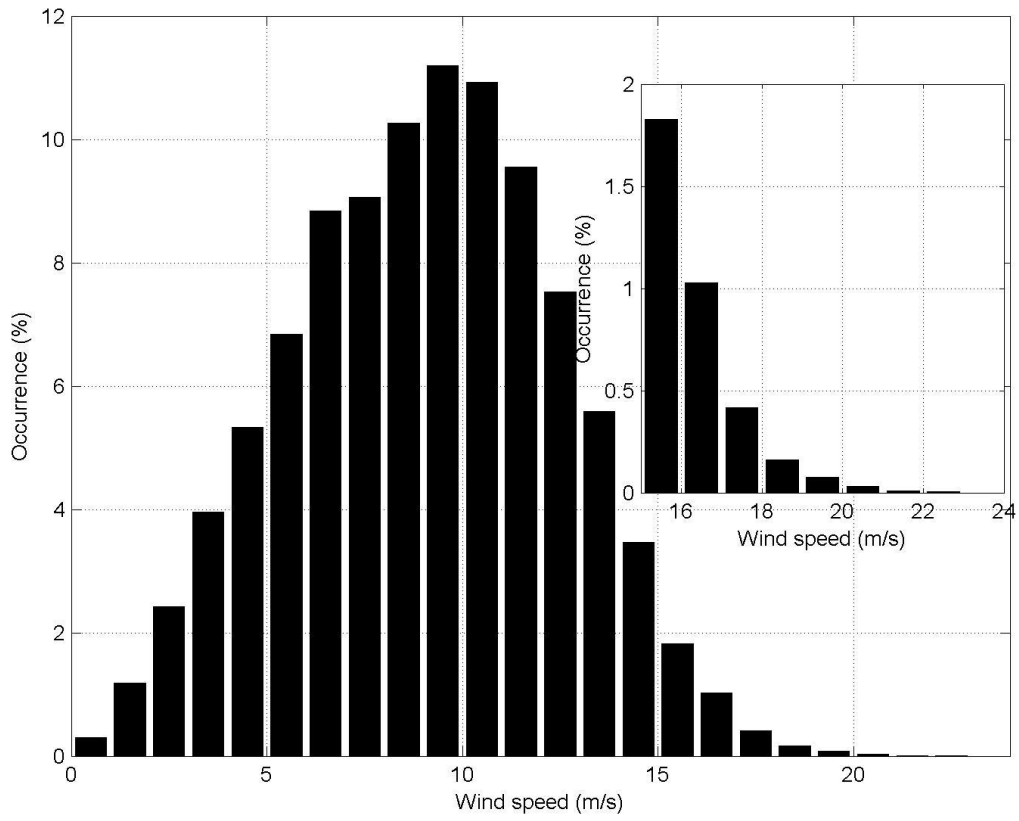


Fig. 3.1.1.26. Occurrence of wind speed in December based on ERA5 data

3.1.2. Extreme wind conditions

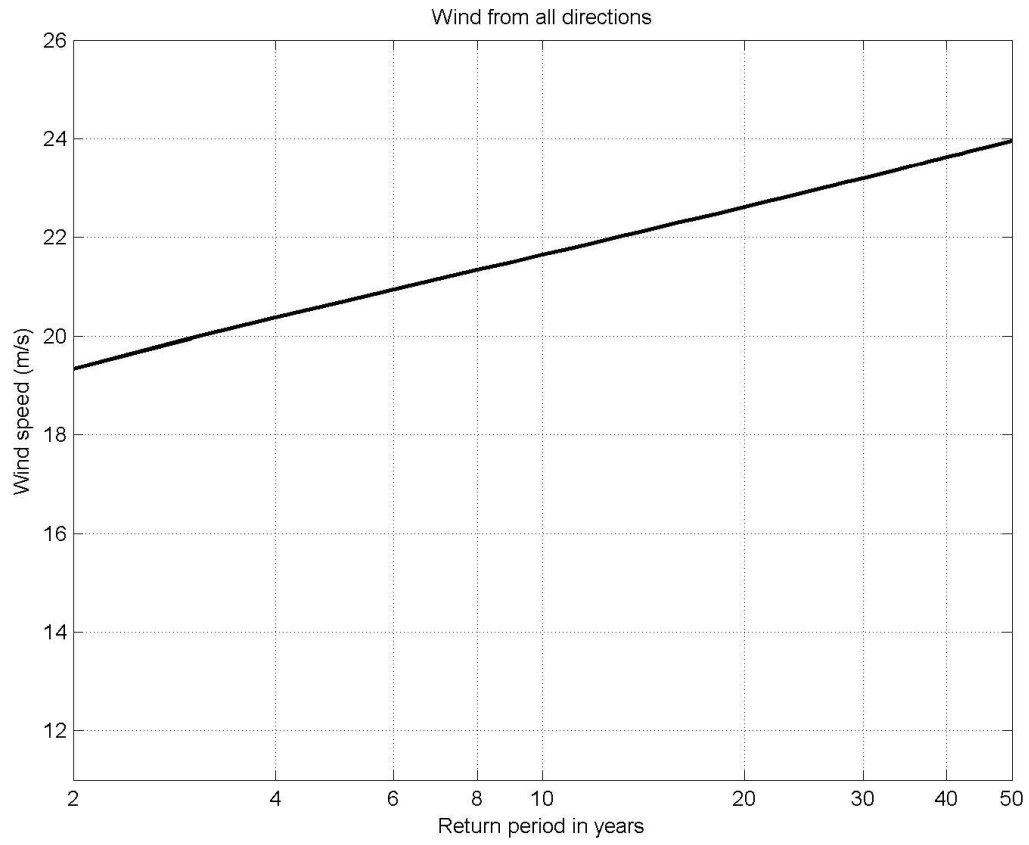


Fig. 3.1.2.1. Return periods of 1-h wind speed acquired from ERA5 data.

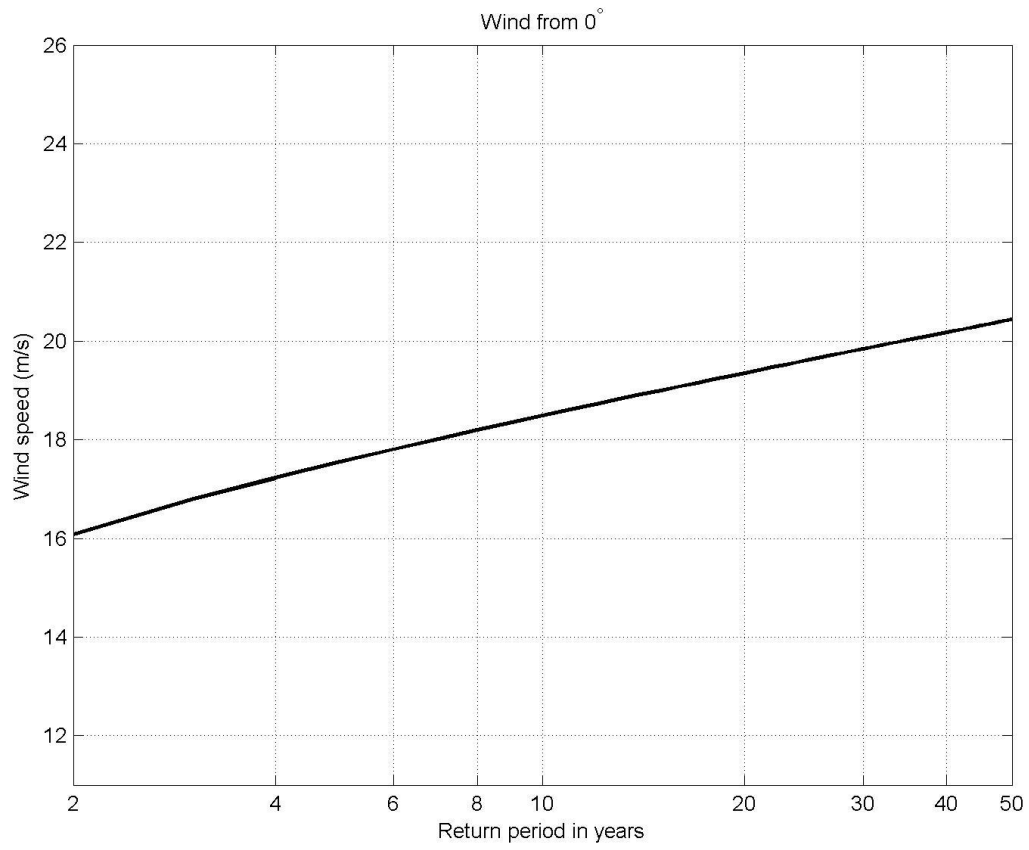


Fig. 3.1.2.2. Return periods of 1-h wind speed from 0° direction acquired from ERA5 data.

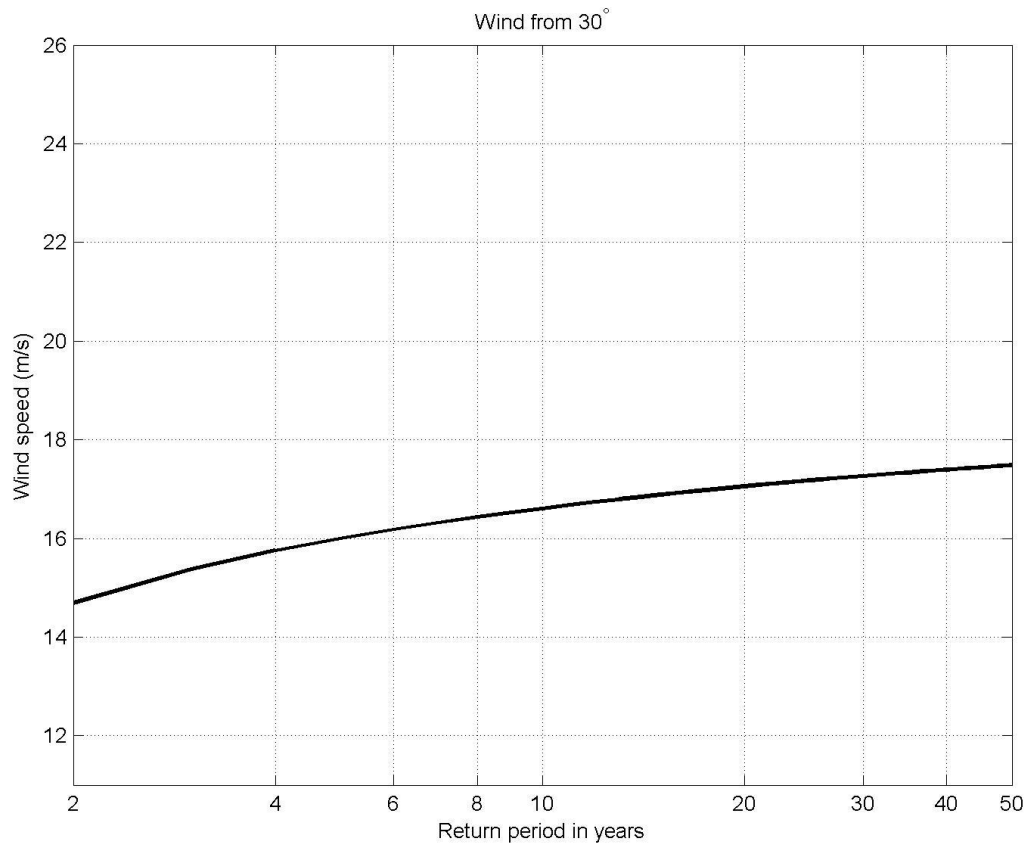


Fig. 3.1.2.3. Return periods of 1-h wind speed from 30° direction acquired from ERA5 data.

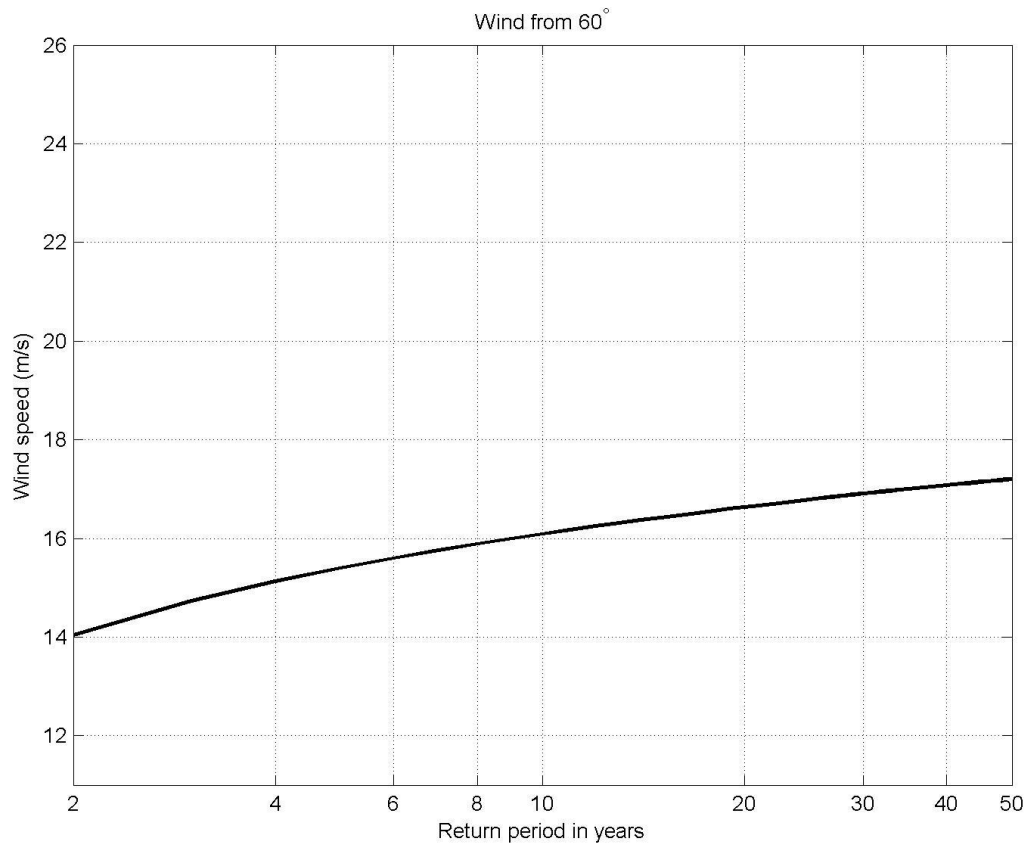


Fig. 3.1.2.4. Return periods of 1-h wind speed from 60° direction acquired from ERA5 data.

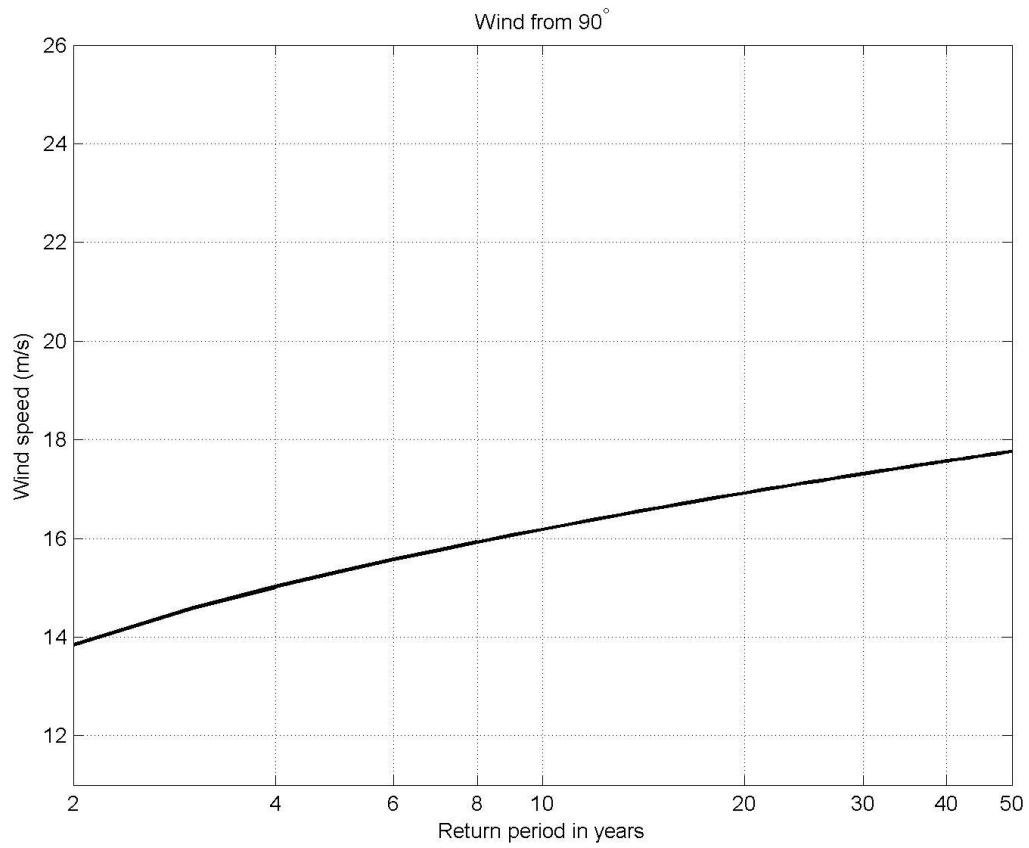


Fig. 3.1.2.5. Return periods of 1-h wind speed from 90° direction acquired from ERA5 data.

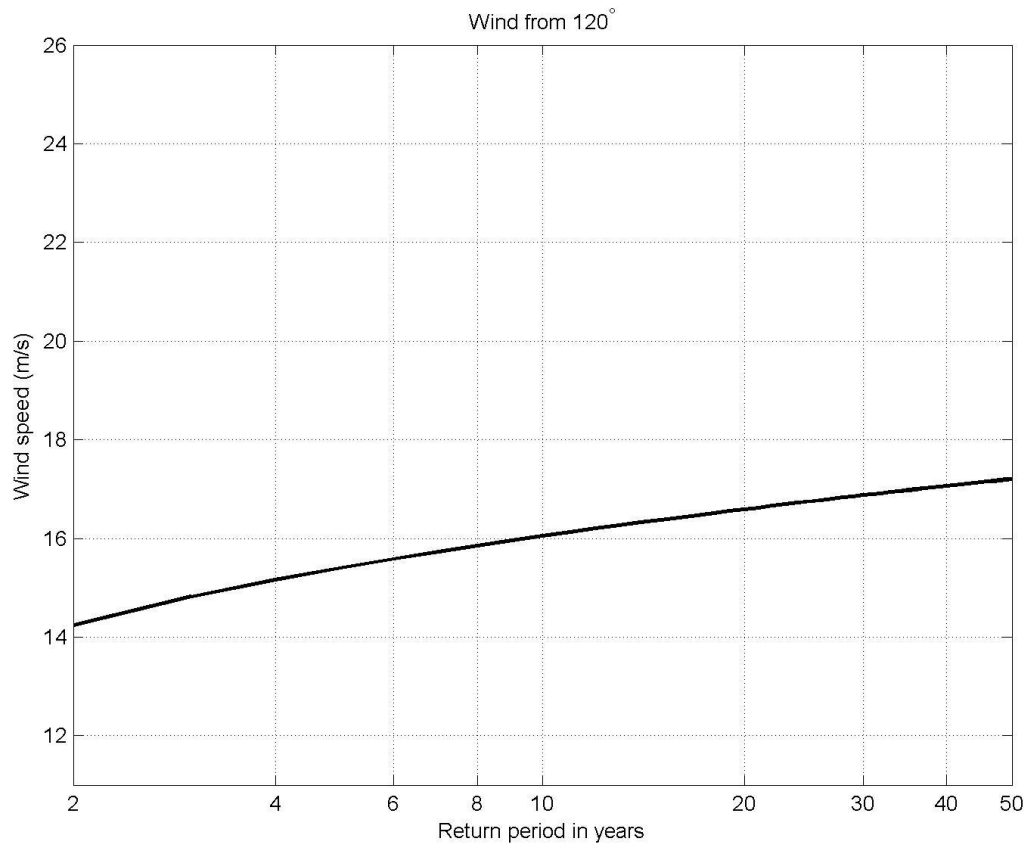


Fig. 3.1.2.6. Return periods of 1-h wind speed from 120° direction acquired from ERA5 data.

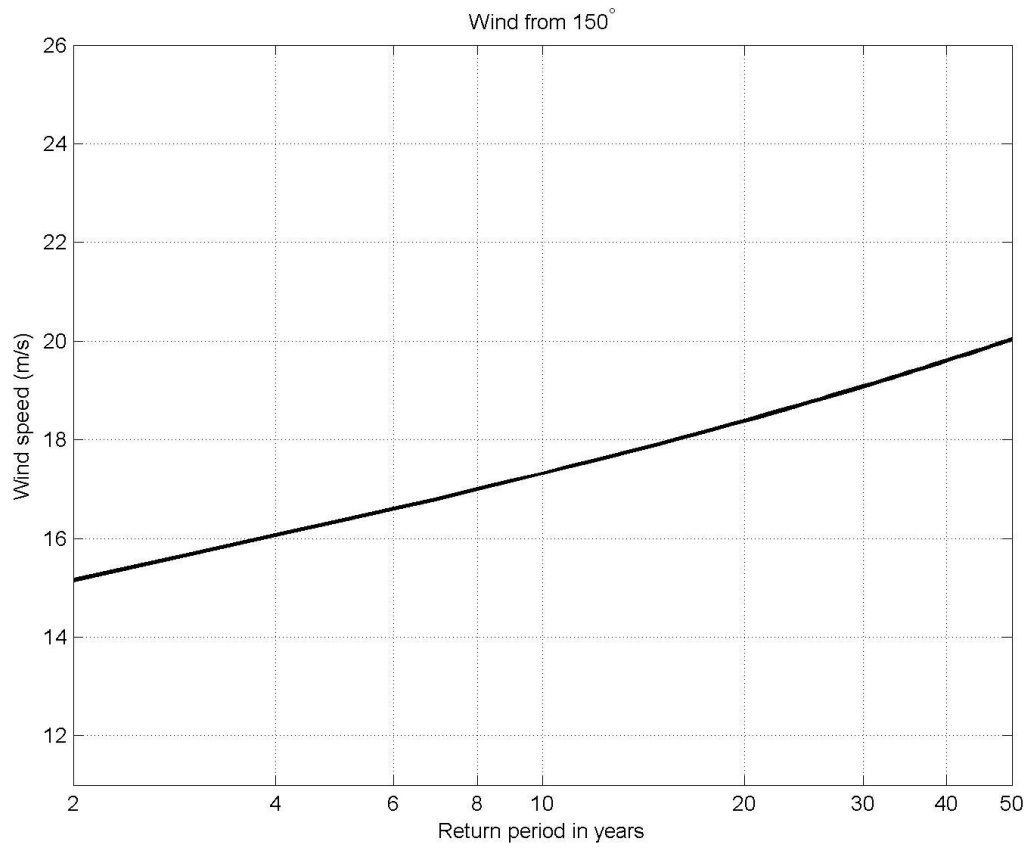


Fig. 3.1.2.7. Return periods of 1-h wind speed from 150° direction acquired from ERA5 data.

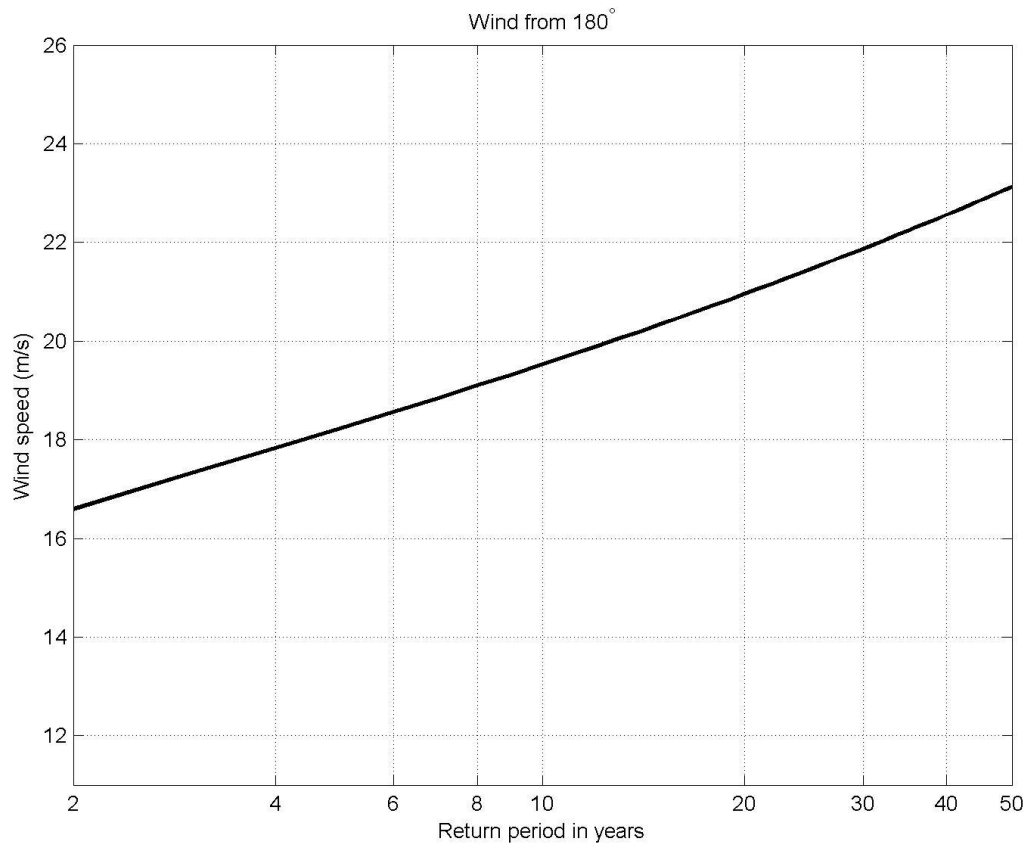


Fig. 3.1.2.8. Return periods of 1-h wind speed from 180° direction acquired from ERA5 data.

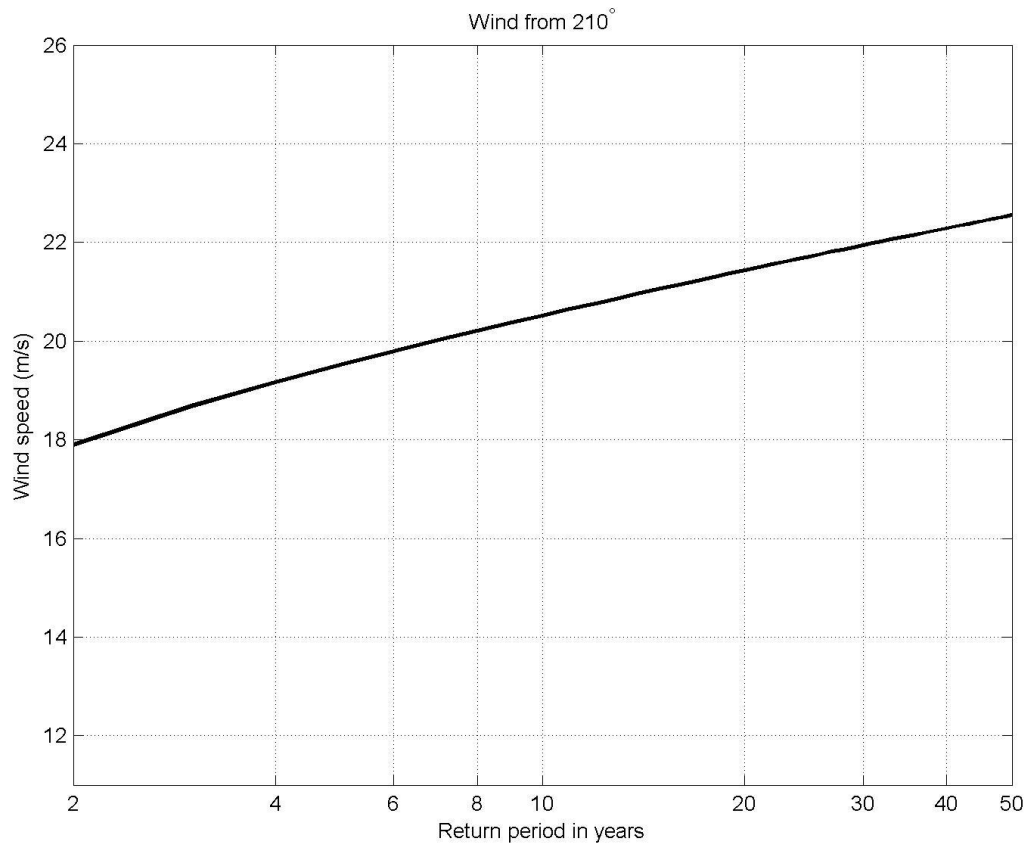


Fig. 3.1.2.9. Return periods of 1-h wind speed from 210° direction acquired from ERA5 data.

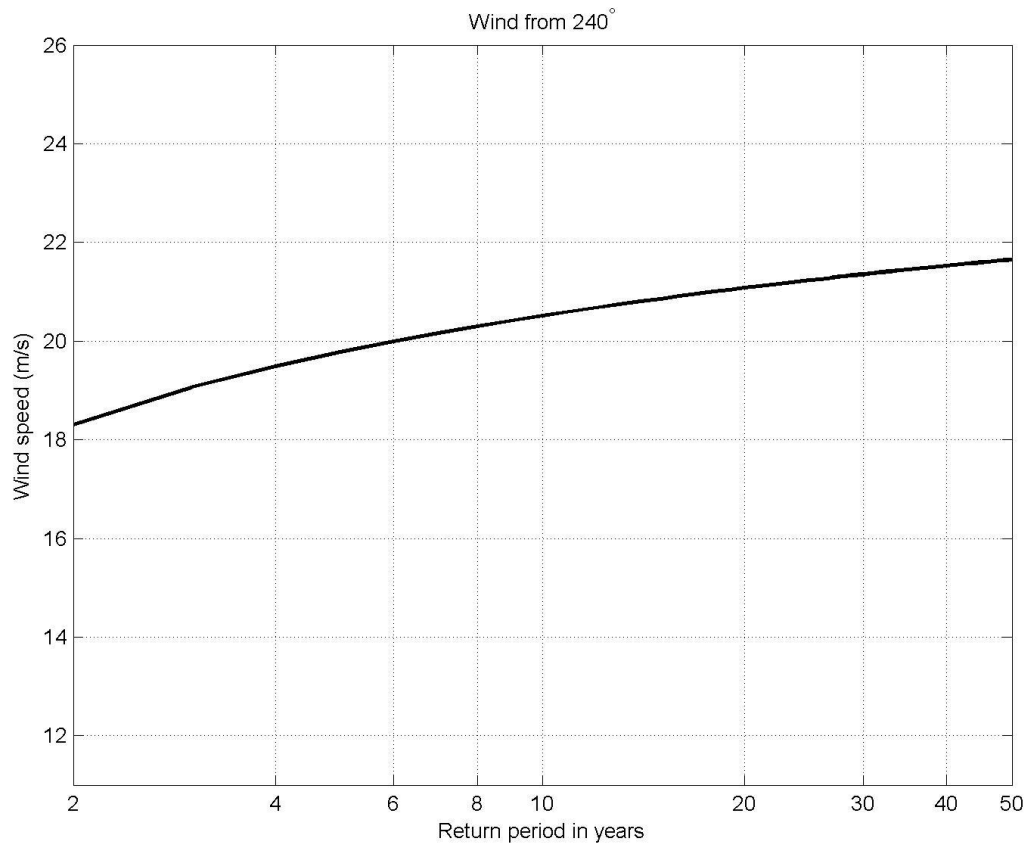


Fig. 3.1.2.10. Return periods of 1-h wind speed from 240° direction acquired from ERA5 data.

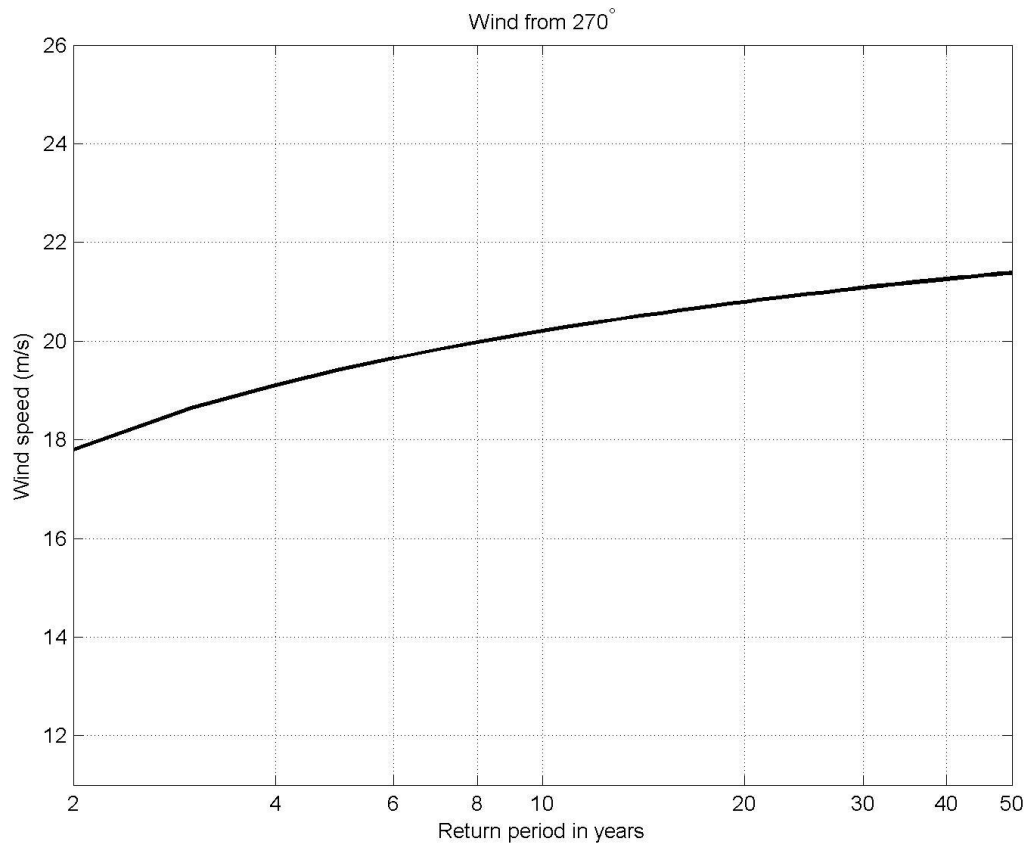


Fig. 3.1.2.11. Return periods of 1-h wind speed from 270° direction acquired from ERA5 data.

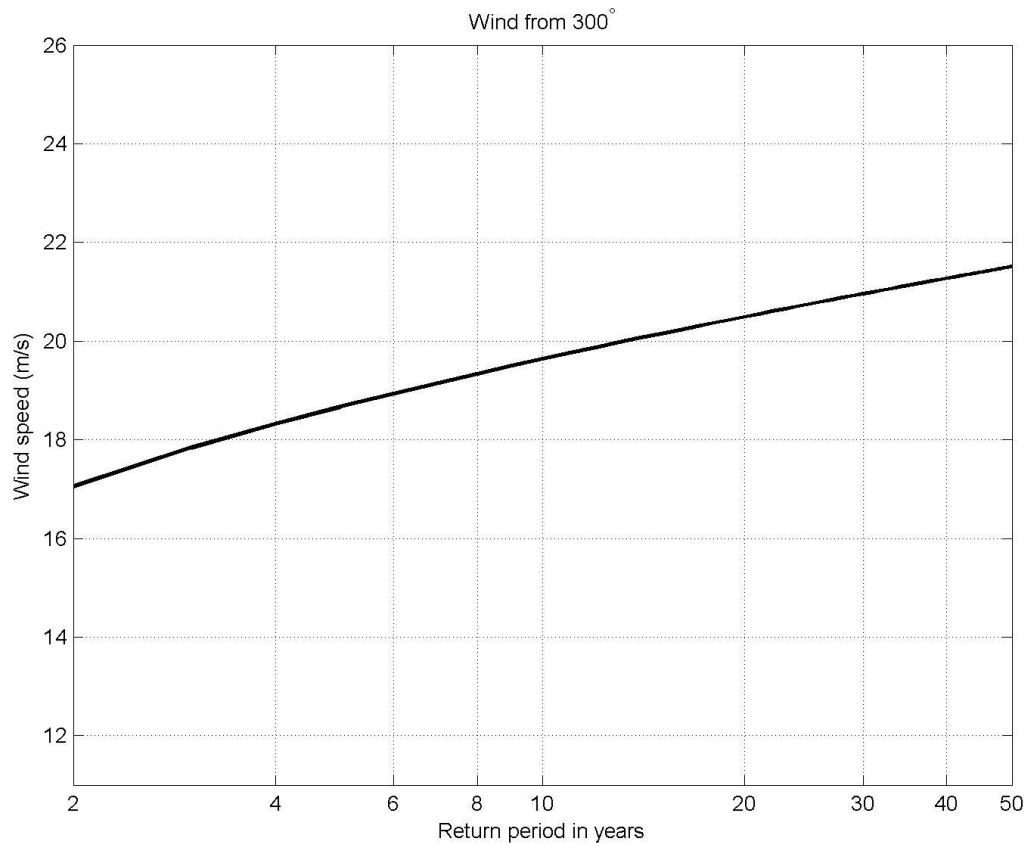


Fig. 3.1.2.12. Return periods of 1-h wind speed from 300° direction acquired from ERA5 data.

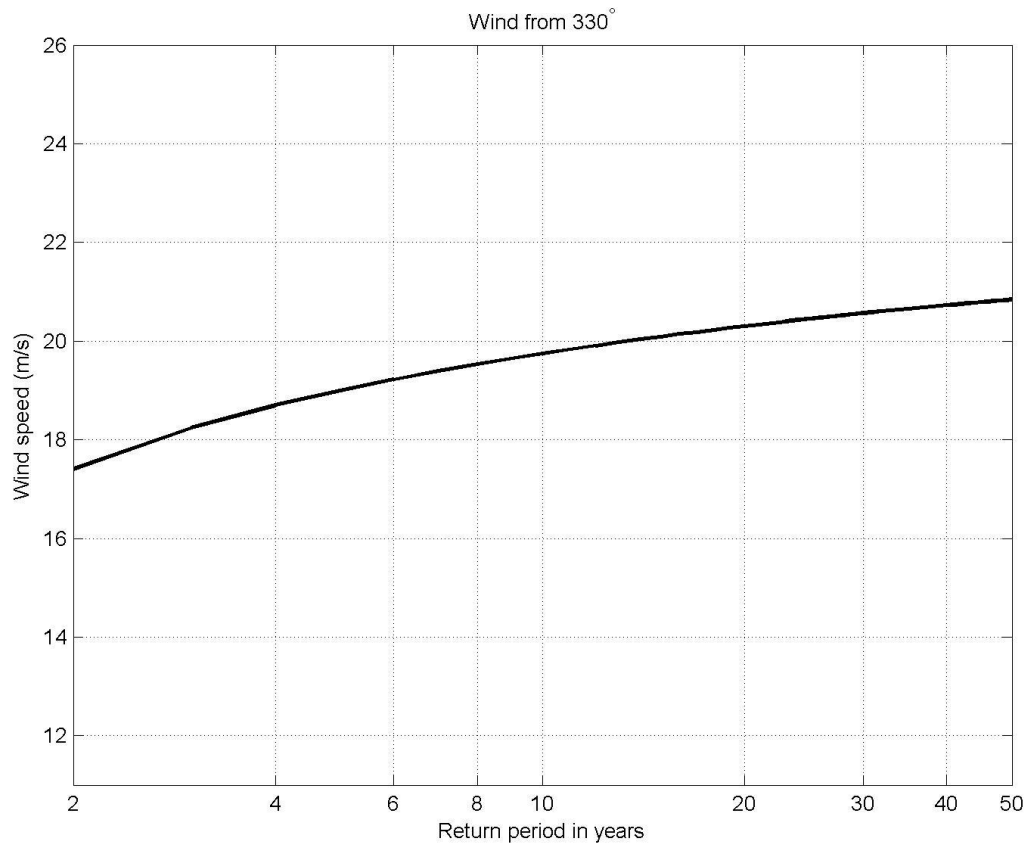


Fig. 3.1.2.13. Return periods of 1-h wind speed from 330° direction acquired from ERA5 data.

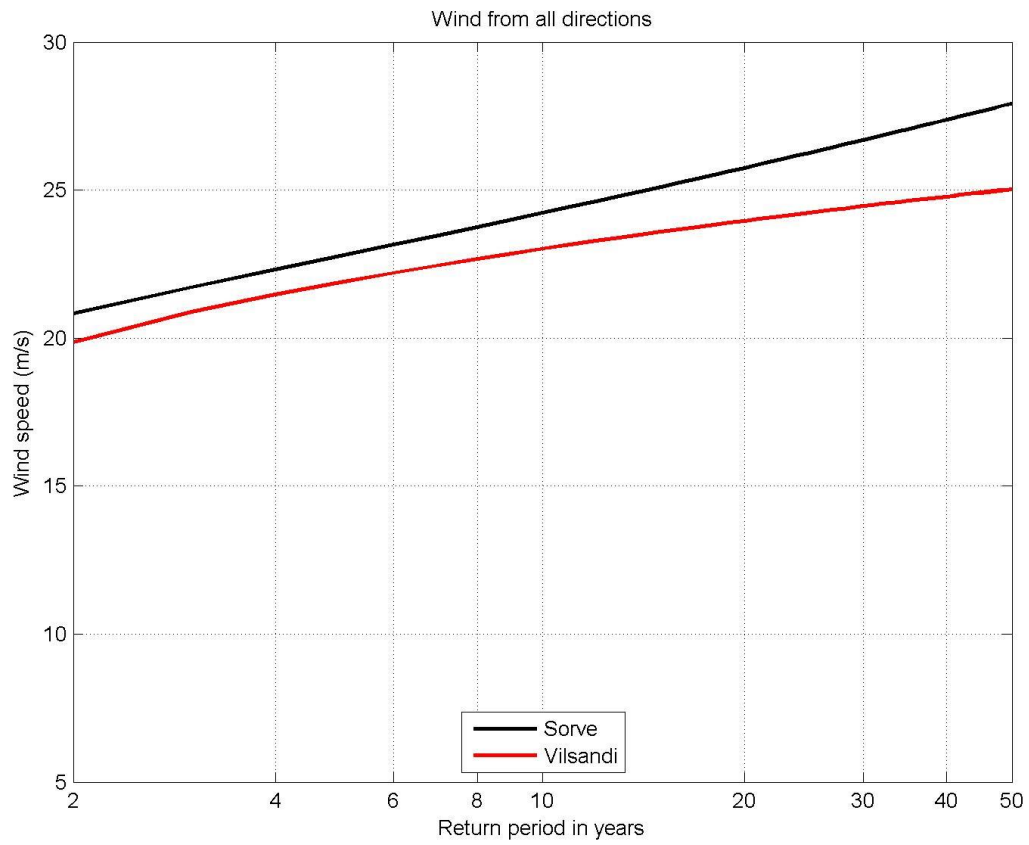


Fig. 3.1.2.14. Return periods of 10-minute wind speed at Vilsandi and Sörve meteorological stations.

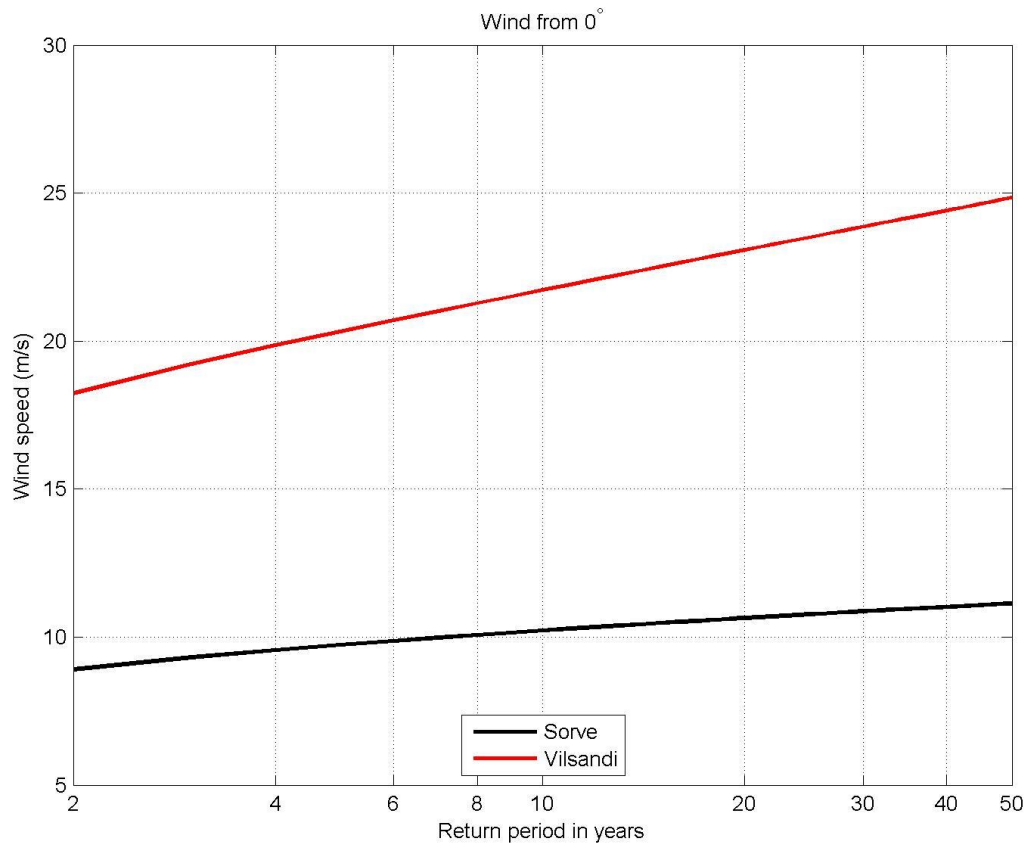


Fig. 3.1.2.15. Return periods of 10-minute wind speed from 0° direction at Vilsandi and Sörve meteorological stations.

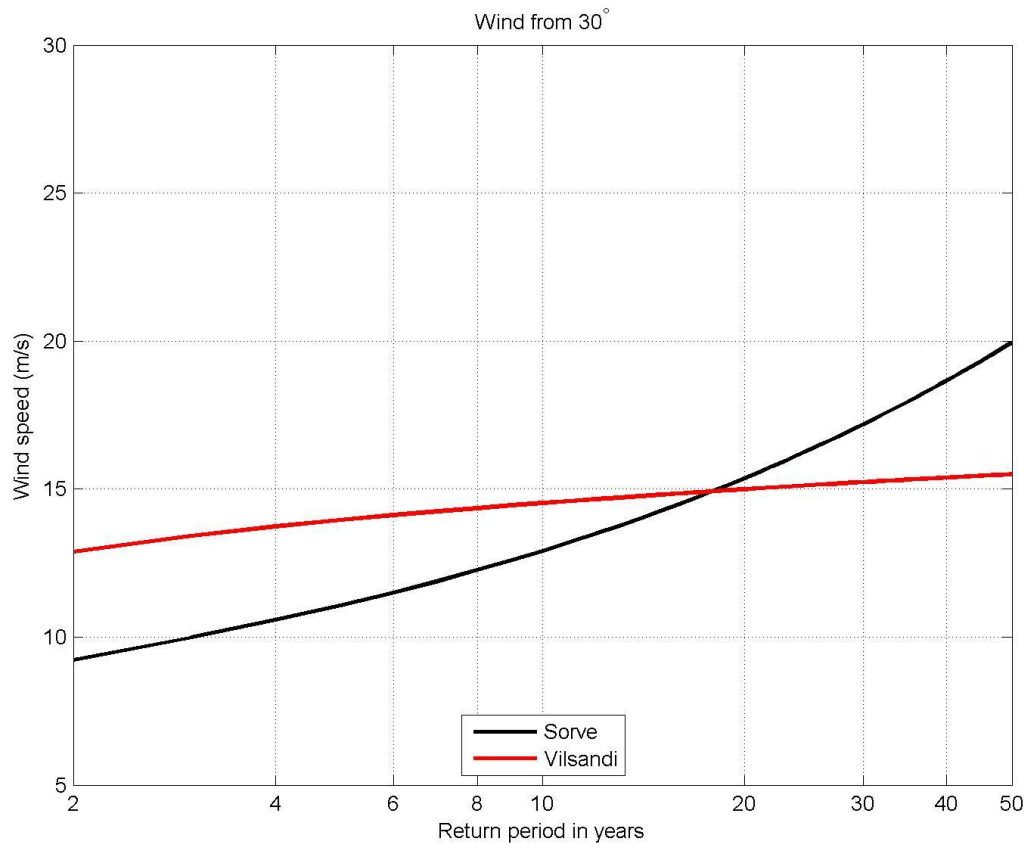


Fig. 3.1.2.16. Return periods of 10-minute wind speed from 30° direction at Vilsandi and Sørve meteorological stations.

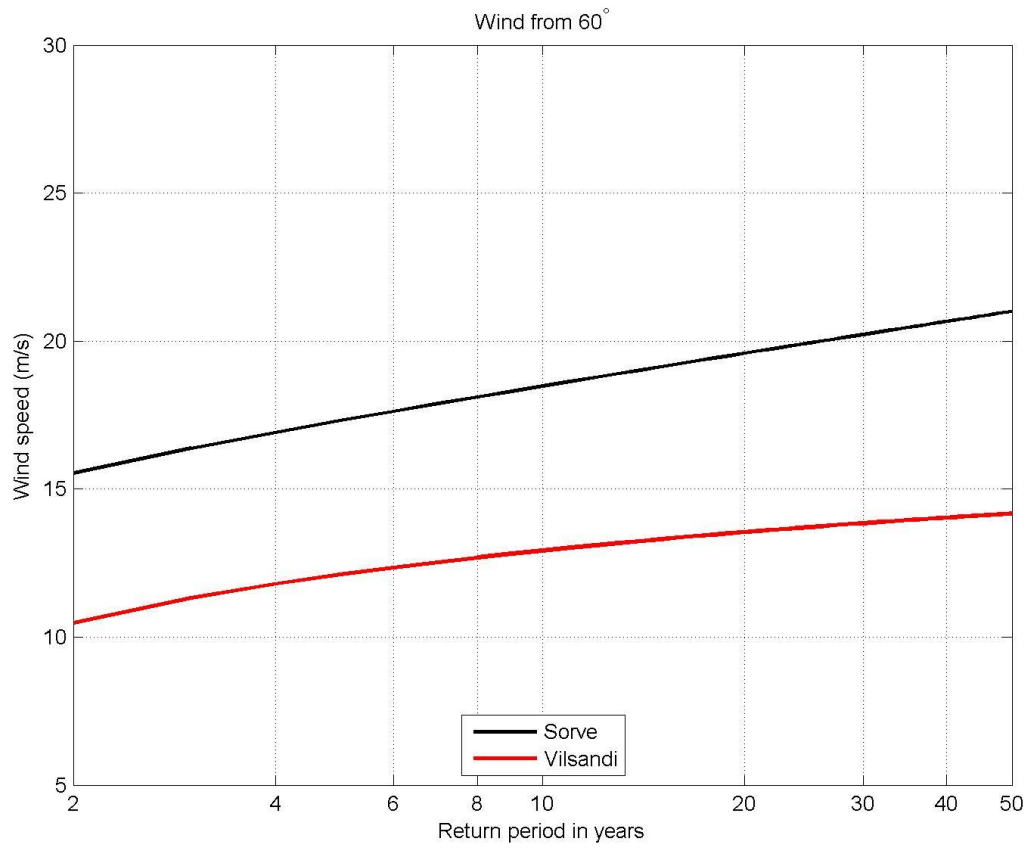


Fig. 3.1.2.17. Return periods of 10-minute wind speed from 60° direction at Vilsandi and Sørve meteorological stations.

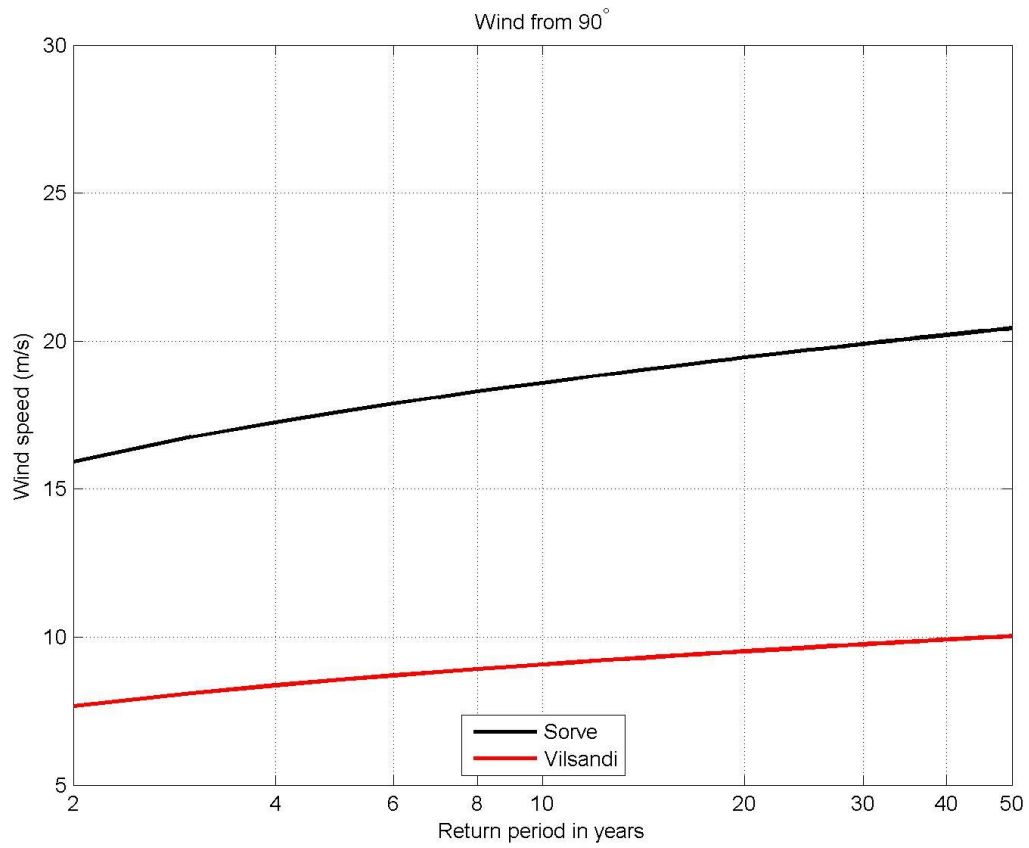


Fig. 3.1.2.18. Return periods of 10-minute wind speed from 90° direction at Vilsandi and Sørve meteorological stations.

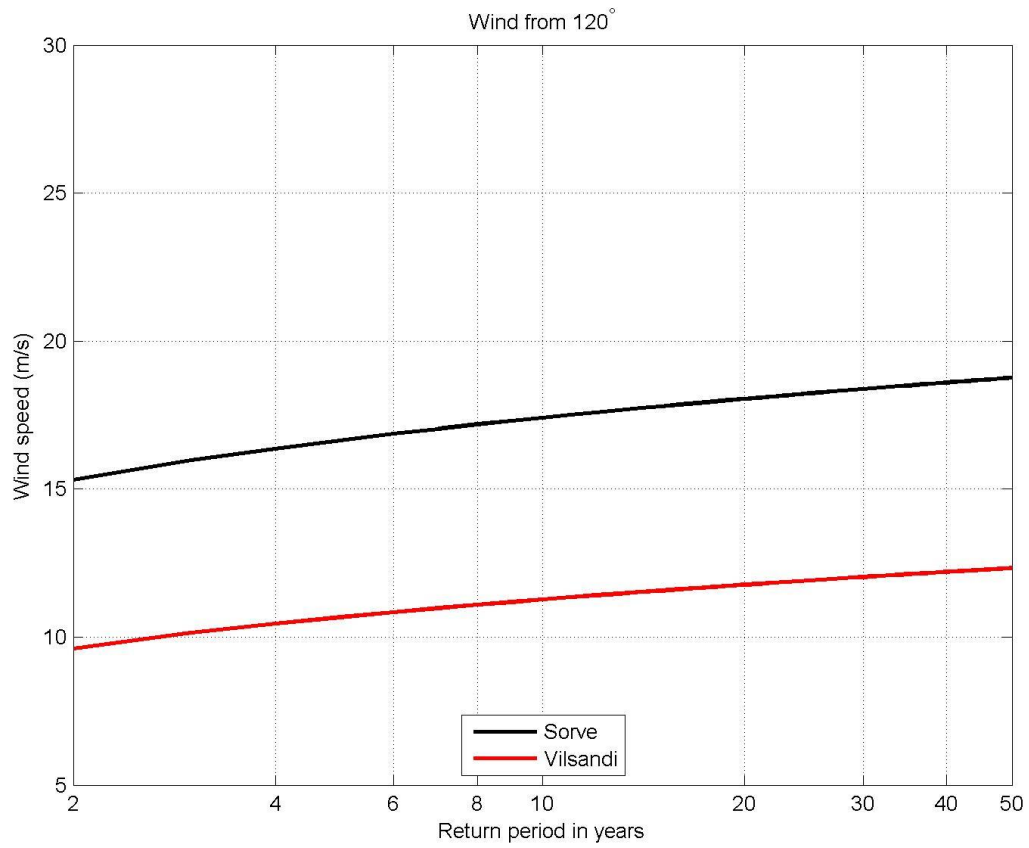


Fig. 3.1.2.19. Return periods of 10-minute wind speed from 120° direction at Vilsandi and Sørve meteorological stations.

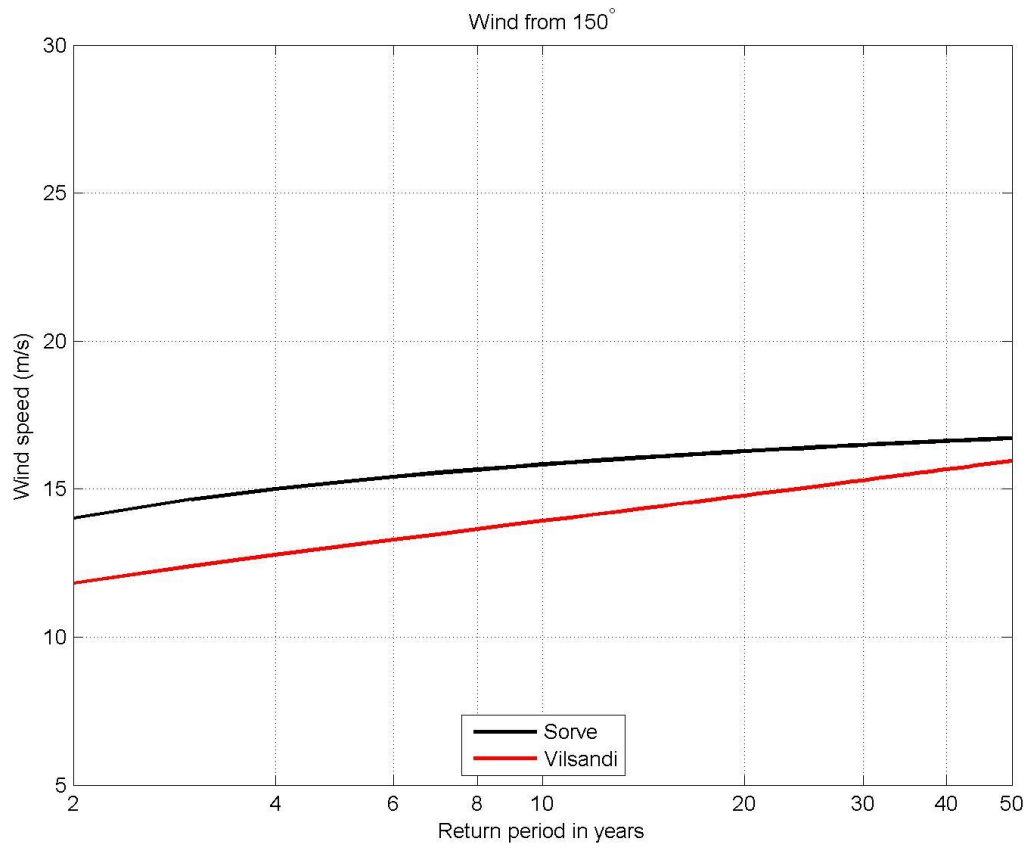


Fig. 3.1.2.20. Return periods of 10-minute wind speed from 150° direction at Vilsandi and Sørve meteorological stations.

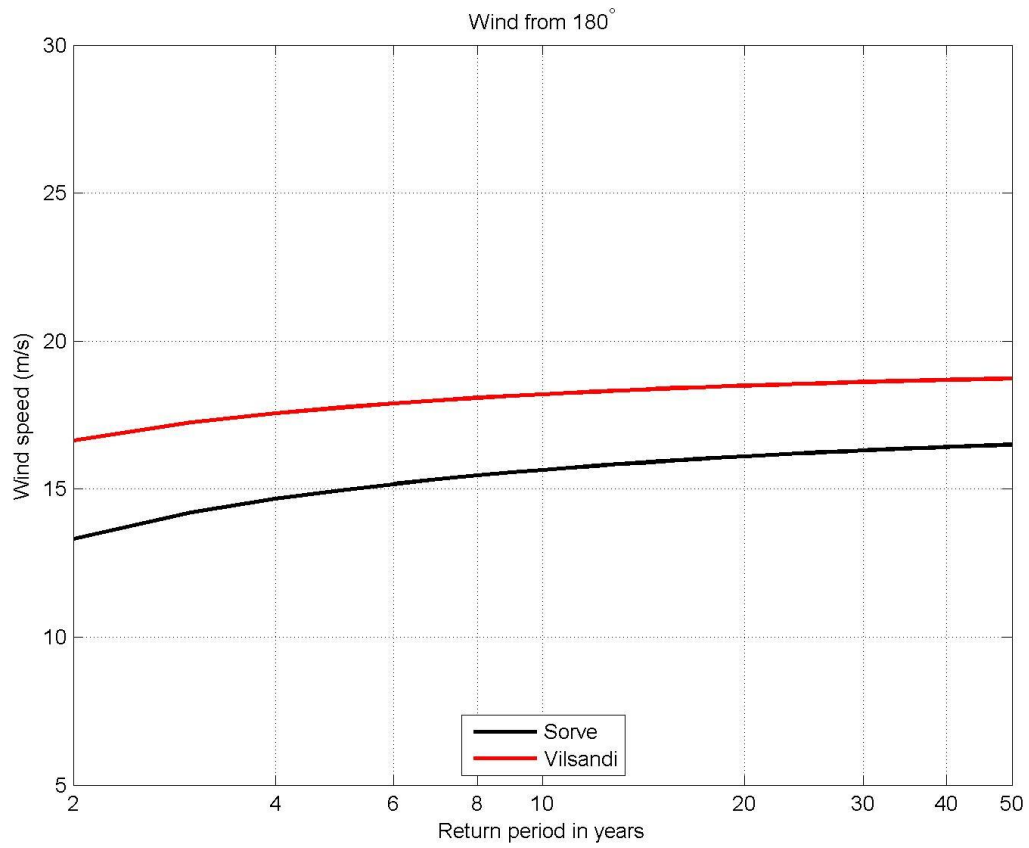


Fig. 3.1.2.21. Return periods of 10-minute wind speed from 180° direction at Vilsandi and Sørve meteorological stations.

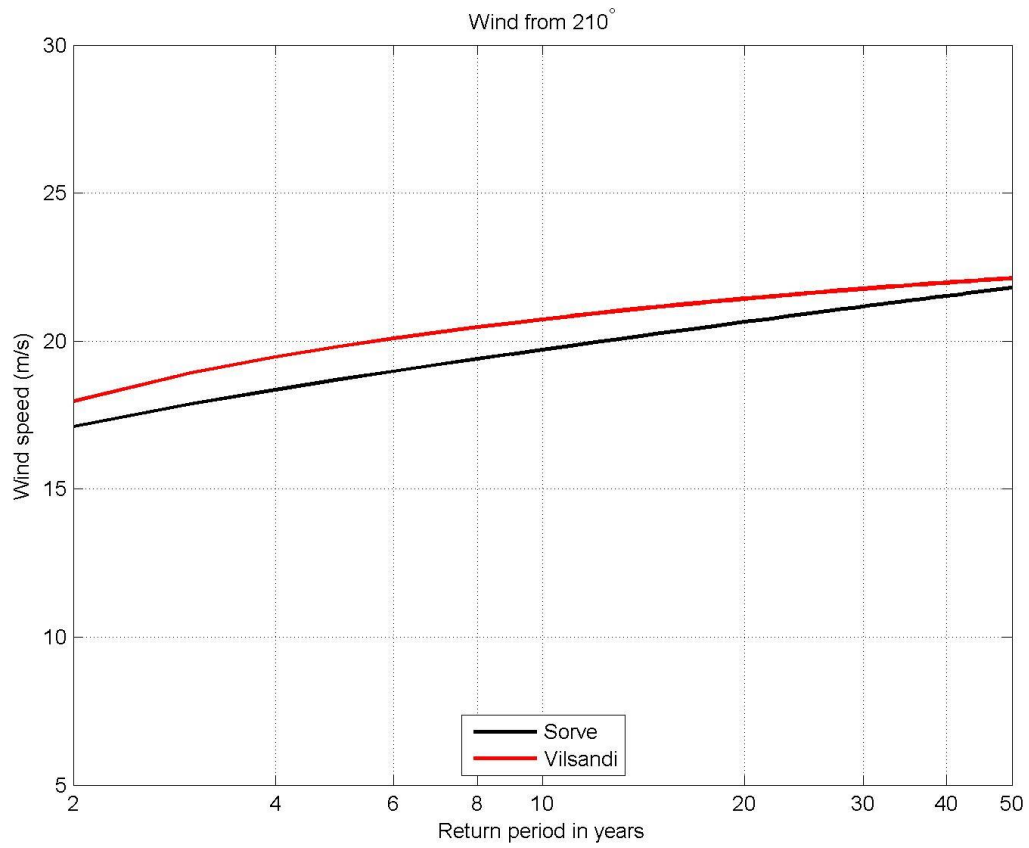


Fig. 3.1.2.22. Return periods of 10-minute wind speed from 210° direction at Vilsandi and Sørve meteorological stations.

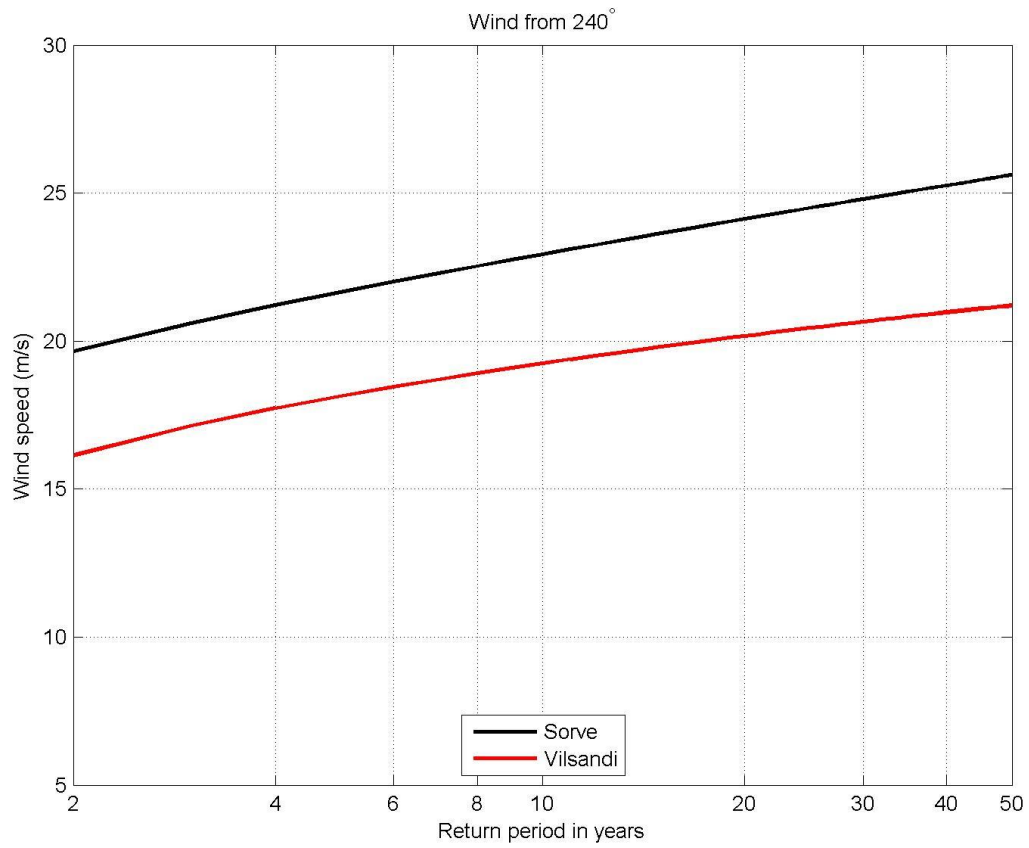


Fig. 3.1.2.23. Return periods of 10-minute wind speed from 240° direction at Vilsandi and Sørve meteorological stations.

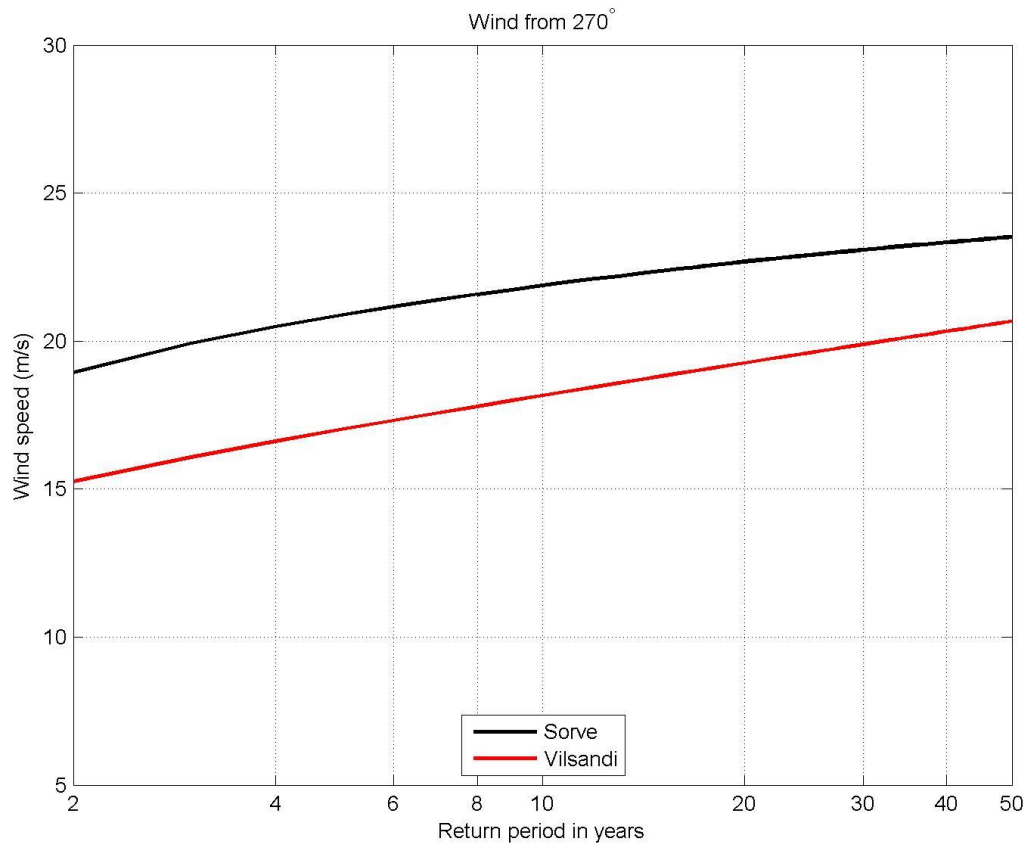


Fig. 3.1.2.24. Return periods of 10-minute wind speed from 270° direction at Vilsandi and Sørve meteorological stations.

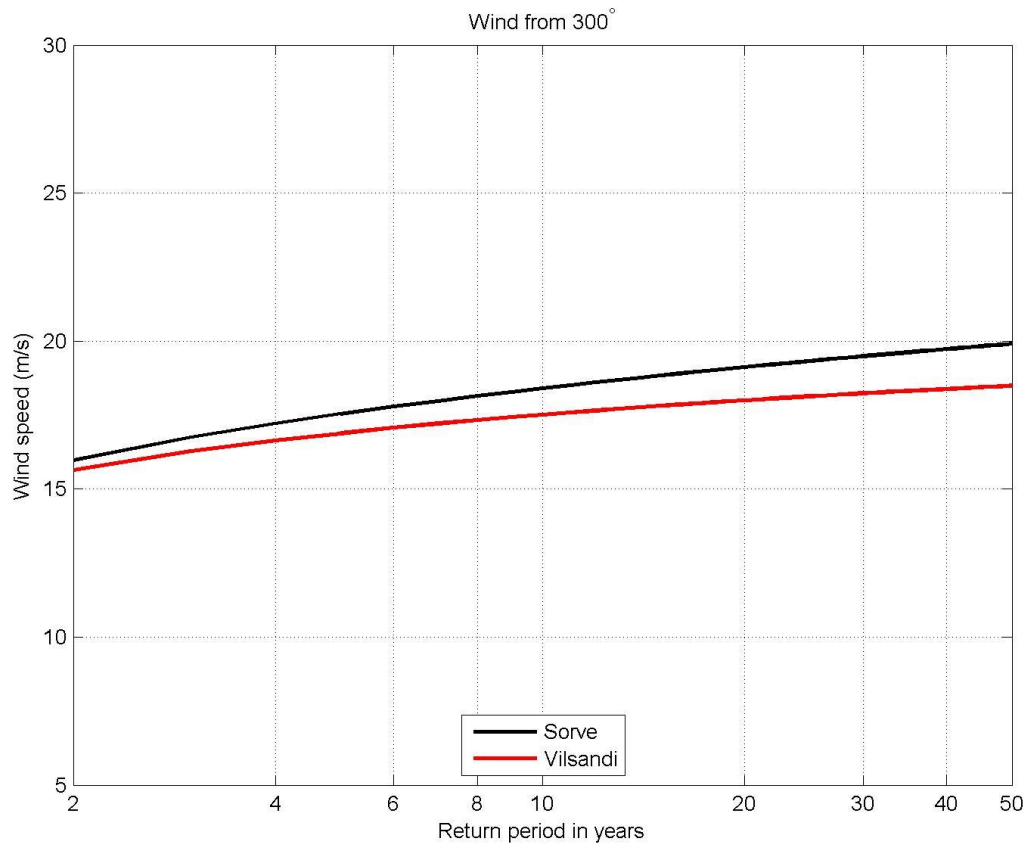


Fig. 3.1.2.25. Return periods of 10-minute wind speed from 300° direction at Vilsandi and Sørve meteorological stations.

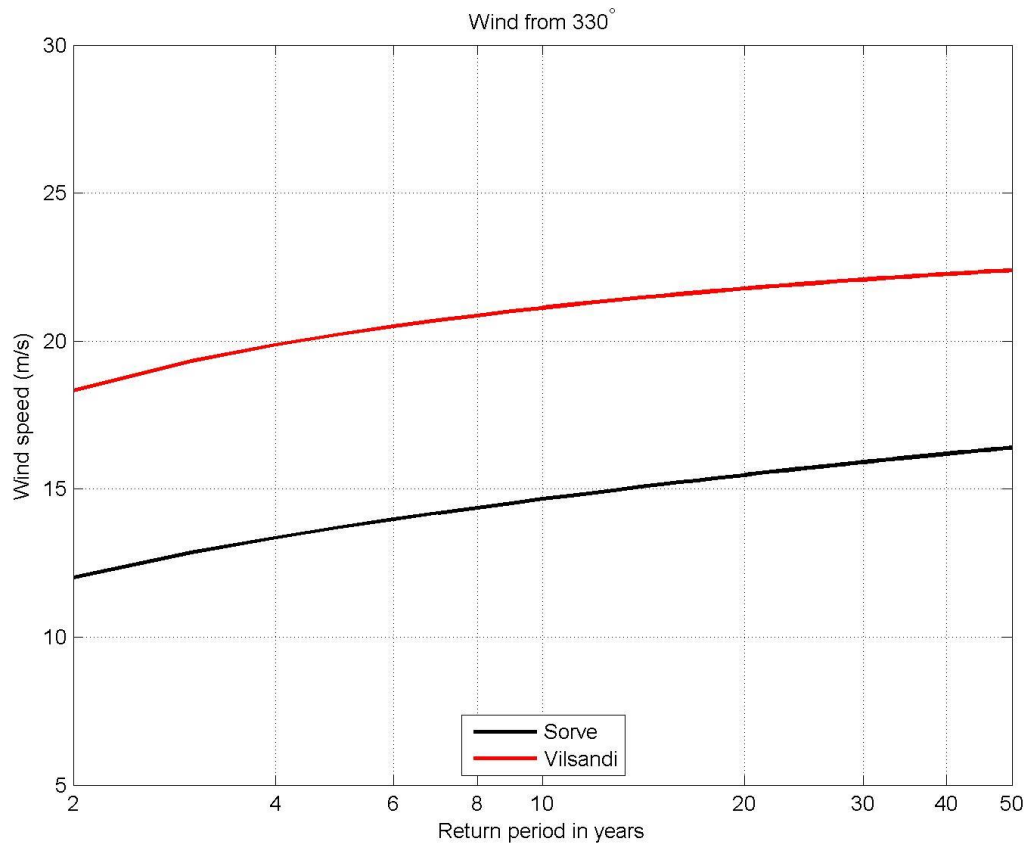
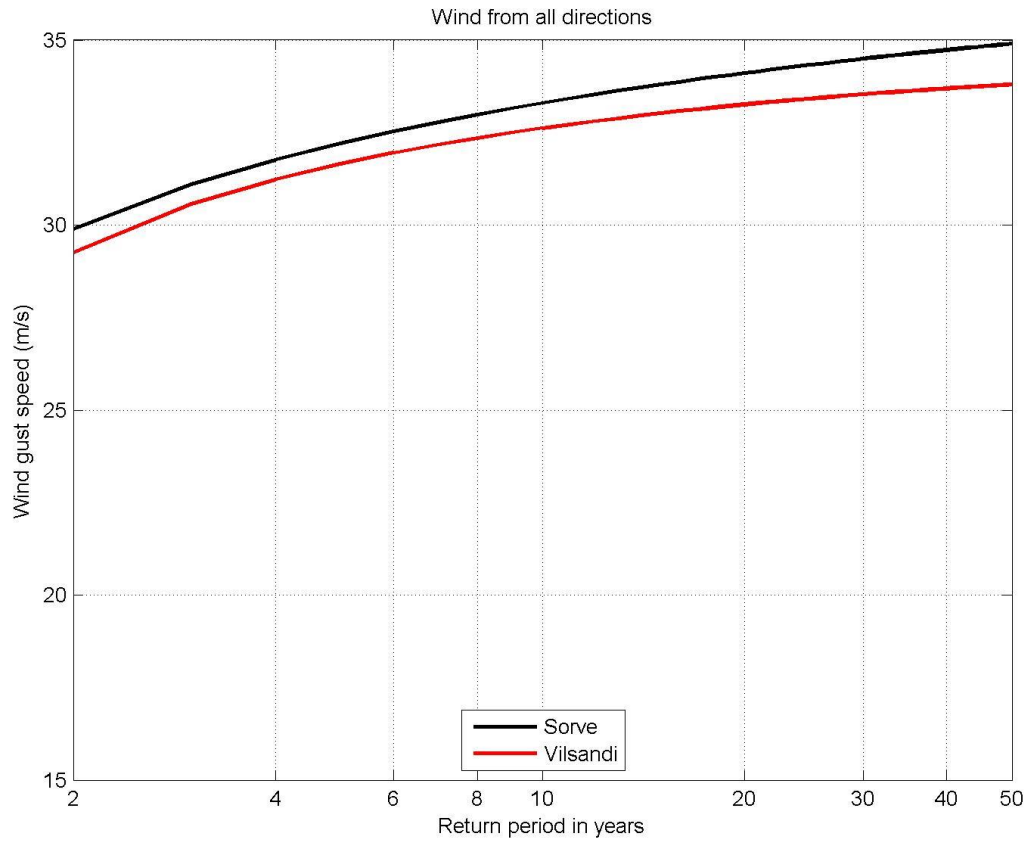
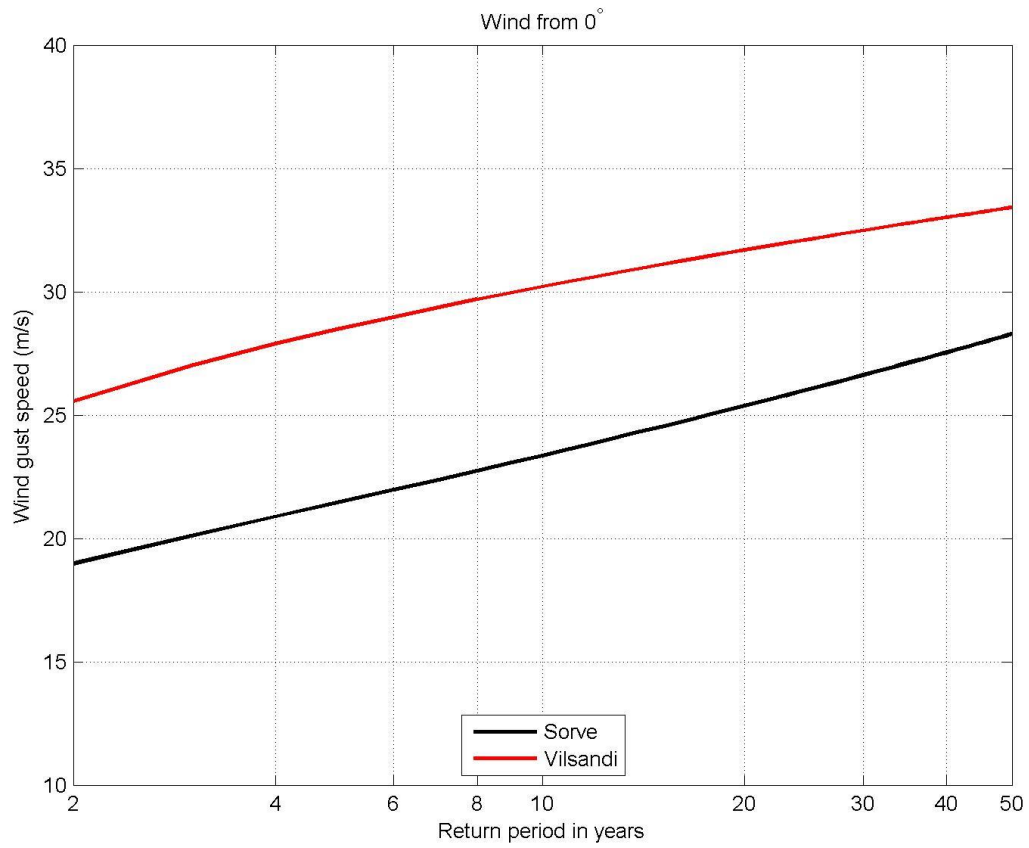


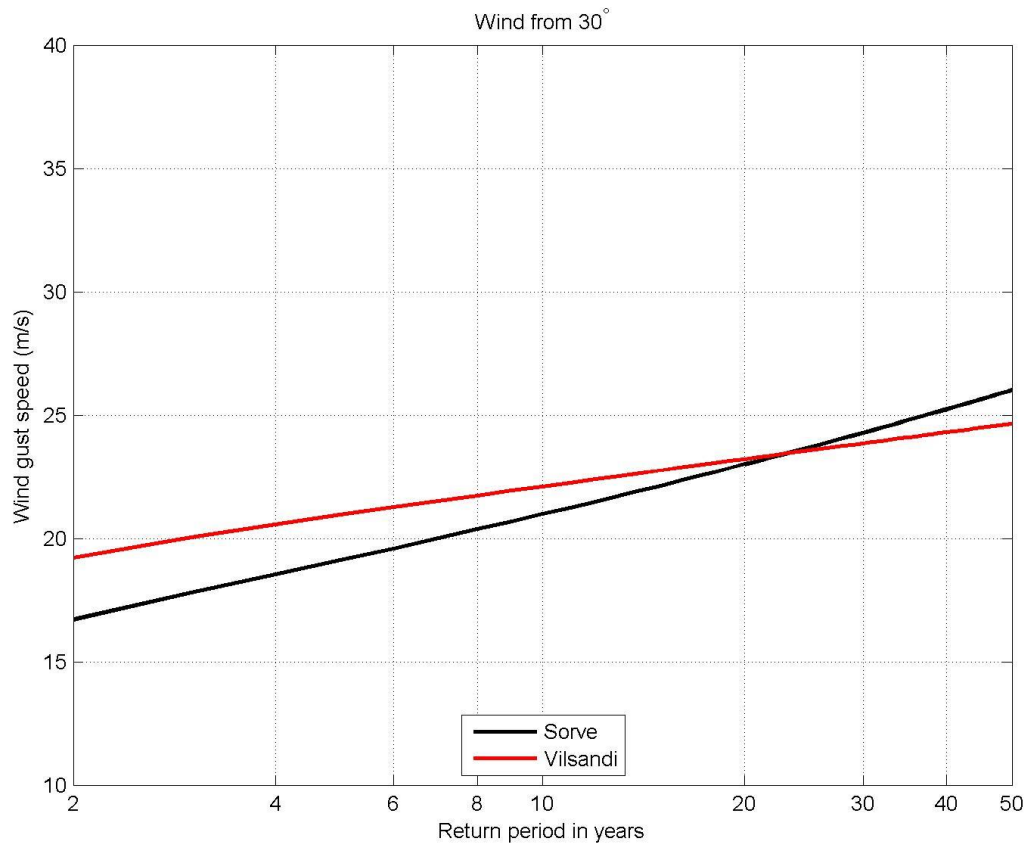
Fig. 3.1.2.26. Return periods of 10-minute wind speed from 330° direction at Vilsandi and Sørve meteorological stations.



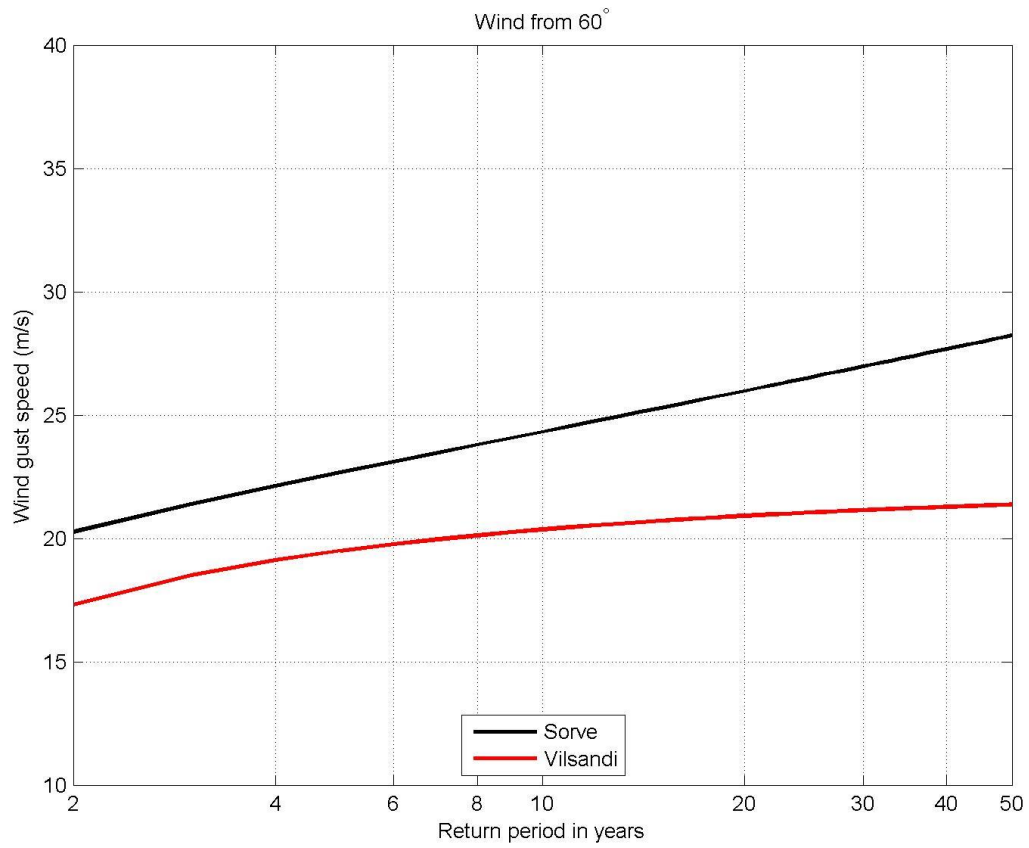
3.1.2.27. Return periods of wind gust speed at Vilsandi and Sørve meteorological stations.



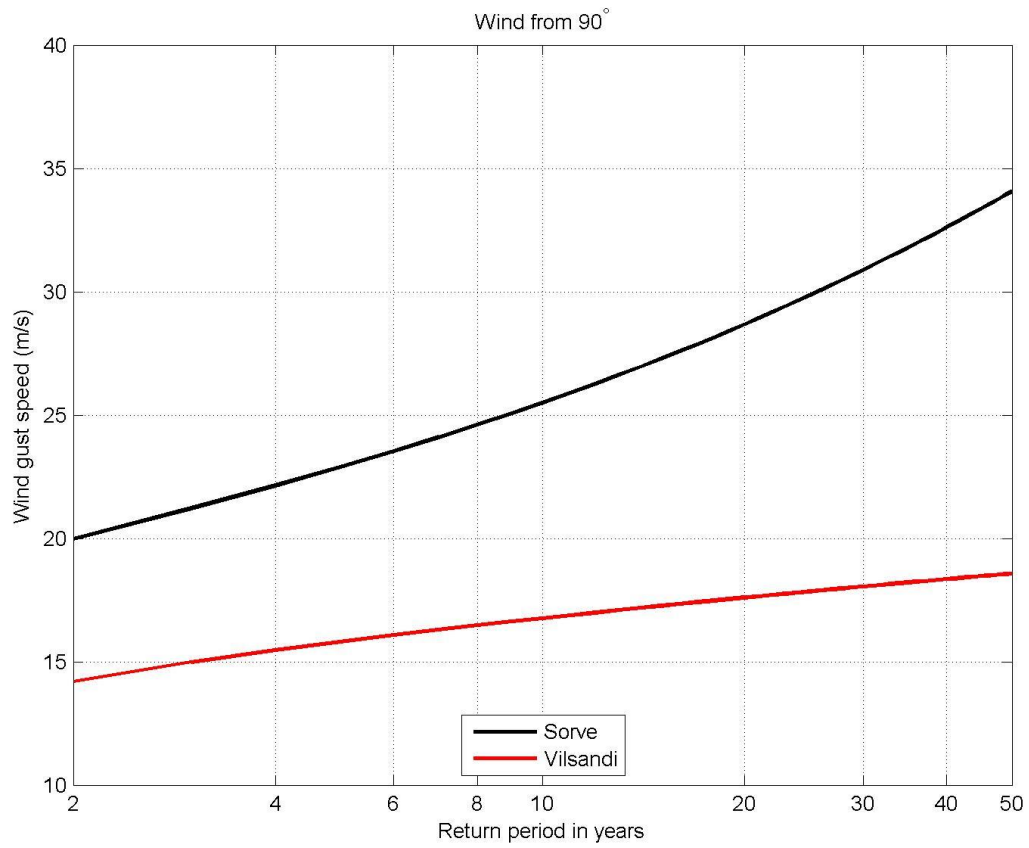
3.1.2.28. Return periods of wind gust speed from 30° direction at Vilsandi and Sörve meteorological stations.



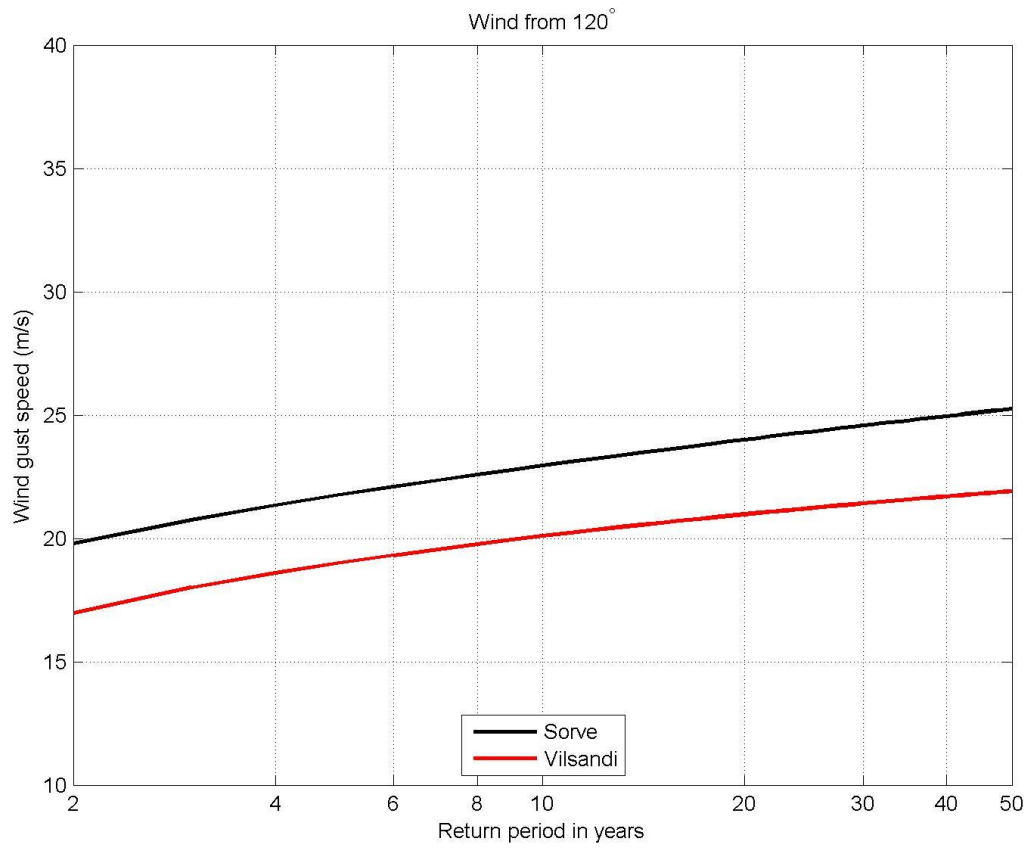
3.1.2.29. Return periods of wind gust speed from 30° direction at Vilsandi and Sörve meteorological stations.



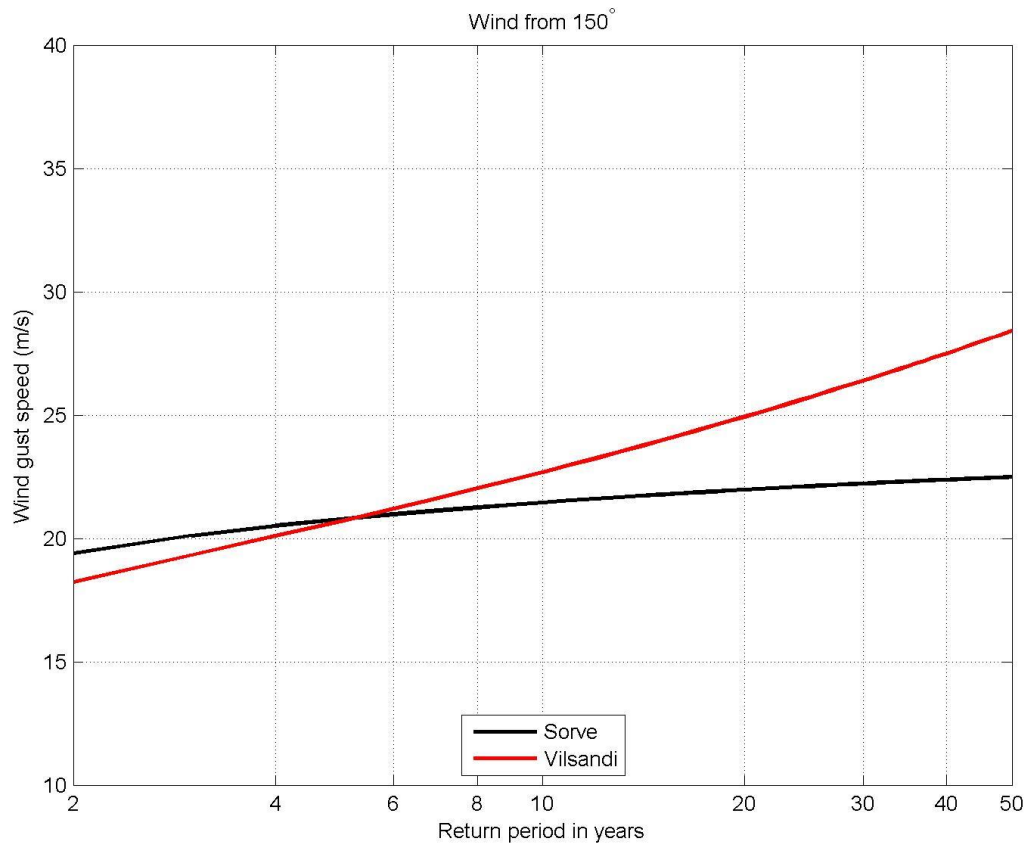
3.1.2.30. Return periods of wind gust speed from 60° direction at Vilsandi and Sörve meteorological stations.



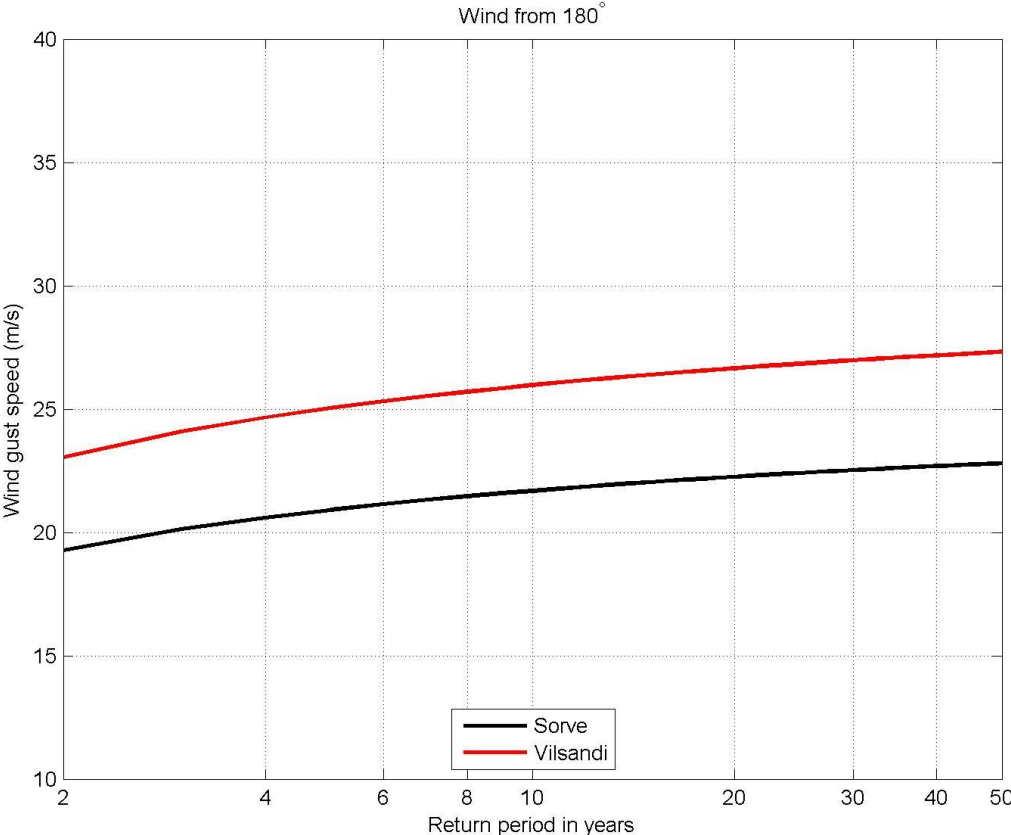
3.1.2.31. Return periods of wind gust speed from 90° direction at Vilsandi and Sörve meteorological stations.



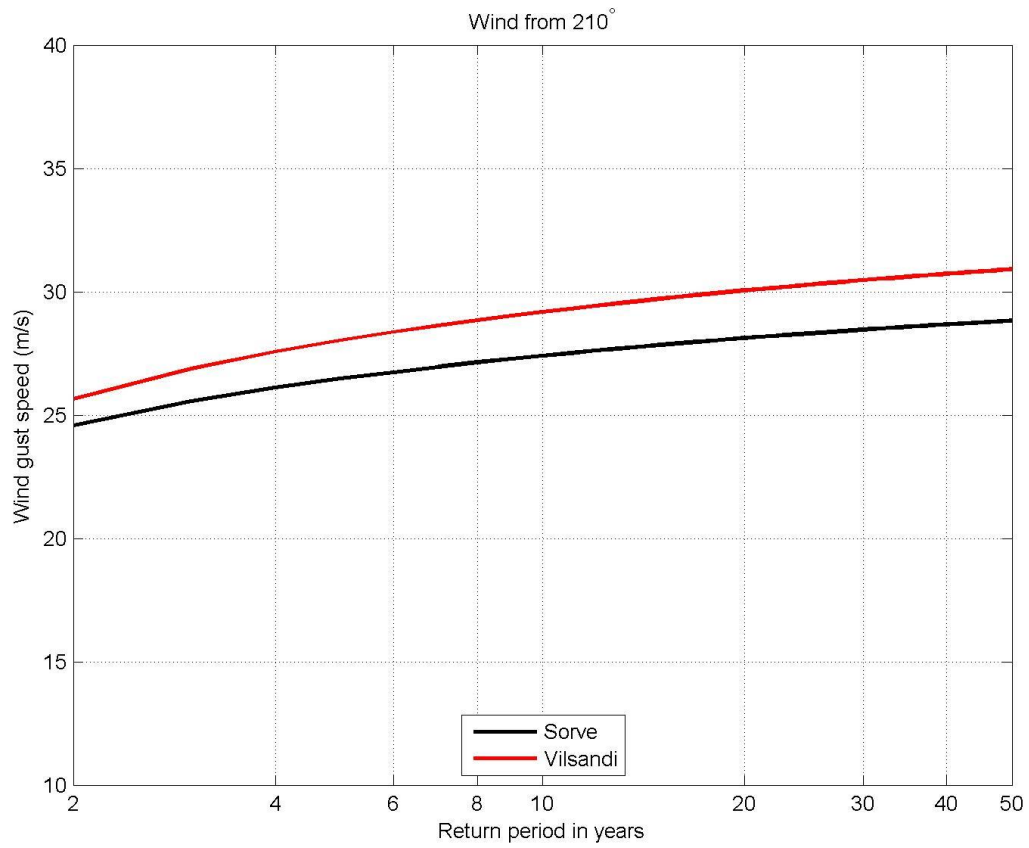
3.1.2.32. Return periods of wind gust speed from 120° direction at Vilsandi and Sörve meteorological stations.



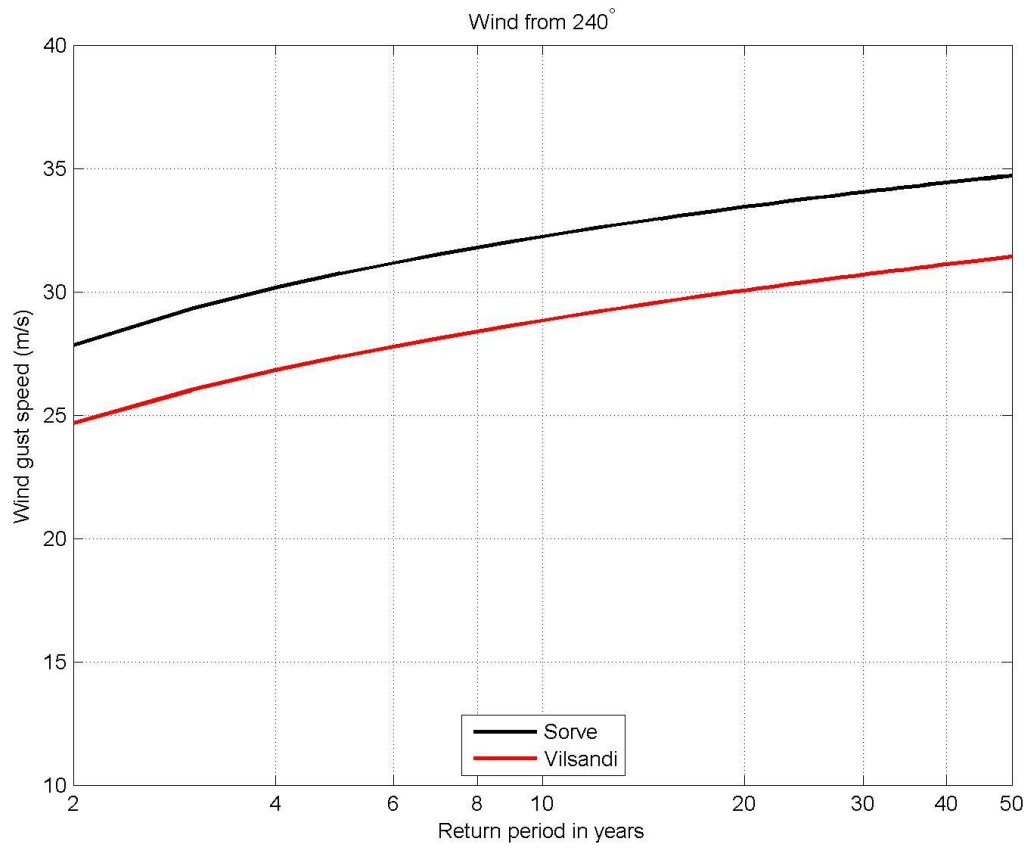
3.1.2.33. Return periods of wind gust speed from 150° direction at Vilsandi and Sörve meteorostations.



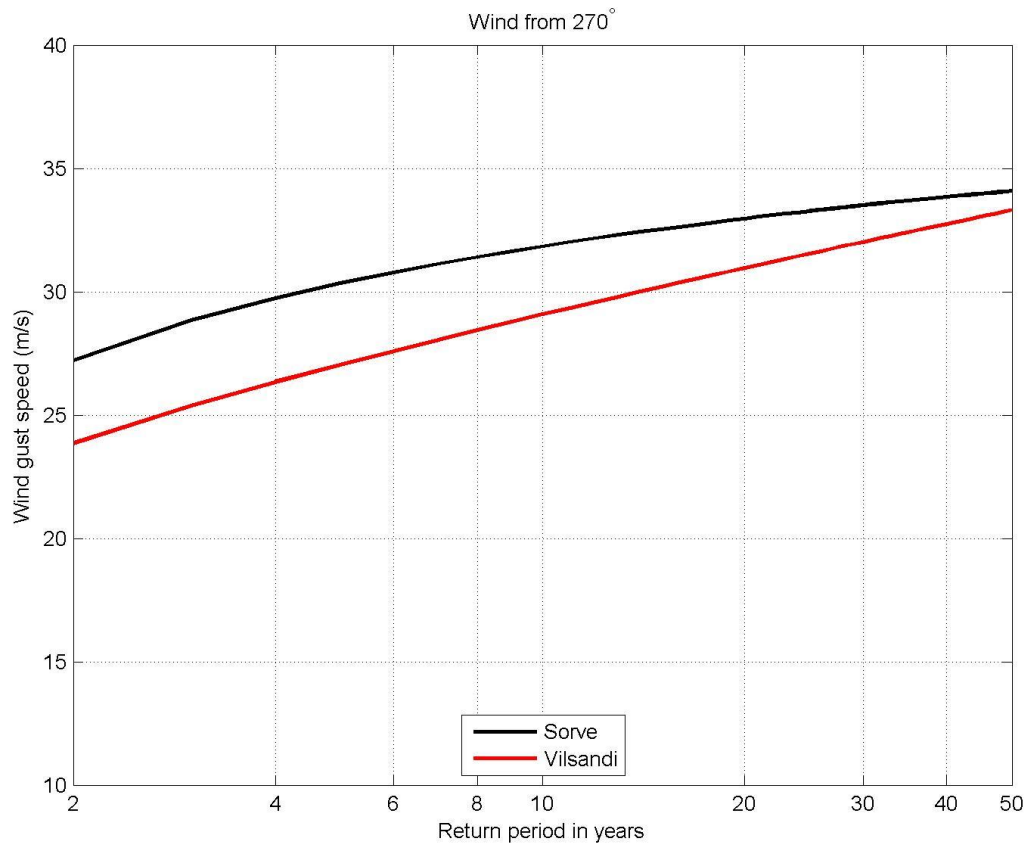
3.1.2.34. Return periods of wind gust speed from 180° direction at Vilsandi and Sörve meteorostations.



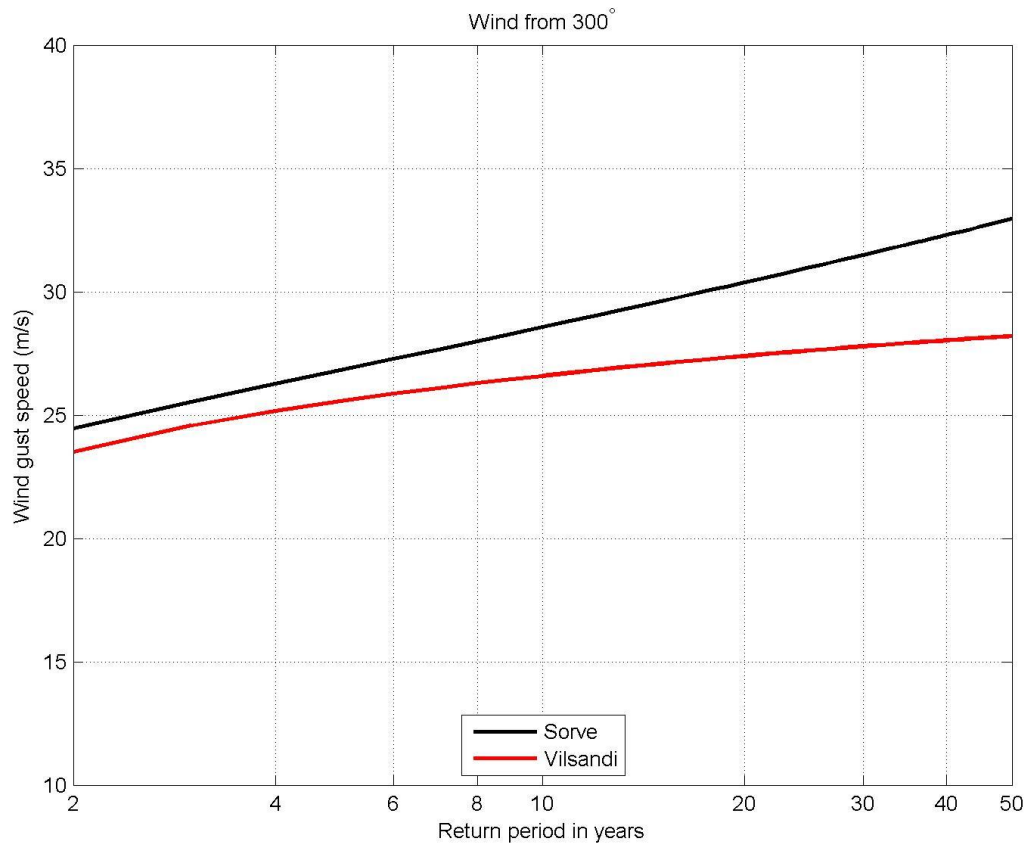
3.1.2.35. Return periods of wind gust speed from 210° direction at Vilsandi and Sörve meteorological stations.



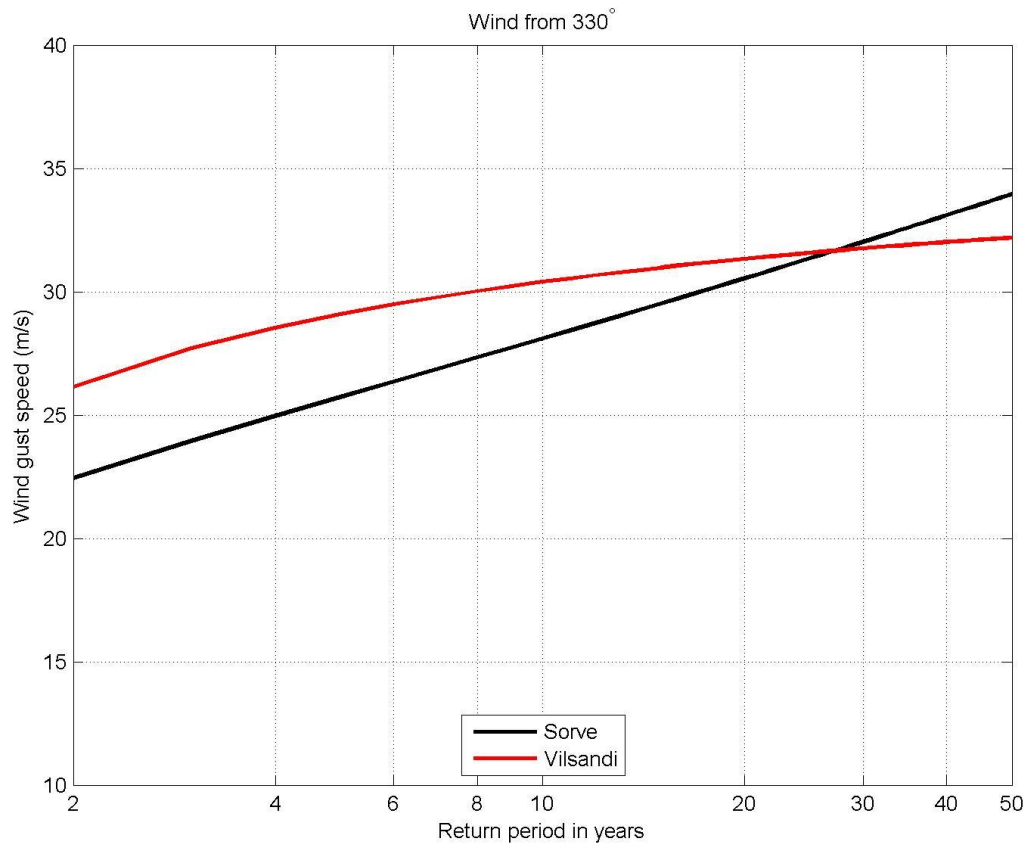
3.1.2.36. Return periods of wind gust speed from 240° direction at Vilsandi and Sörve meteorological stations.



3.1.2.37. Return periods of wind gust speed from 270° direction at Vilsandi and Sörve meteorological stations.



3.1.2.38. Return periods of wind gust speed from 300° direction at Vilsandi and Sörve meteorological stations.



3.1.2.39. Return periods of wind gust speed from 330° direction at Vilsandi and Sörve meteorological stations.

3.1.3. Characteristic wind profiles

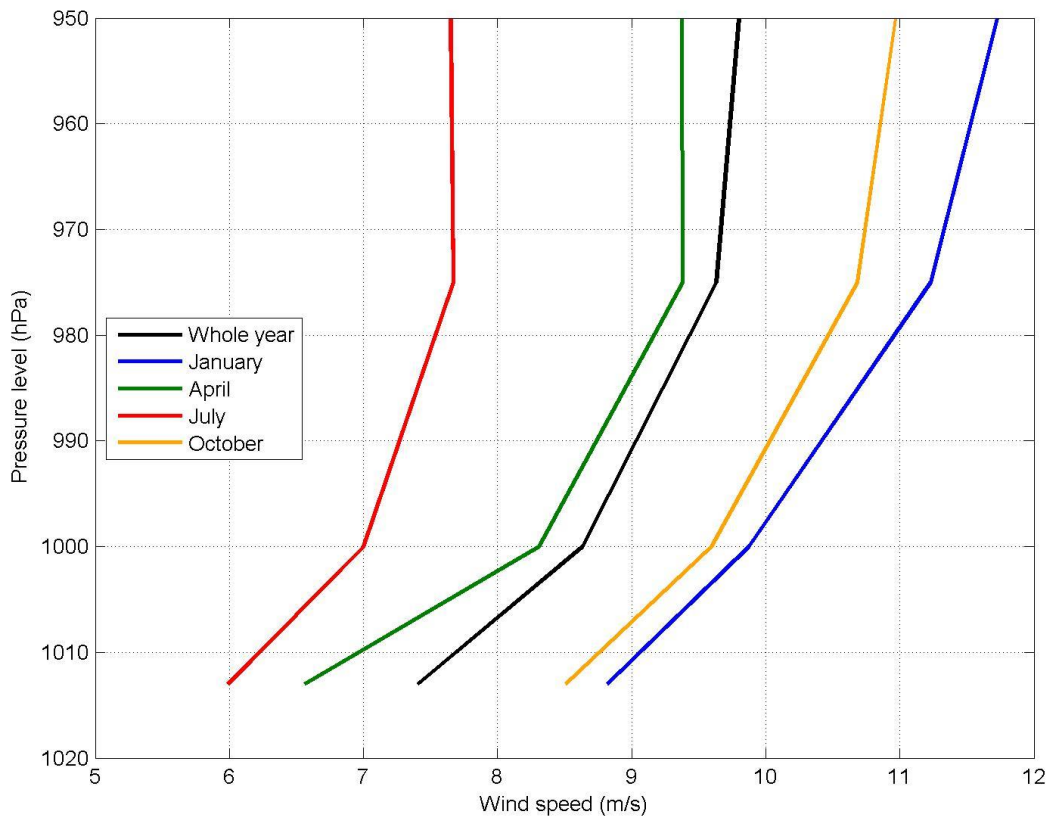


Fig. 3.1.3.1. Mean wind profiles in January, April, July, October and for a year.

3.1.4. Spatial variation of wind speed across the ELWIND site

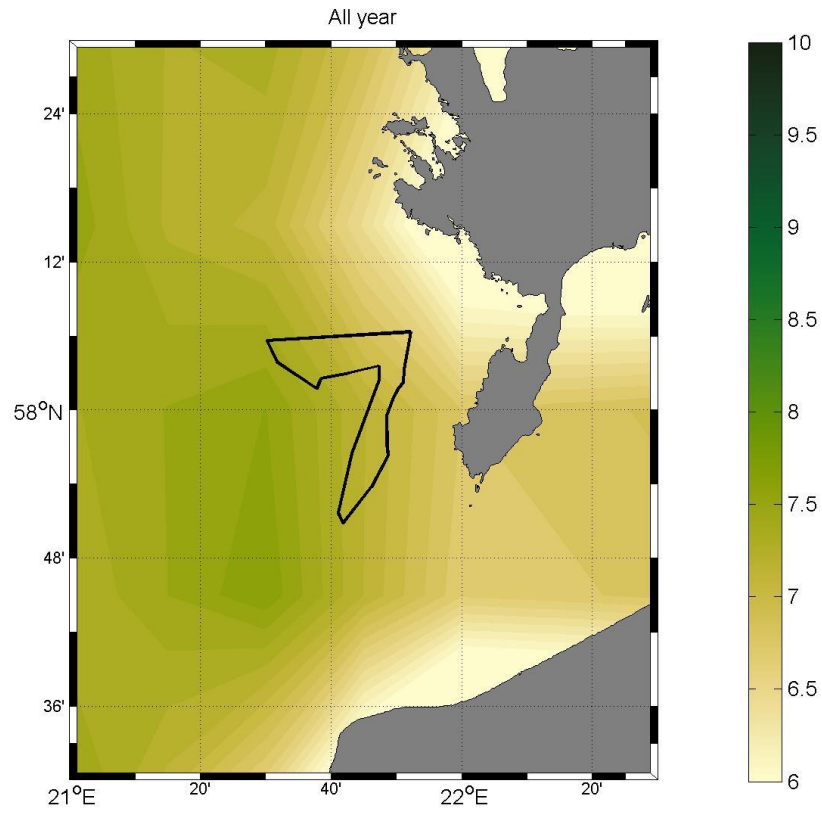


Fig. 3.1.4.1. Mean wind speed derived from ERA5.

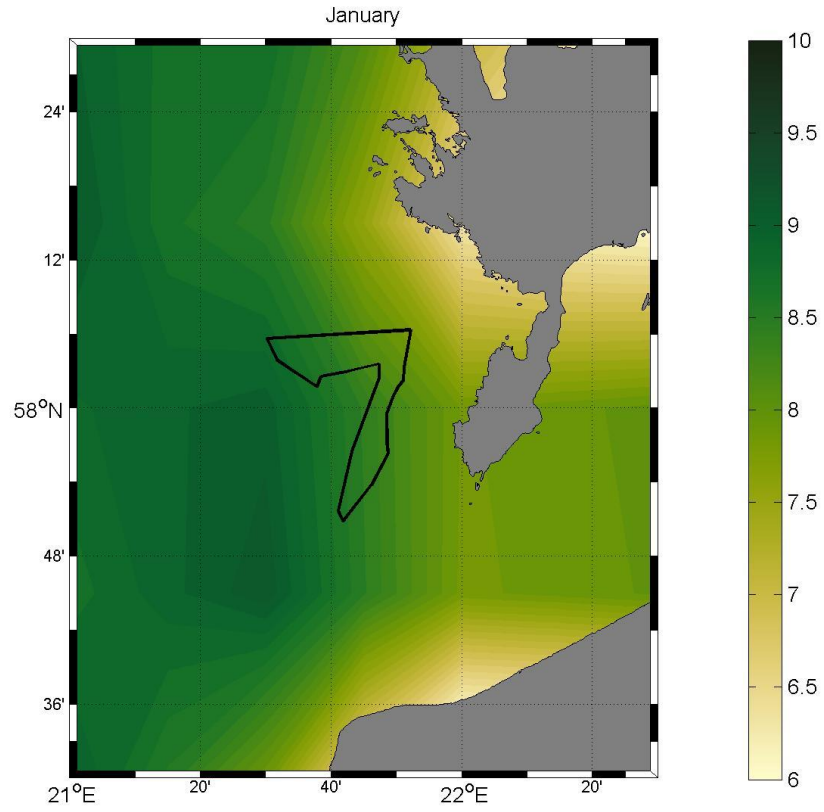


Fig. 3.1.4.2. Mean wind speed in January derived from ERA5.

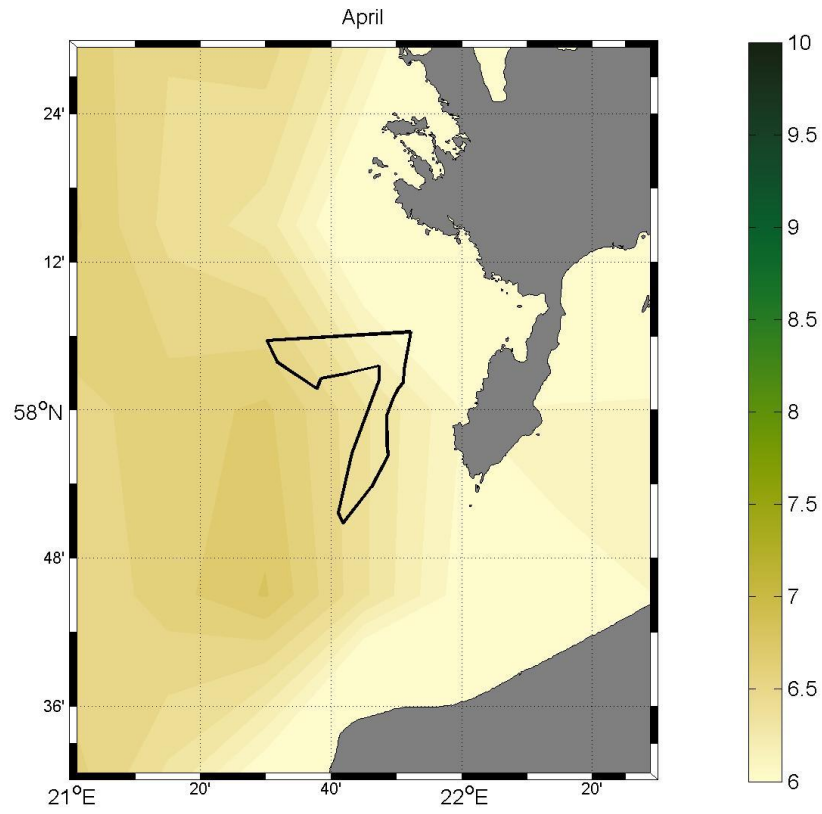


Fig. 3.1.4.3. Mean wind speed in April derived from ERA5.

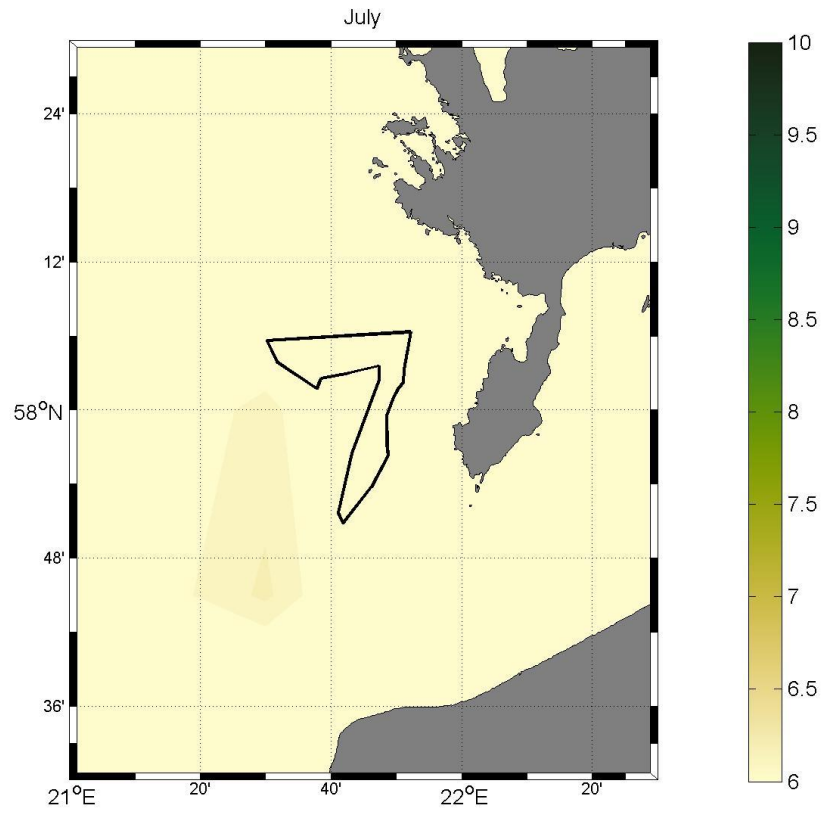


Fig. 3.1.4.4. Mean wind speed in July derived from ERA5.

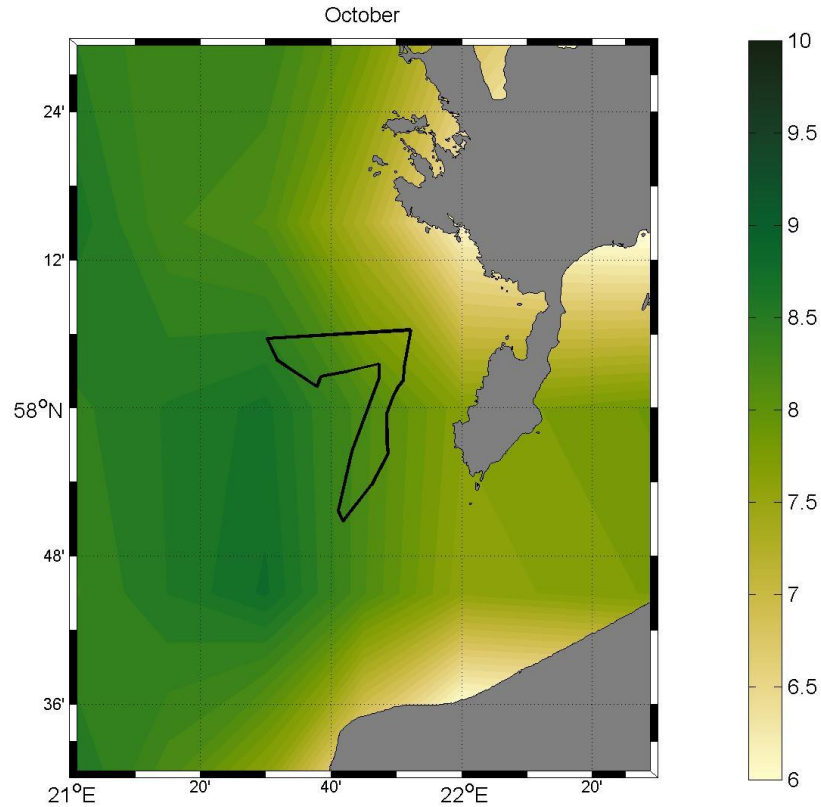


Fig. 3.1.4.5. Mean wind speed in October derived from ERA5.

3.1.5. Qualitative assessment of effect of other wind farms under development in the Baltic Sea

There are no operating wind farms near the ELWIND site, but there are plenty of wind farms planned to the north, northwest, and west of the ELWIND area (Fig. 3.1.5.1). There are no wind farms planned southwest of the EWLIND site, which is the most frequent wind direction. Particularly the northern part of the ELWIND area would be impacted by wind wake effect from northerly and northwesterly wind directions and less with winds from the west. The decrease in wind speed due to the wake effect in the northern part of the ELWIND area in the case of northerly or northeasterly winds could be in the order of 10-30% (Barthelmie and Jensen, 2010; Maas and Raasch, 2022; Westerhellweg et al., 2014). According to the ERA5 data, approximately 24% of the wind is coming from the sector between north and west. The wind wake effect generated in the neighboring wind farms also alters waves, current and circulation, and stratification in the ELWIND area.

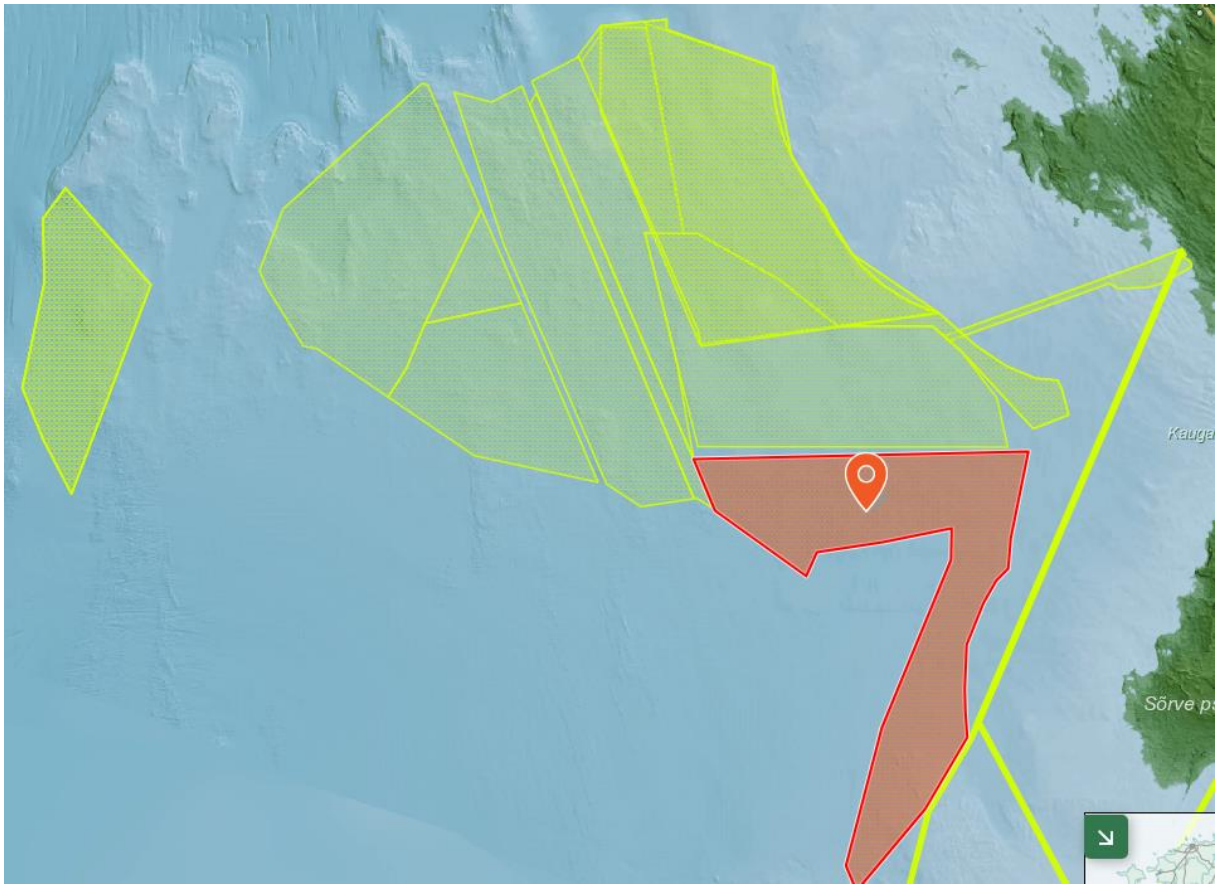


Fig. 3.1.5.1. The areas of superficies license applied or the superficies license procedure initiated near the offshore wind farm (<https://xgis.maaamet.ee/xgis2/page/app/TTJAhoonestusload>, accessed 20.04.2025). ELWIND area is marked with red.

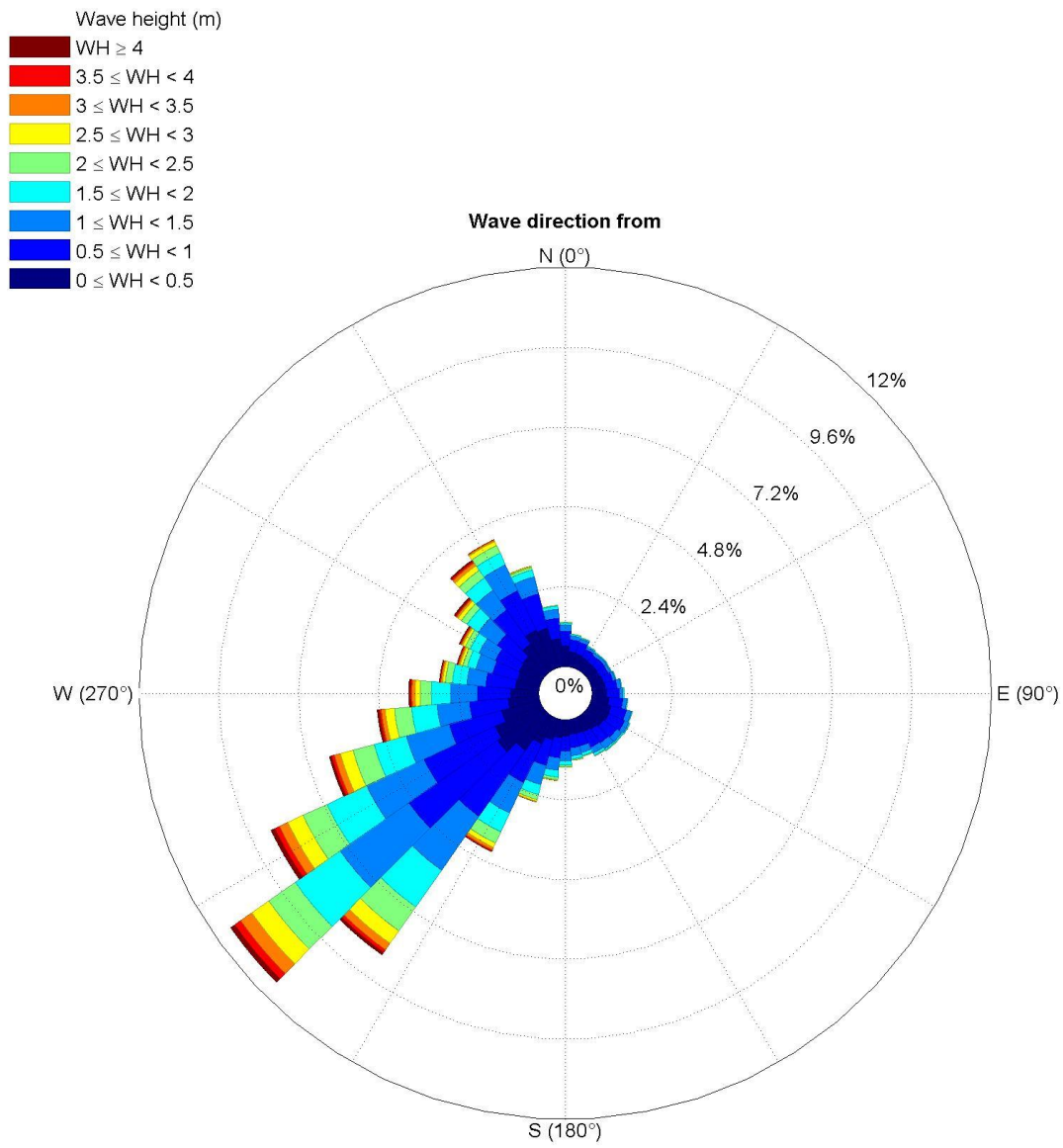
3.2. Wave conditions

The wave conditions in the ELWIND areas largely dependent on the direction and speed of the wind. Thus, the wave climate is well connected to the wind climate, and the dominant wave propagation occurs from the southwest, and the secondary peak is from the northwest (Figs 3.1.1-3.1.25). The highest waves approach from northwest, west, and southwest and the same applies for the longest wave periods (Figs. 3.2.2.1-3.2.2.18). Significant wave height up to 8 meters could occur in severe storms (Fig. 3.1.26). Since the maximum waves could be as high as 1.8 times larger than the significant wave height, single waves of 14 m high could occur in heavy storms. The highest waves during the selected 30-year period likely occurred during the storm Gudrun in January 2005 (Soomere et al., 2008; Suursaar et al., 2006). The significant wave height at the peak of Gudrun is shown in Fig. 3.2.3.2. Significant wave height exceeded 8 m in the westernmost part of the ELWIND area during that storm. Due to the land coverage from north, east, southeast, and northeast, no very high waves approach the ELWIND area from these directions (Figs 3.1.1-3.1.25). On average, slightly higher waves occur in the western than southeastern part of the ELWIND area (Fig. 3.2.3.1). However, compared to the temporal variability of wave properties spatial variability is minor within the ELWIND area.

A significant wave height of 2 m and higher is common in the area. There are about 20 events a year when significant wave height is 2 m and higher at least 24 hours (Fig. 3.2.2.18). The occurrence of higher (e.g. ≥ 3 m) wave conditions is smaller but still considerable. For instance, there are about 10-11 events a year, when significant wave height is ≥ 3 m for at least 12 hours. The duration and occurrence of the events of significant wave height ≥ 4 m, ≥ 5 m, and so on, is much rarer.

The active breaking of waves occurs when the wave height is approximately 80% of the sea depth. Thus, taking depths of the ELWIND area, the area is not an active breaking or shoaling zone for wind waves.

3.2.1. Average conditions



3.2.1.1. Annual occurrence of significant wave height.

Fig.

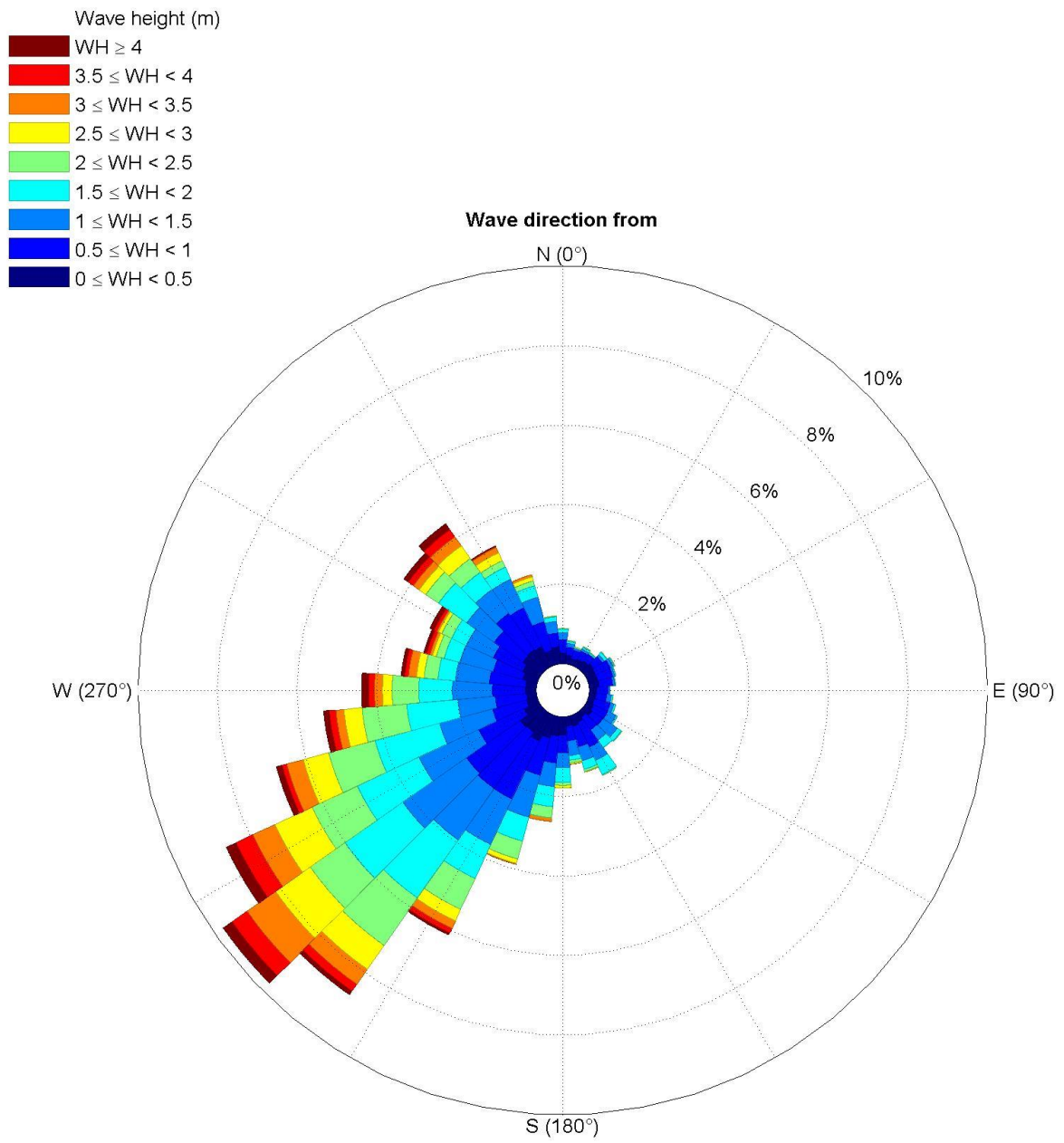


Fig. 3.2.1.2. Occurrence of significant wave height in January.

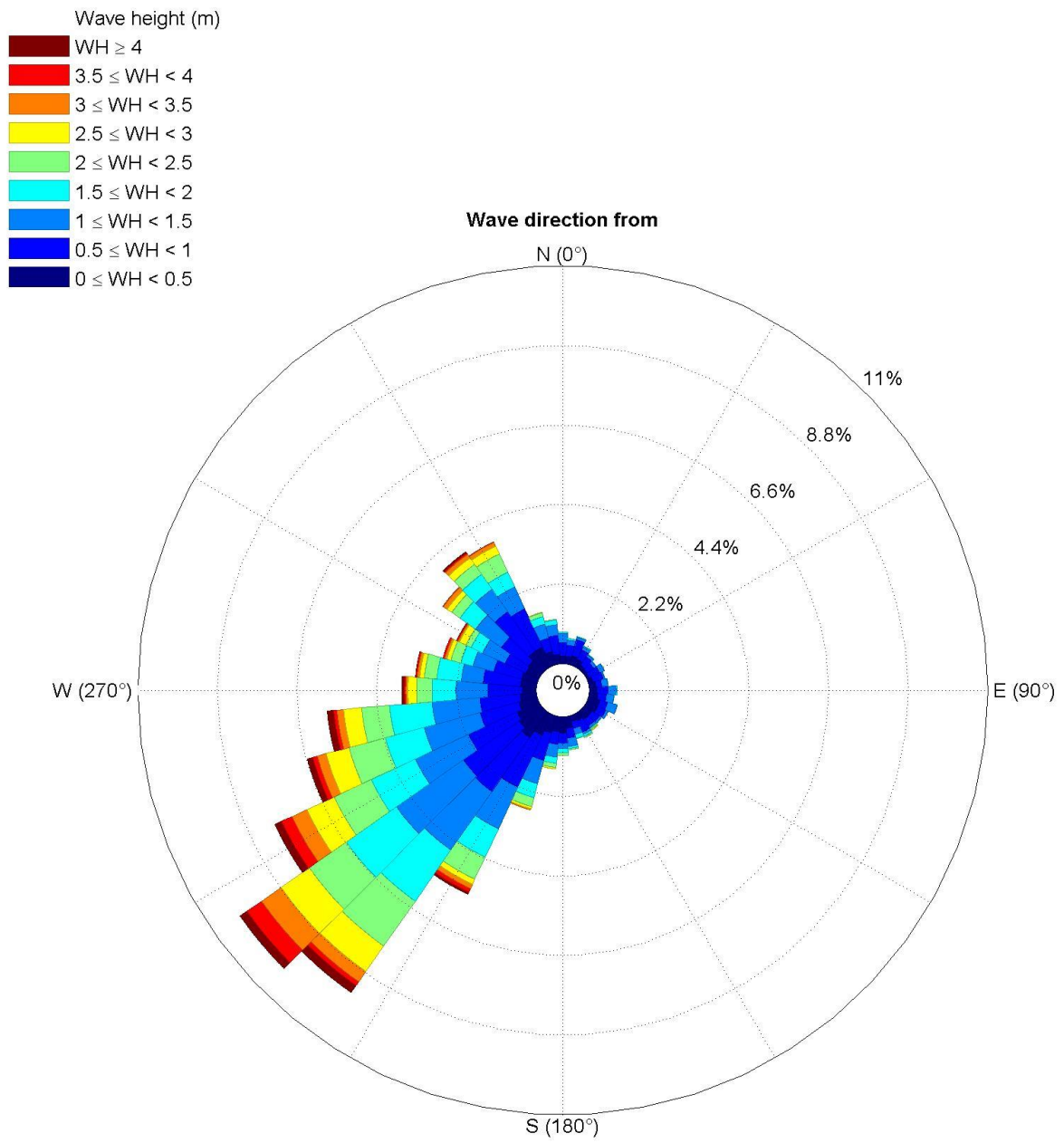


Fig. 3.2.1.3. Occurrence of significant wave height in February.

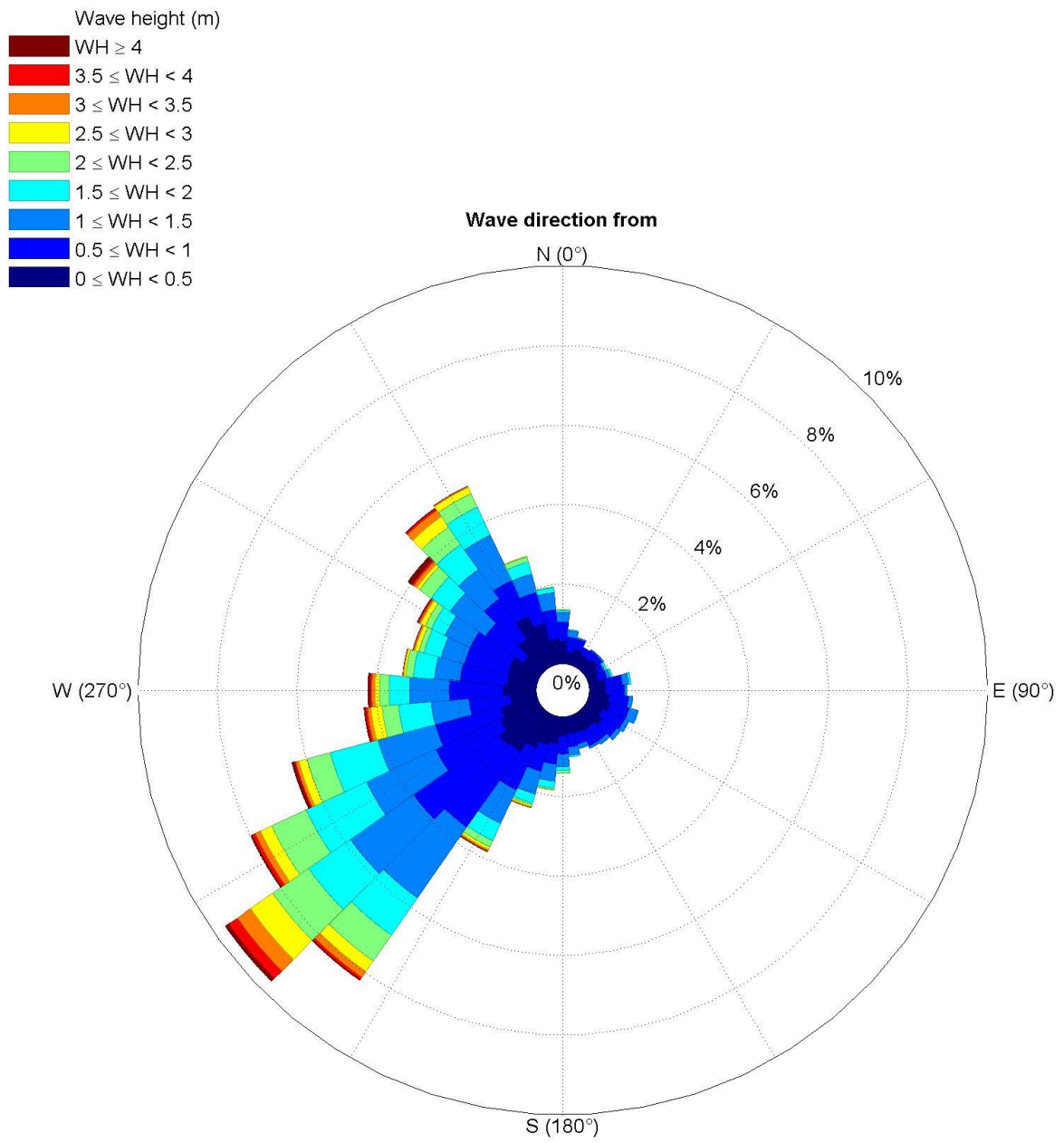


Fig. 3.2.1.4. Occurrence of significant wave height in March.

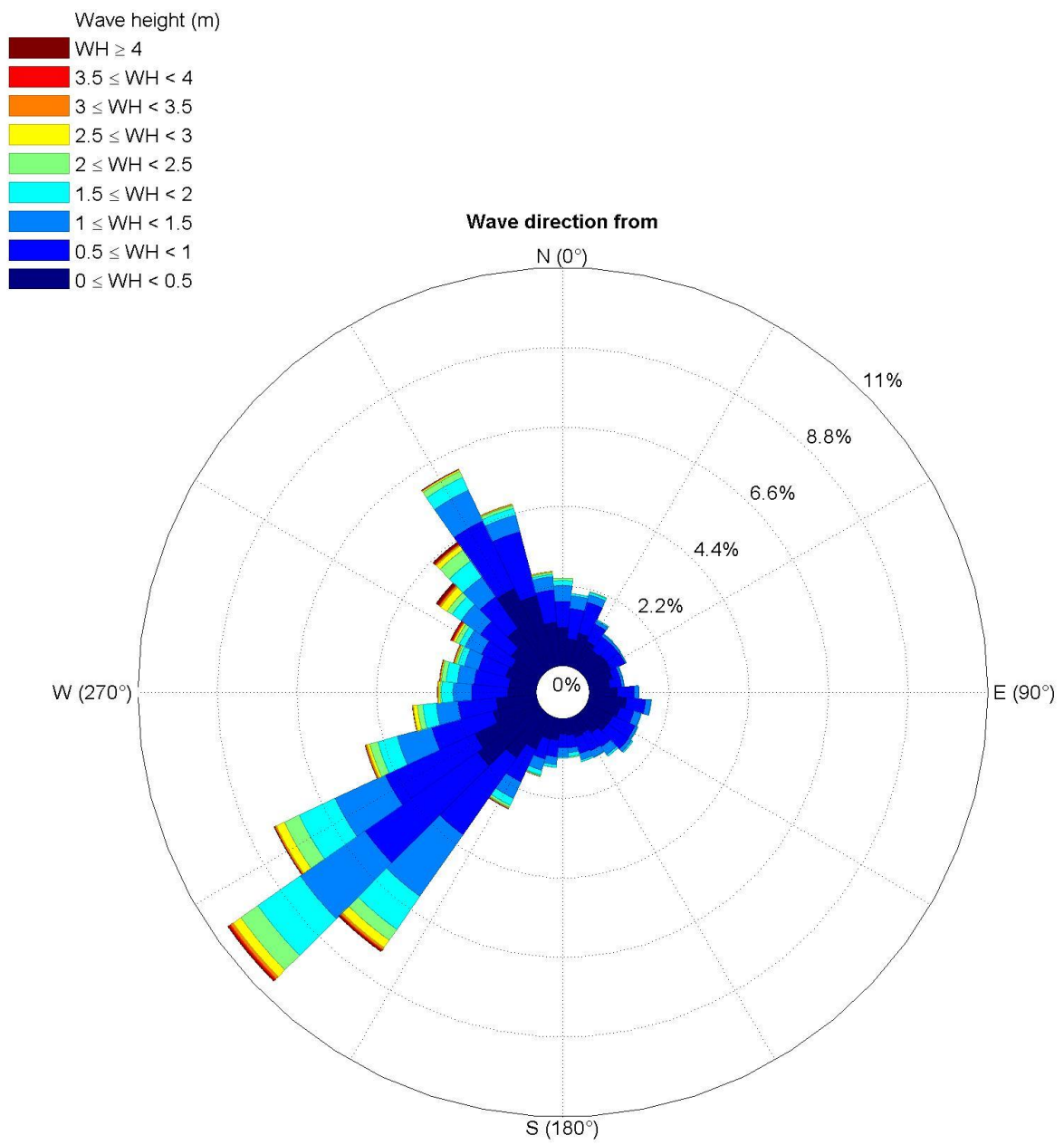


Fig. 3.2.1.5. Occurrence of significant wave height in April.

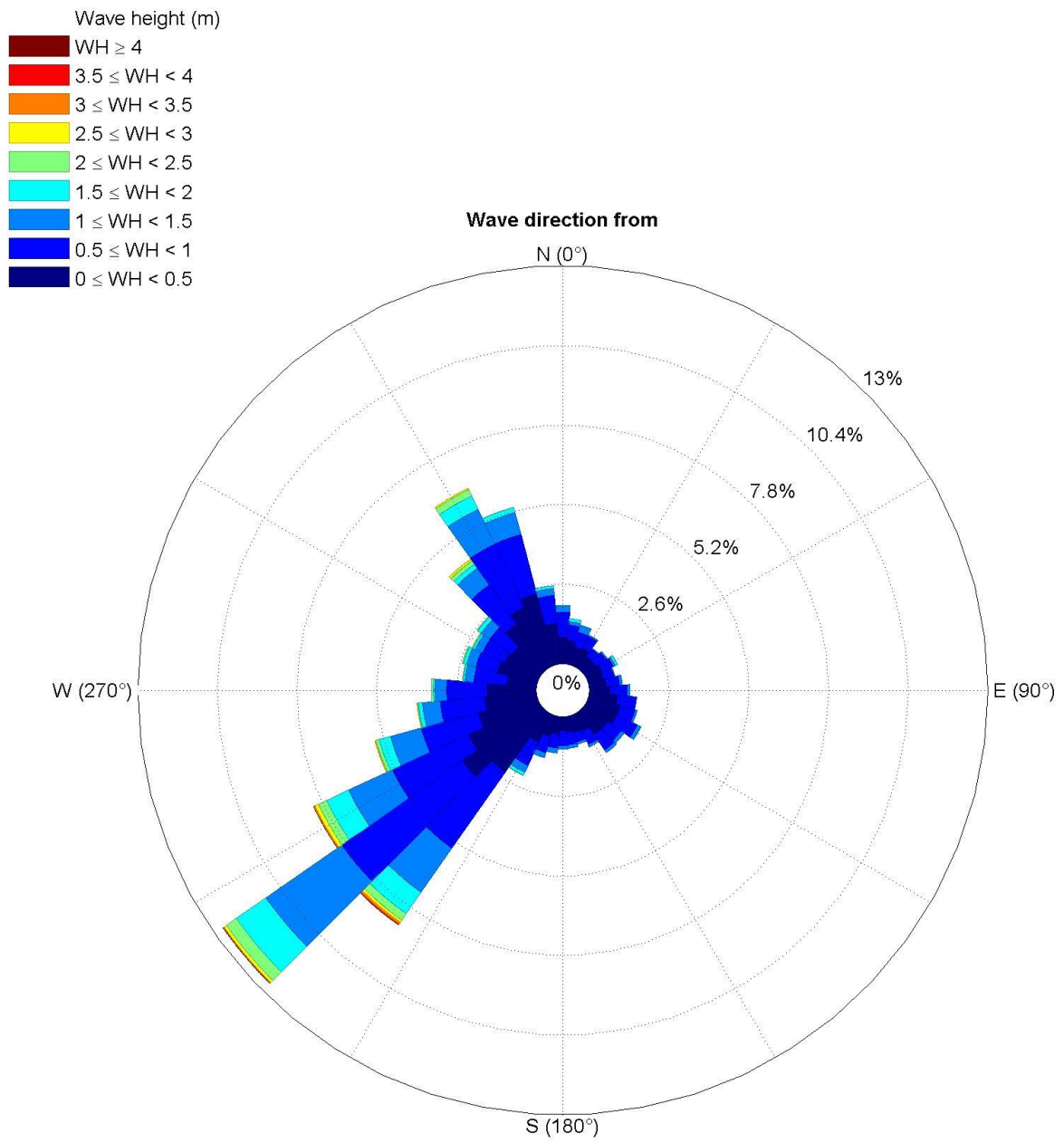


Fig. 3.2.1.6. Occurrence of significant wave height in May.

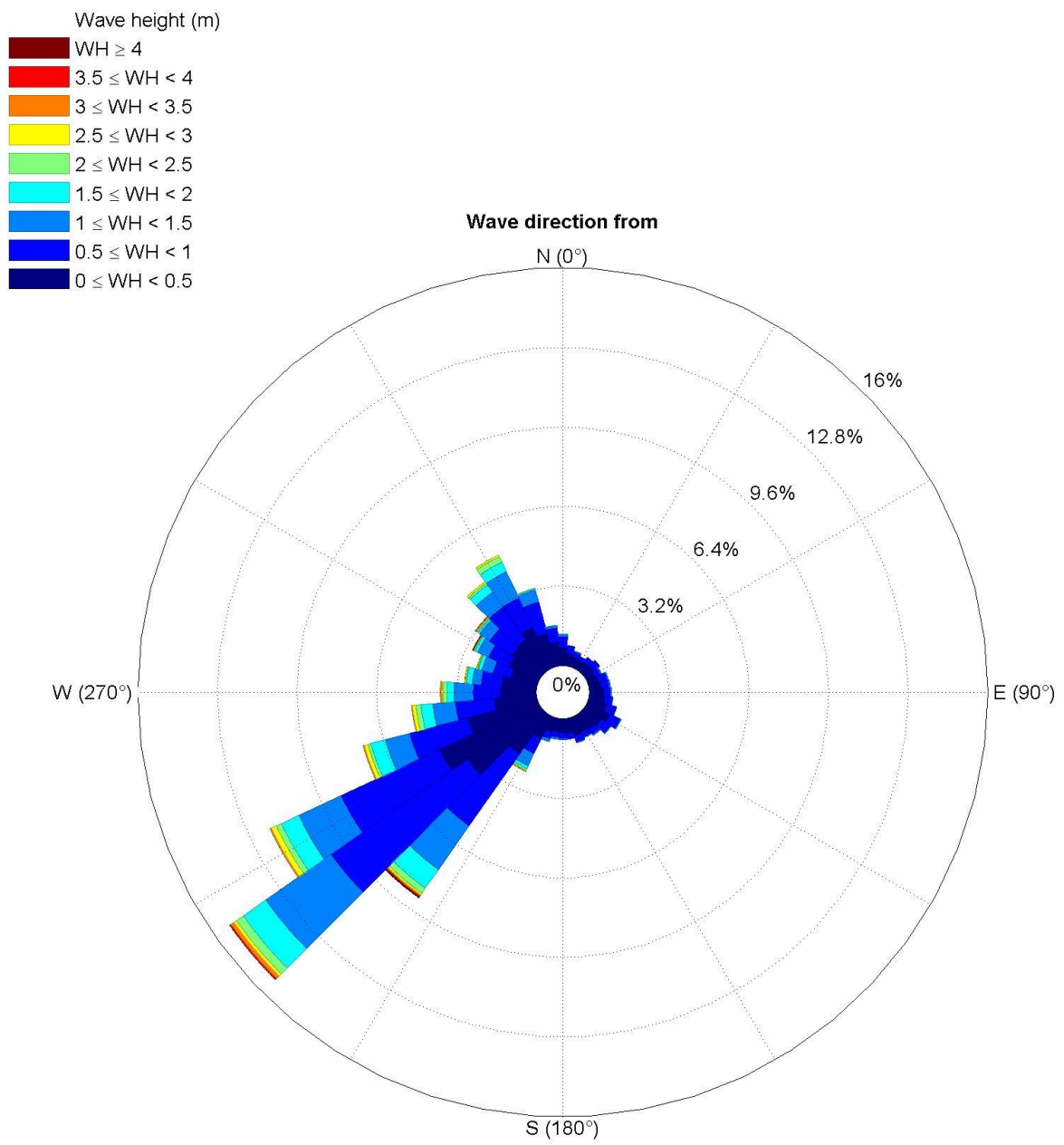


Fig. 3.2.1.7. Occurrence of significant wave height in June.

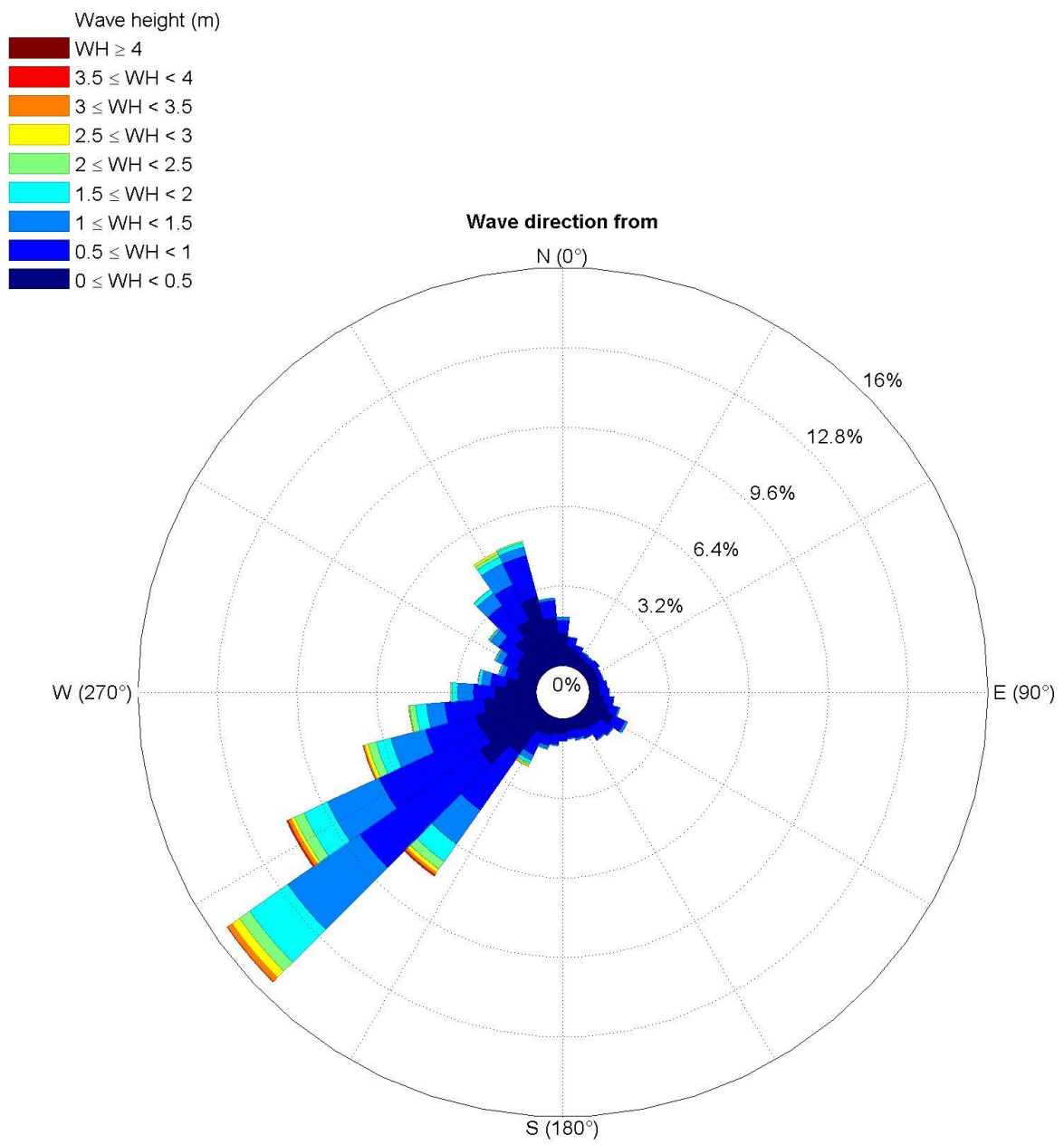


Fig. 3.2.1.8. Occurrence of significant wave height in July.

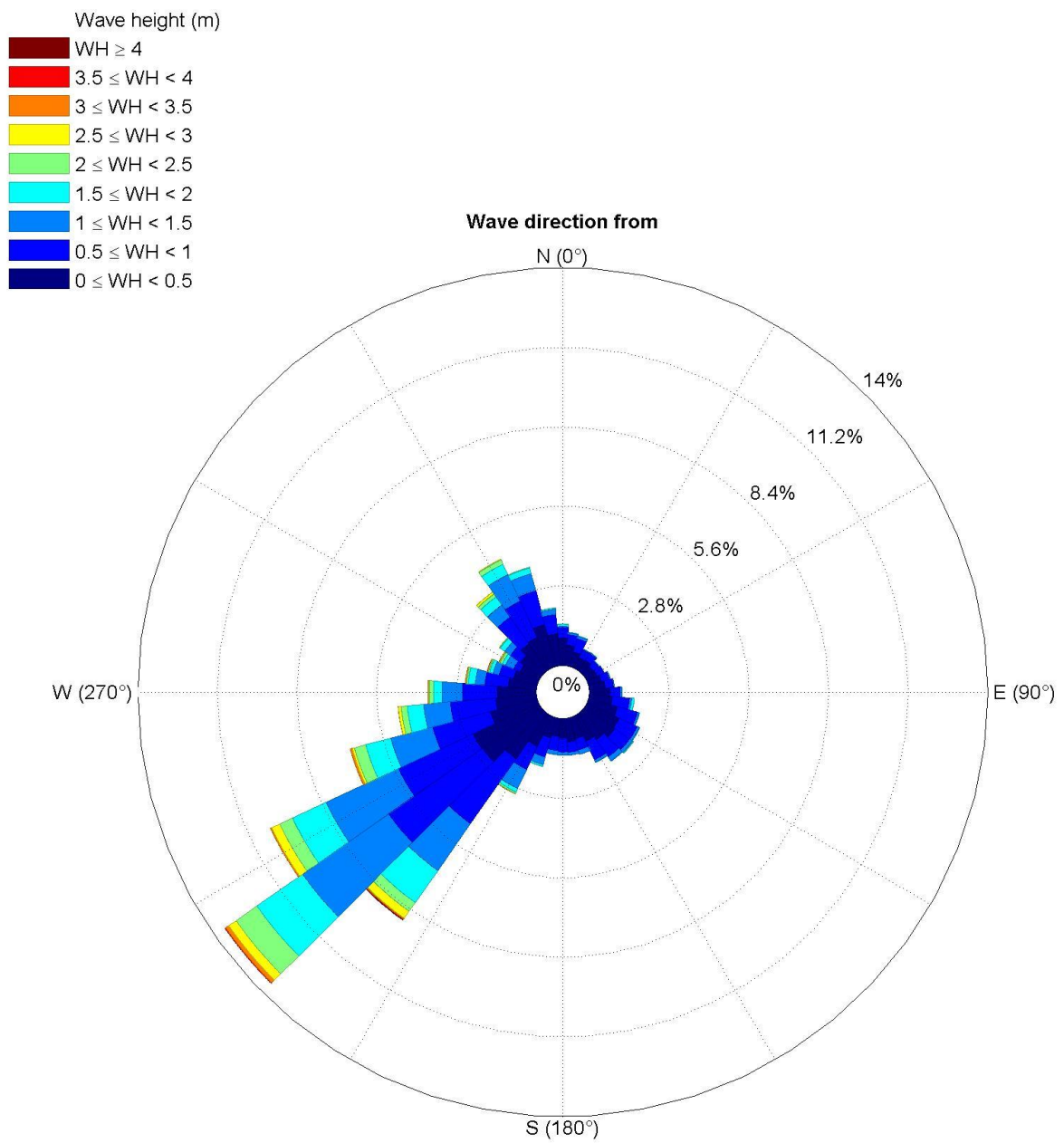


Fig. 3.2.1.9. Occurrence of significant wave height in August.

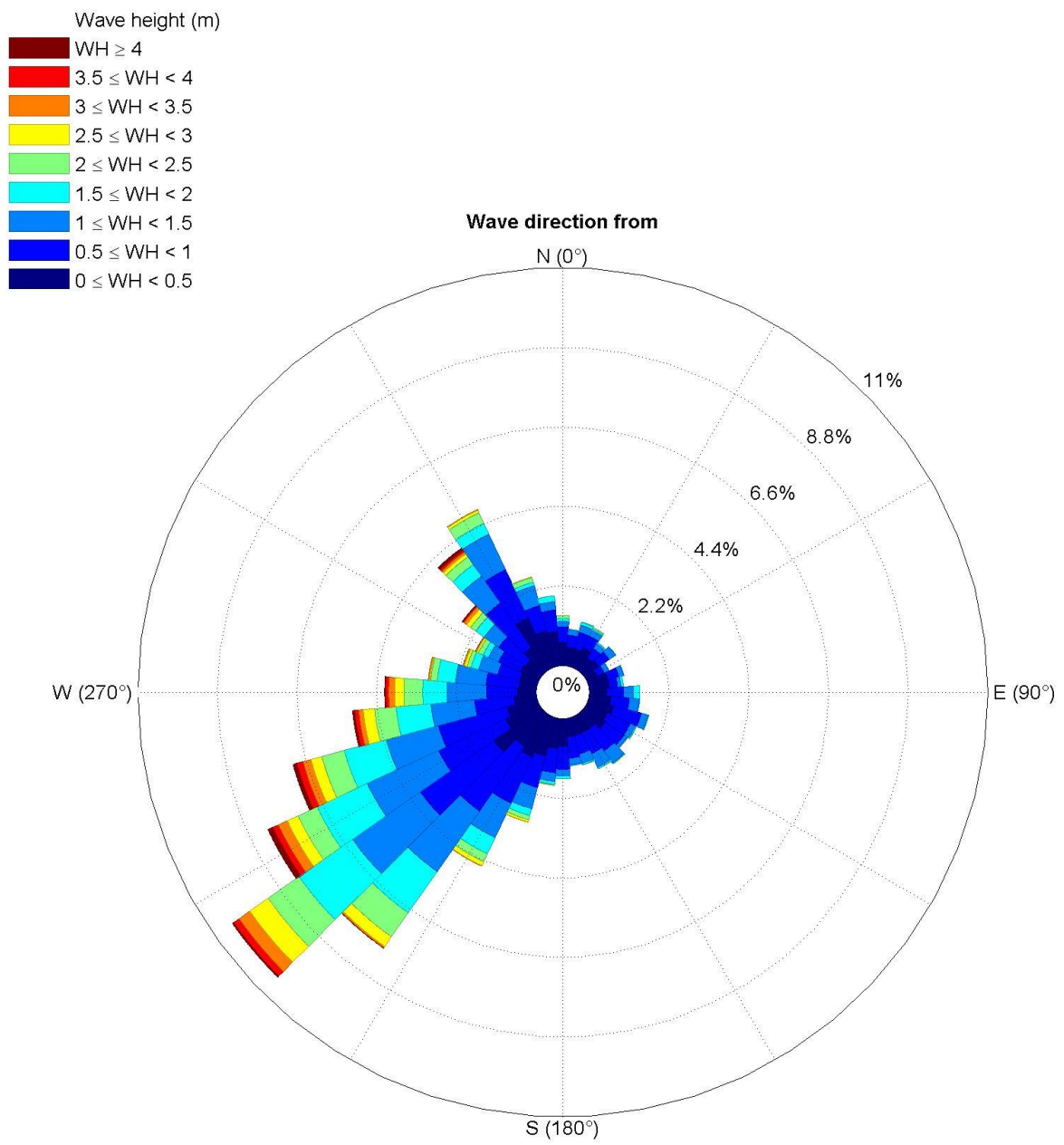


Fig. 3.2.1.10. Occurrence of significant wave height in September.

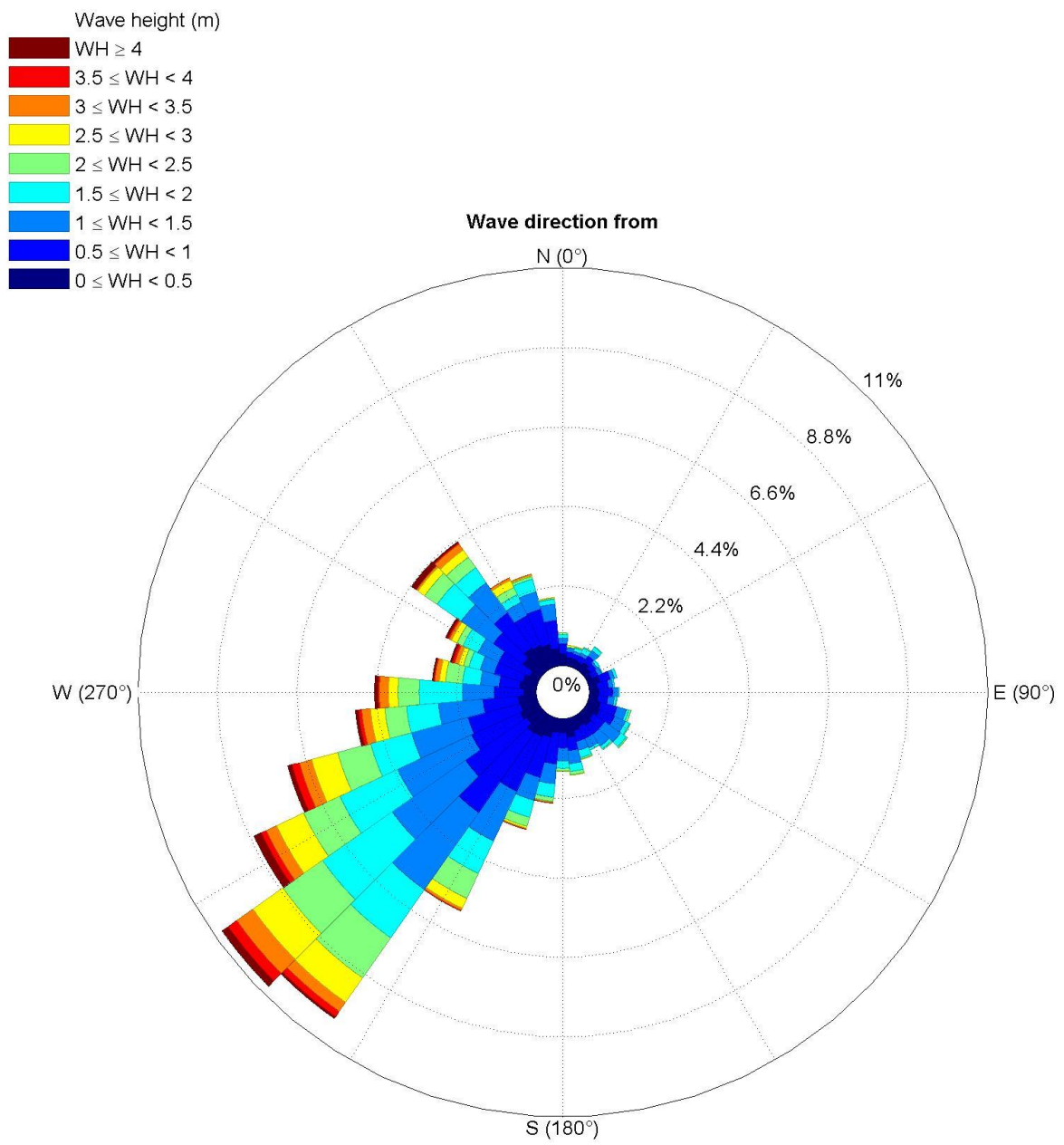


Fig. 3.2.1.11. Occurrence of significant wave height in October.

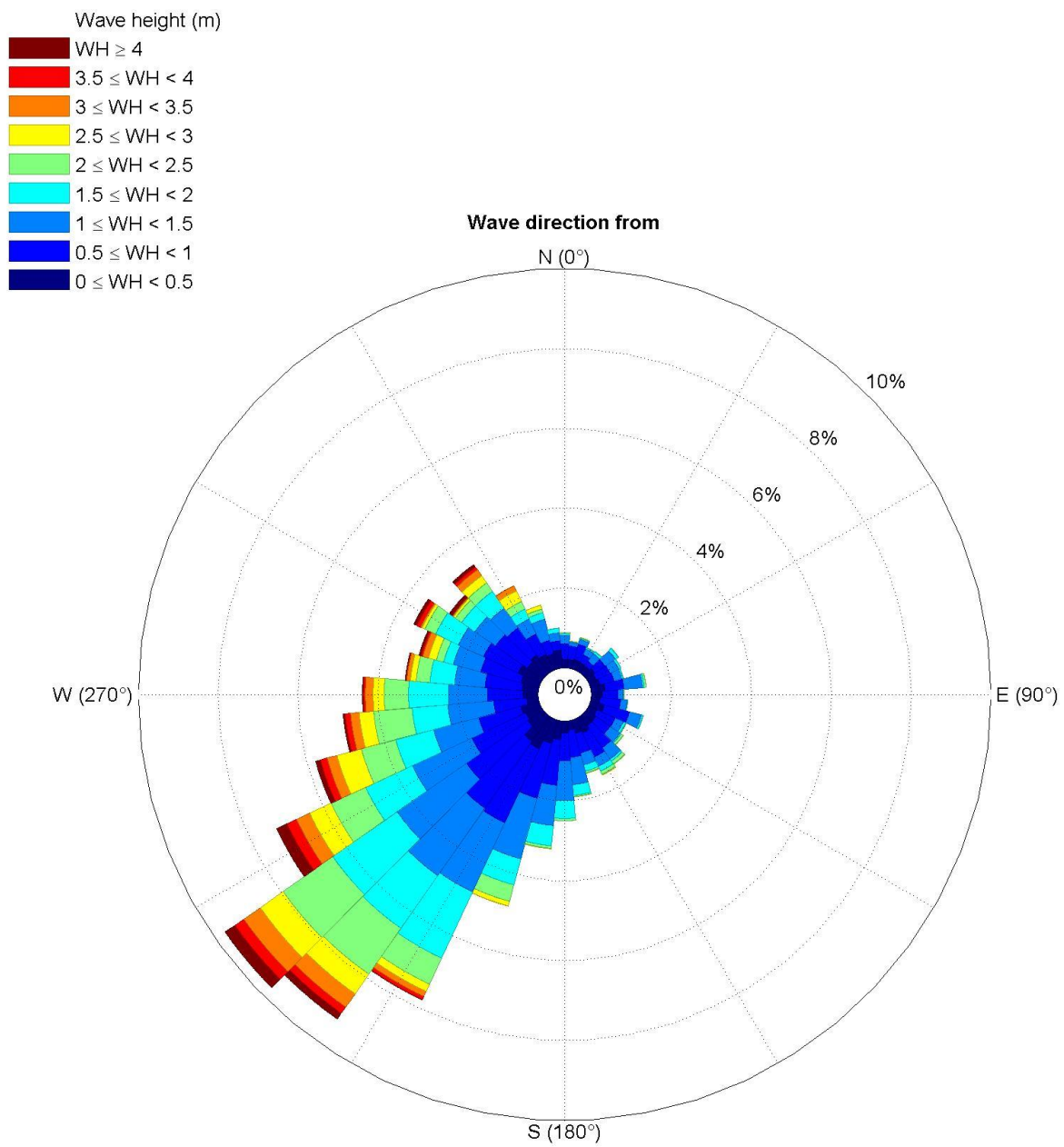


Fig. 3.2.1.11. Occurrence of significant wave height in November.

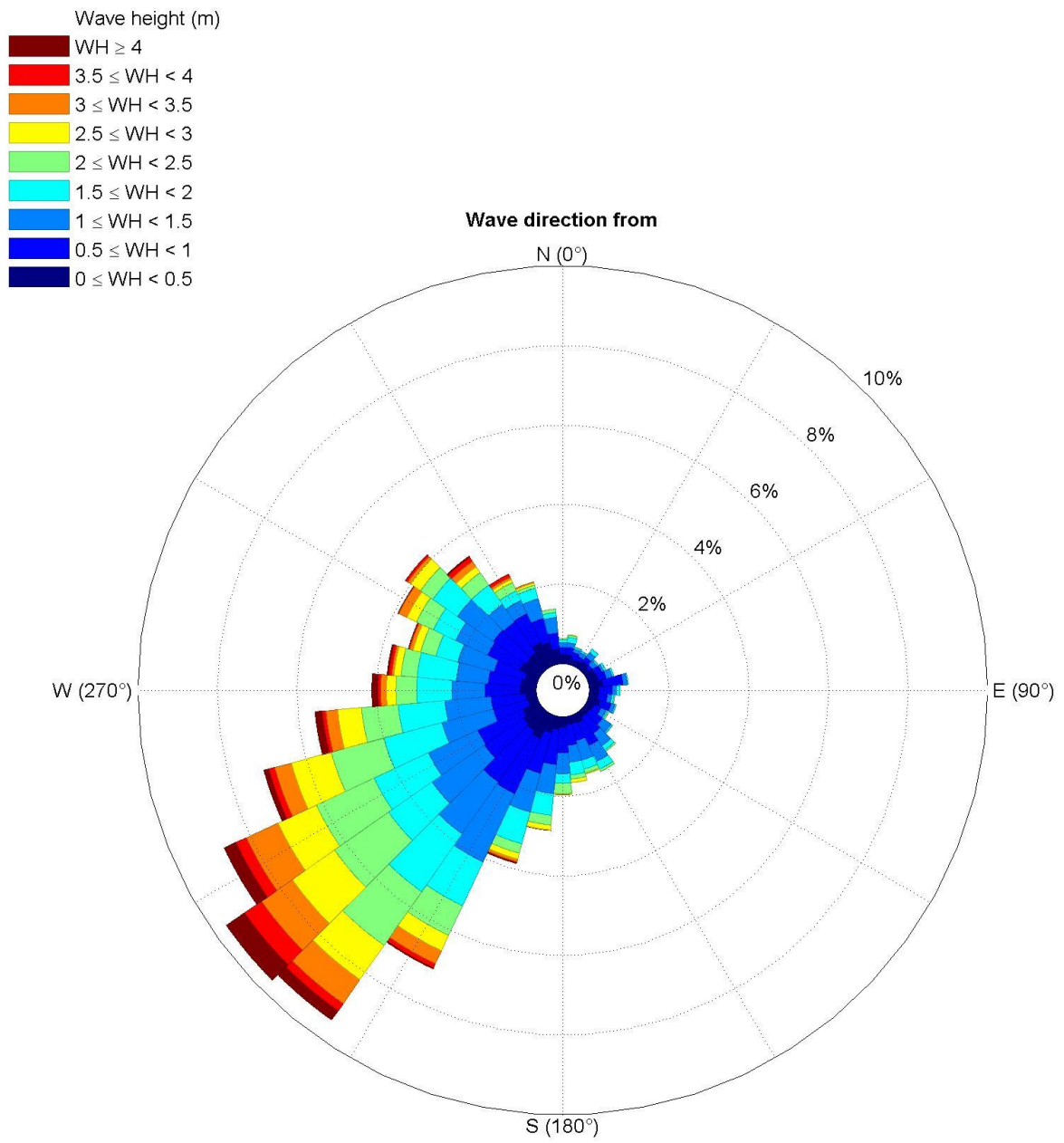


Fig. 3.2.1.12. Occurrence of significant wave height in December.

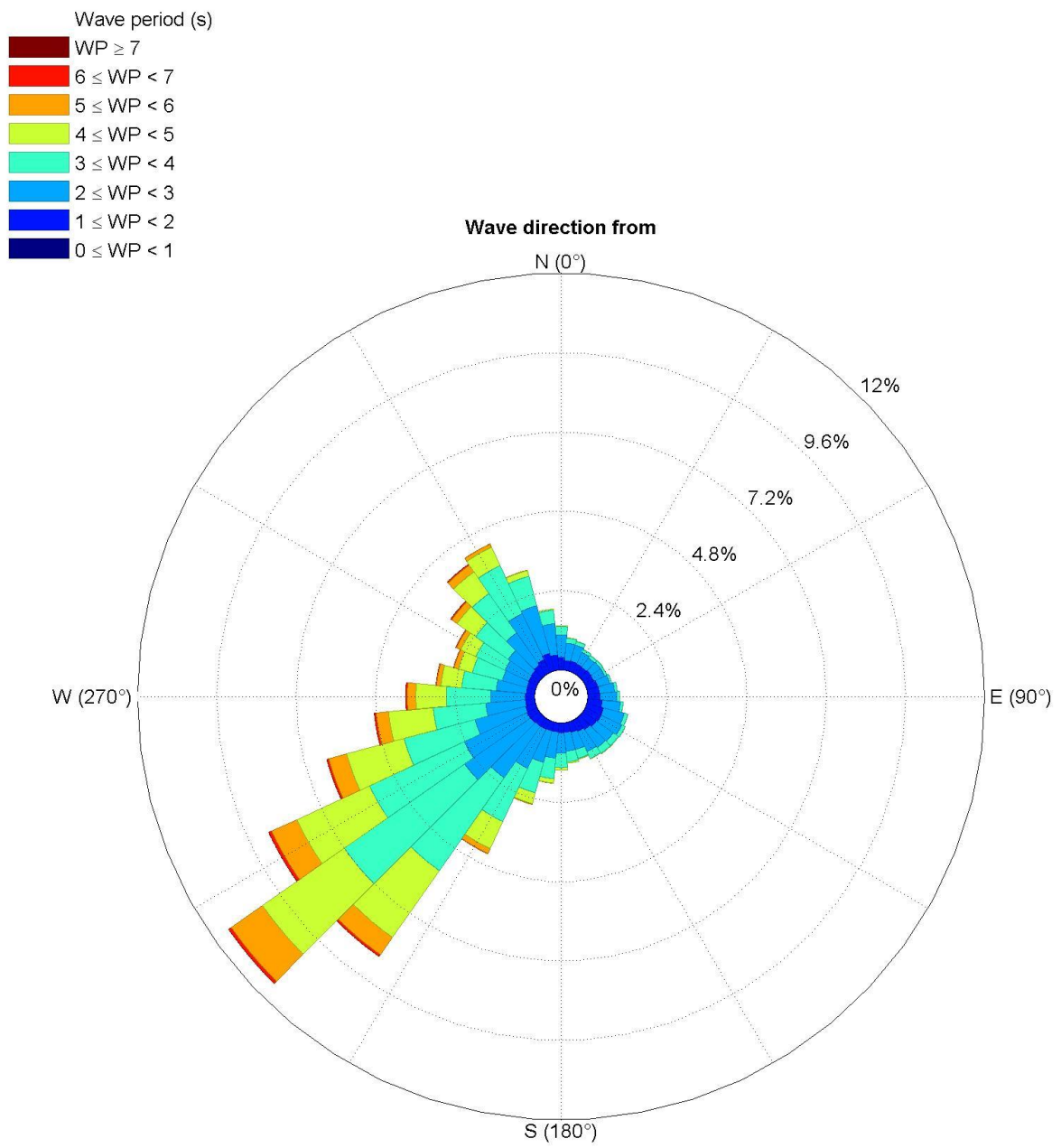


Fig. 3.2.1.13. Annual occurrence of mean wave period.

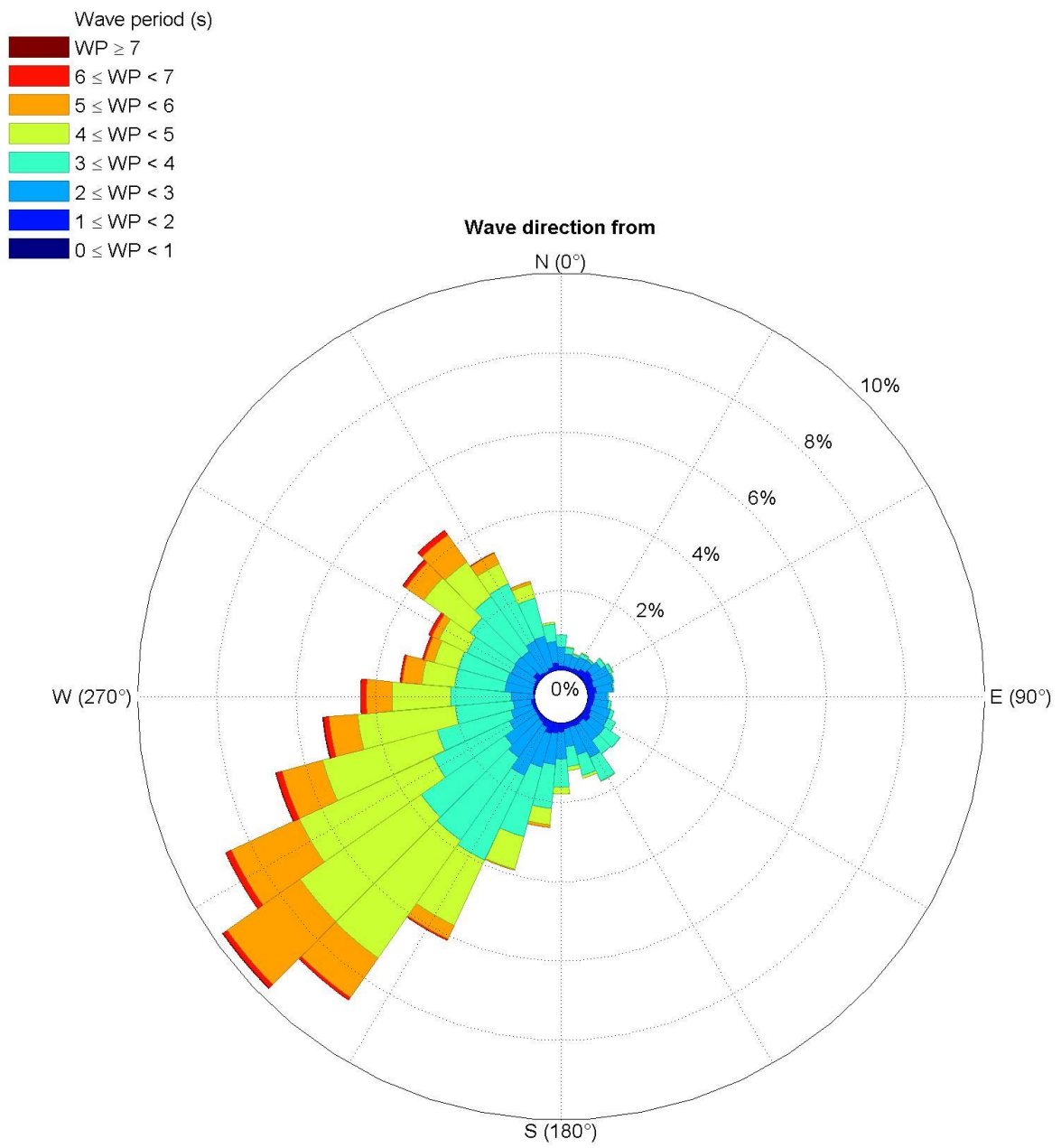


Fig. 3.2.1.14. Occurrence of mean wave period in January.

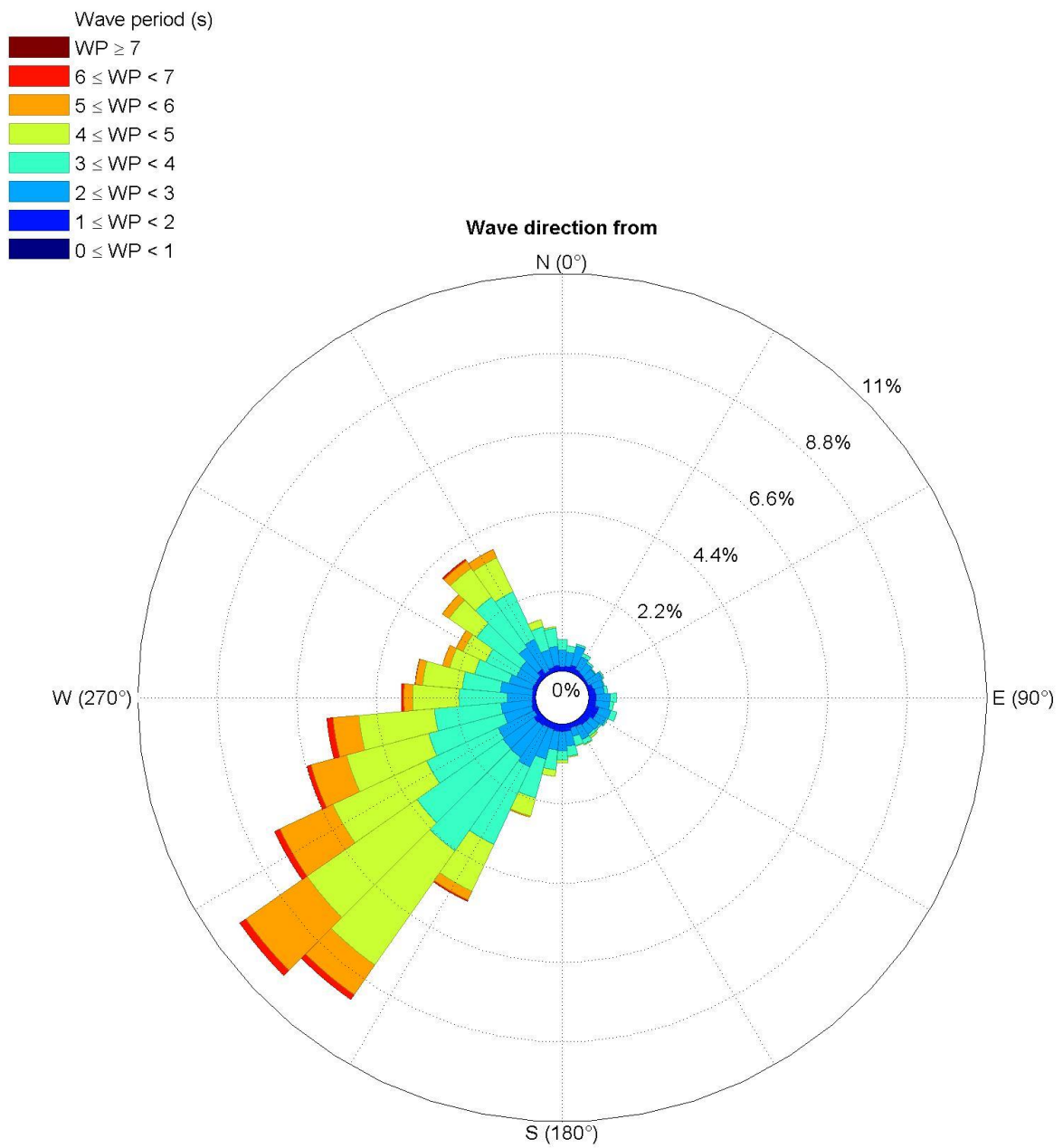


Fig. 3.2.1.15. Occurrence of mean wave period in February.

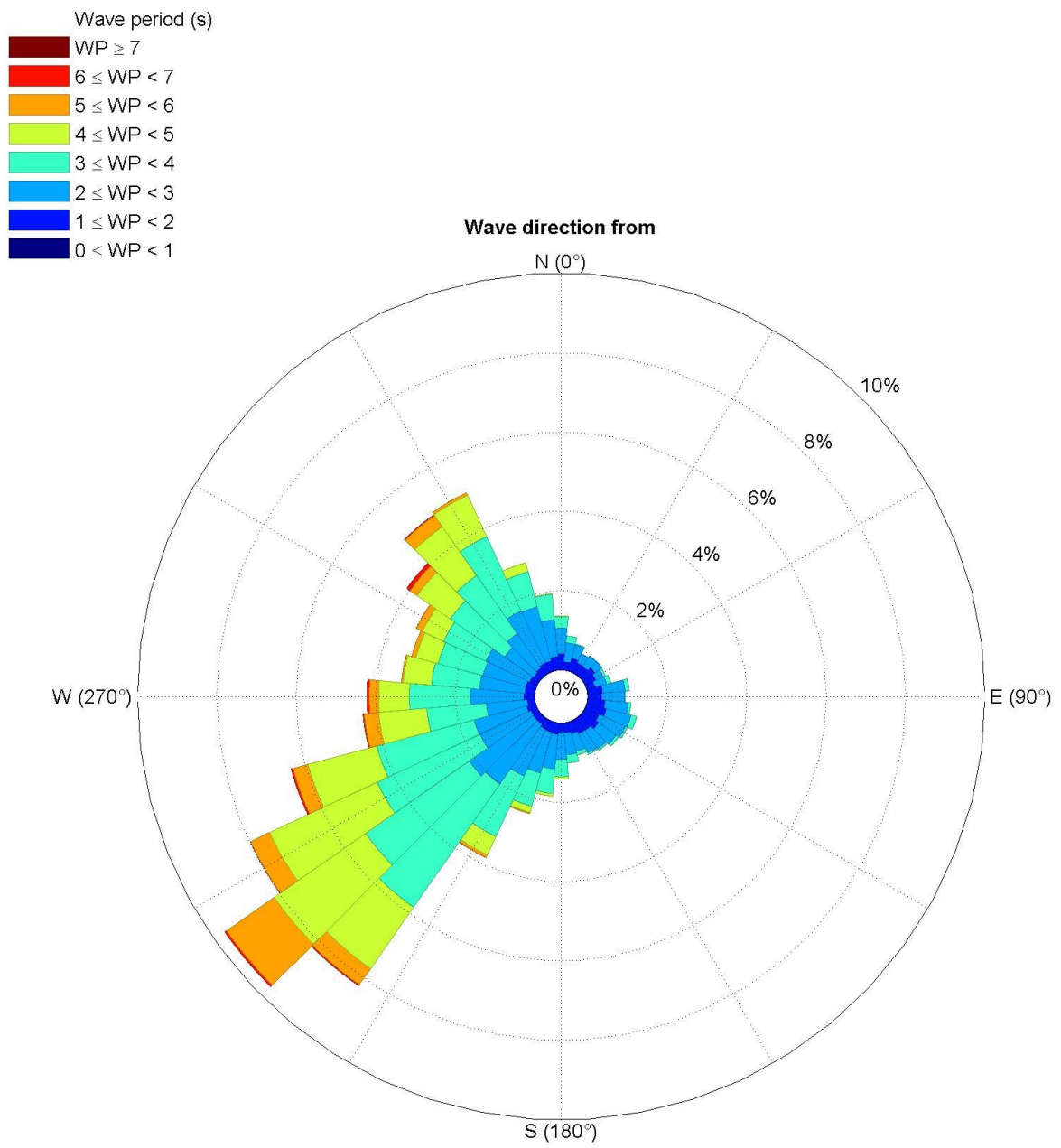


Fig. 3.2.1.16. Occurrence of mean wave period in March.

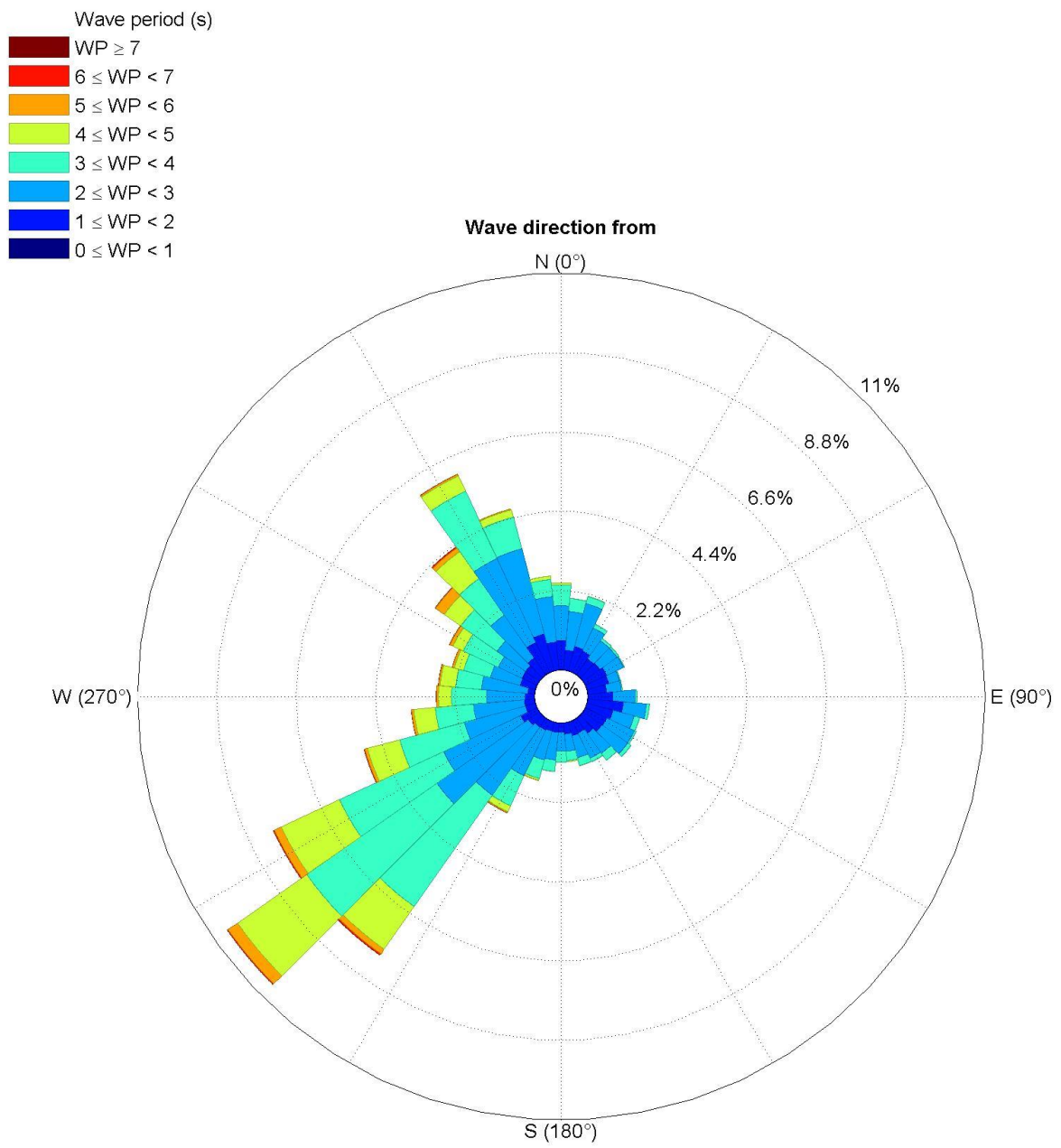


Fig. 3.2.1.17. Occurrence of mean wave period in April.

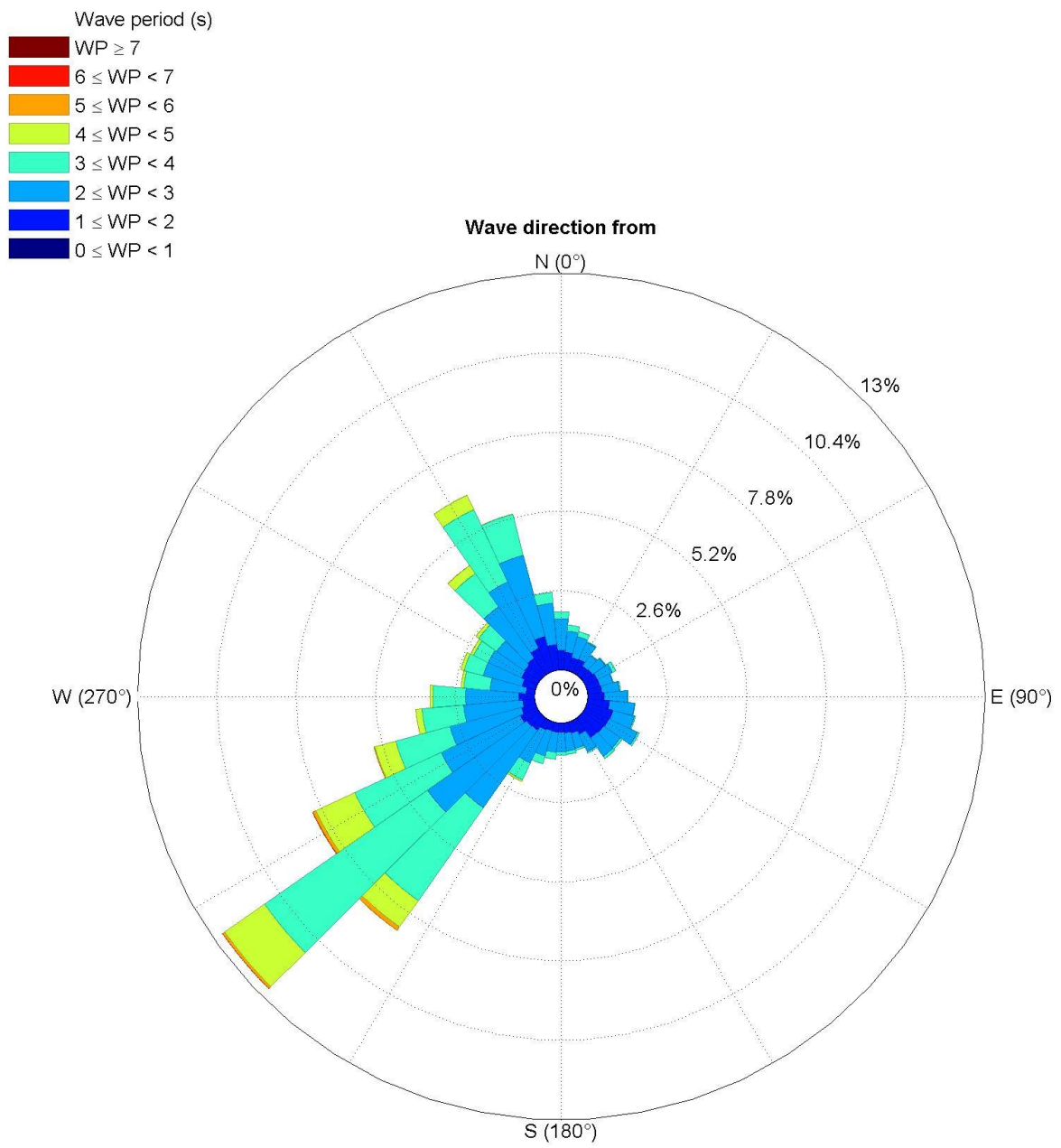


Fig. 3.2.1.18. Occurrence of mean wave period in May.

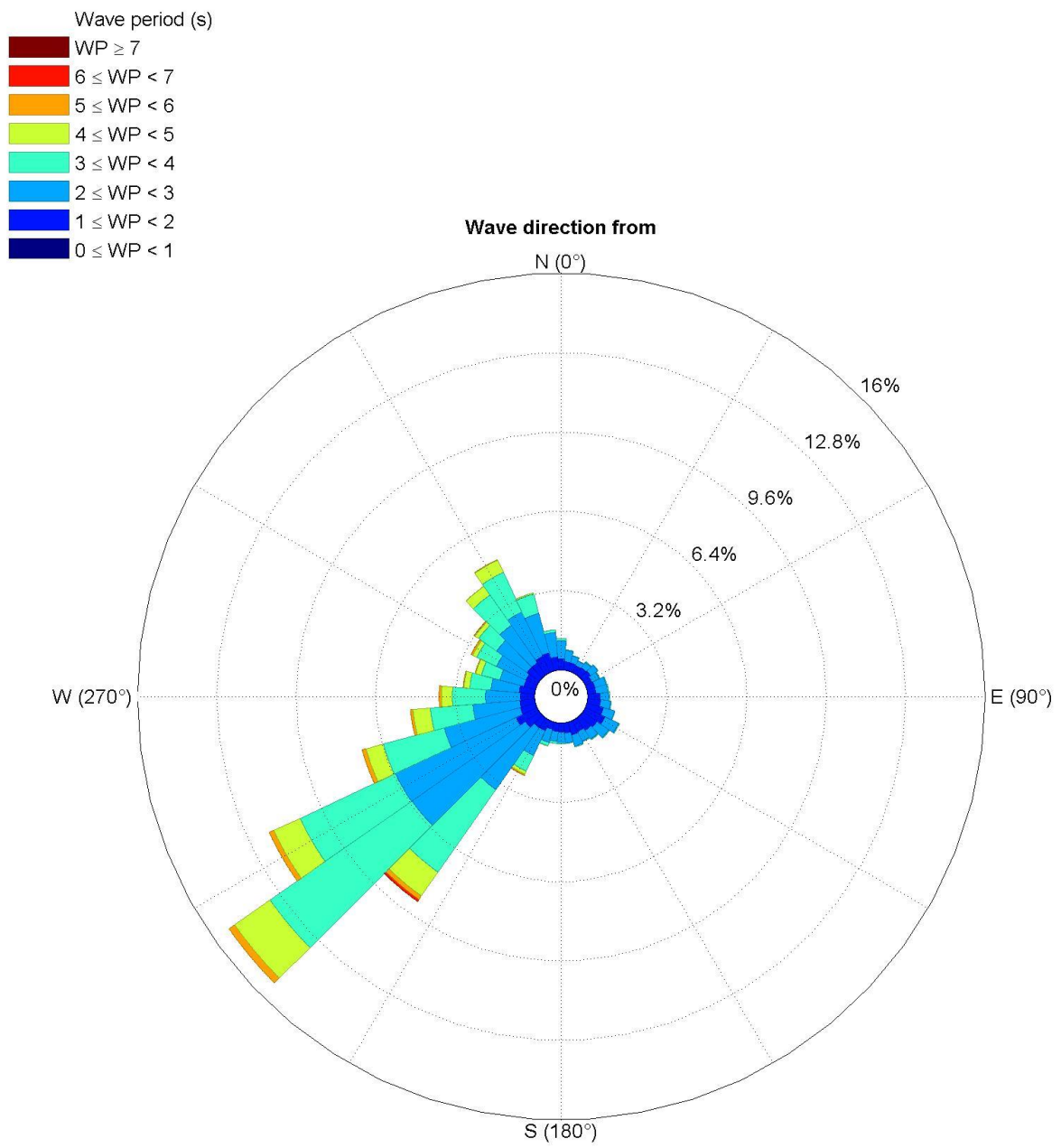


Fig. 3.2.1.19. Occurrence of mean wave period in June.

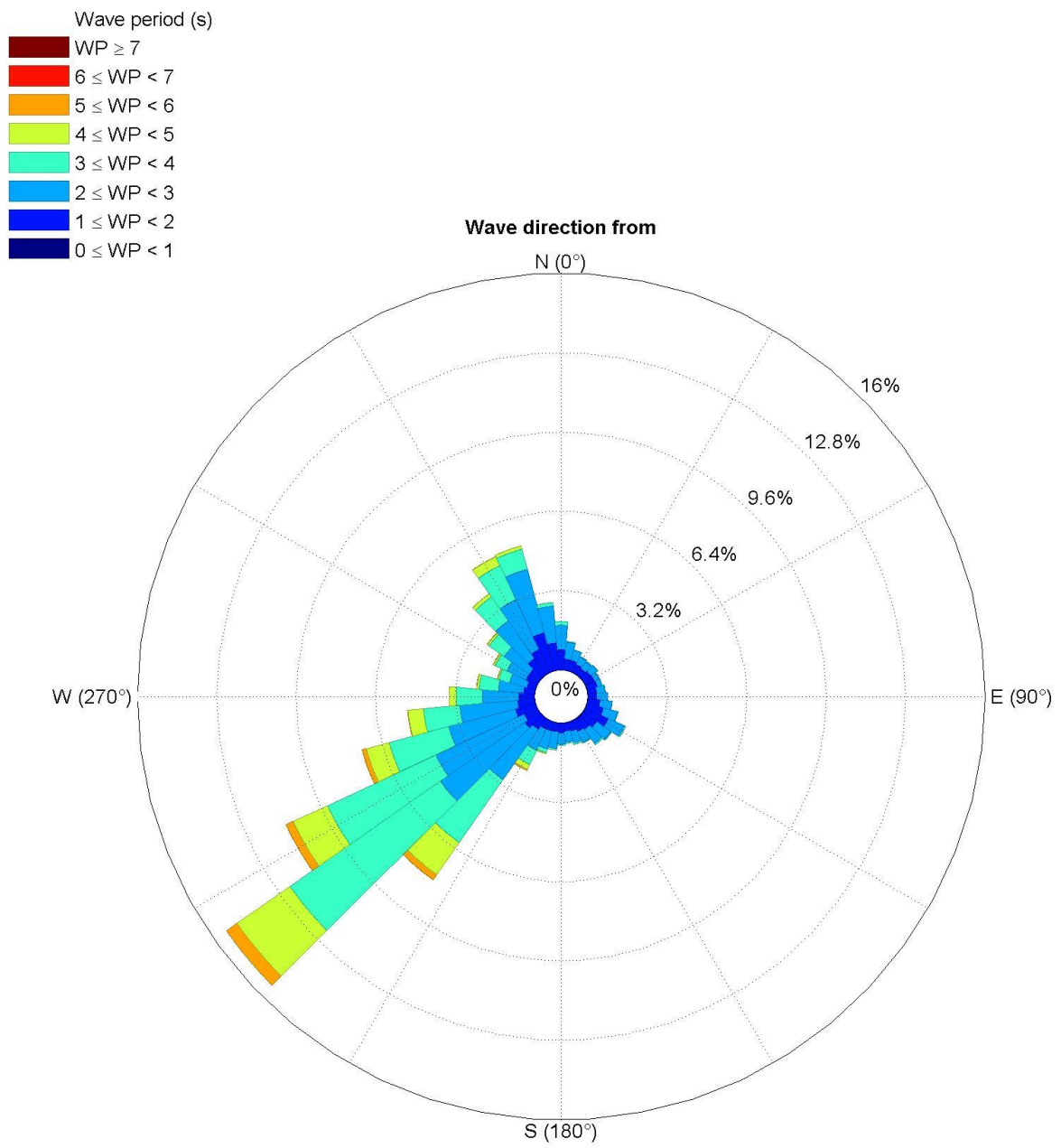


Fig. 3.2.1.20. Occurrence of mean wave period in July.

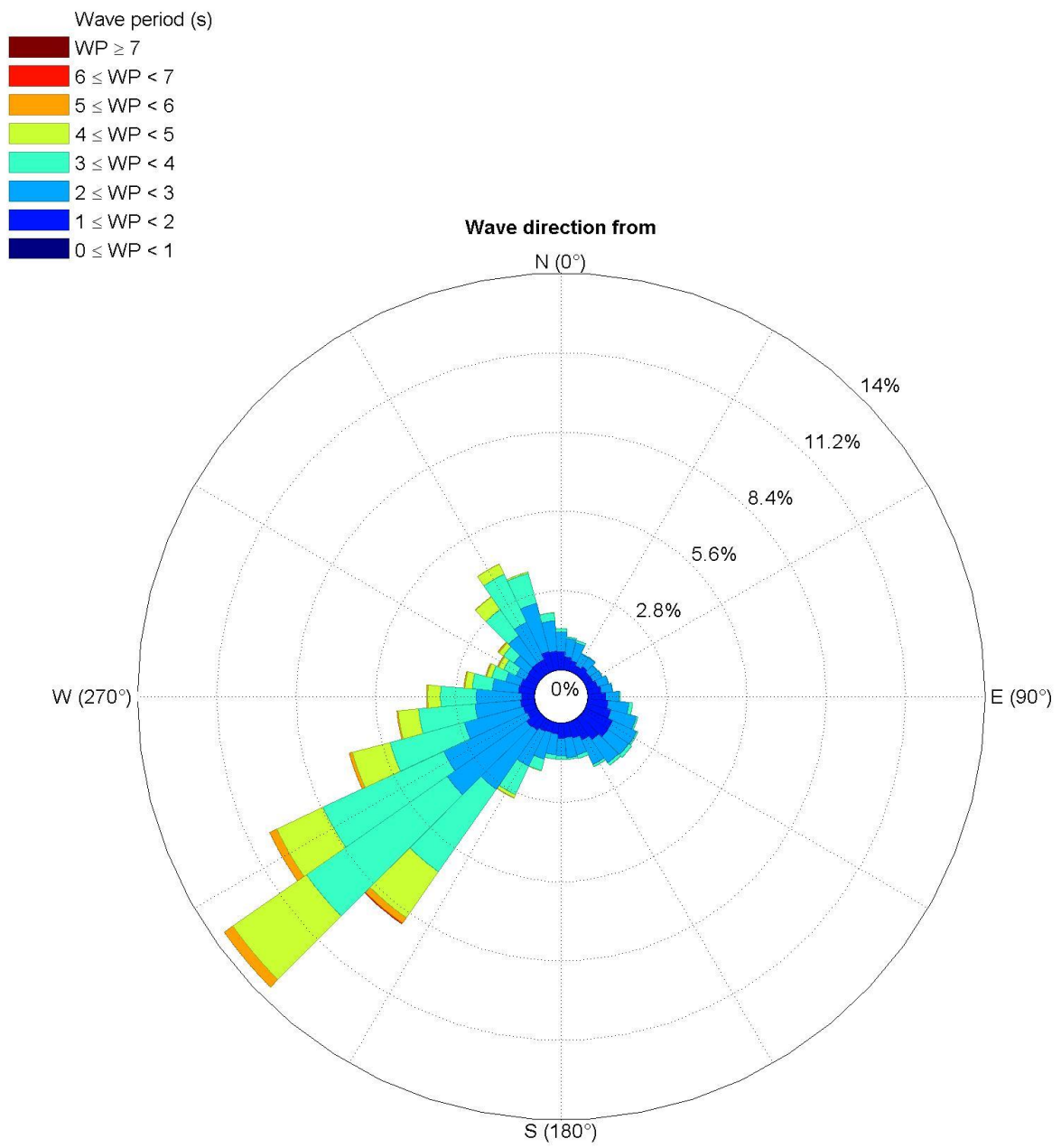


Fig. 3.2.1.21. Occurrence of mean wave period in August.

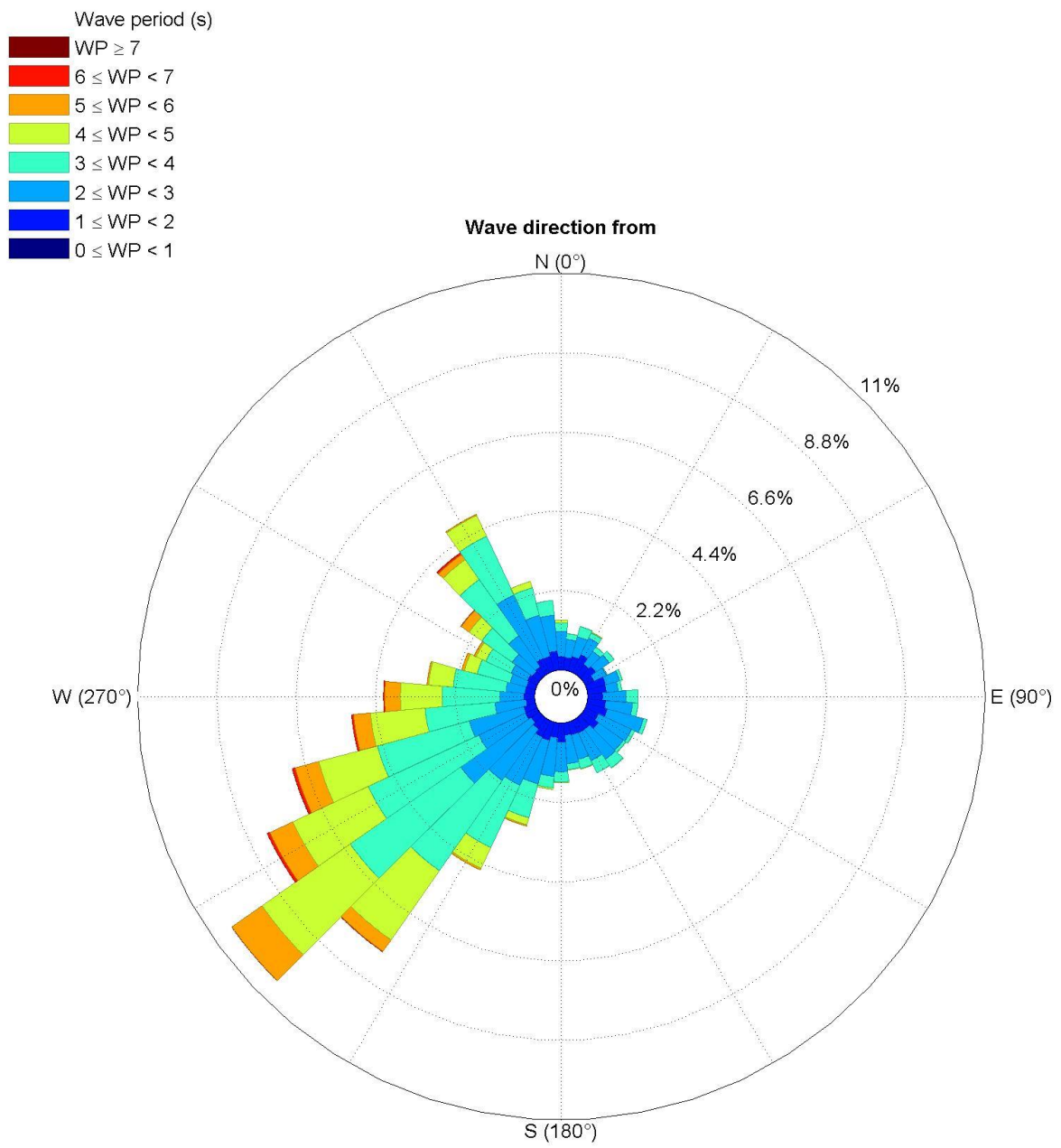


Fig. 3.2.1.22. Occurrence of mean wave period in September.

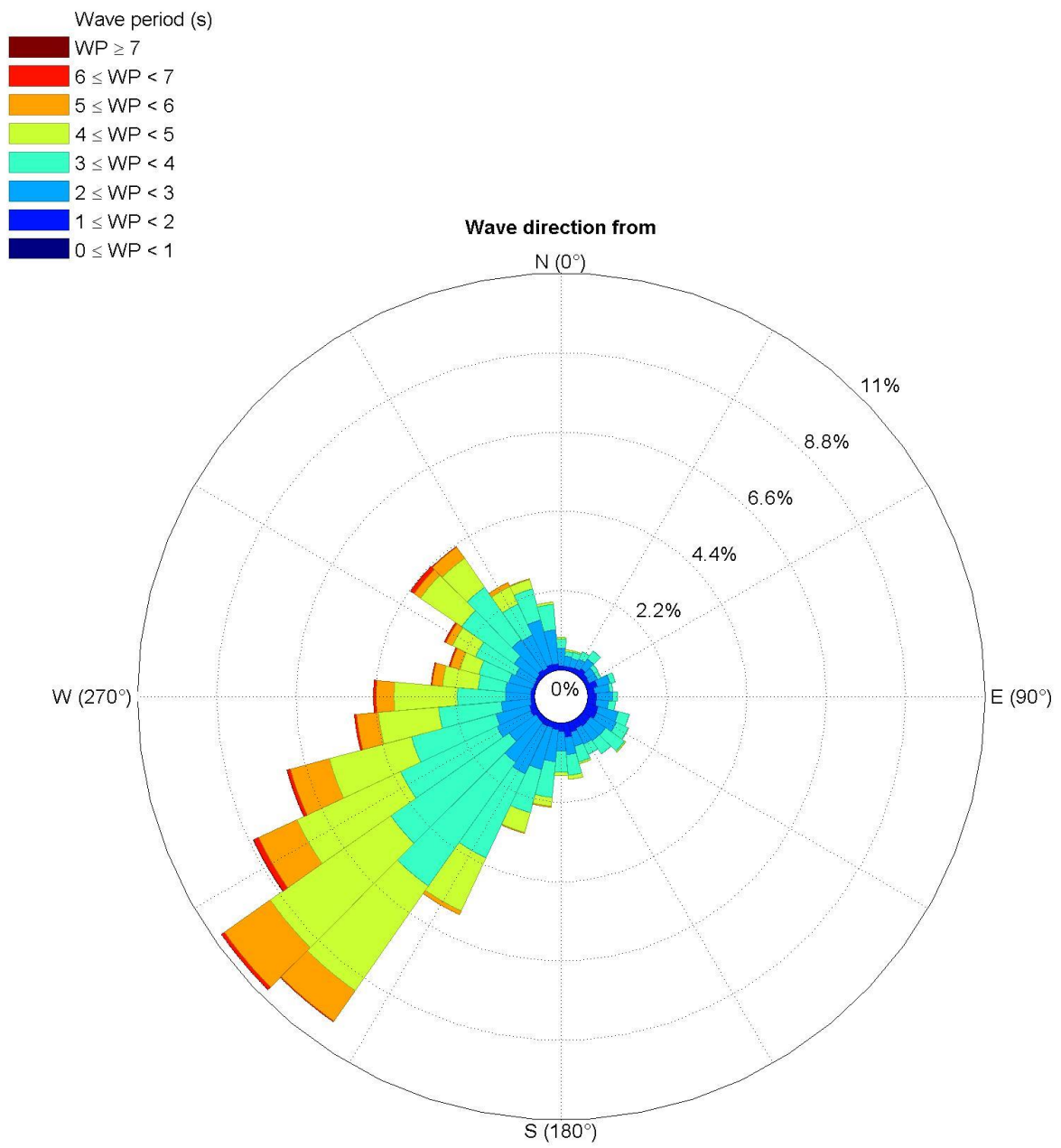


Fig. 3.2.1.23. Occurrence of mean wave period in October.

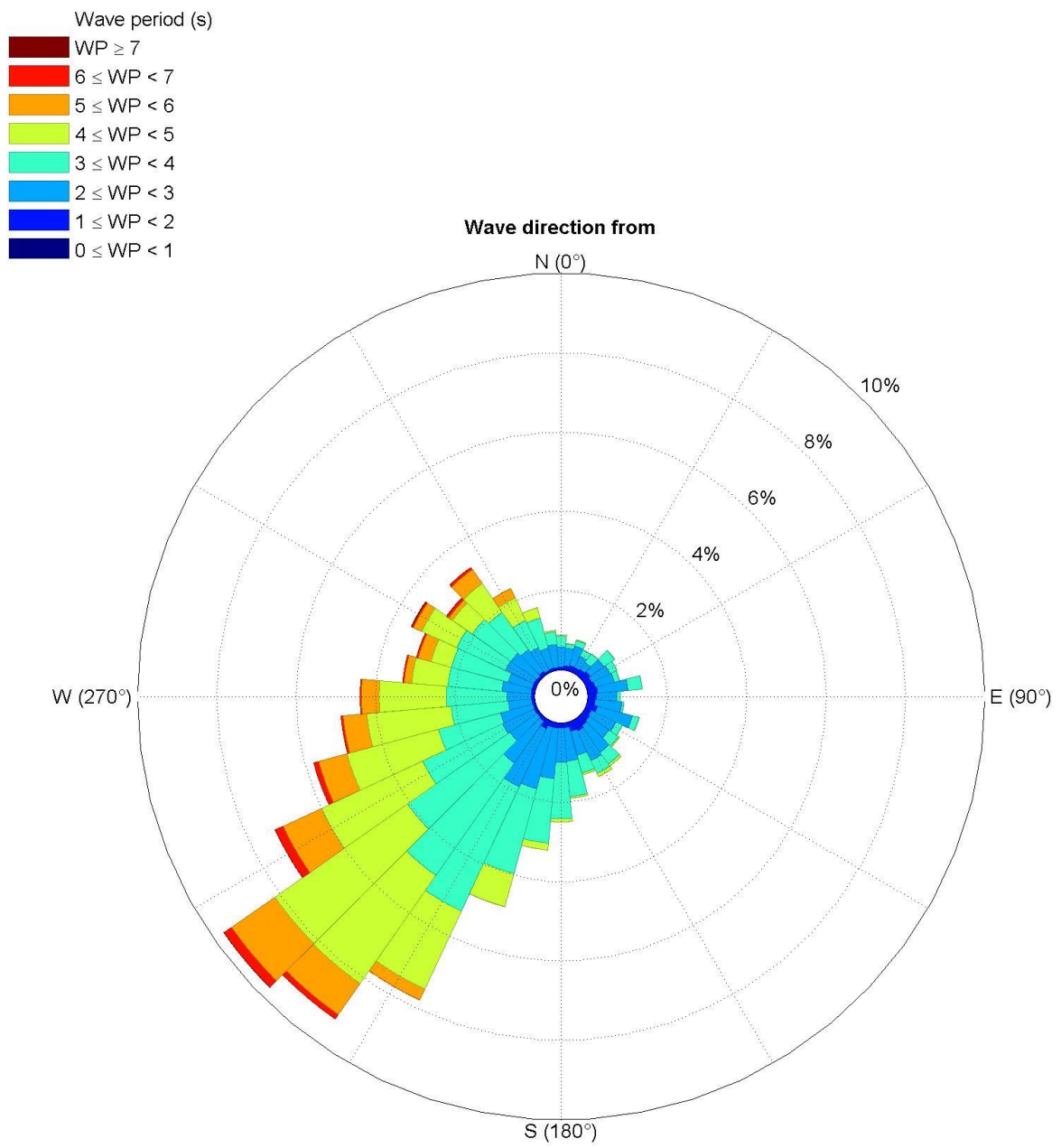


Fig. 3.2.1.24. Occurrence of mean wave period in November.

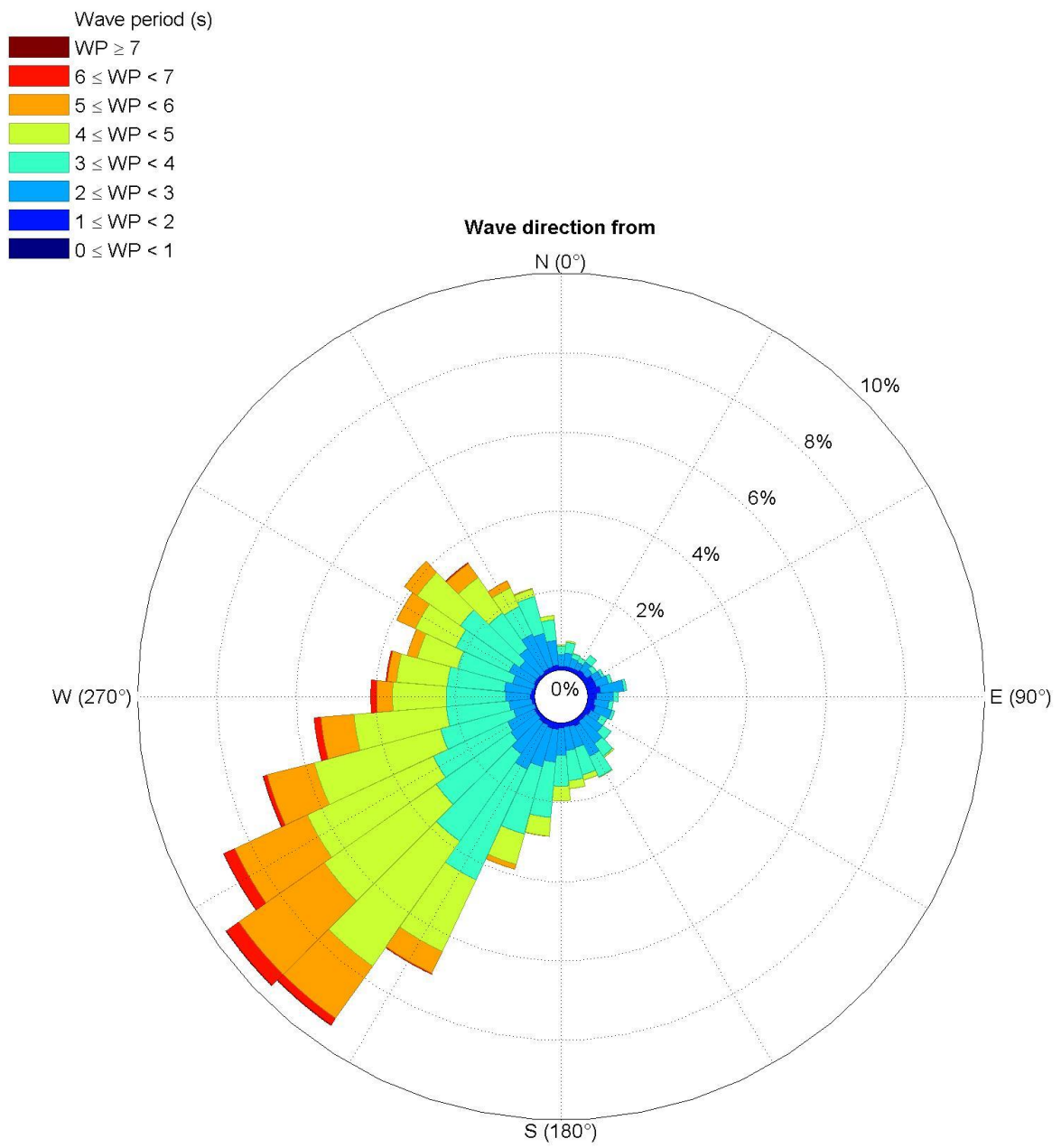


Fig. 3.2.1.25. Occurrence of mean wave period in December.

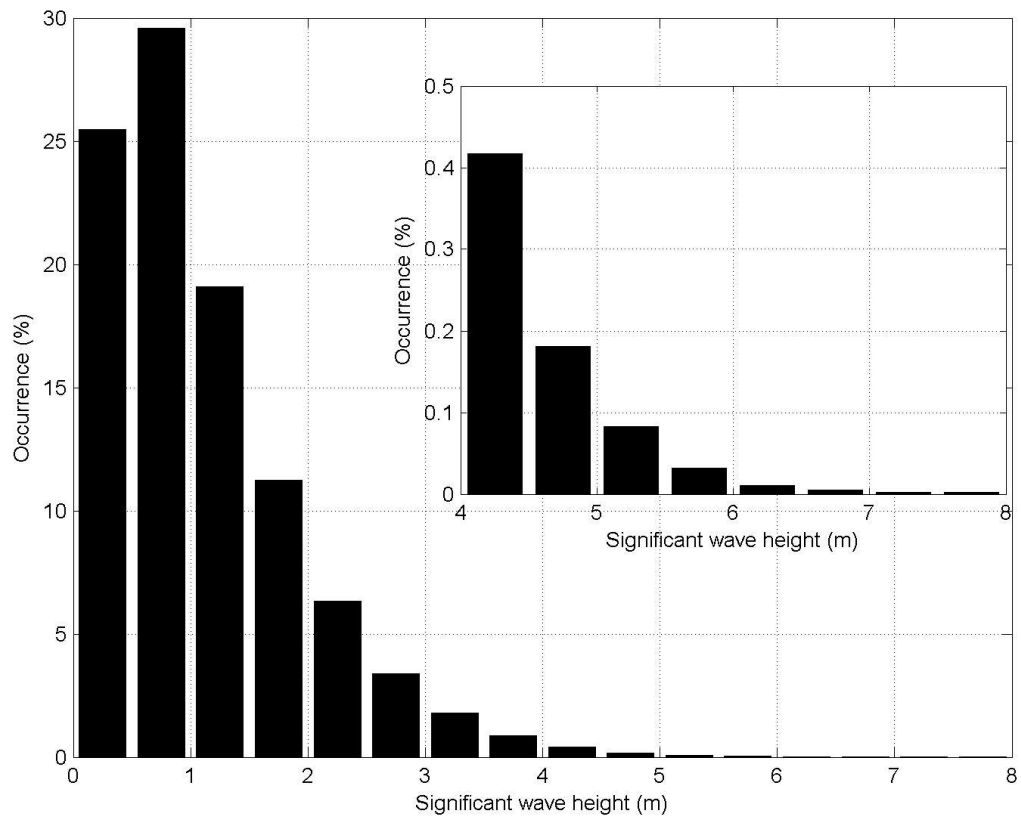


Fig. 3.2.1.26. Occurrence of significant wave height

3.2.2. Extreme wave conditions

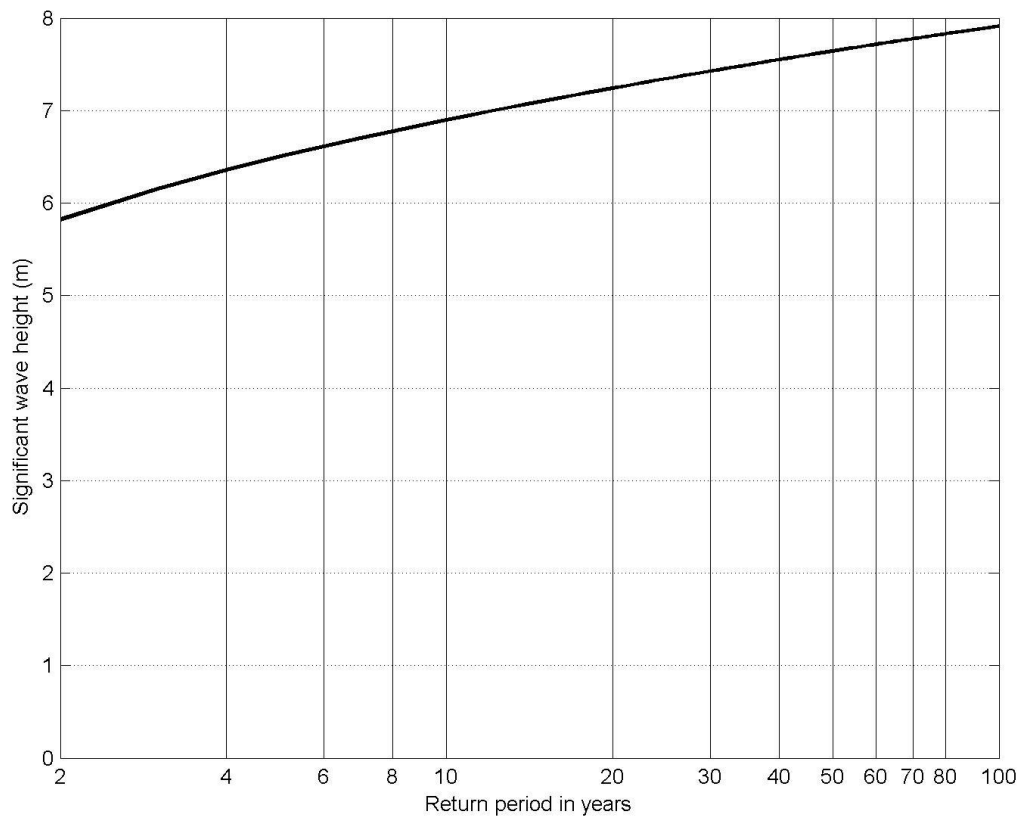


Fig. 3.2.2.1. Return periods of significant wave height.

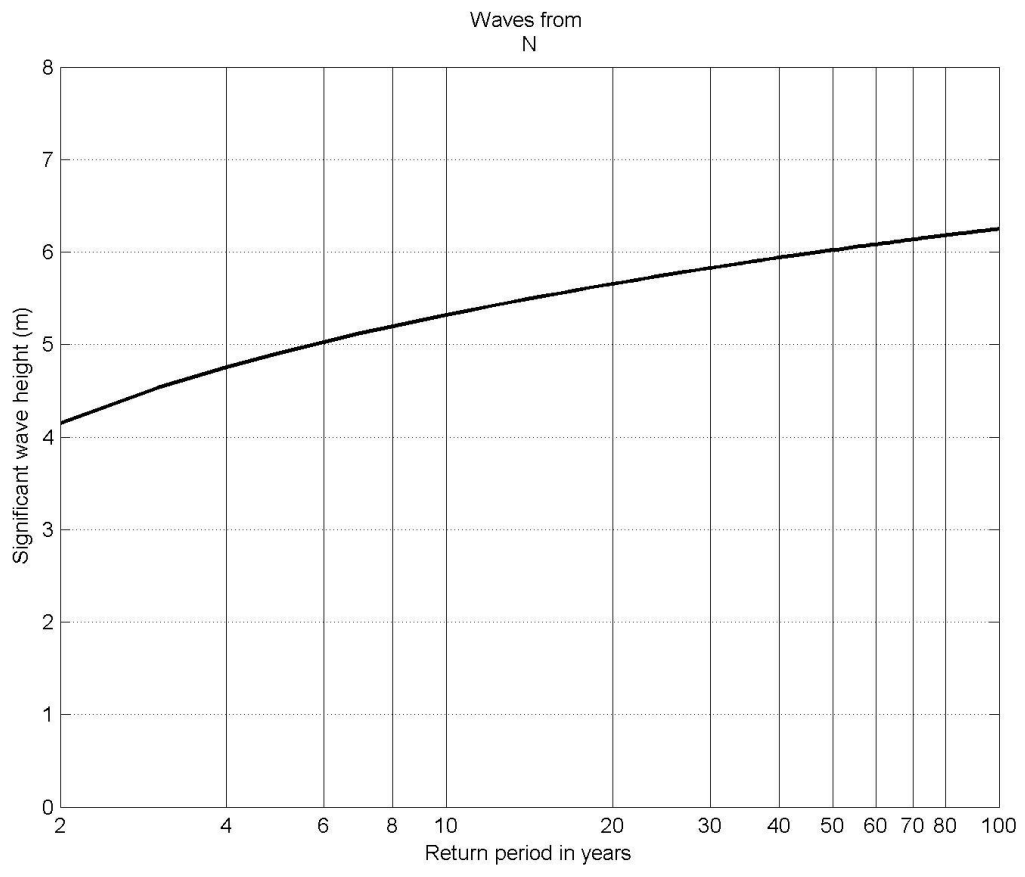


Fig. 3.2.2.2. Return periods of significant wave height from north.

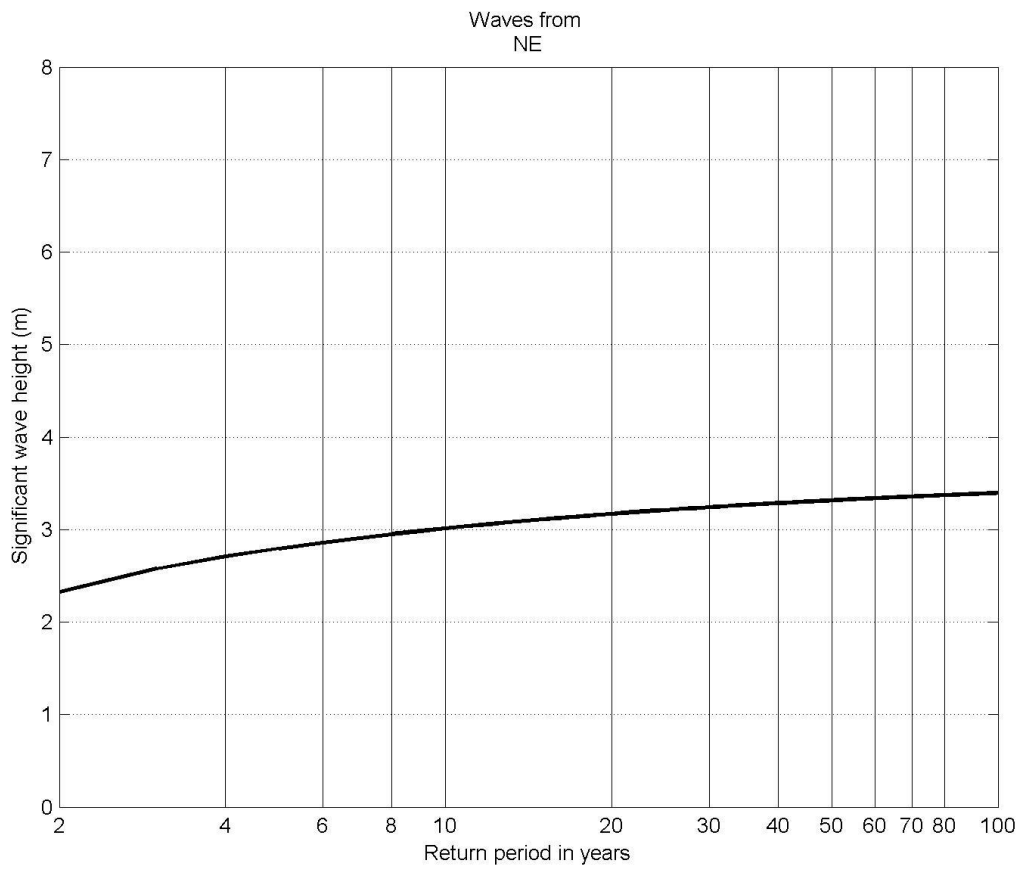


Fig. 3.2.2.3. Return periods of significant wave height from northeast.

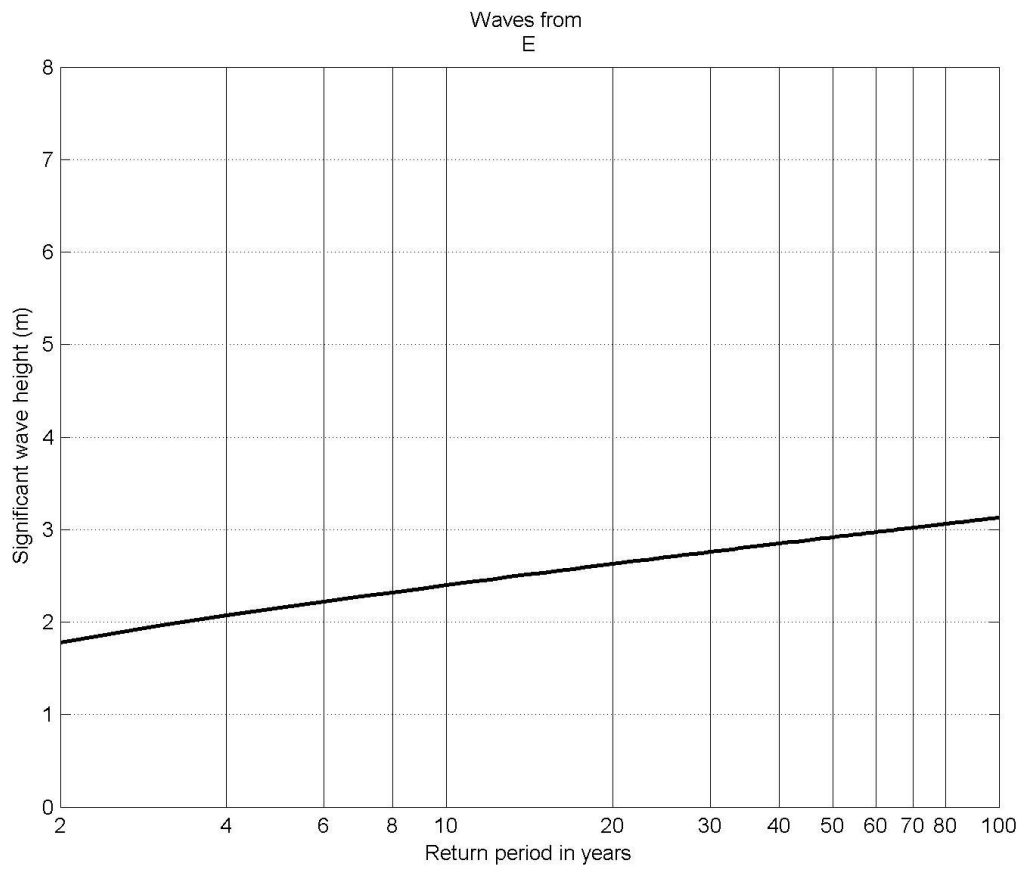


Fig. 3.2.2.4. Return periods of significant wave height from east.

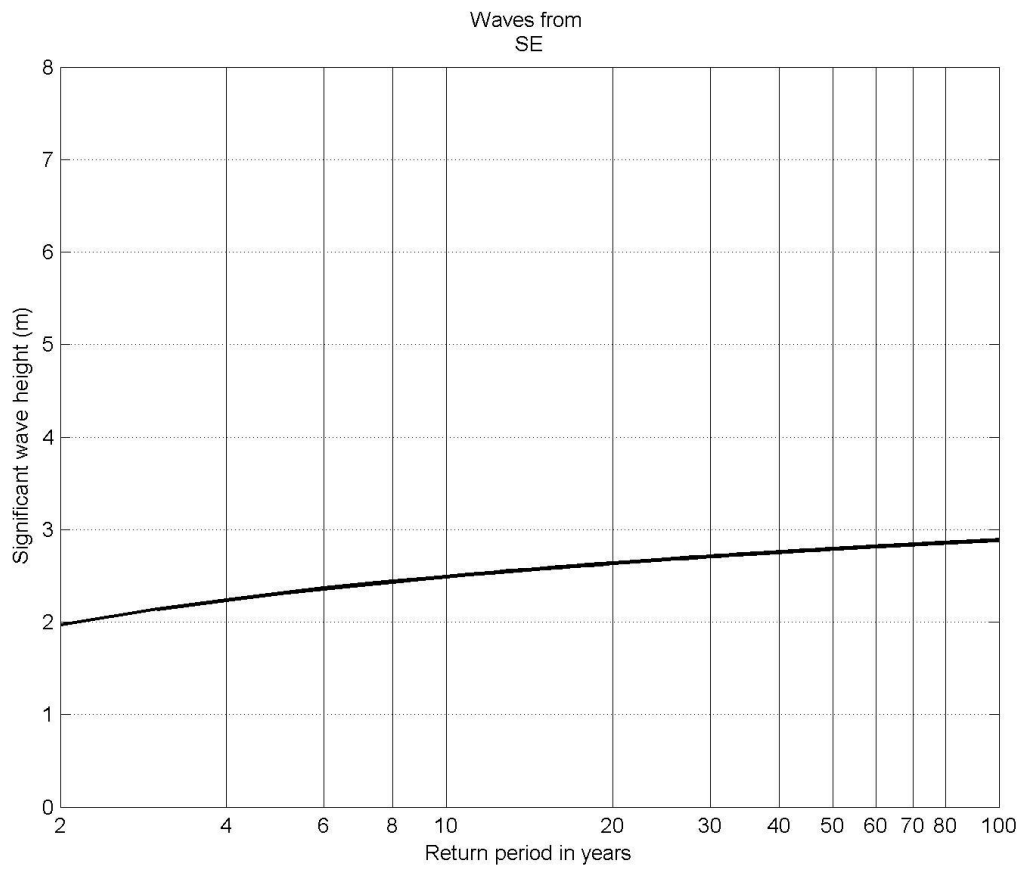


Fig. 3.2.2.5. Return periods of significant wave height from southeast.

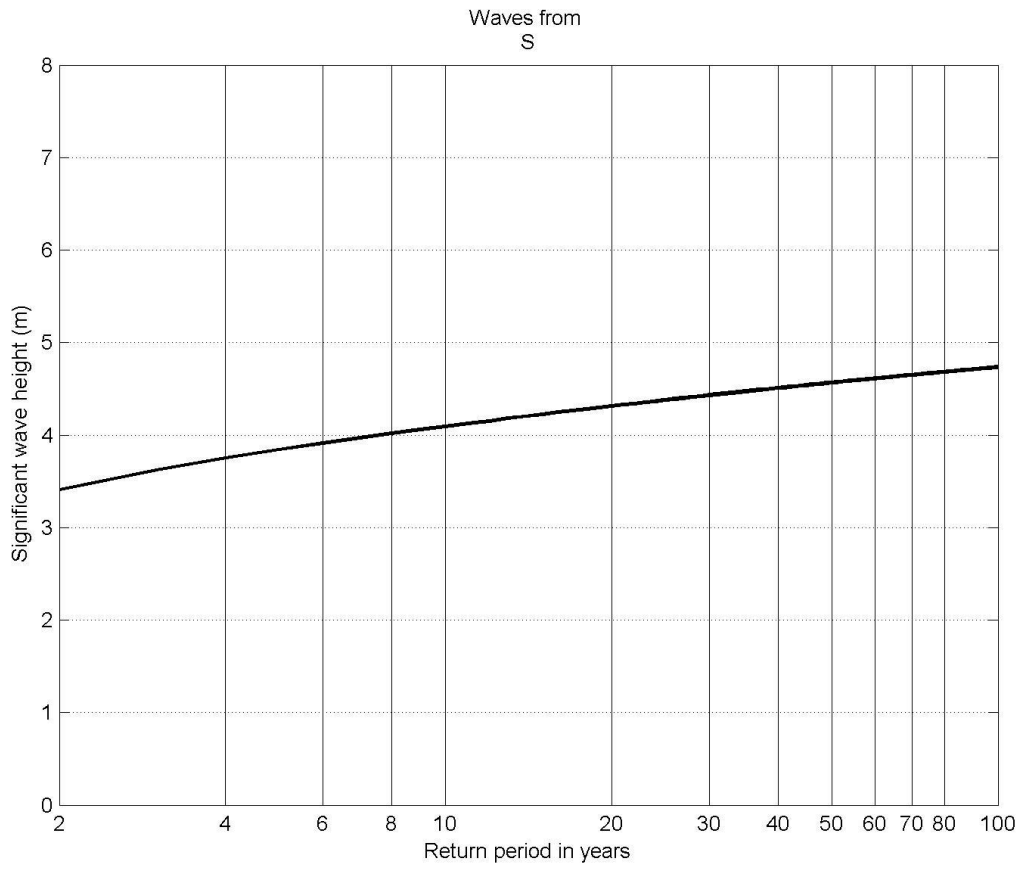


Fig. 3.2.2.6. Return periods of significant wave height from south.

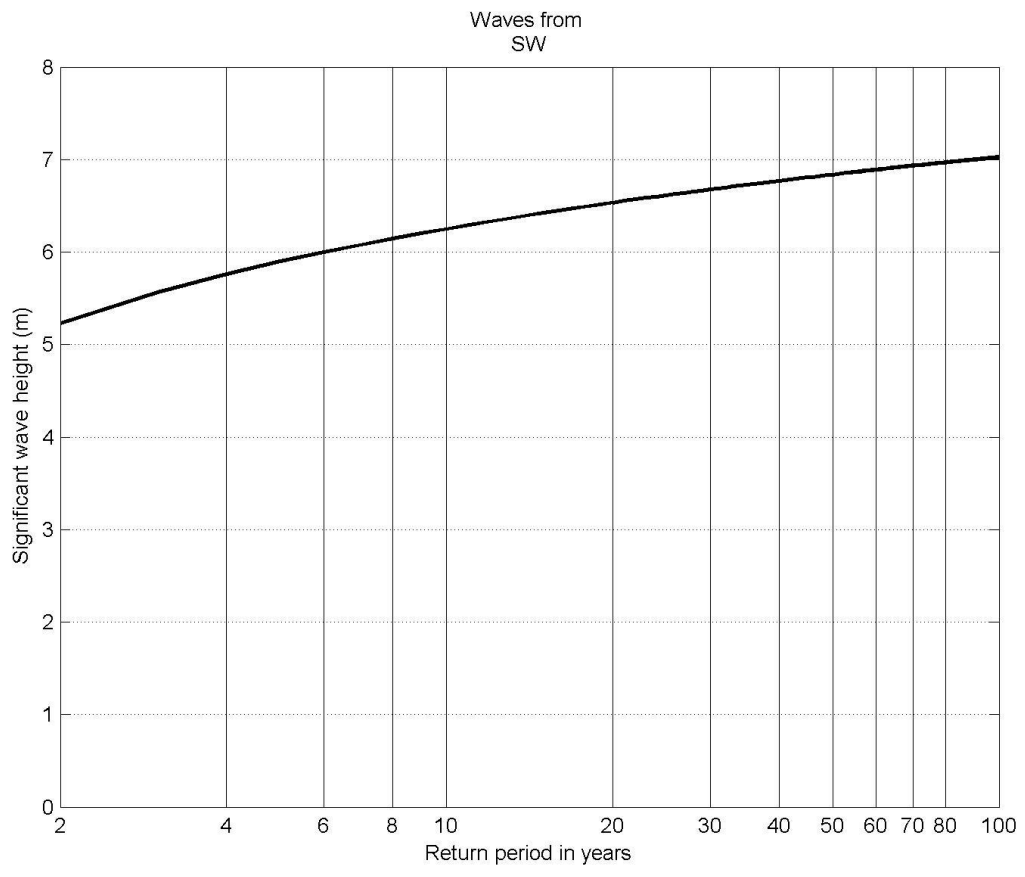


Fig. 3.2.2.7. Return periods of significant wave height from southwest.

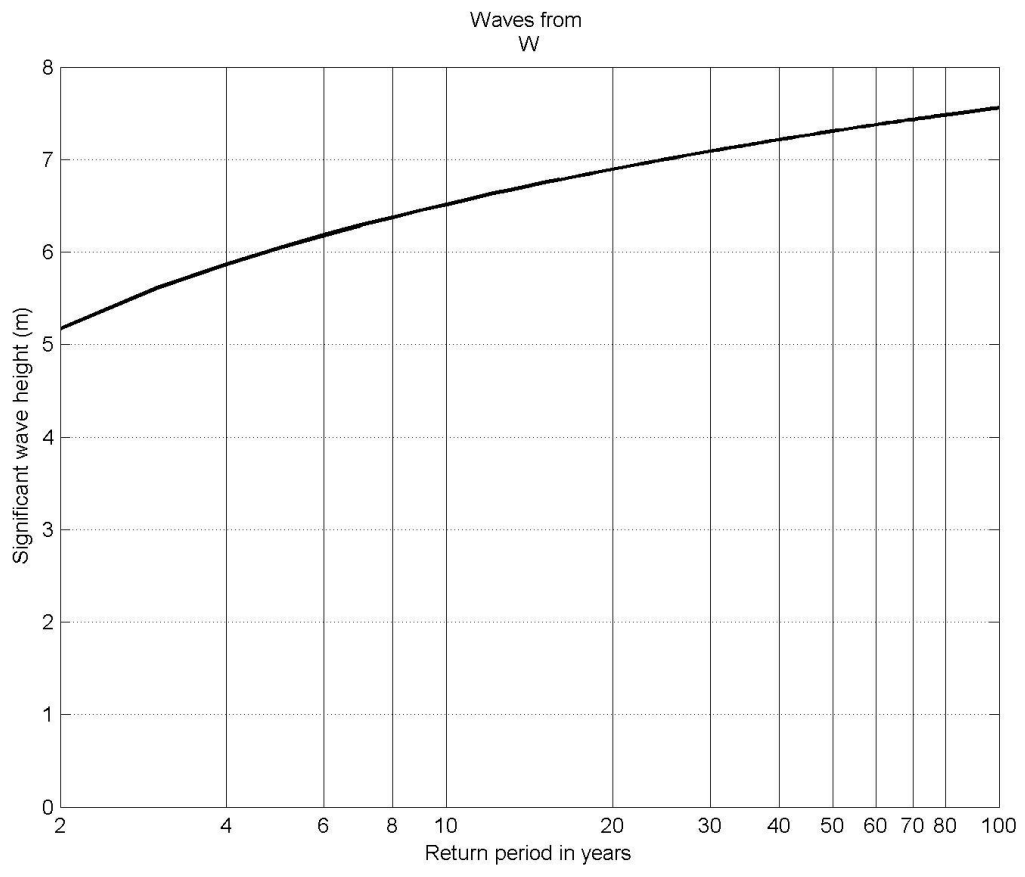


Fig. 3.2.2.8. Return periods of significant wave height from west.

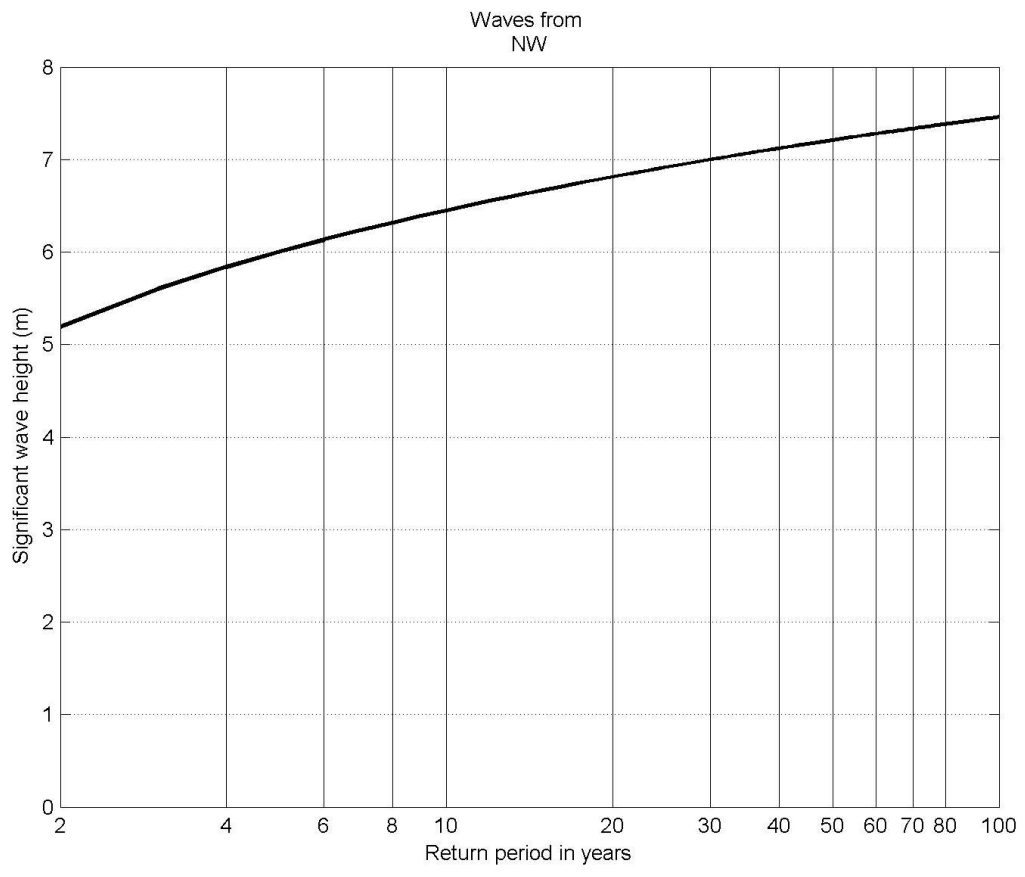


Fig. 3.2.2.9. Return periods of significant wave height from northwest.

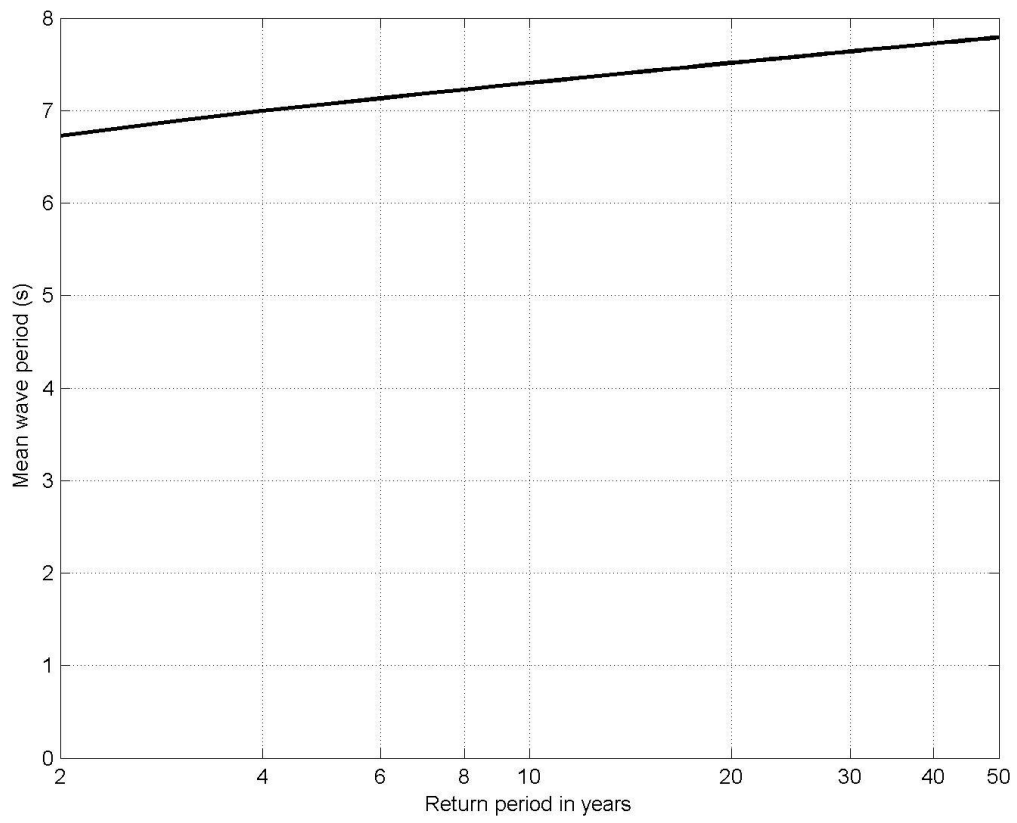


Fig. 3.2.2.10. Return periods of mean wave period.

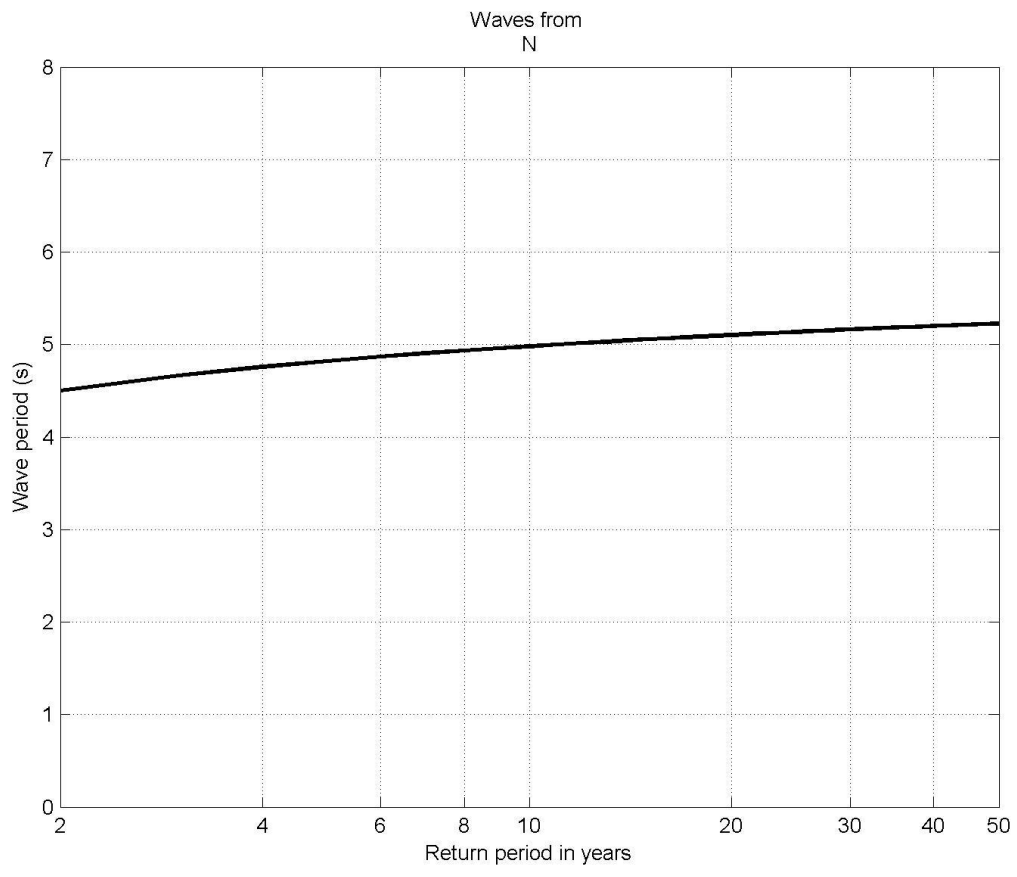


Fig. 3.2.2.11. Return periods of mean wave period from north.

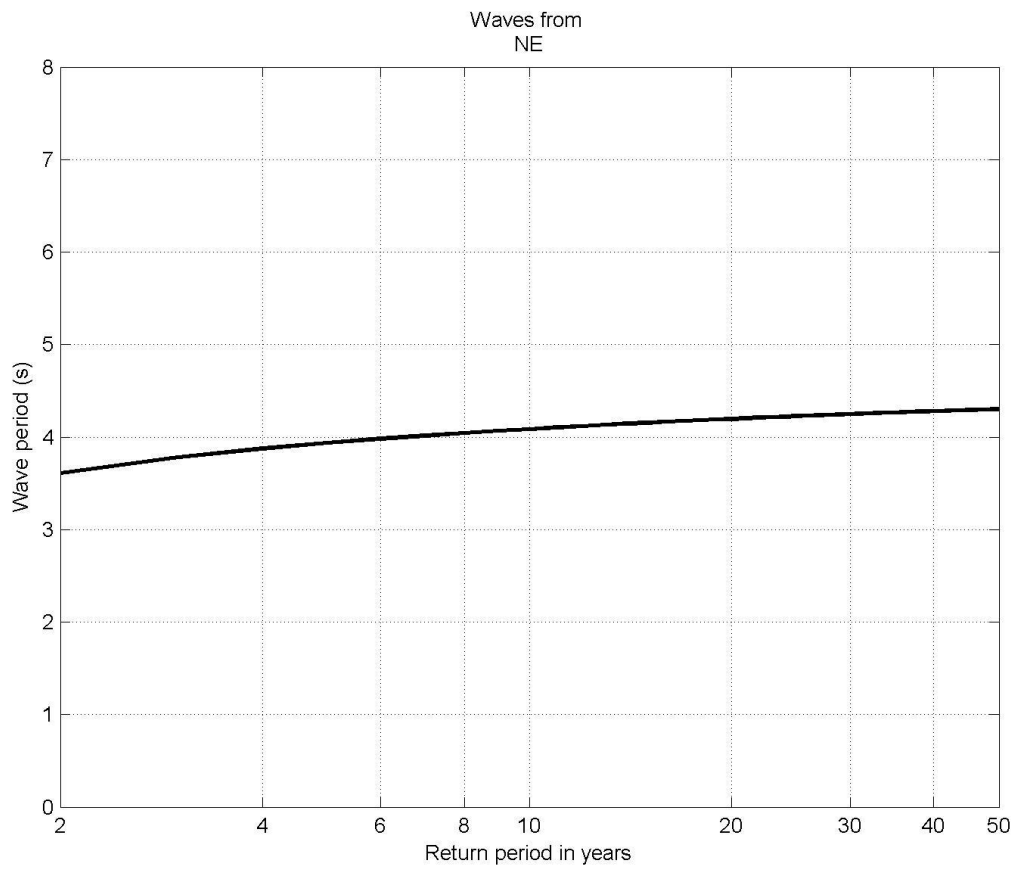


Fig. 3.2.2.12. Return periods of mean wave period from northeast.

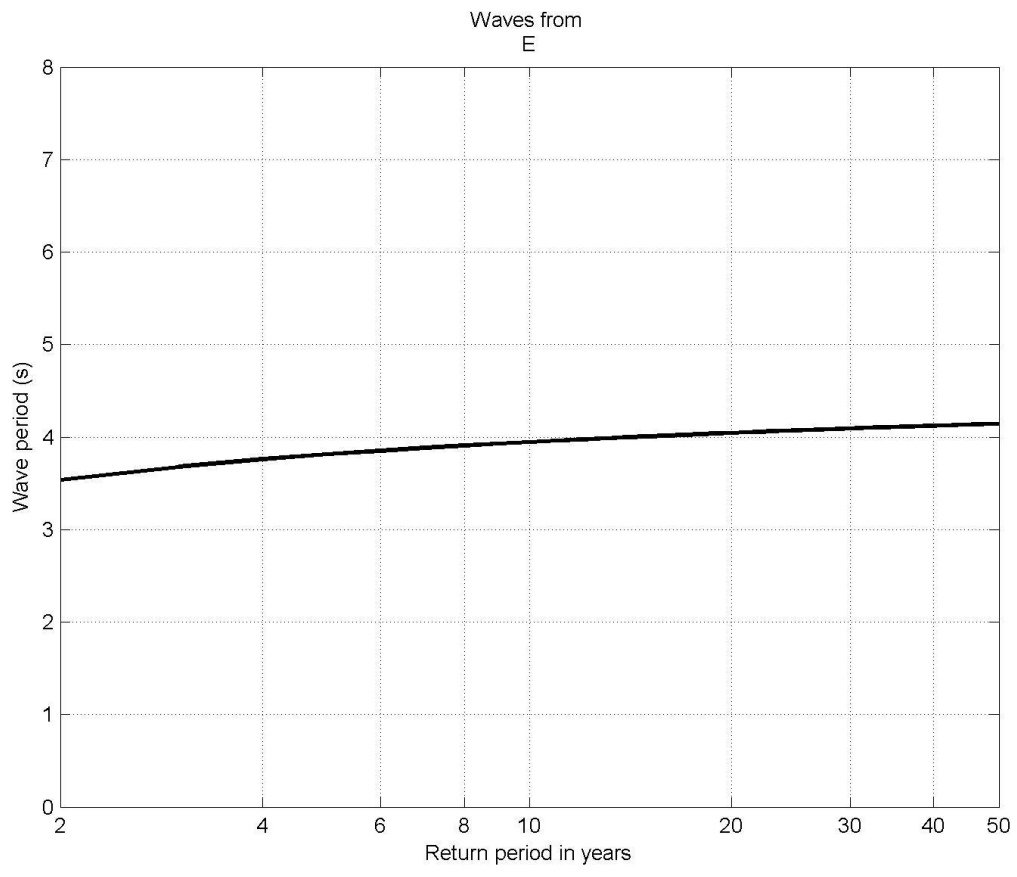


Fig. 3.2.2.13. Return periods of mean wave period from east.

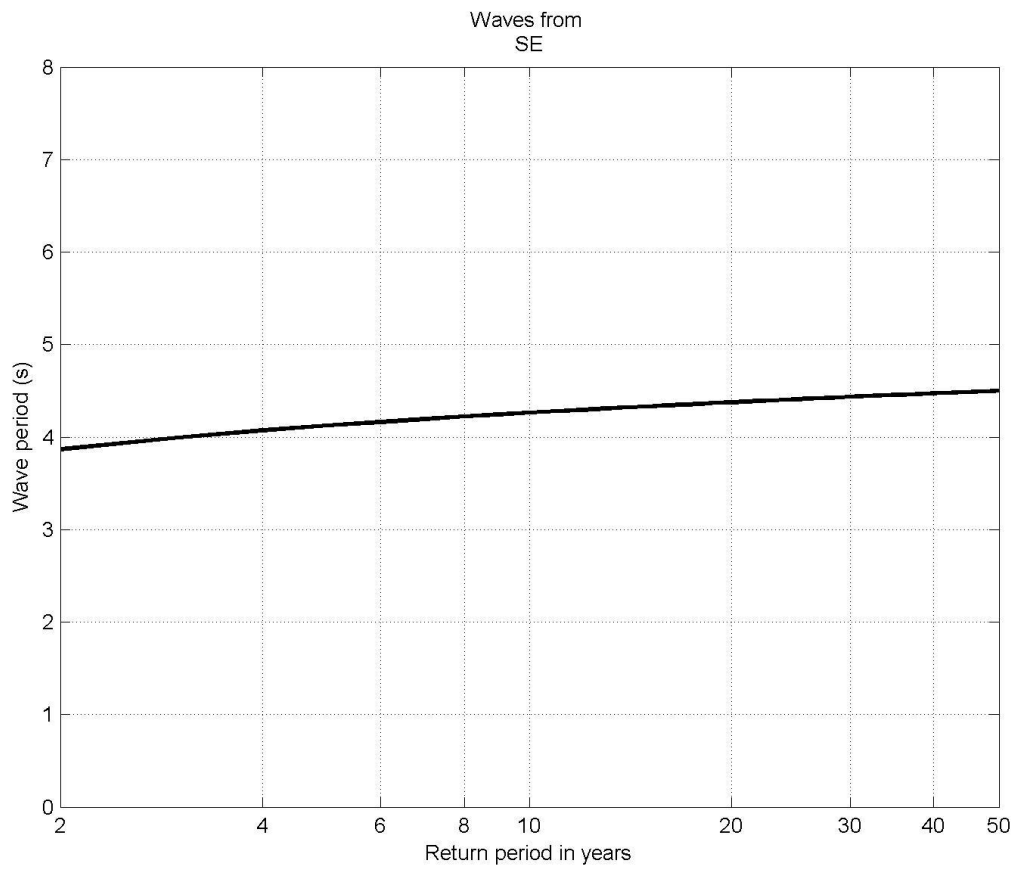


Fig. 3.2.2.14. Return periods of mean wave period from southeast.

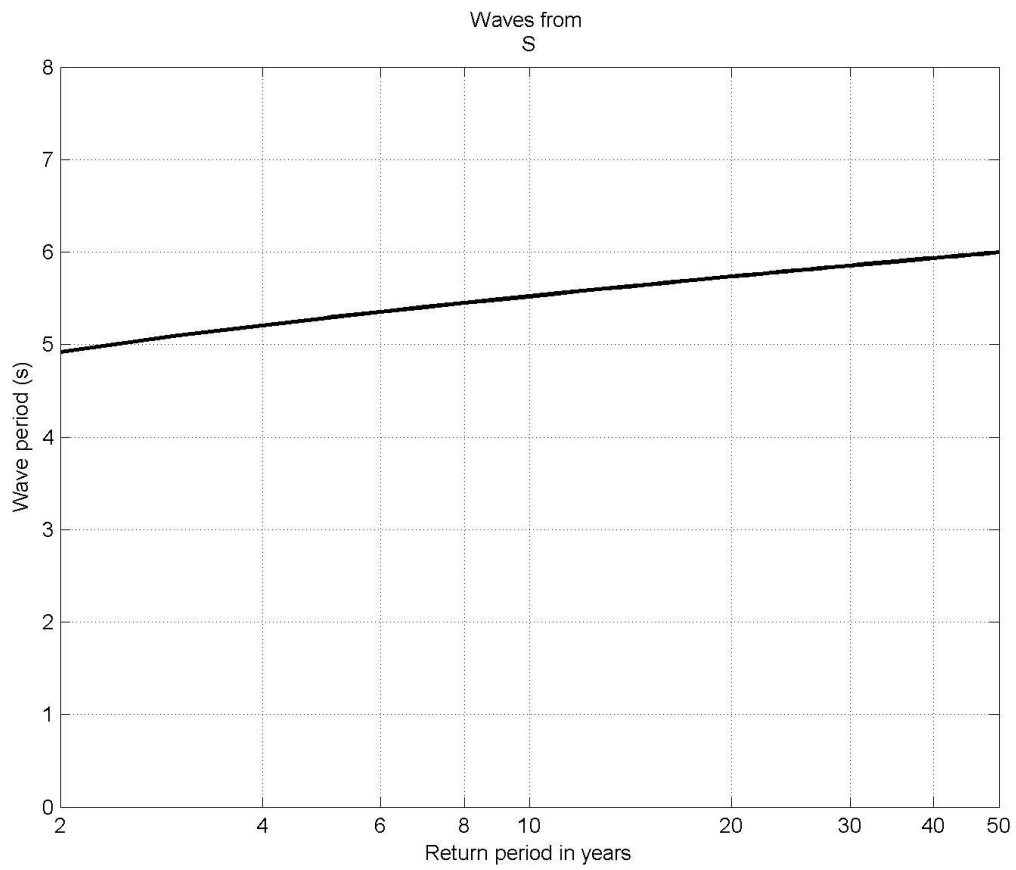


Fig. 3.2.2.15. Return periods of mean wave period from south.

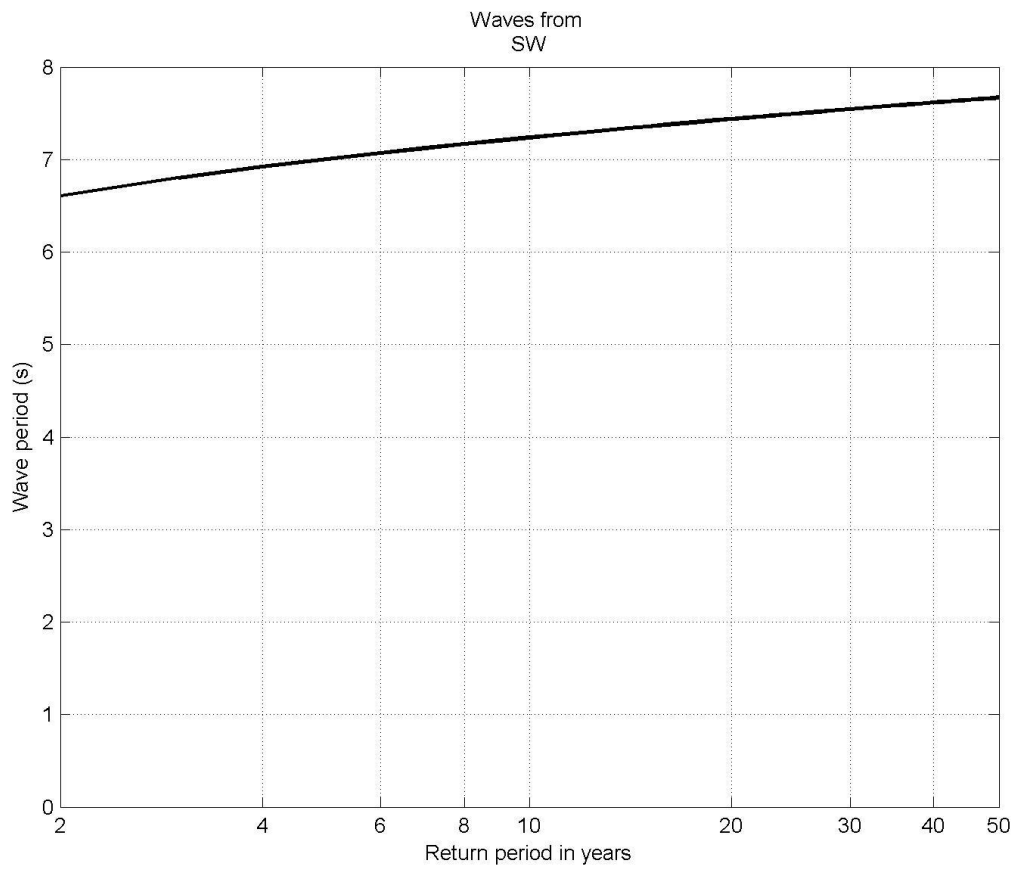


Fig. 3.2.2.16. Return periods of mean wave period from southwest.

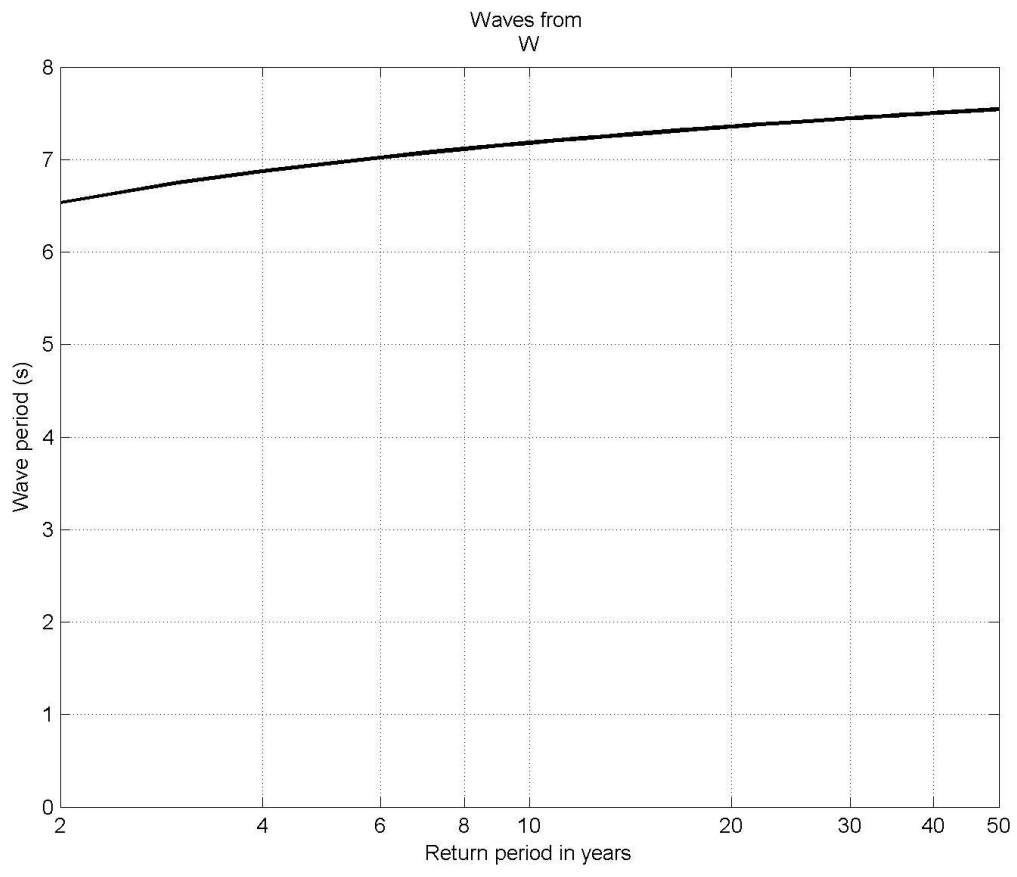


Fig. 3.2.2.17. Return periods of mean wave period from west.

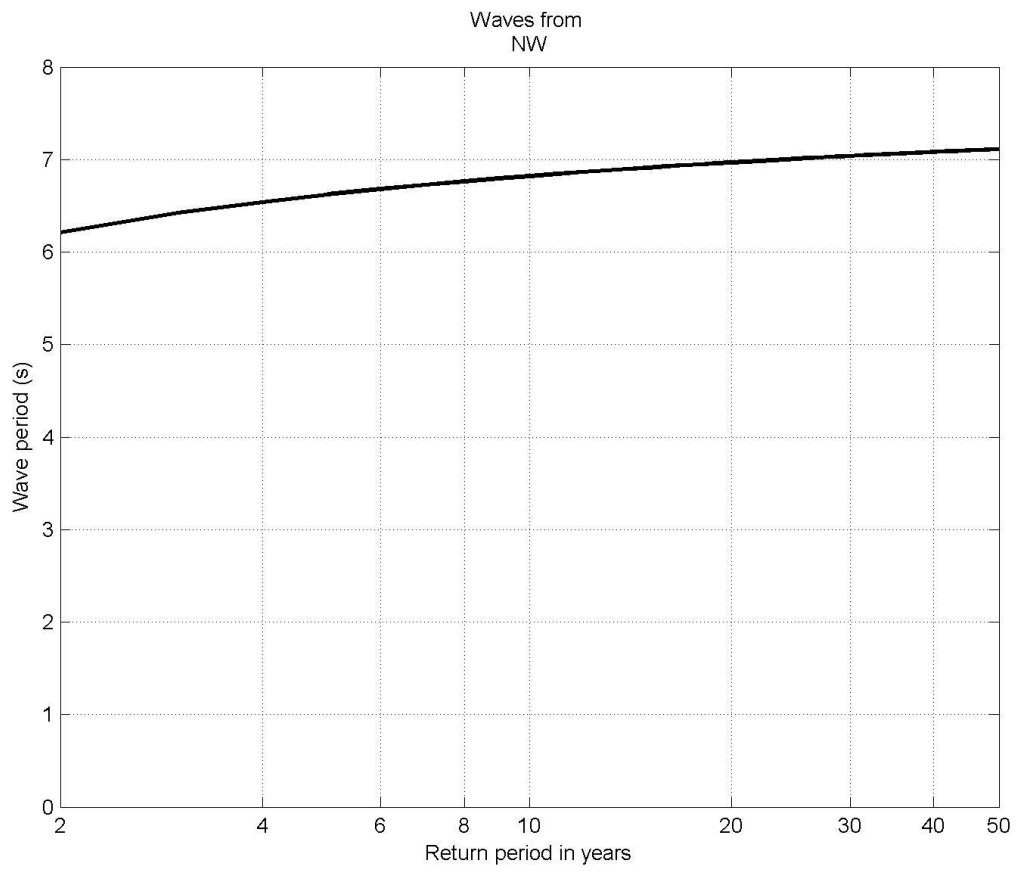


Fig. 3.2.2.18. Return periods of mean wave period from northwest.

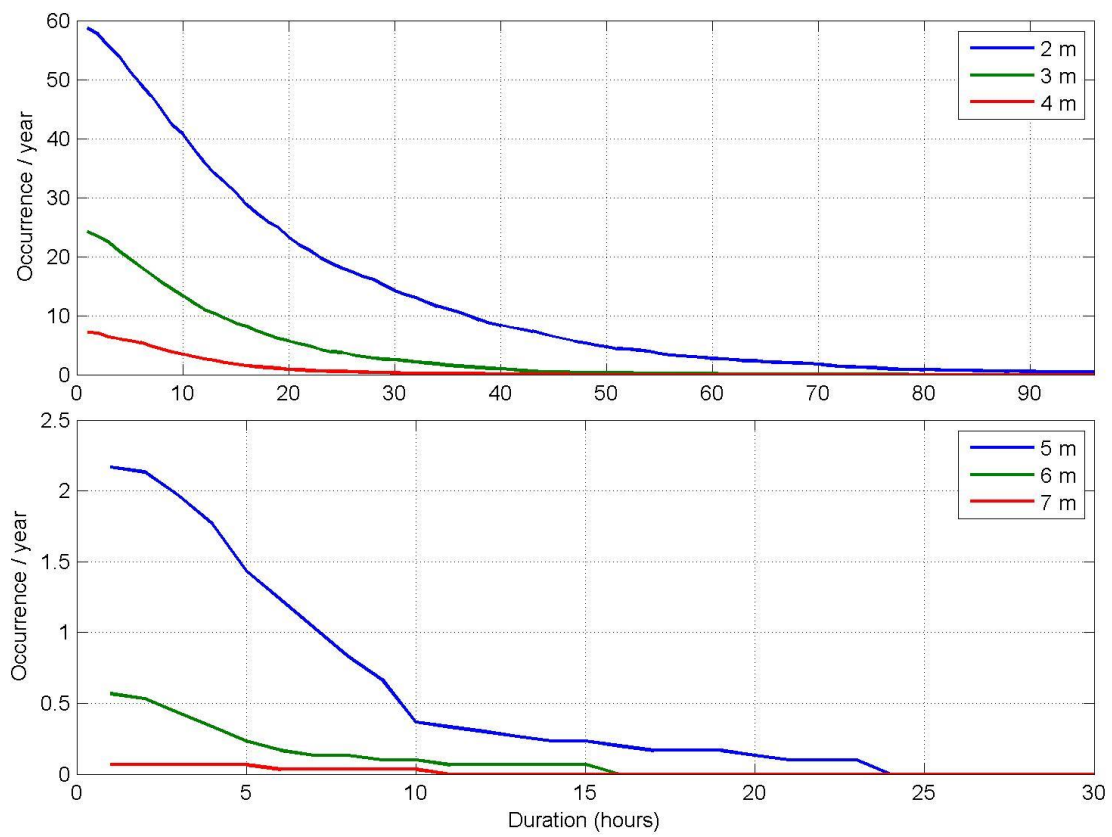


Fig. 3.2.2.18. Occurrence and duration of events with significant wave height (m) over 2, 3, 4, 6, 7 m.

Table. 3.2.2.1. Co-occurrence of wave height and wave period.

Wave height (m)		Wave period (s)															
		0.25	0.75	1.25	1.75	2.25	2.75	3.25	3.75	4.25	4.75	5.25	5.75	6.25	6.75	7.25	7.75
0.25	0.0000	0.0407	2.0000	9.1175	9.4225	2.9774	0.7522	0.1251	0.0118	0.0011	0.0000	0.0000	0.0000	0.0000	0.0000	0.0000	0.0000
0.75	0.0000	0.0000	0.0000	0.0152	5.7704	13.6302	7.9990	1.6897	0.3358	0.0825	0.0171	0.0042	0.0011	0.0000	0.0000	0.0000	0.0000
1.25	0.0000	0.0000	0.0000	0.0000	0.0000	0.7572	8.2626	8.5619	1.3699	0.2107	0.0555	0.0141	0.0015	0.0000	0.0000	0.0000	0.0000
1.75	0.0000	0.0000	0.0000	0.0000	0.0000	0.0000	0.1491	4.0742	6.6710	0.7766	0.0814	0.0118	0.0030	0.0008	0.0000	0.0000	0.0000
2.25	0.0000	0.0000	0.0000	0.0000	0.0000	0.0000	0.0000	0.0647	2.4998	3.7152	0.2556	0.0148	0.0019	0.0000	0.0000	0.0000	0.0000
2.75	0.0000	0.0000	0.0000	0.0000	0.0000	0.0000	0.0000	0.0000	0.0437	1.9479	1.5125	0.0525	0.0023	0.0000	0.0000	0.0000	0.0000
3.25	0.0000	0.0000	0.0000	0.0000	0.0000	0.0000	0.0000	0.0000	0.0654	1.4608	0.3442	0.0057	0.0000	0.0000	0.0000	0.0000	0.0000
3.75	0.0000	0.0000	0.0000	0.0000	0.0000	0.0000	0.0000	0.0000	0.0004	0.1704	0.7648	0.0361	0.0008	0.0000	0.0000	0.0000	0.0000
4.25	0.0000	0.0000	0.0000	0.0000	0.0000	0.0000	0.0000	0.0000	0.0000	0.0015	0.2491	0.1978	0.0019	0.0000	0.0000	0.0000	0.0000
4.75	0.0000	0.0000	0.0000	0.0000	0.0000	0.0000	0.0000	0.0000	0.0000	0.0000	0.0087	0.1947	0.0157	0.0000	0.0000	0.0000	0.0000
5.25	0.0000	0.0000	0.0000	0.0000	0.0000	0.0000	0.0000	0.0000	0.0000	0.0000	0.0004	0.0472	0.0562	0.0000	0.0000	0.0000	0.0000
5.75	0.0000	0.0000	0.0000	0.0000	0.0000	0.0000	0.0000	0.0000	0.0000	0.0000	0.0000	0.0027	0.0377	0.0030	0.0000	0.0000	0.0000
6.25	0.0000	0.0000	0.0000	0.0000	0.0000	0.0000	0.0000	0.0000	0.0000	0.0000	0.0000	0.0000	0.0000	0.0126	0.0106	0.0000	0.0000
6.75	0.0000	0.0000	0.0000	0.0000	0.0000	0.0000	0.0000	0.0000	0.0000	0.0000	0.0000	0.0000	0.0000	0.0000	0.0049	0.0000	0.0000
7.25	0.0000	0.0000	0.0000	0.0000	0.0000	0.0000	0.0000	0.0000	0.0000	0.0000	0.0000	0.0000	0.0000	0.0000	0.0019	0.0000	0.0015
7.75	0.0000	0.0000	0.0000	0.0000	0.0000	0.0000	0.0000	0.0000	0.0000	0.0000	0.0000	0.0000	0.0000	0.0000	0.0004	0.0000	0.0019

3.2.3. Spatial variations

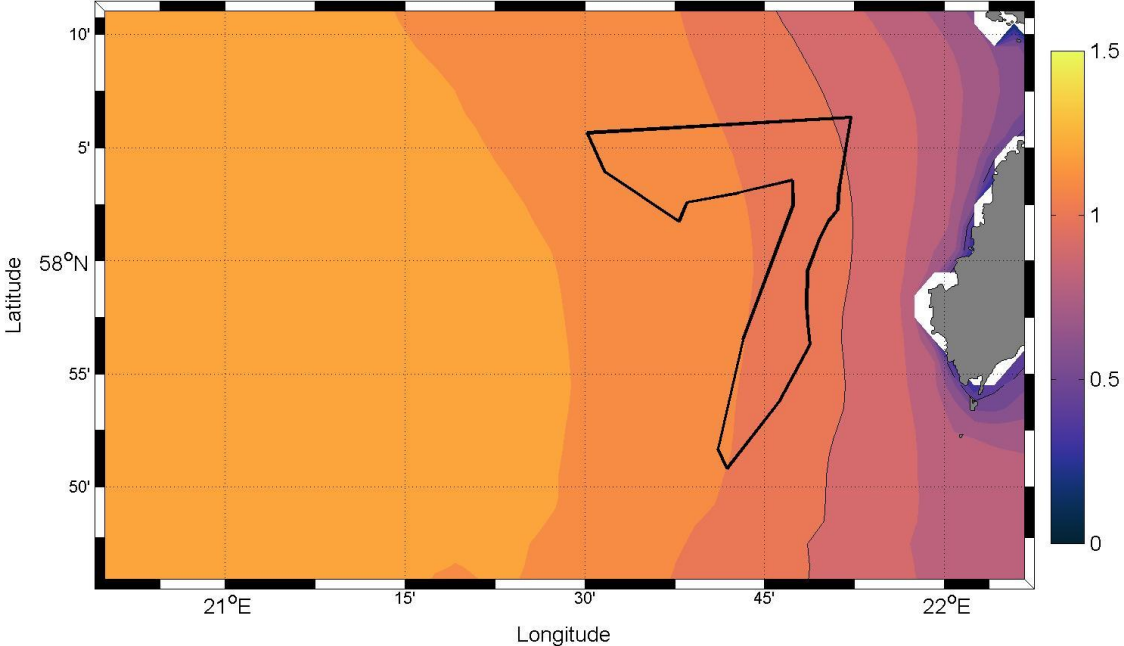


Fig. 3.2.3.1. Mean significant wave height (m). The solid thin line represents isoline 1 m. Thick line represents ELWIND area.

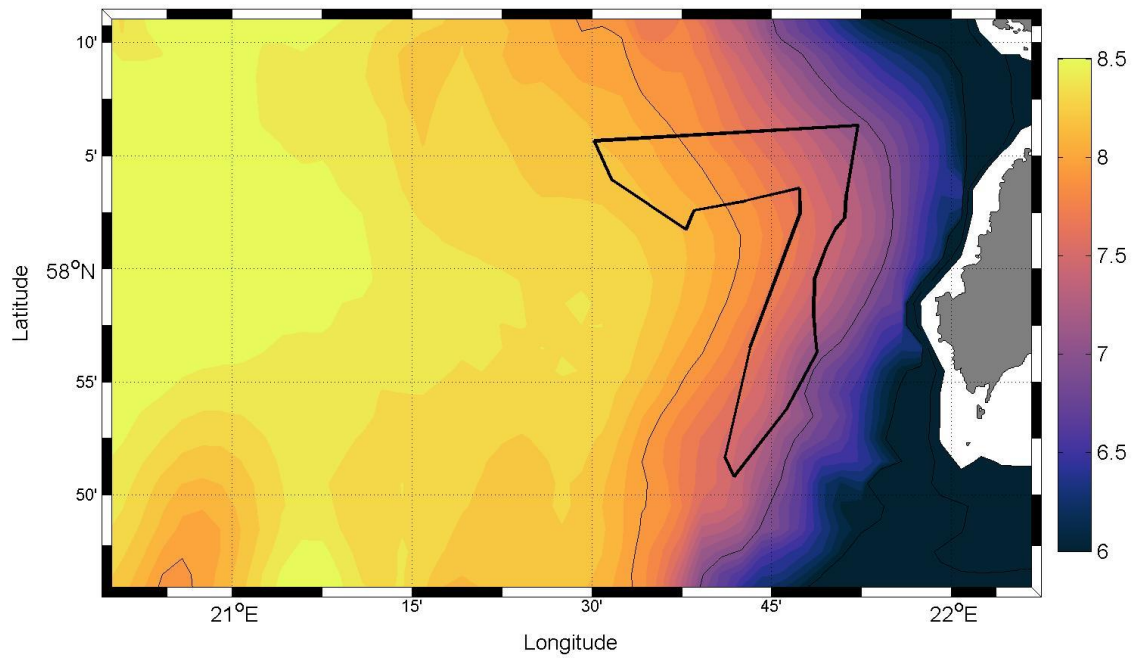


Fig. 3.2.3.2. Highest significant wave height (m) of the time series that occurred on 9 January 2005 during the storm Gudrun. Solid lines represent isolines of 7 m and 8 m. Thick line represents ELWIND area.

3.3. Current conditions

Typically for the Baltic Sea, there are no permanent currents in the ELWIND area. The temporal variability of currents is high and related to the wind forcing and its variability. The prevailing current direction is to the northwest in the location of the time series (Fig. 3.3.1.1-3.3.1.48). In the southern side of the ELWIND area, the long-term mean current is parallel to the Sörve peninsula i.e. to the north (Figs. 3.3.3.1-3.3.3.5). In the northern part of the ELWIND area, the long-term mean current turns to the west. This spatial structure of the mean current is part of the large-scale circulation of the Baltic Proper (Liblik et al., 2022). This pattern is encouraged by southwesterly winds and prevails more in autumn and winter due to supporting wind regime. The current reverses in the case of winds from a northerly sector (Liblik et al., 2022).

There is probably a two-layer current structure during the presence of the seasonal thermocline (April-October) while the flow is one-layer when the thermocline does not exist or is deeper than the sea depth in the area (November-March). The used product might underestimate the current speed. However, the current speed is quite low in the area and the likely long-term mean of hourly current speed does not exceed 10 cm/s. According to the product stronger currents occur in the southern part of the ELWIND area. The maximum current speed likely does not exceed 1 m/s and even currents with speed above 0.5 m/s are rare (Fig. 3.3.2.1-3.3.2.2).

3.3.1. Normal conditions

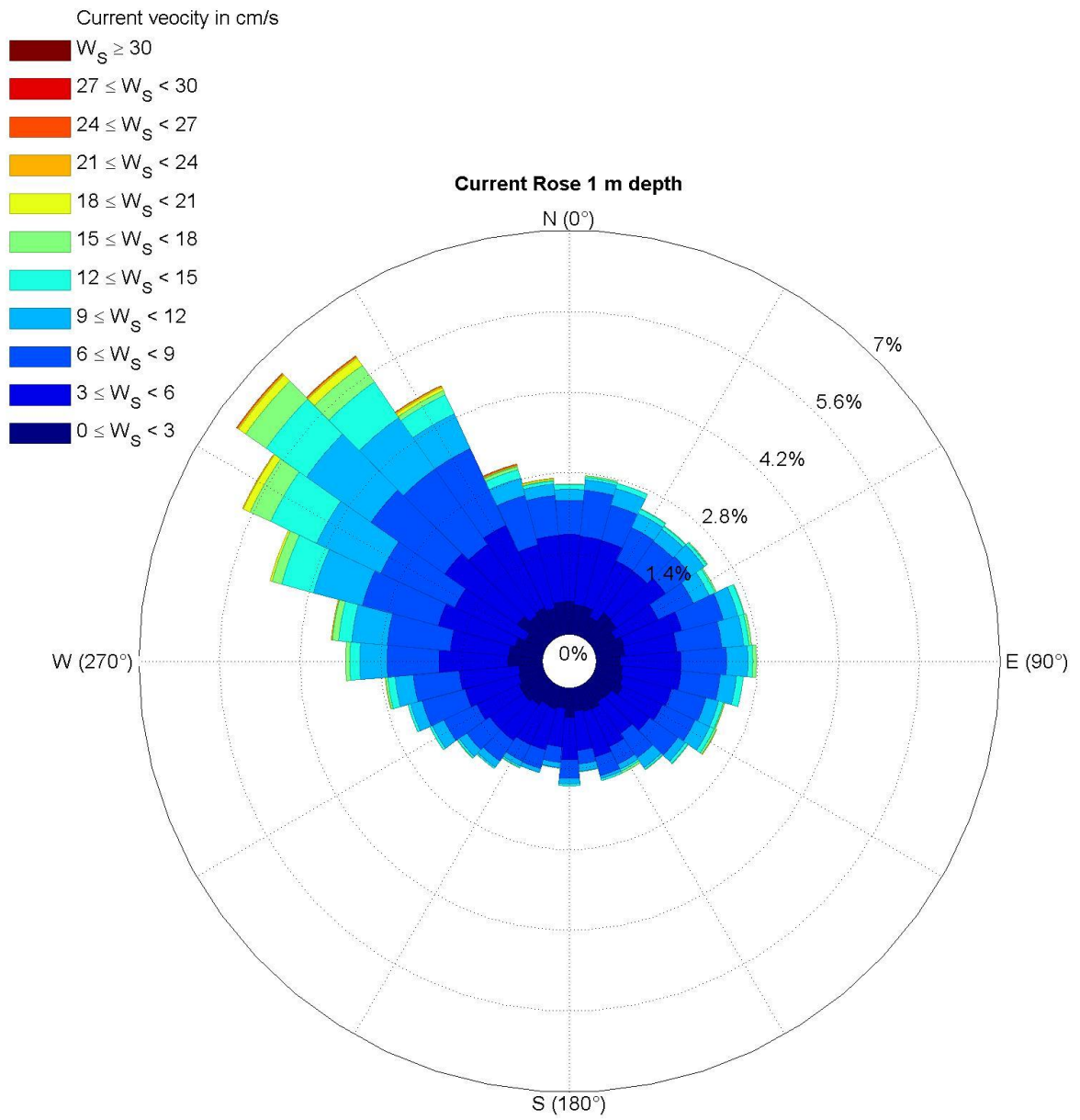


Fig. 3.3.1.1. Annual current rose at 1 m depth

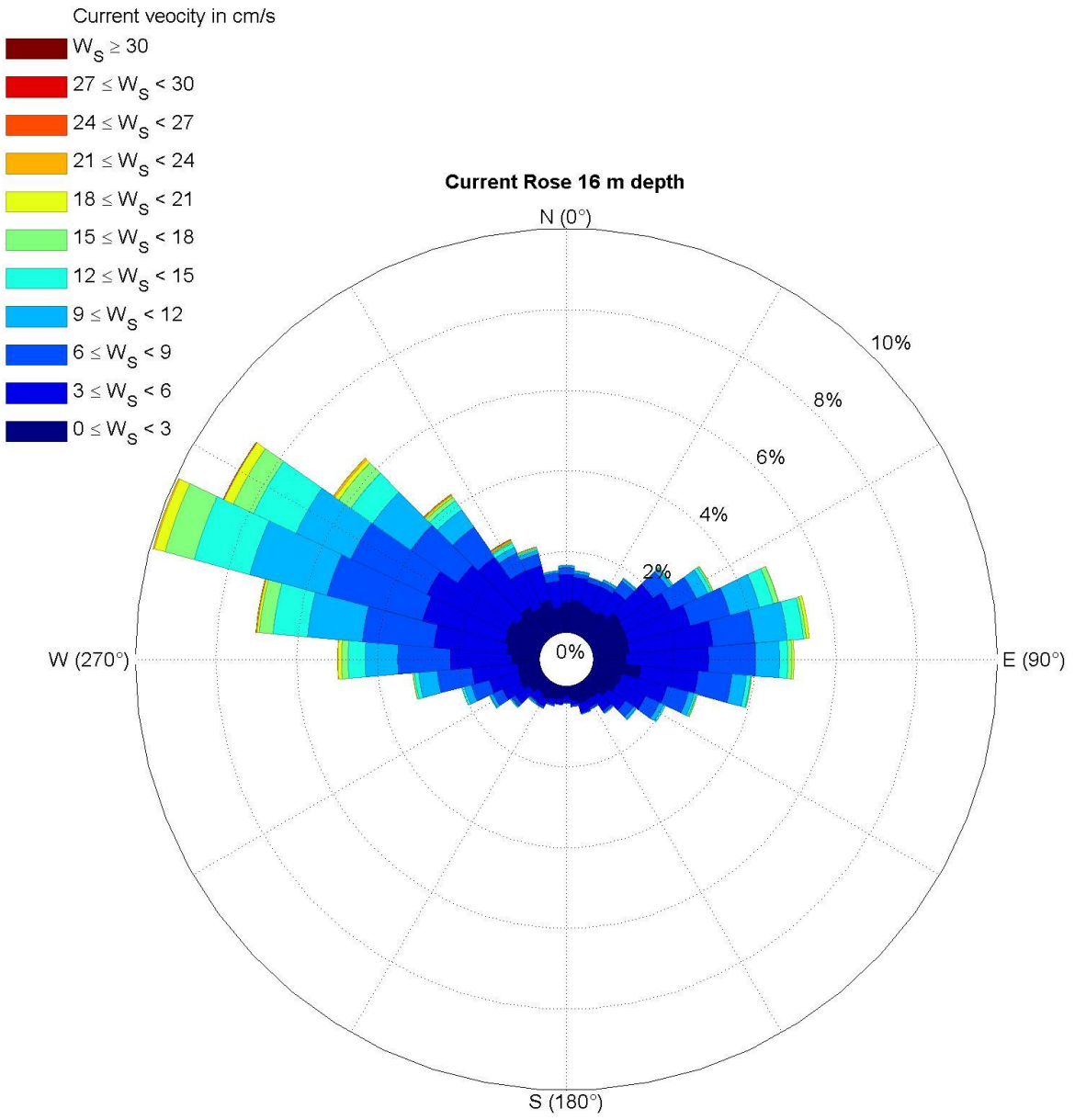


Fig. 3.3.1.2. Annual current rose at 16 m depth.

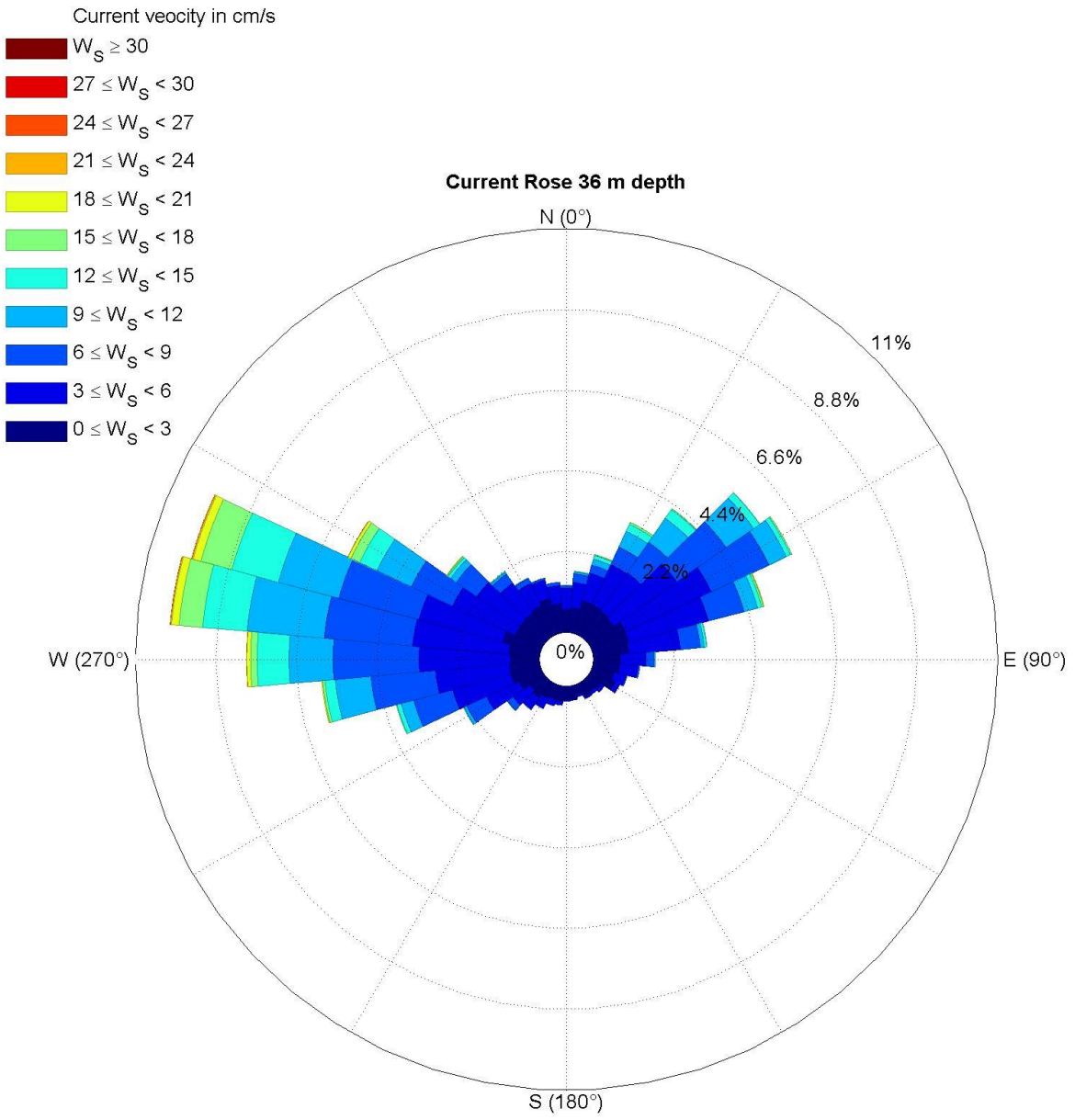


Fig. 3.3.1.3. Annual current rose at 36 m depth.

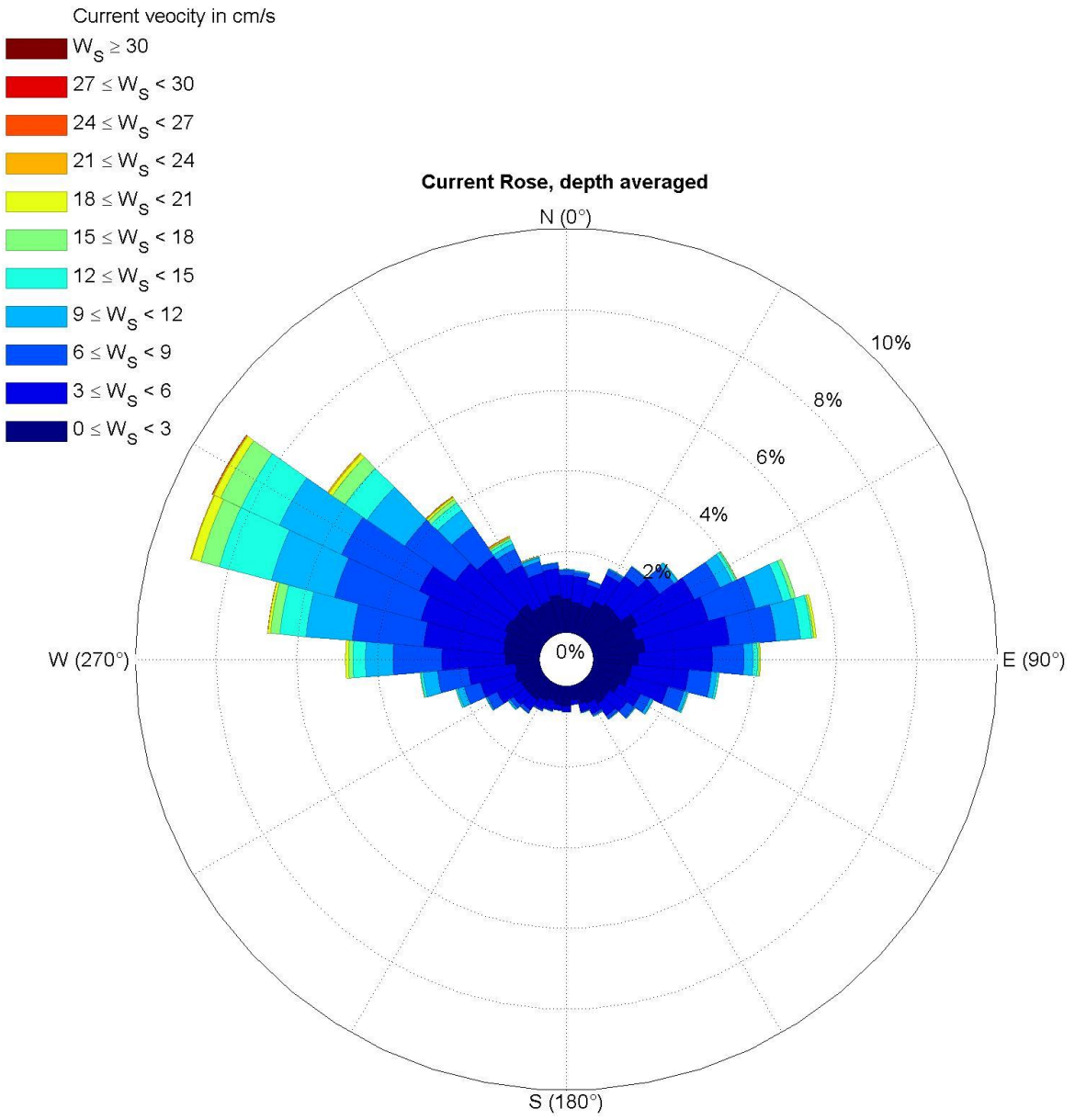


Fig. 3.3.1.4. Annual depth averaged current rose.

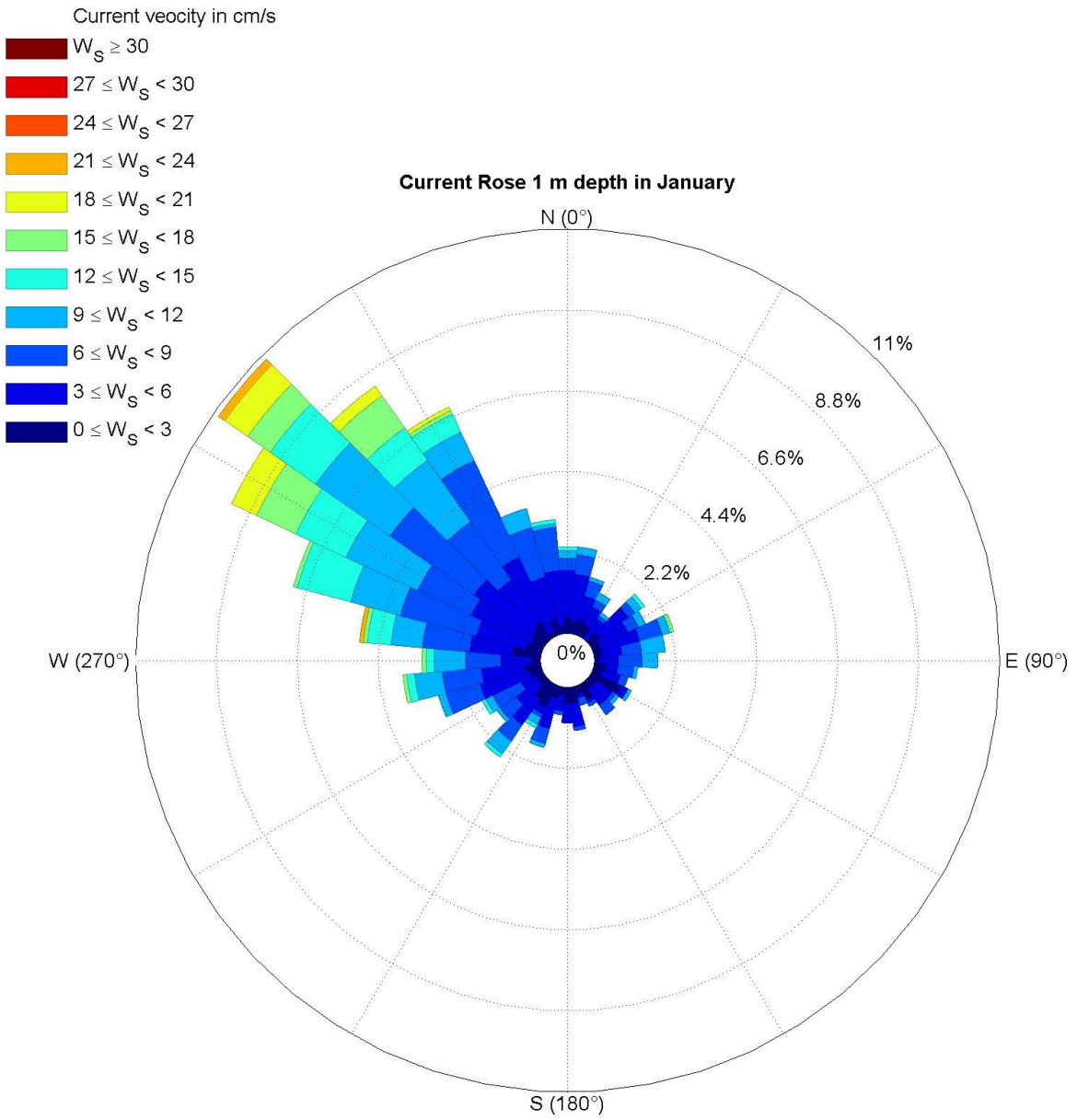


Fig. 3.3.1.1. Current rose at 1 m depth in January

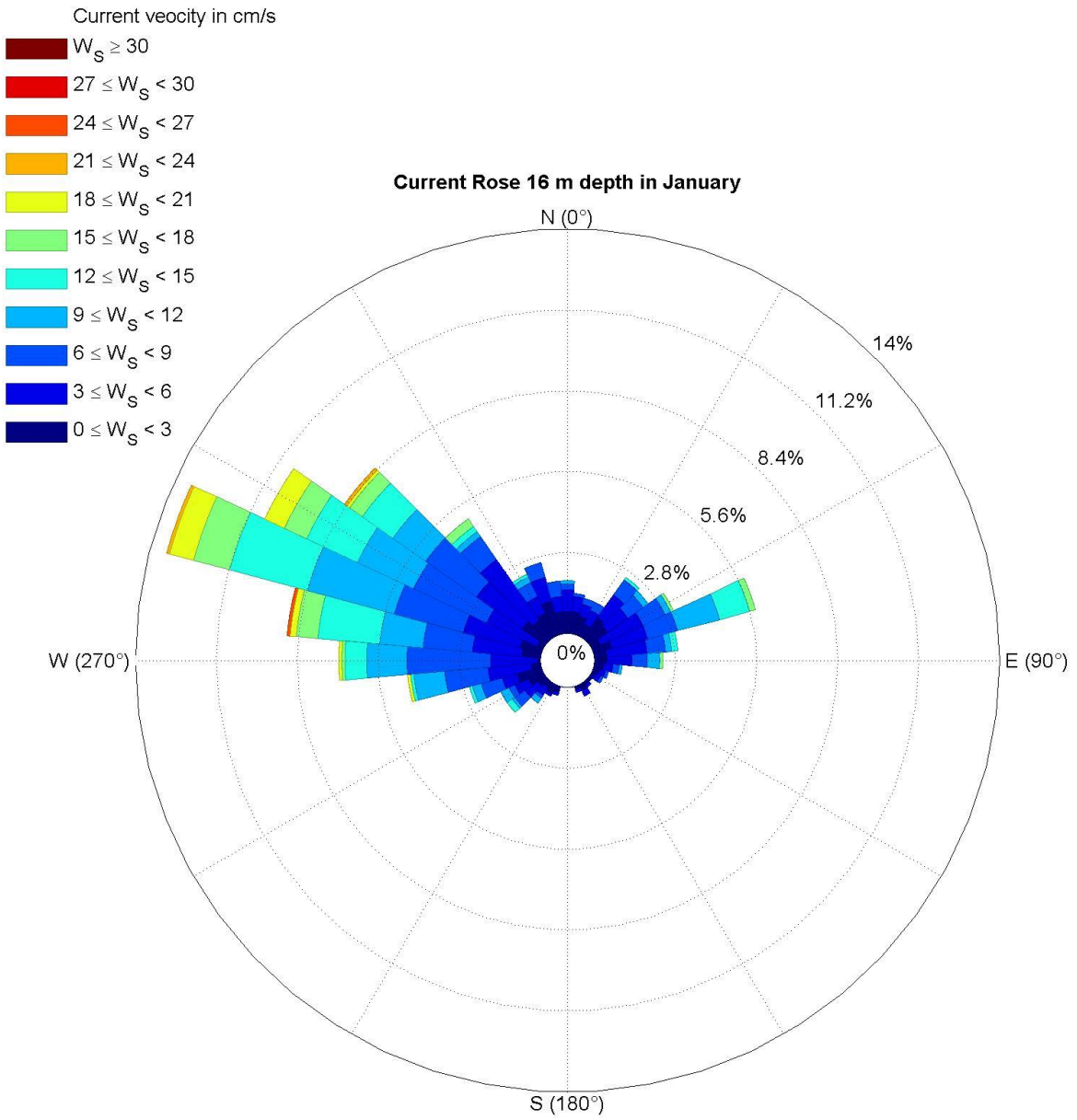


Fig. 3.3.1.2. Current rose at 16 m depth in January.

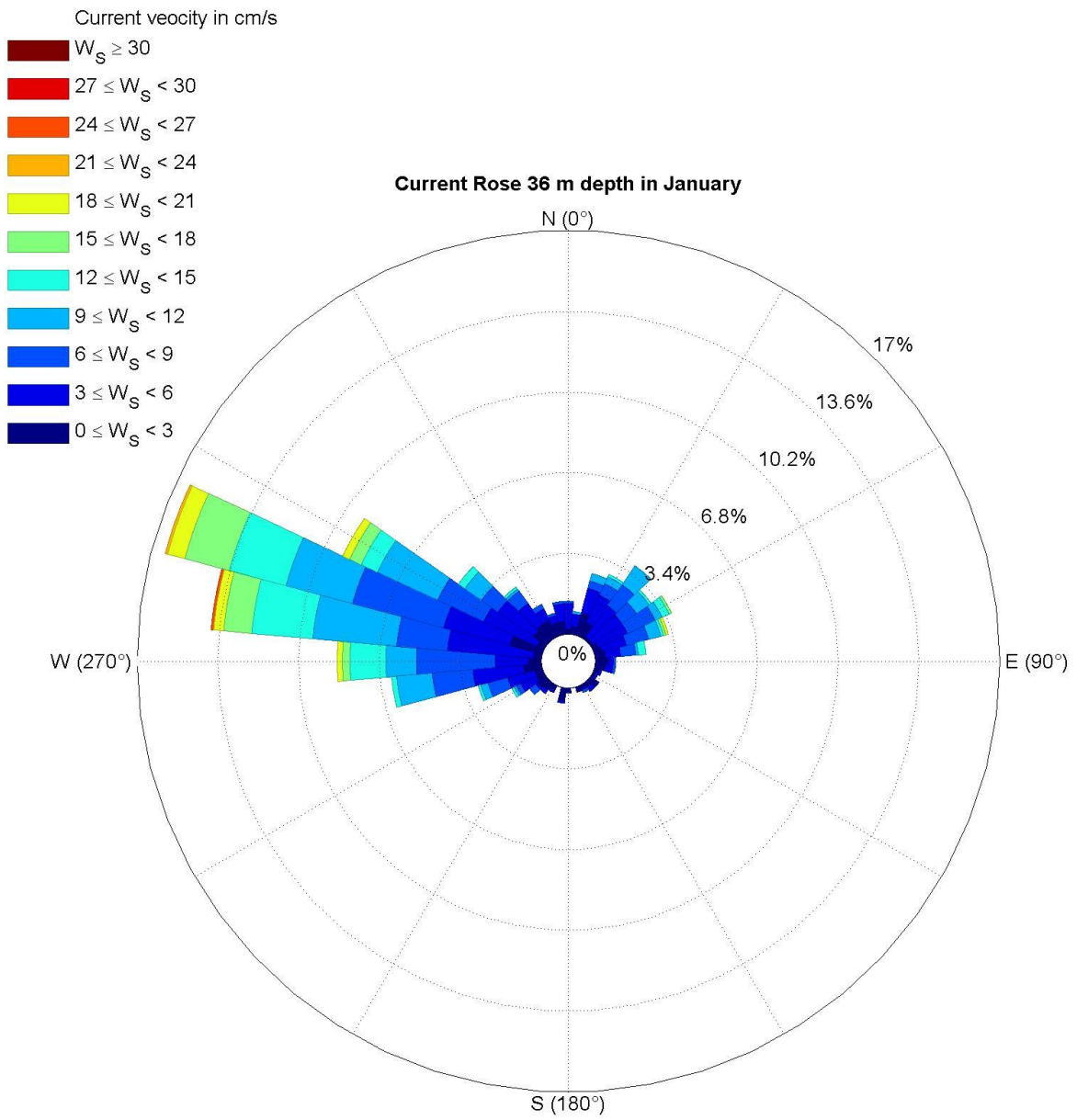


Fig. 3.3.1.3. Current rose at 36 m depth in January.

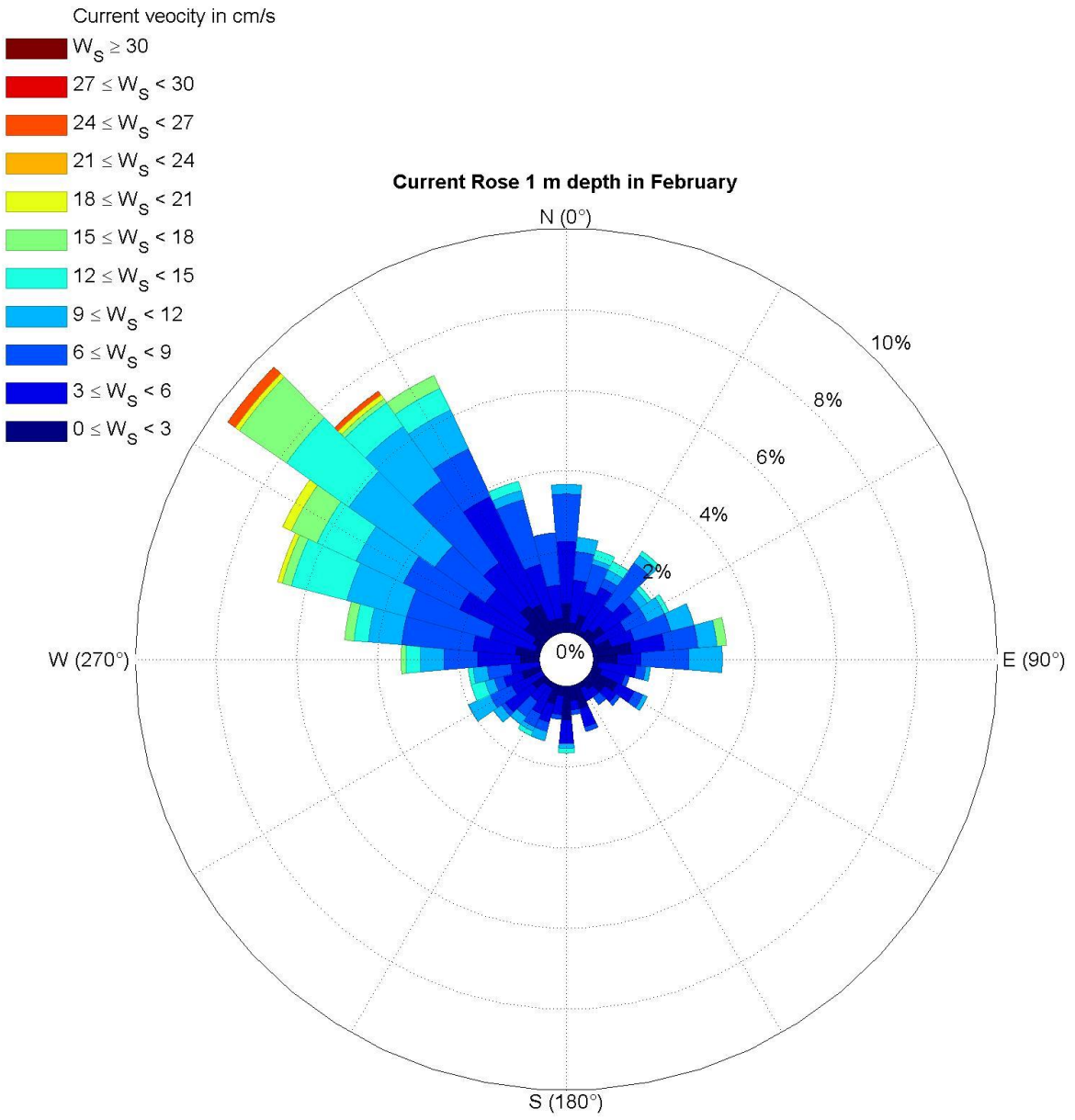


Fig. 3.3.1.5. Current rose at 1 m depth in February.

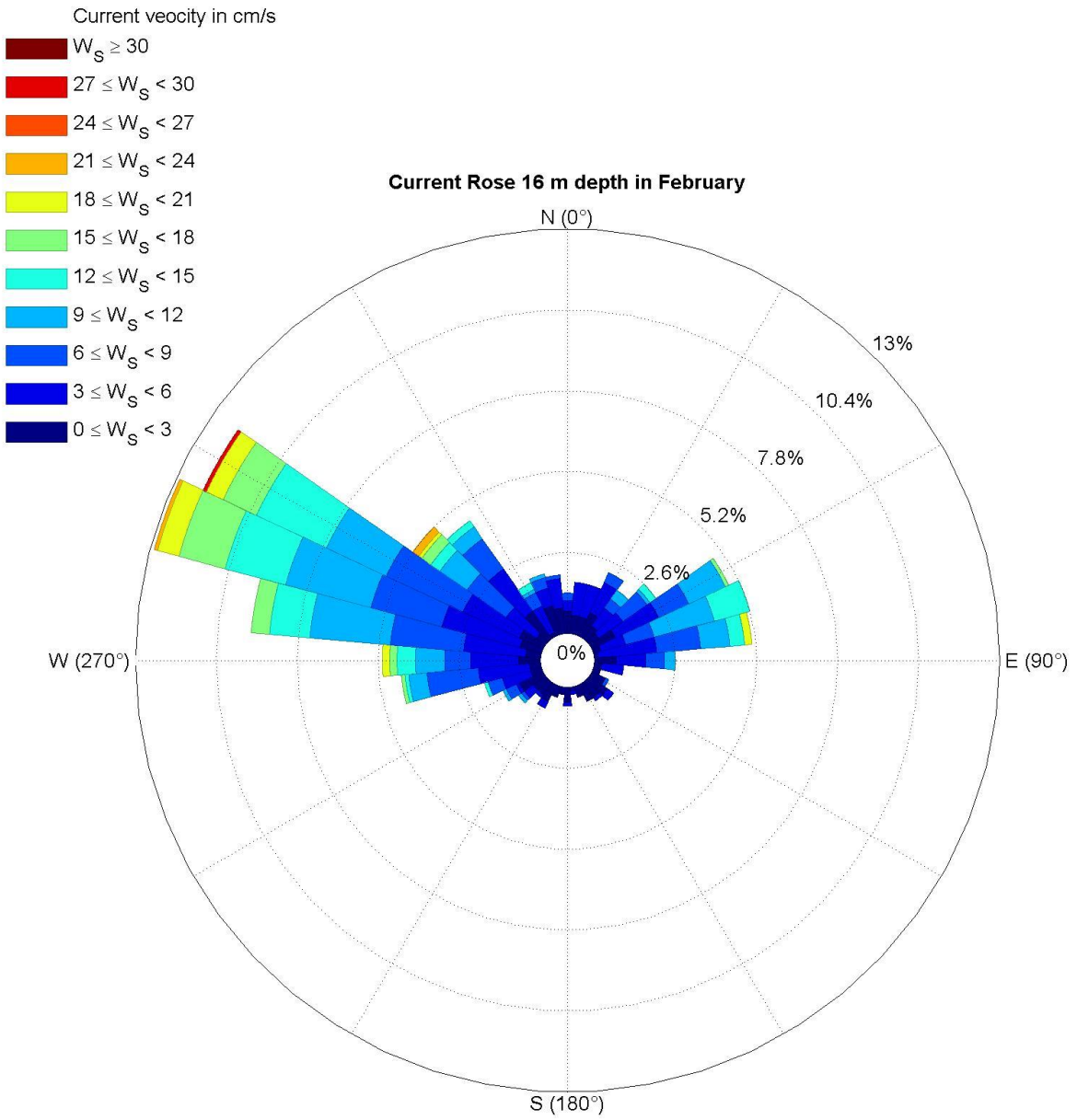


Fig. 3.3.1.6. Current rose at 16 m depth in February.

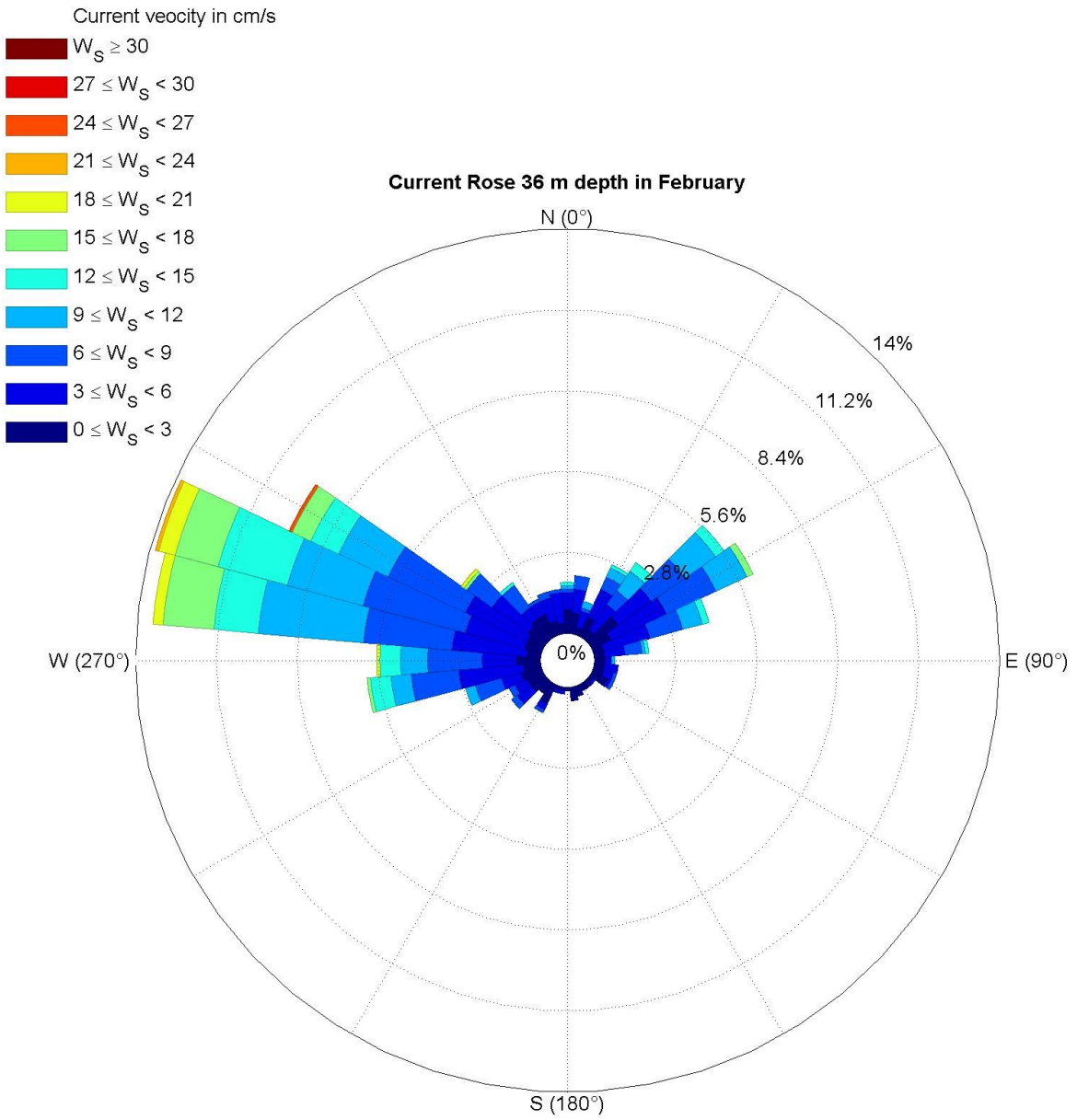


Fig. 3.3.1.7. Current rose at 36 m depth in February.

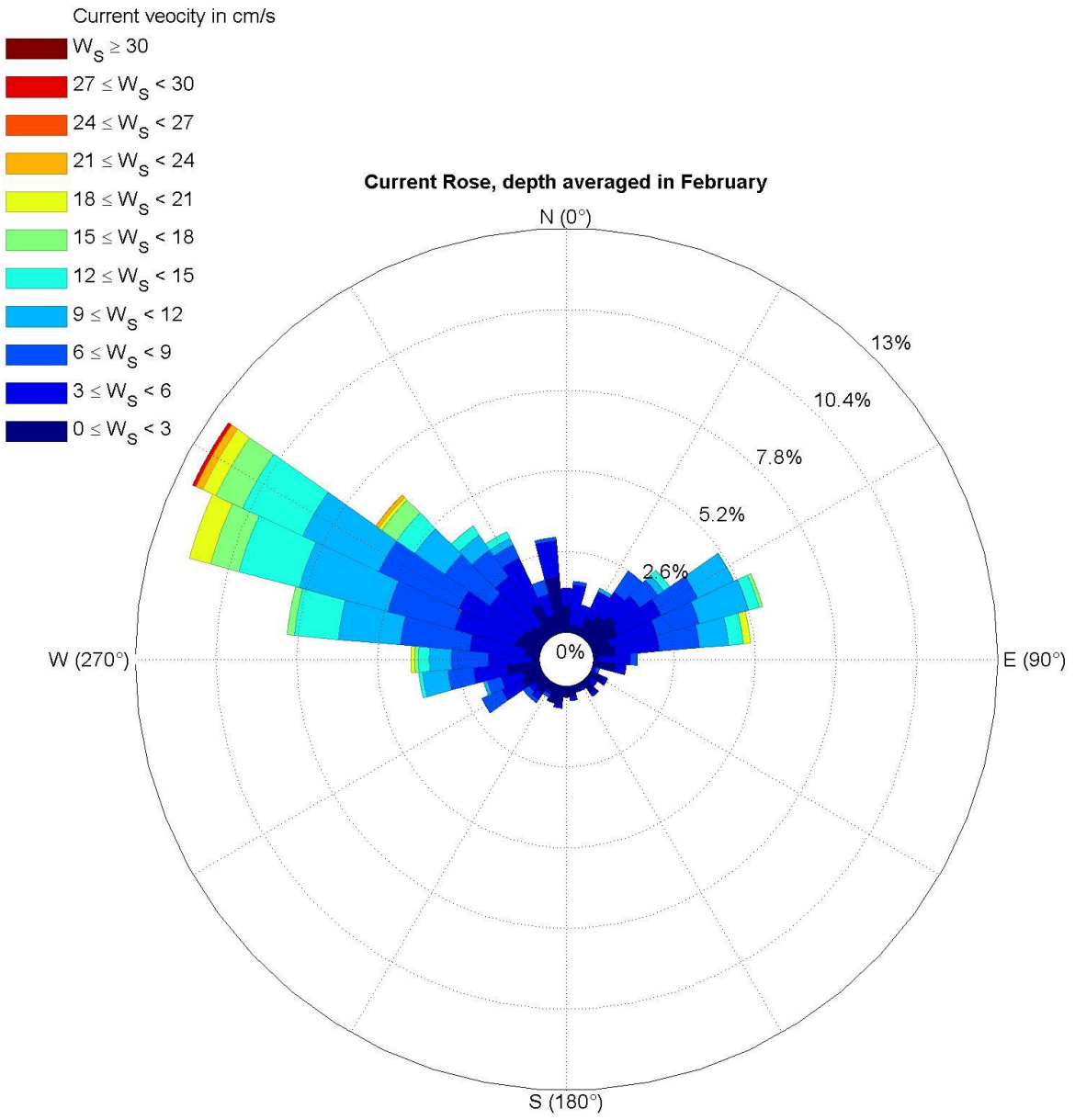


Fig. 3.3.1.8. Depth averaged current rose in February.

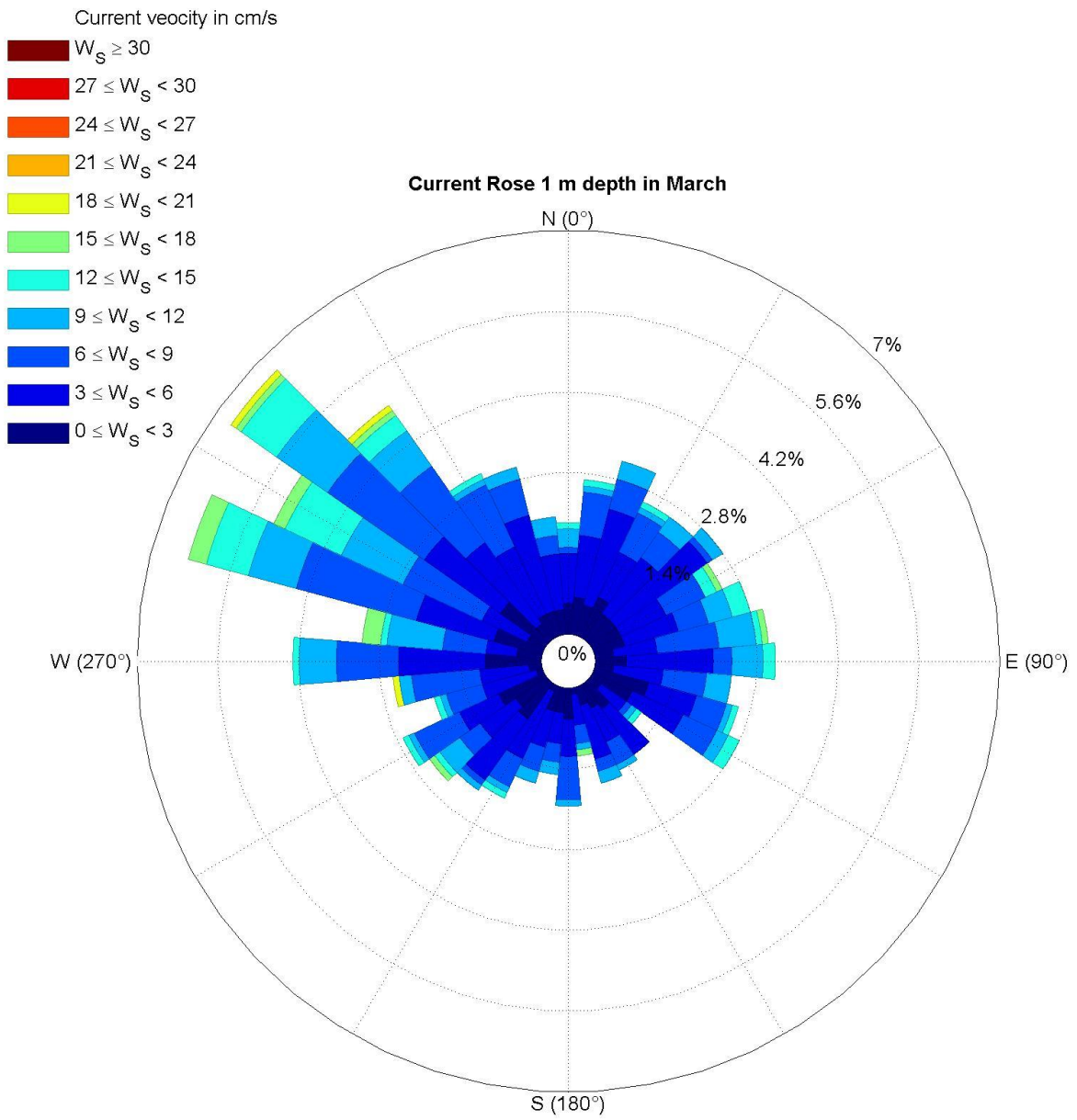


Fig. 3.3.1.9. Current rose at 1 m depth in March.

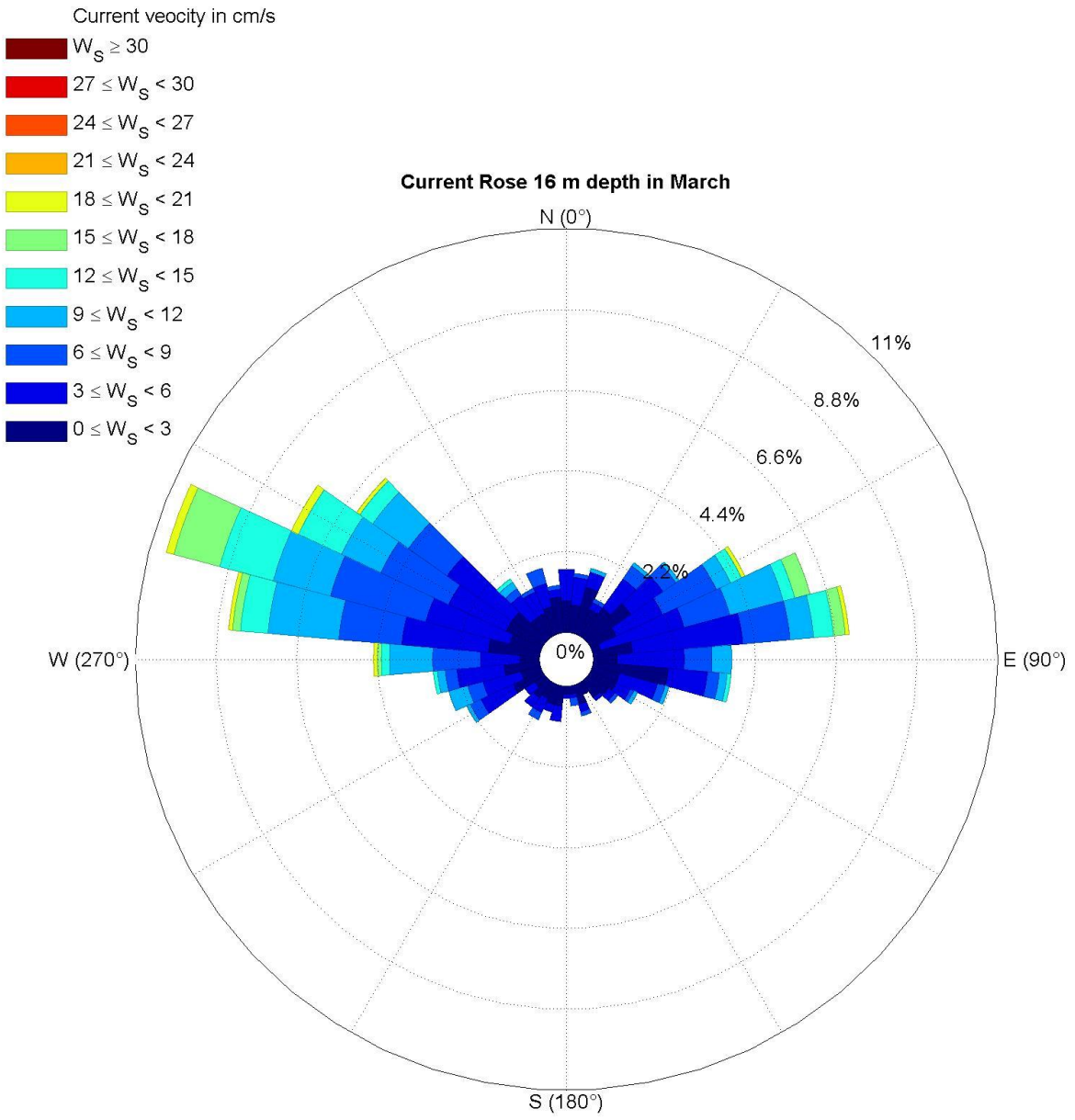


Fig. 3.3.1.10. Current rose at 16 m depth in March.

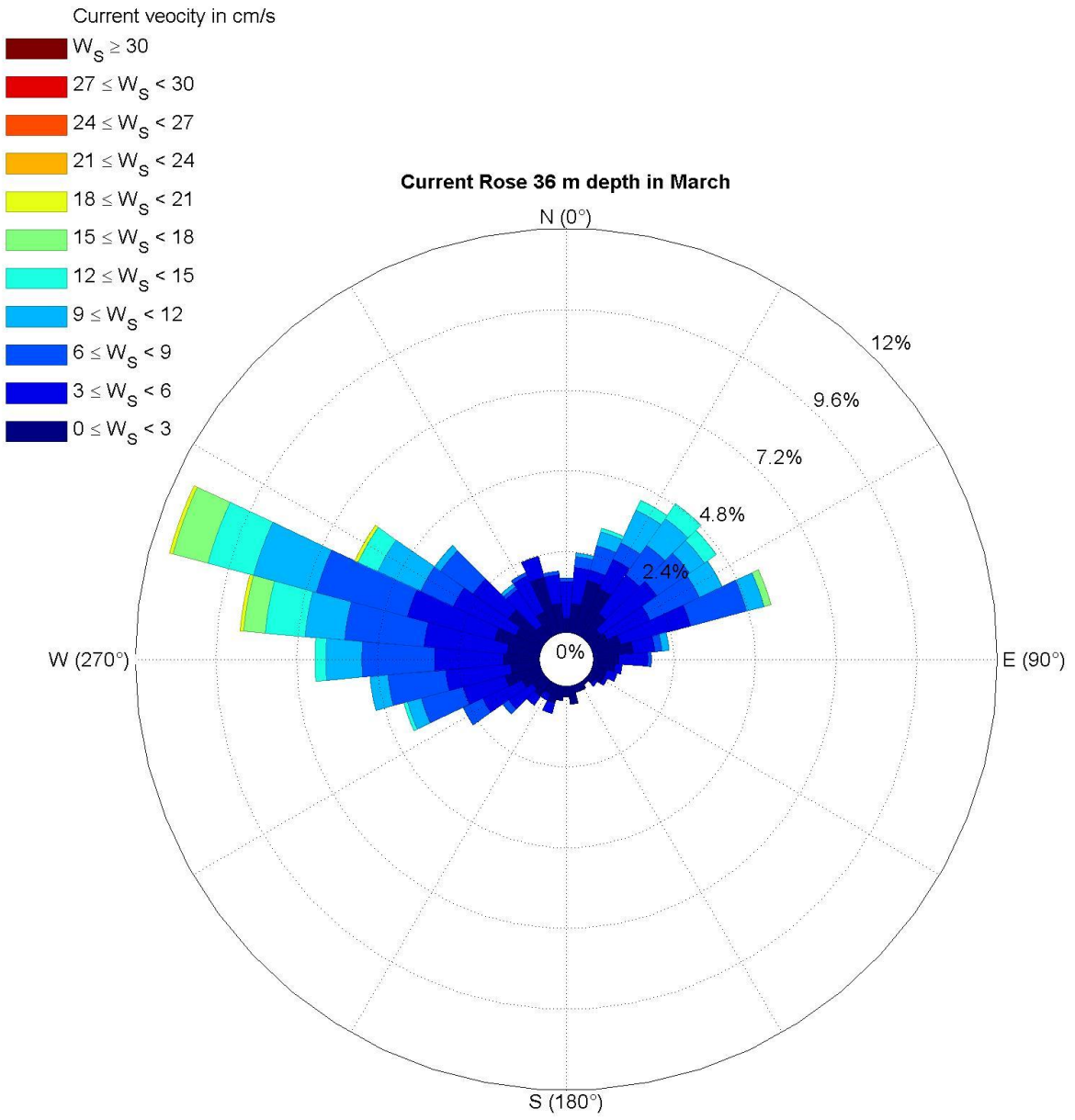


Fig. 3.3.1.11. Current rose at 36 m depth in March.

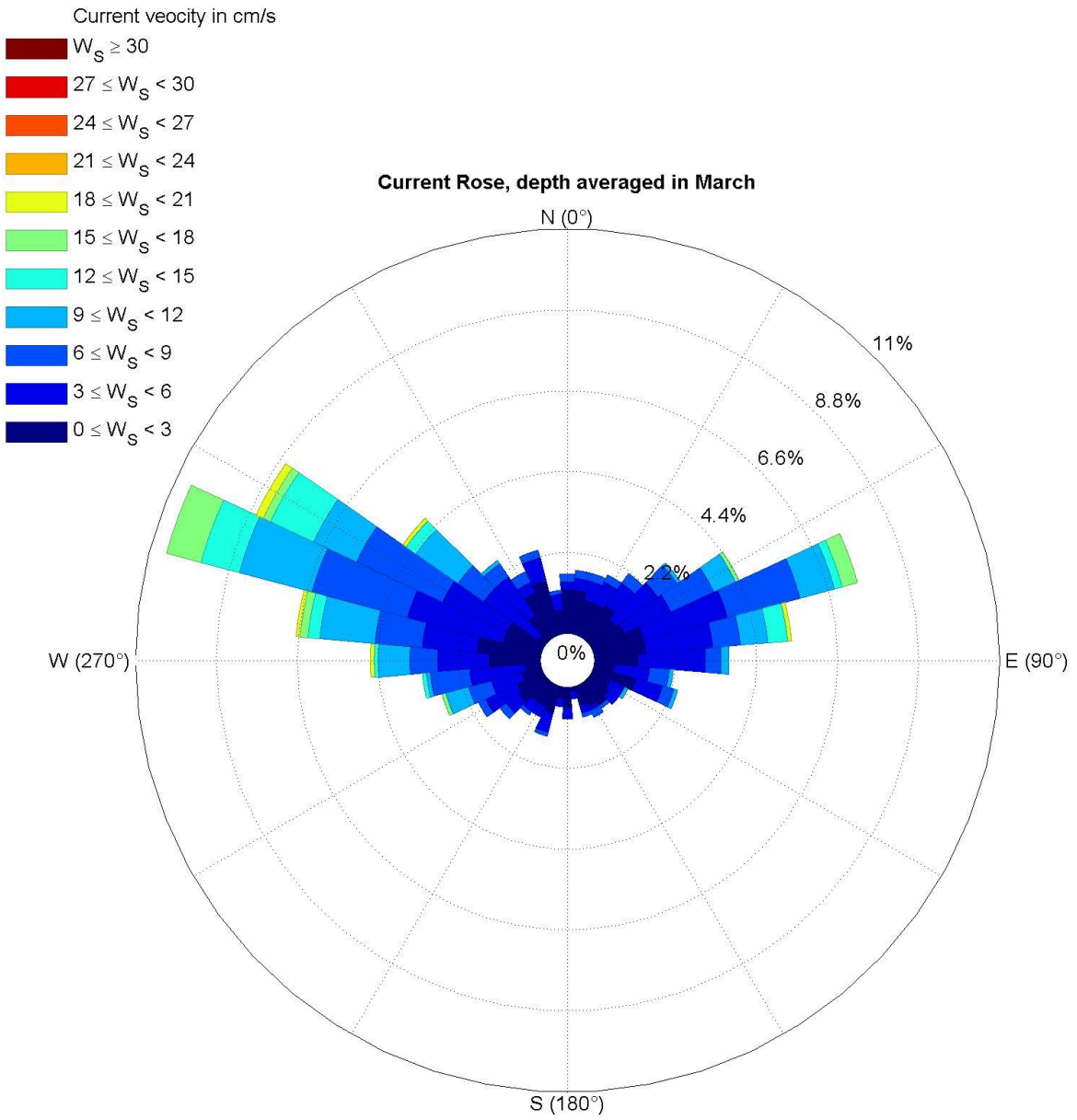


Fig. 3.3.1.12. Depth averaged current rose in March.

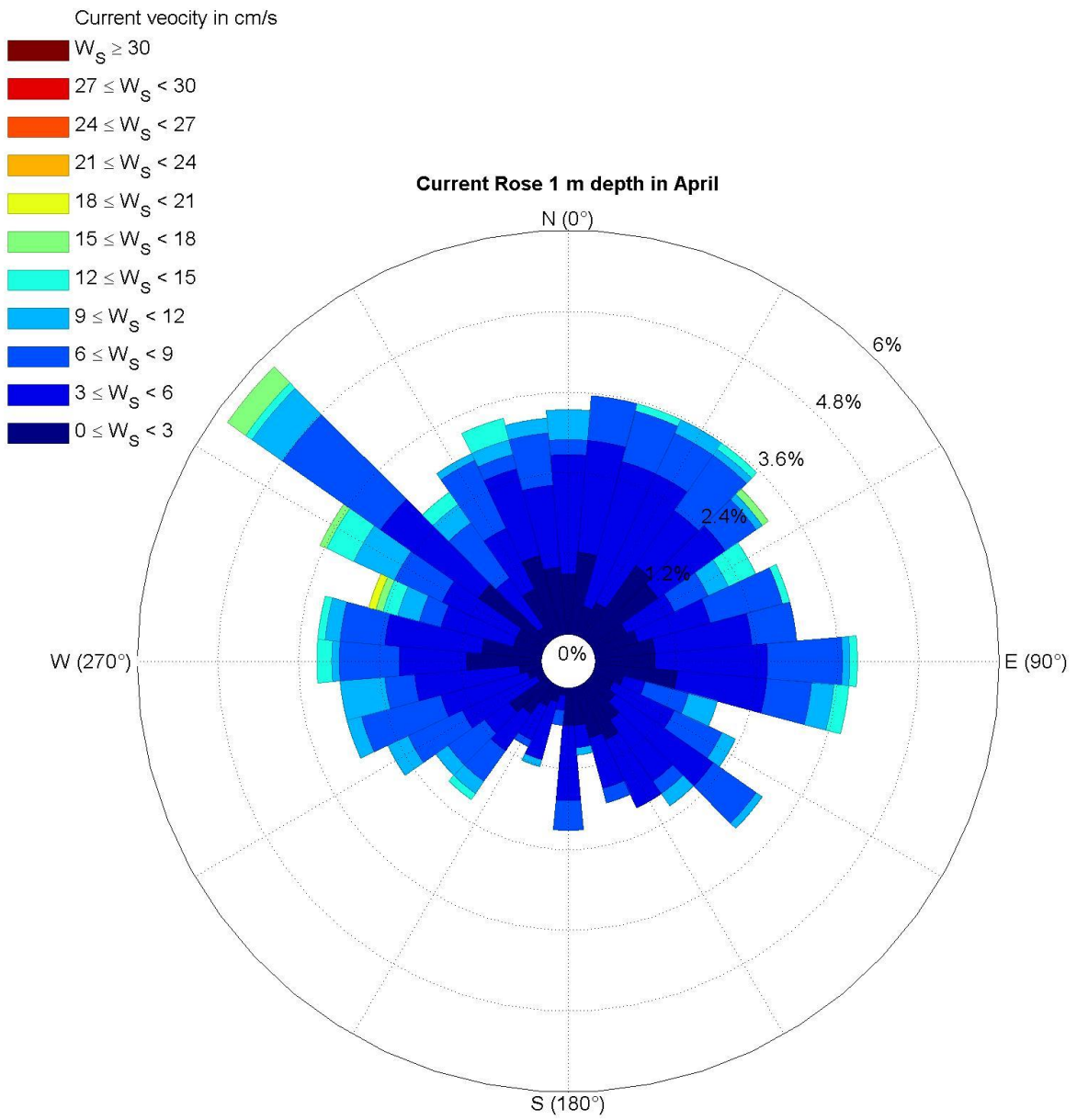


Fig. 3.3.1.13. Current rose at 1 m depth in April.

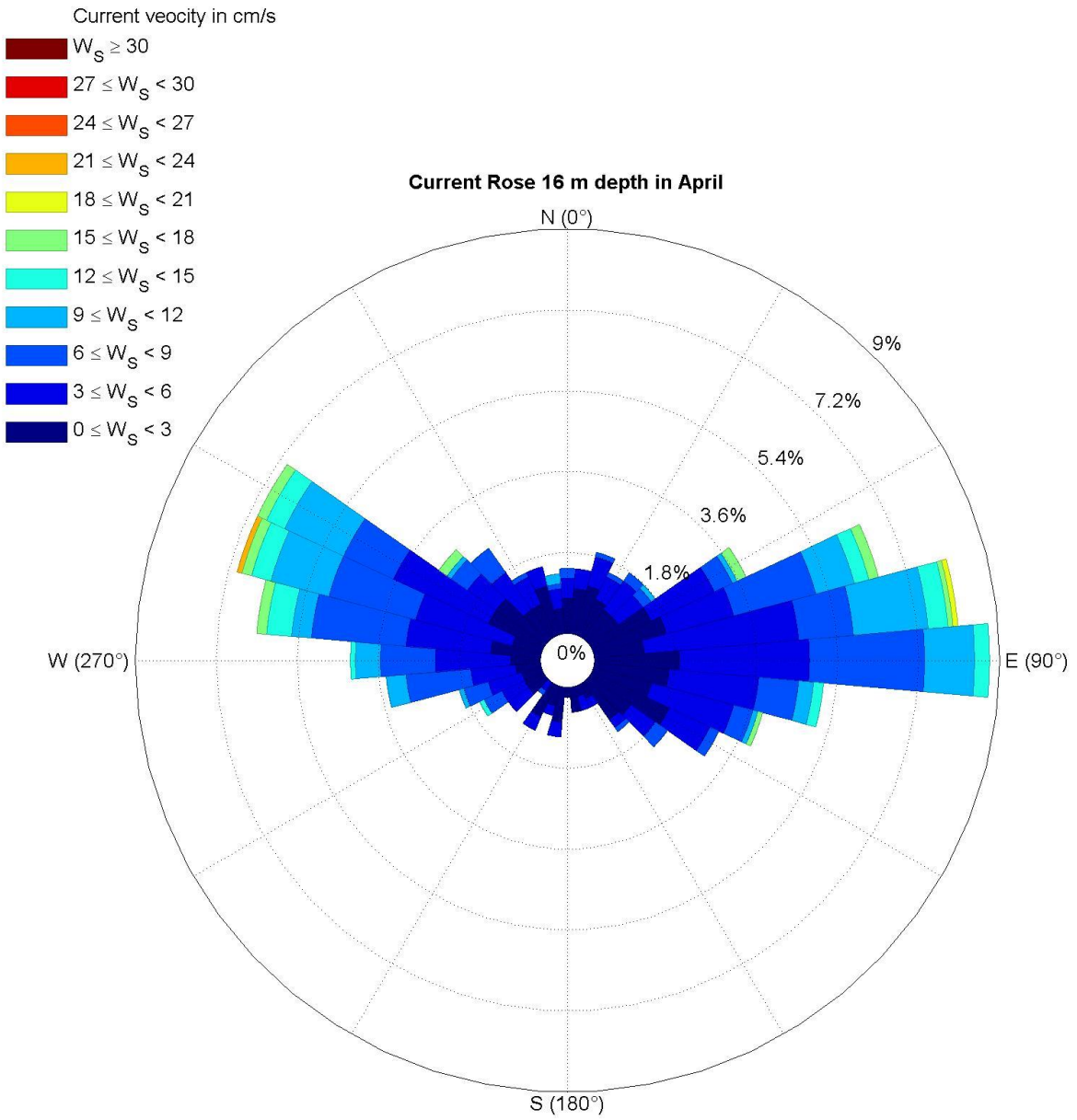


Fig. 3.3.1.14. Current rose at 16 m depth in April.

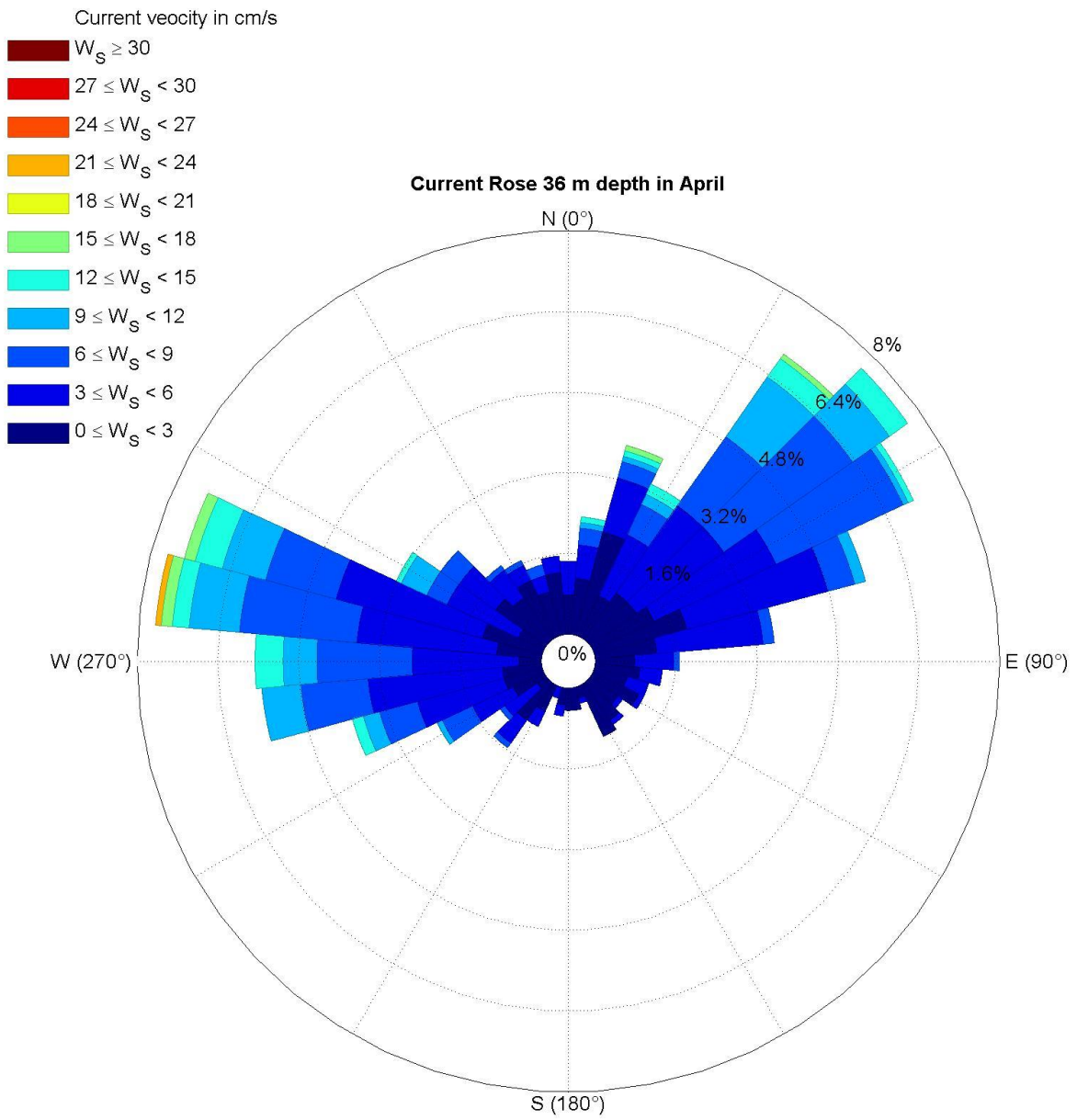


Fig. 3.3.1.15. Current rose at 36 m depth in April.

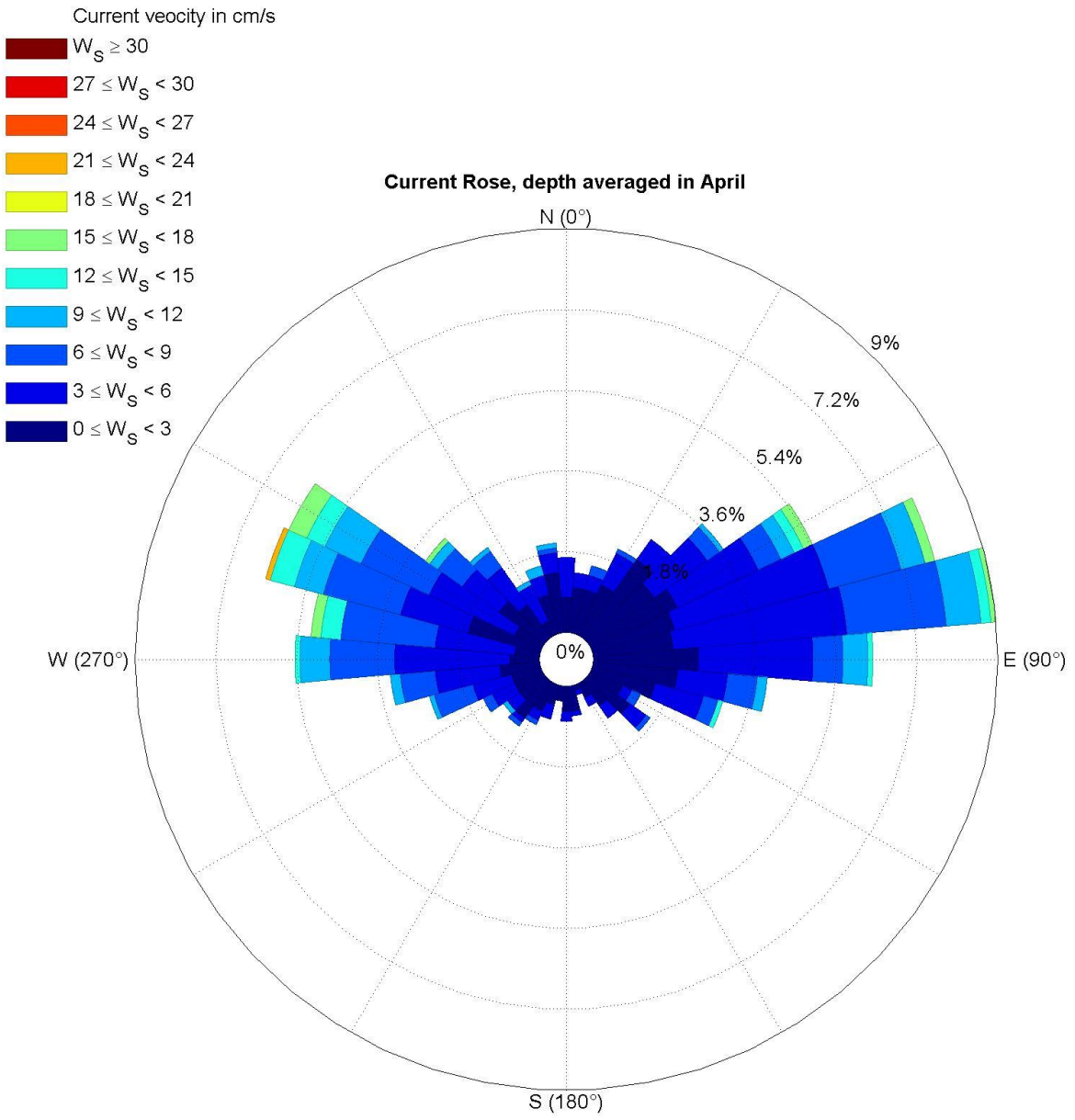


Fig. 3.3.1.16. Depth averaged current rose in April.

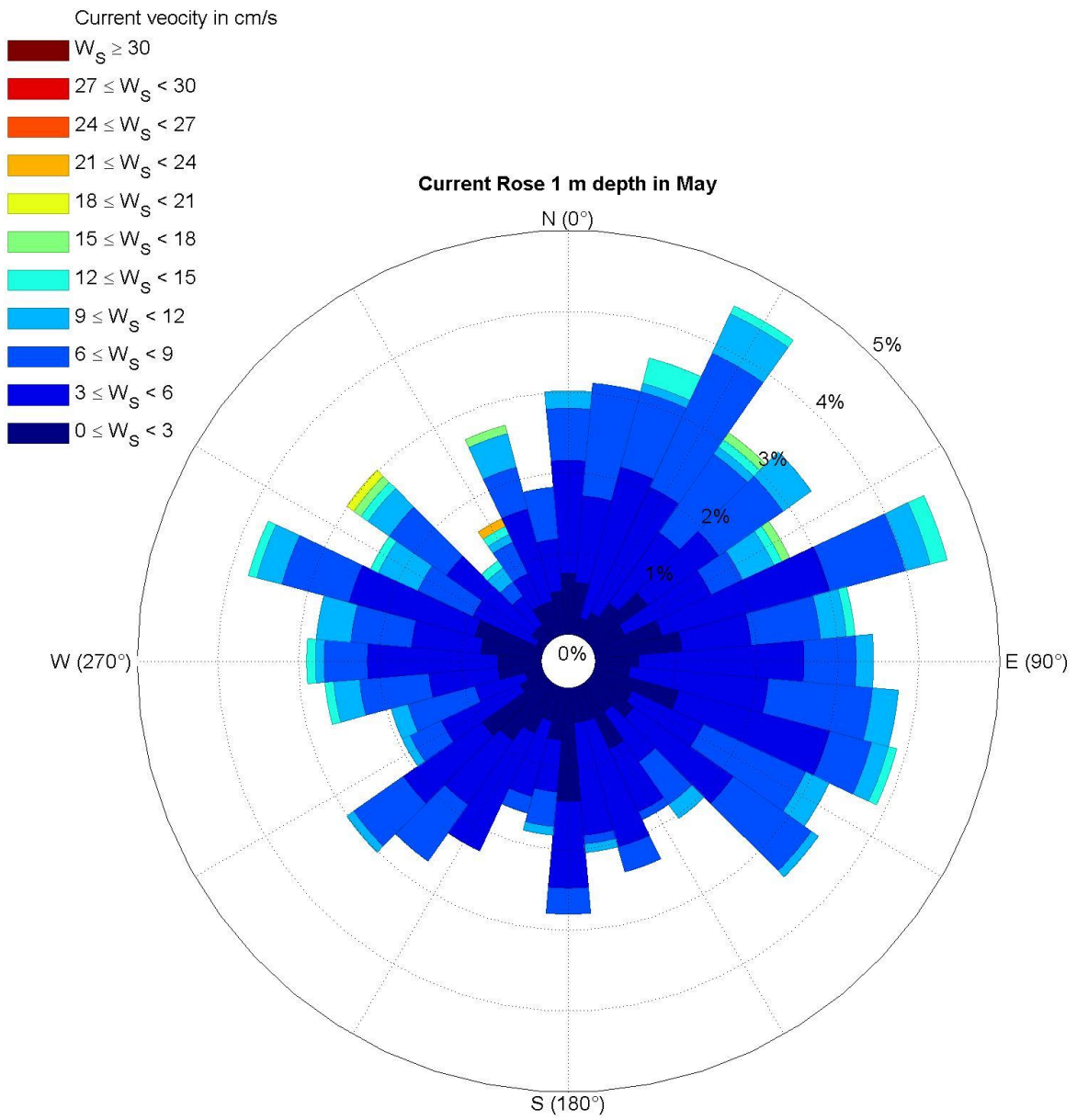


Fig. 3.3.1.17. Current rose at 1 m depth in May.

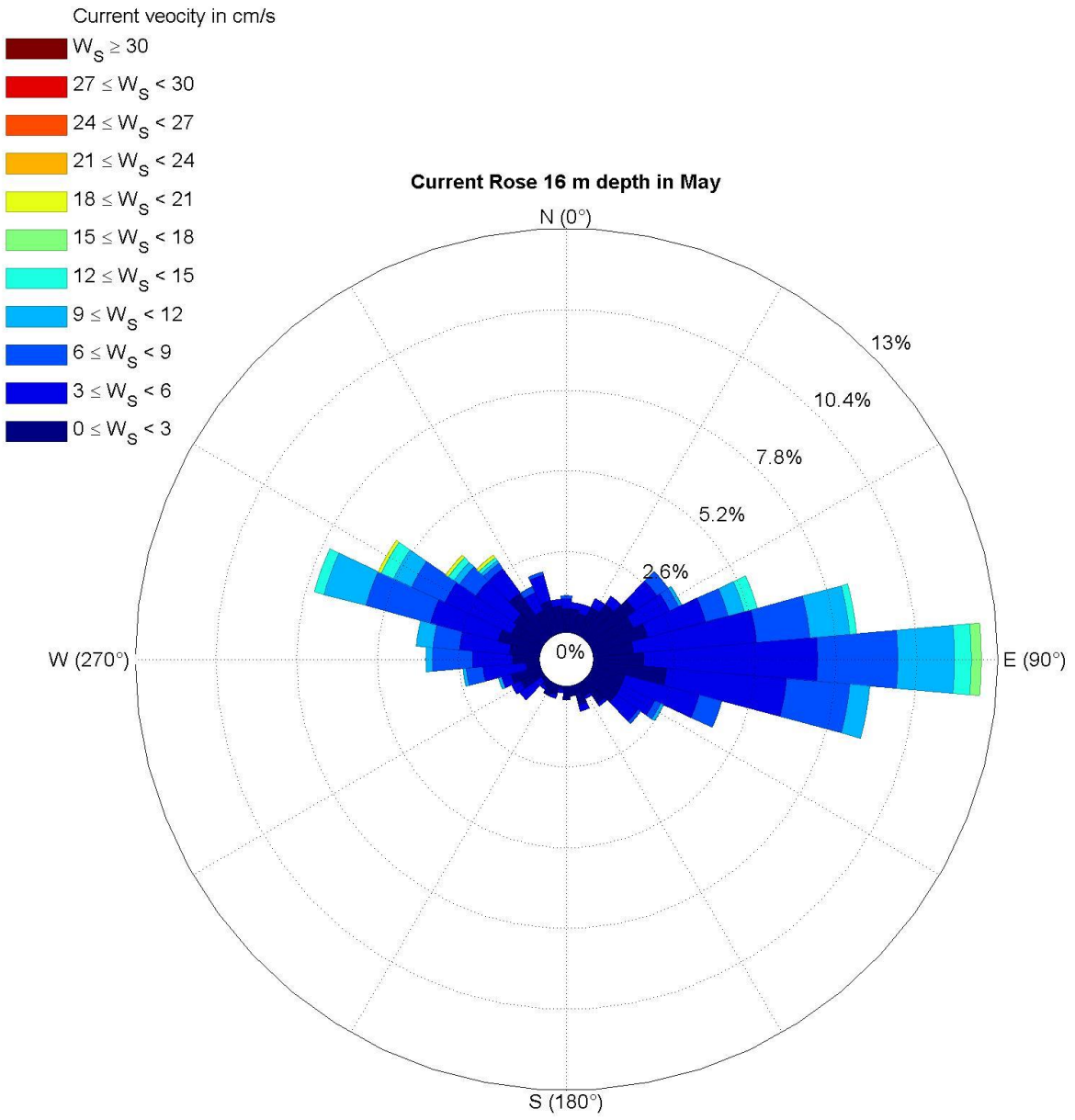


Fig. 3.3.1.18. Current rose at 16 m depth in May.

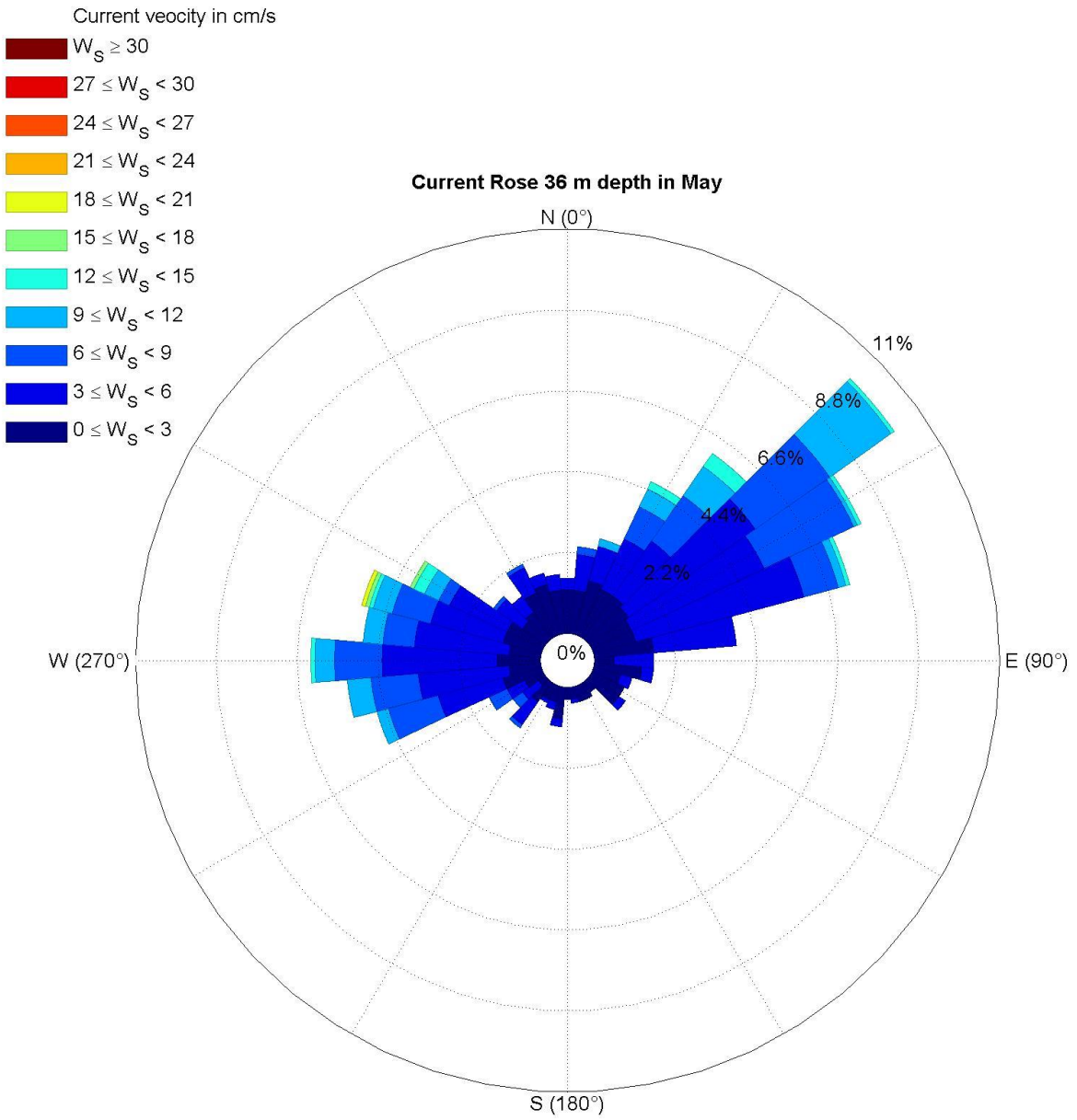


Fig. 3.3.1.19. Current rose at 36 m depth in May.

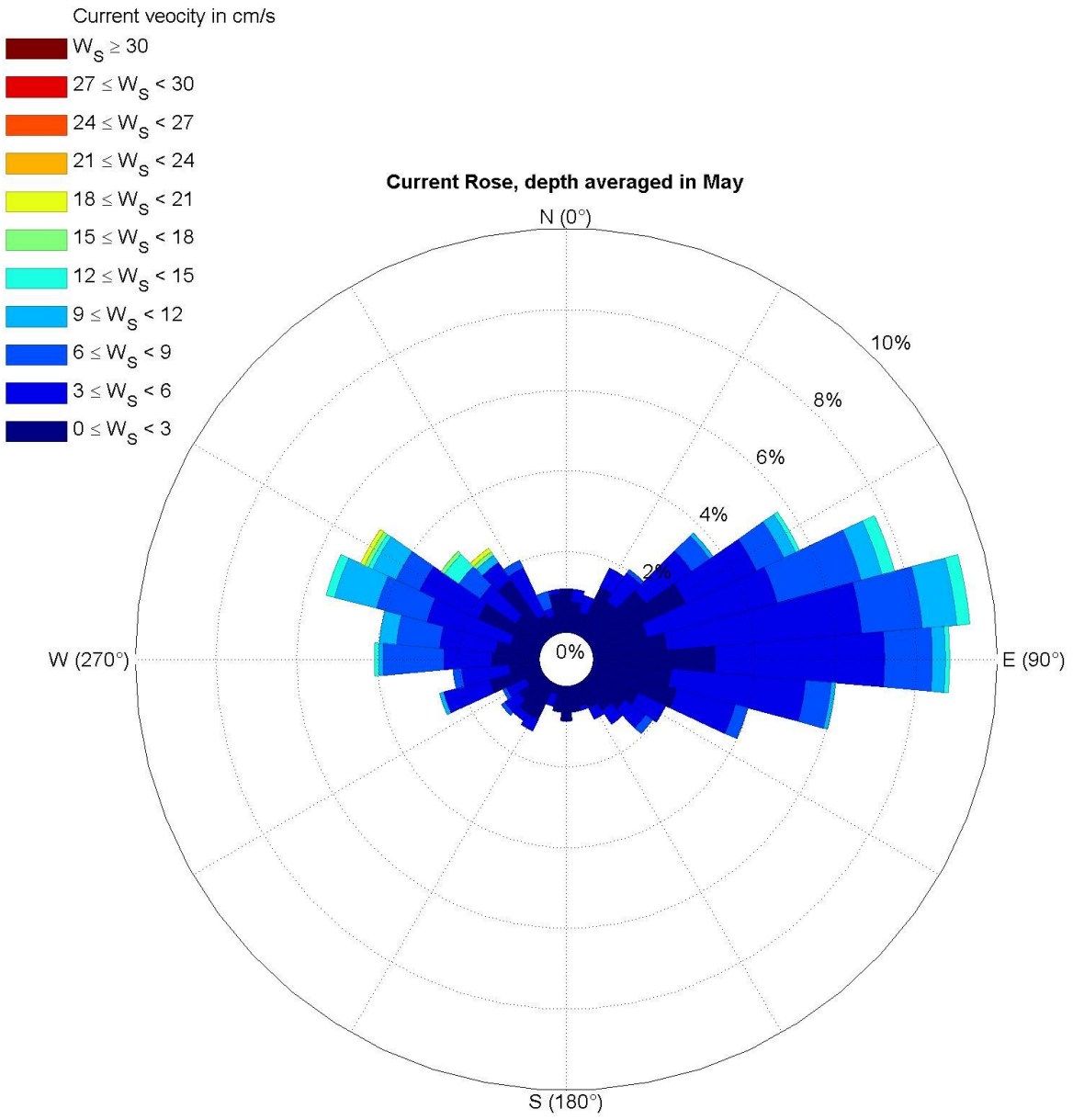


Fig. 3.3.1.20. Depth averaged current rose in May.

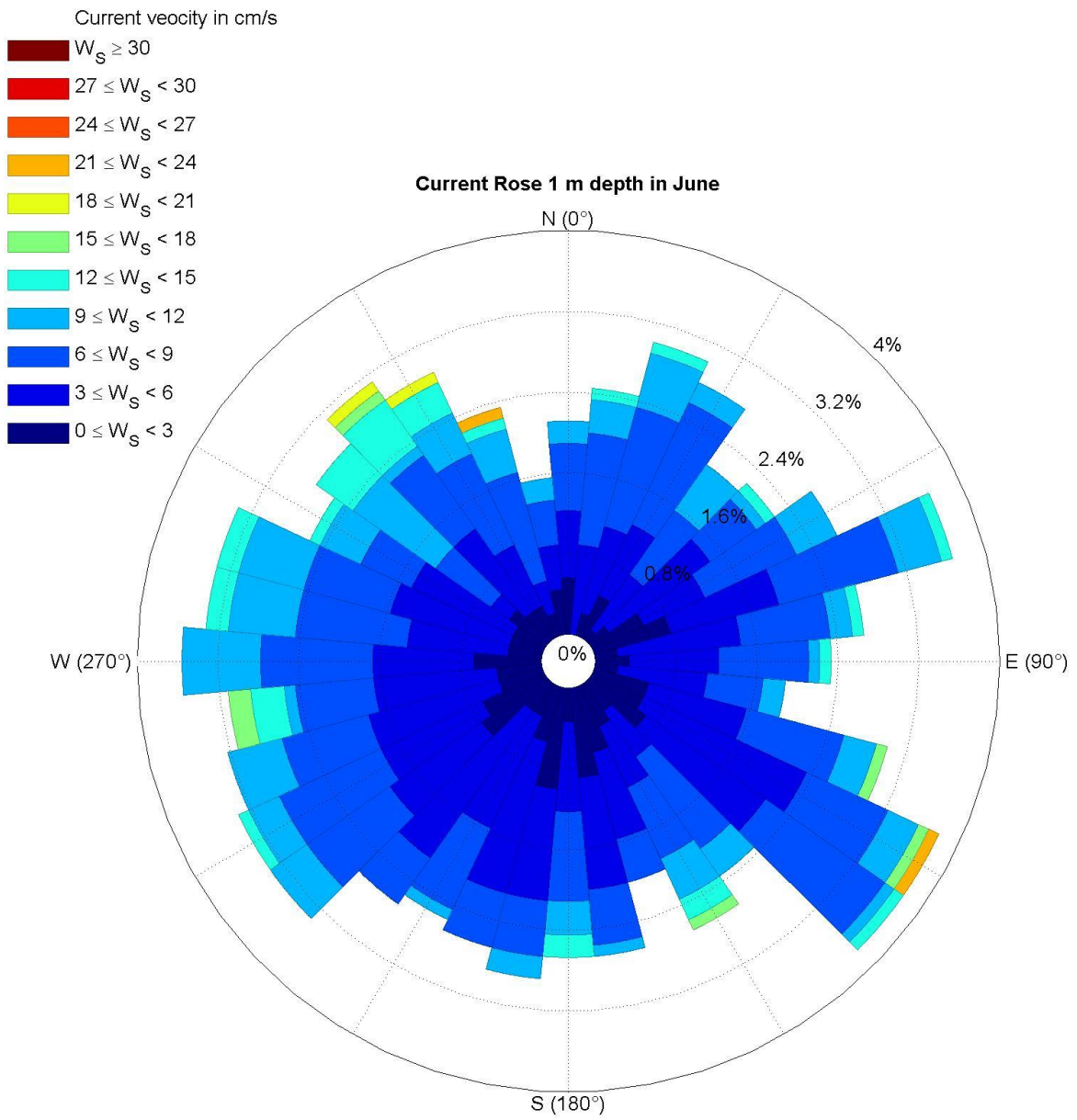


Fig. 3.3.1.21. Current rose at 1 m depth in June.

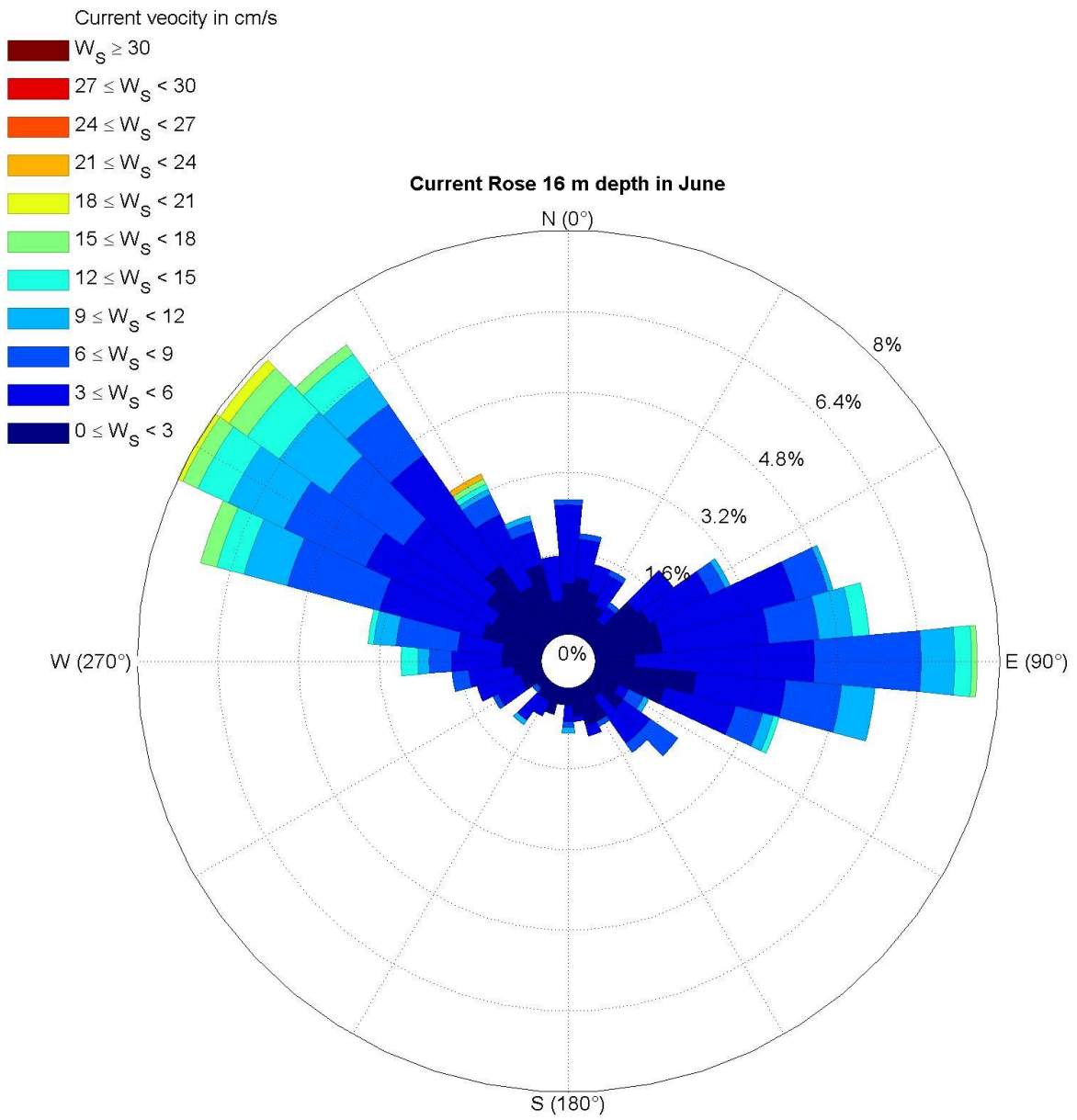


Fig. 3.3.1.22. Current rose at 16 m depth in June.

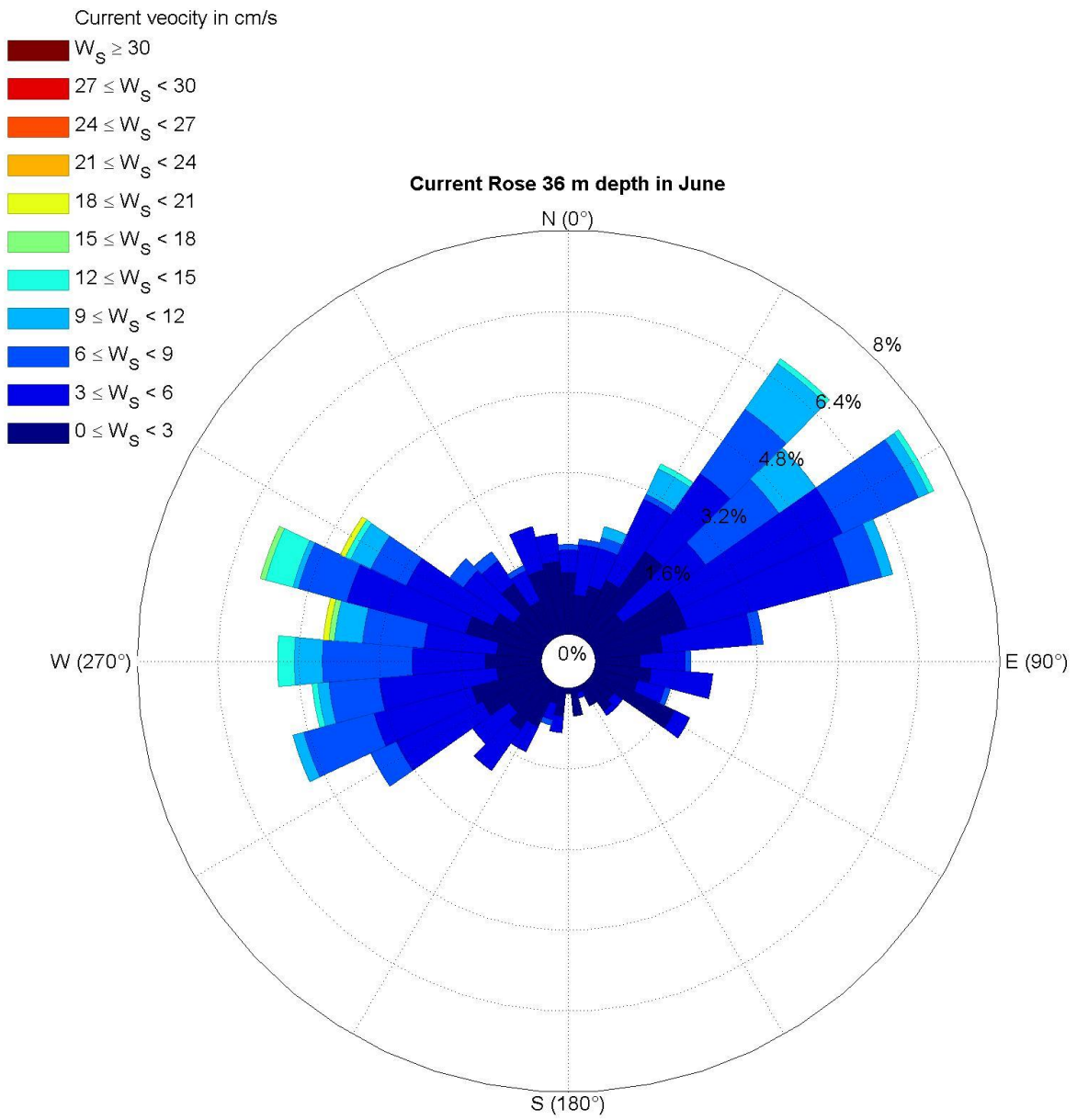


Fig. 3.3.1.23. Current rose at 36 m depth in June.

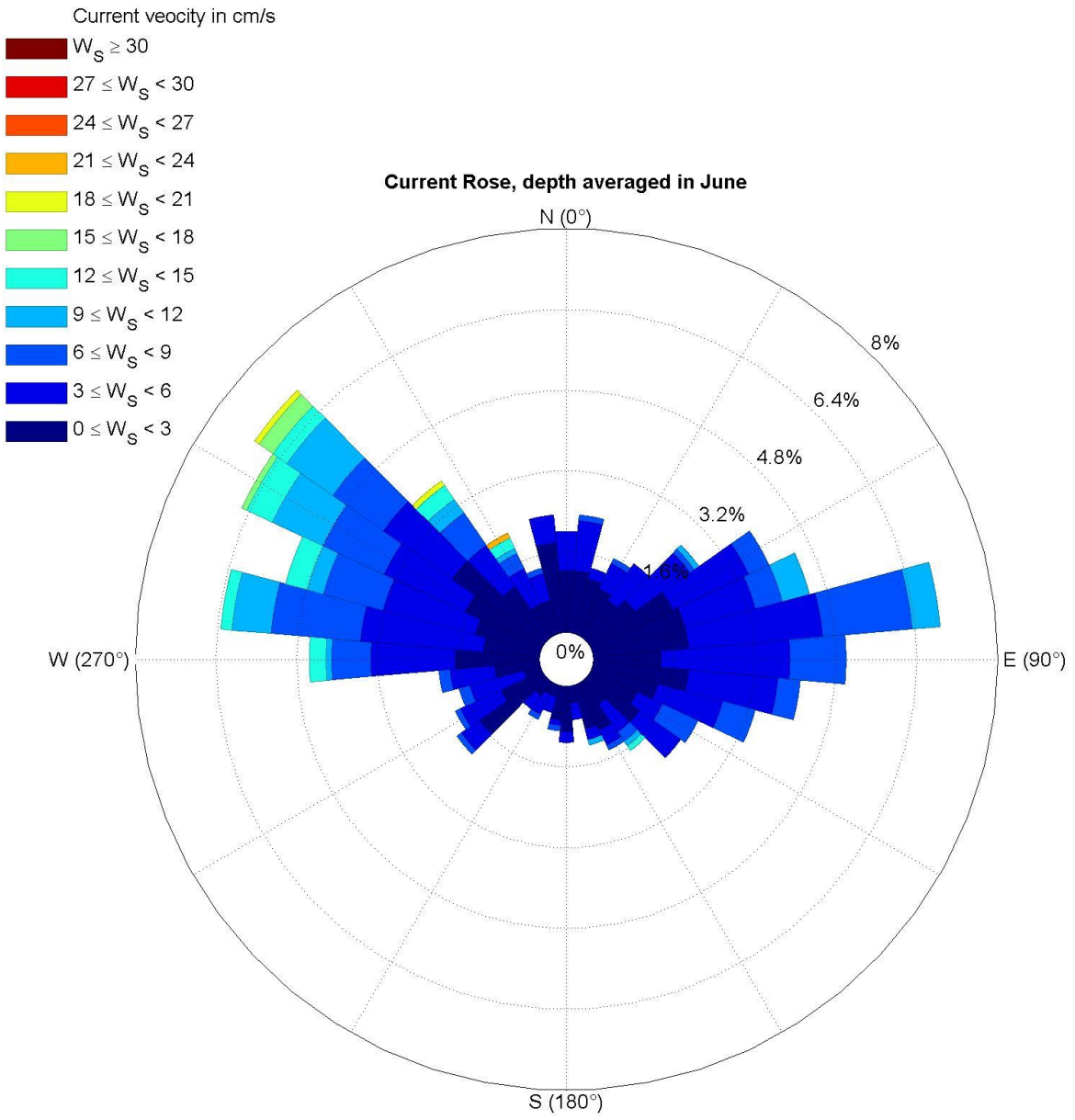


Fig. 3.3.1.24. Depth averaged current rose in June.

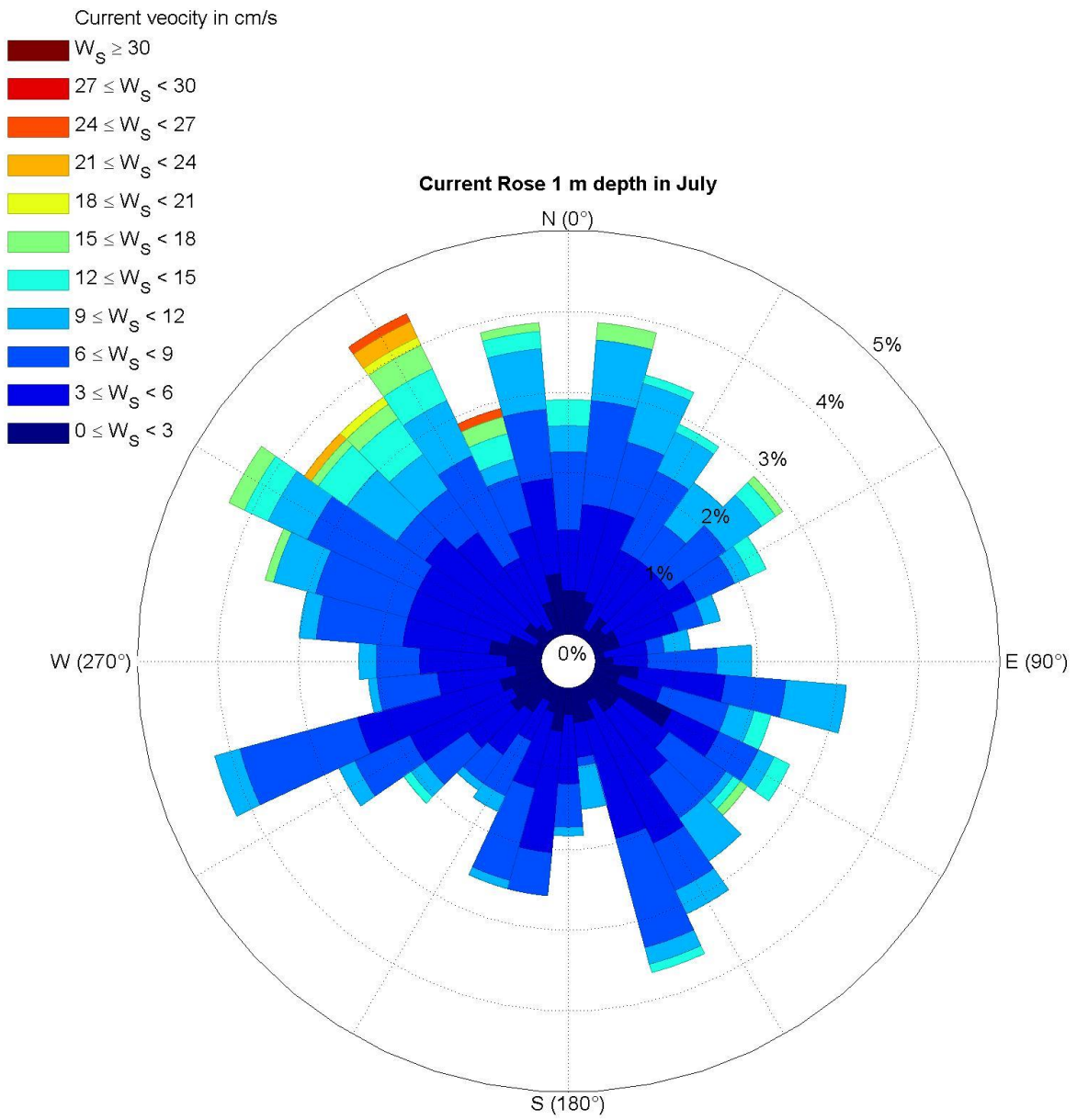


Fig. 3.3.1.25. Current rose at 1 m depth in July.

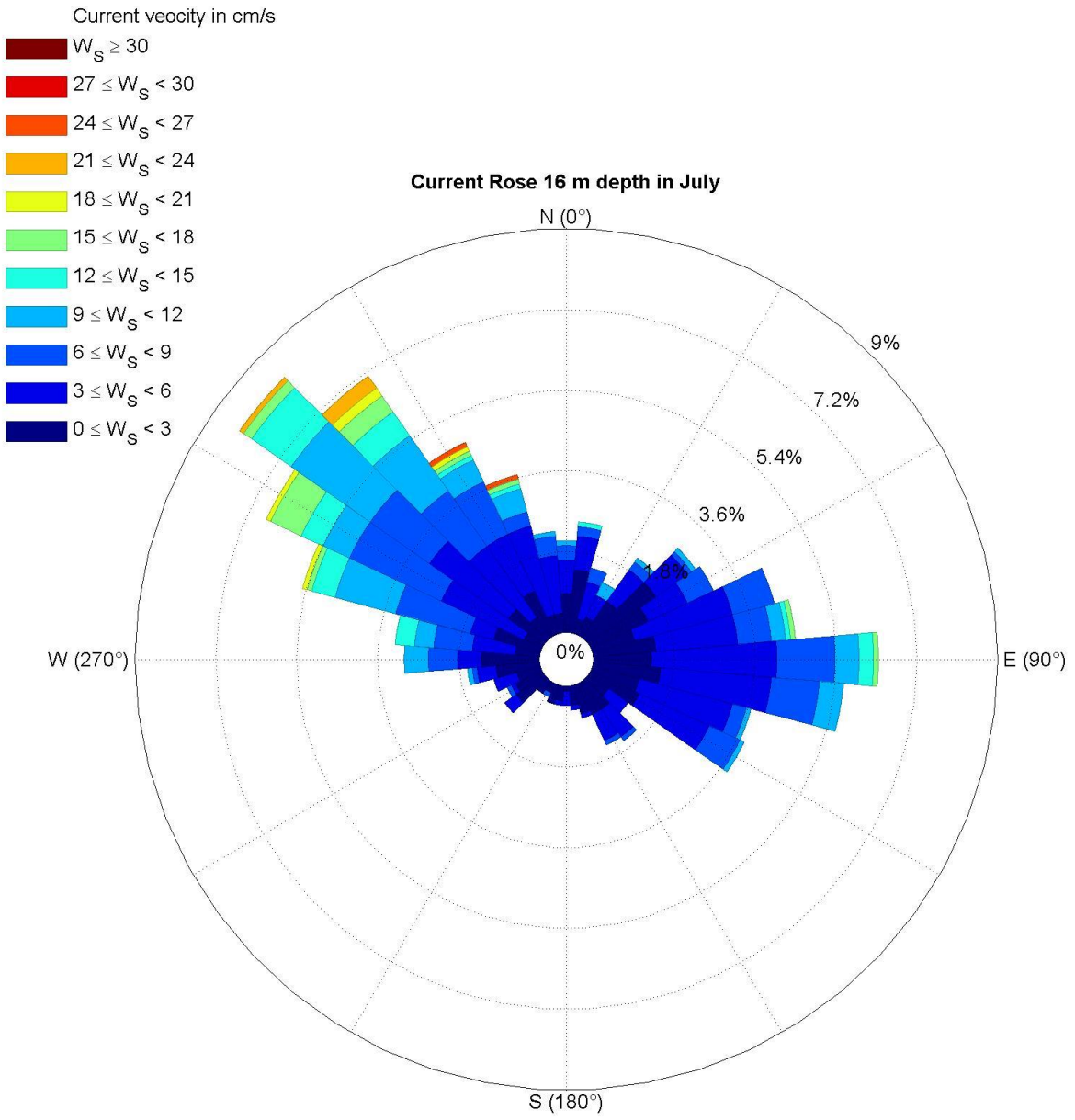


Fig. 3.3.1.26. Current rose at 16 m depth in July.

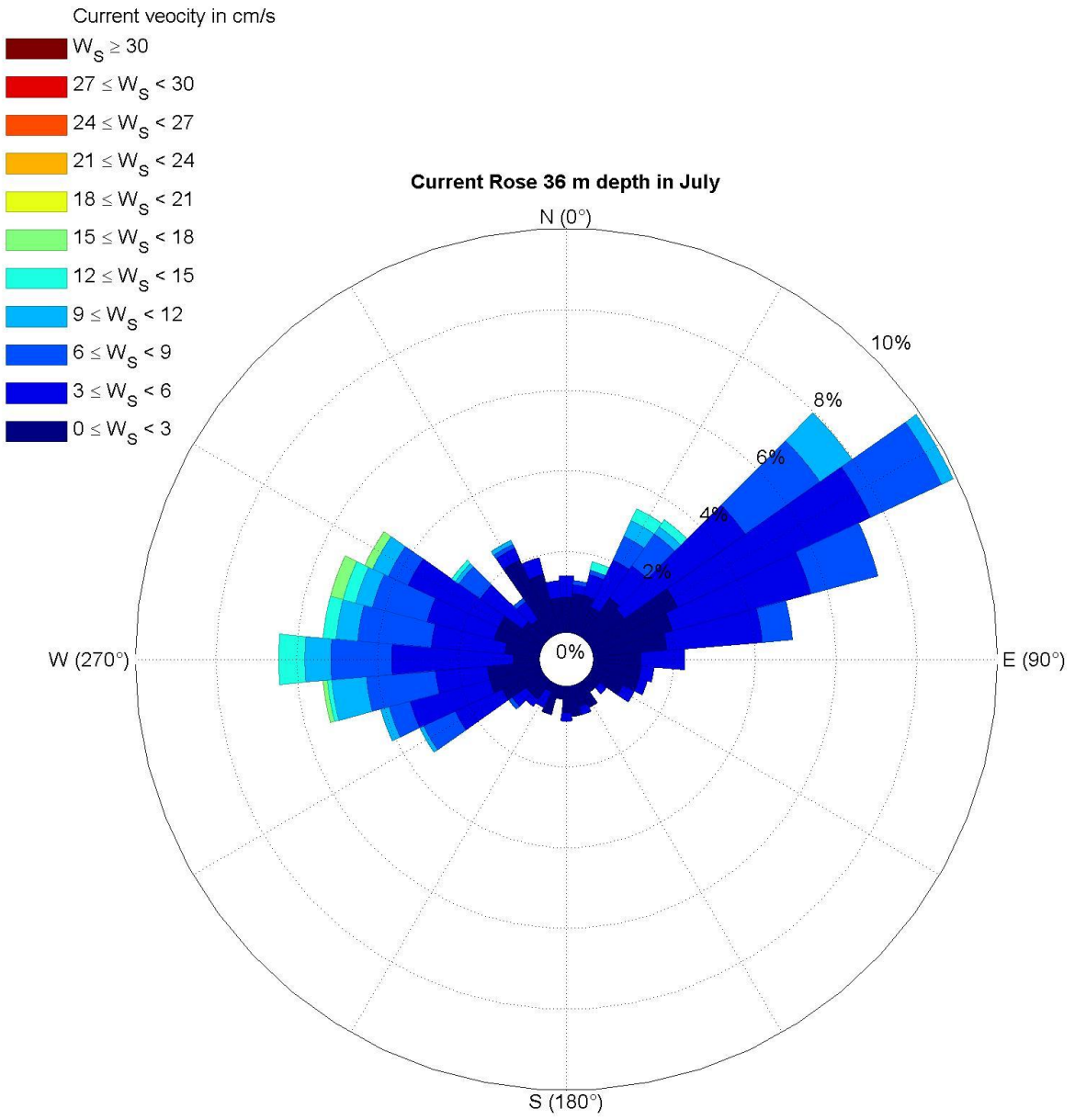


Fig. 3.3.1.27. Current rose at 36 m depth in July.

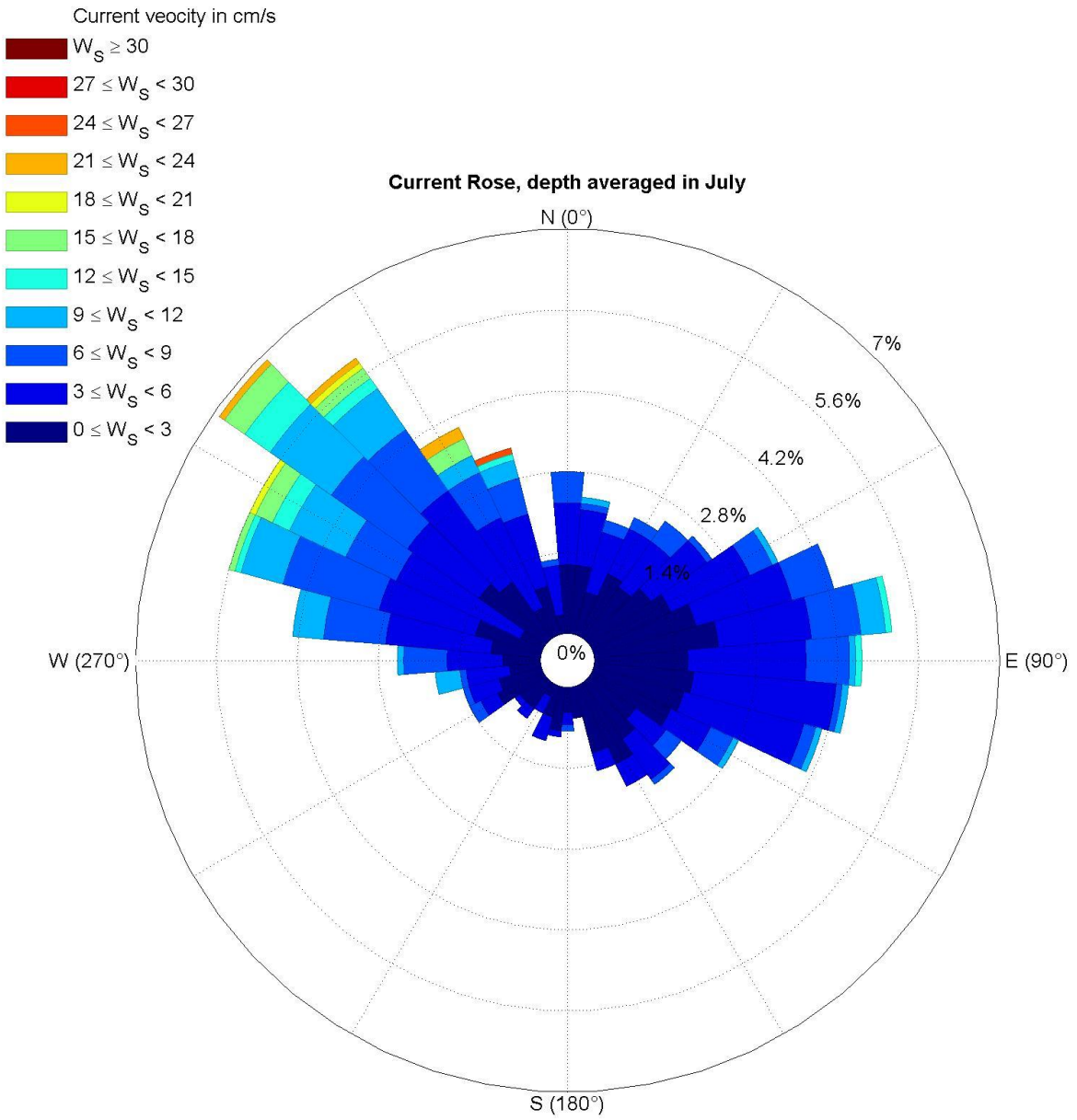


Fig. 3.3.1.28. Depth averaged current rose in July.

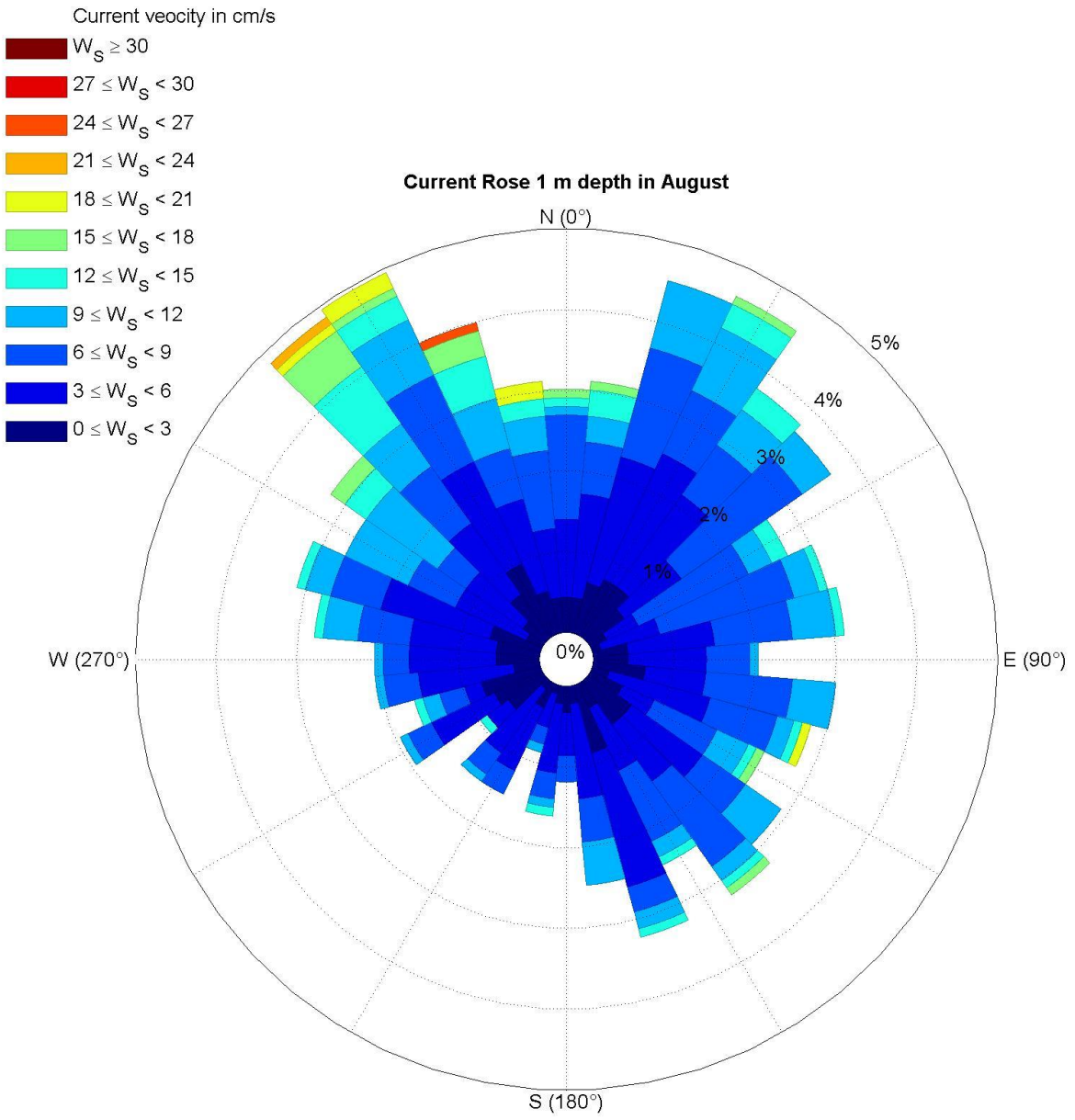


Fig. 3.3.1.29. Current rose at 1 m depth in August.

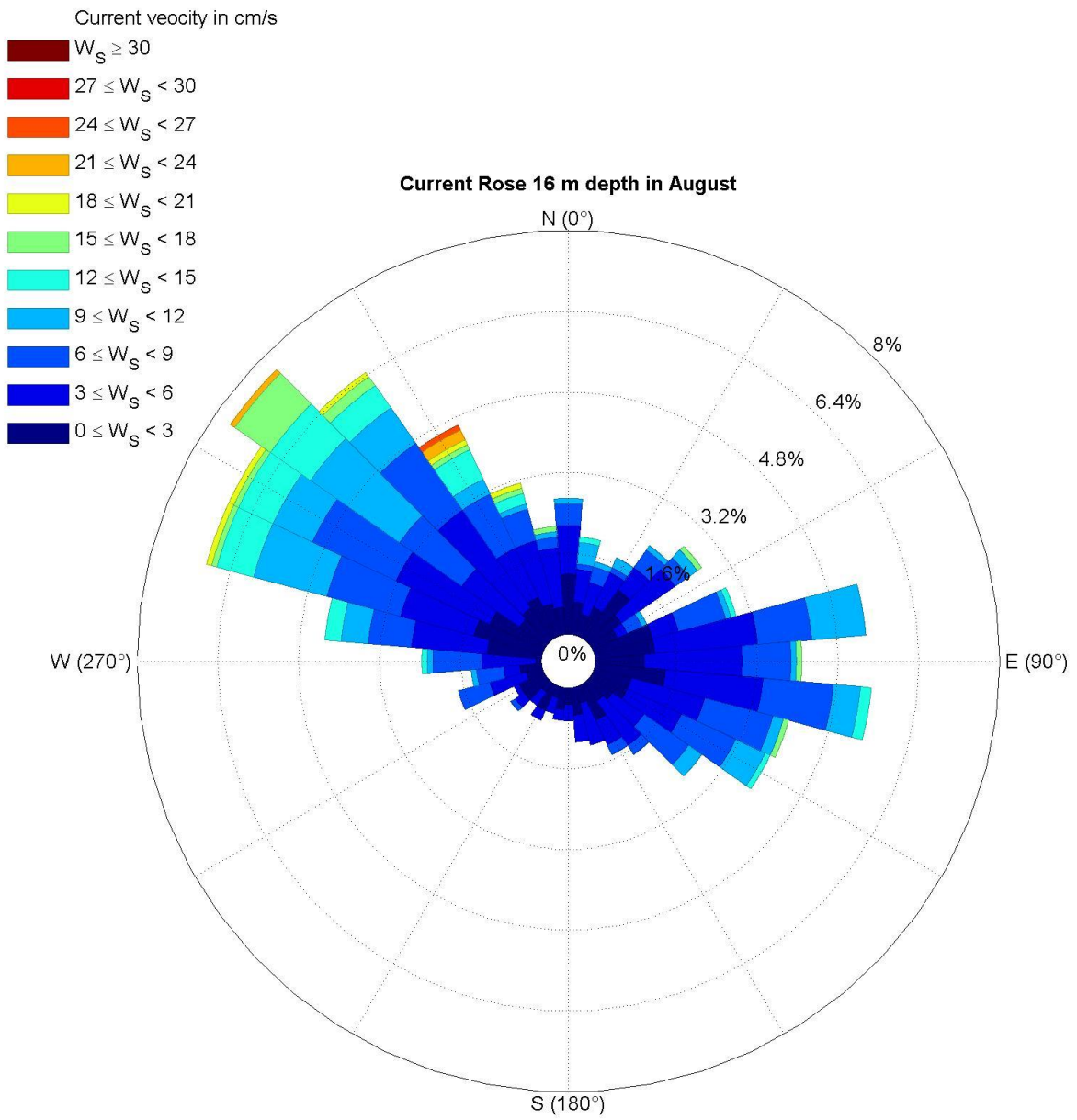


Fig. 3.3.1.30. Current rose at 16 m depth in August.

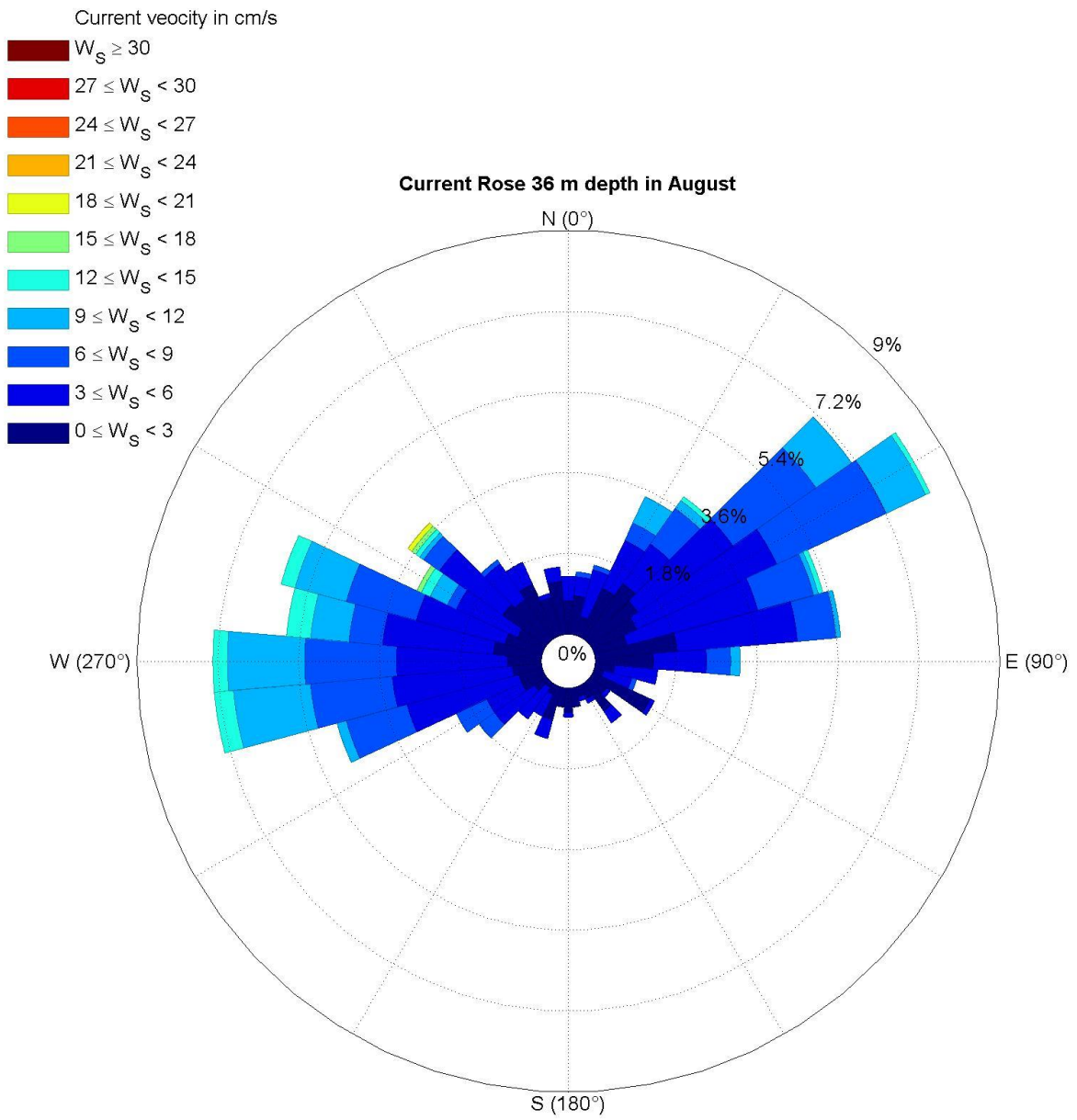


Fig. 3.3.1.31. Current rose at 36 m depth in August.

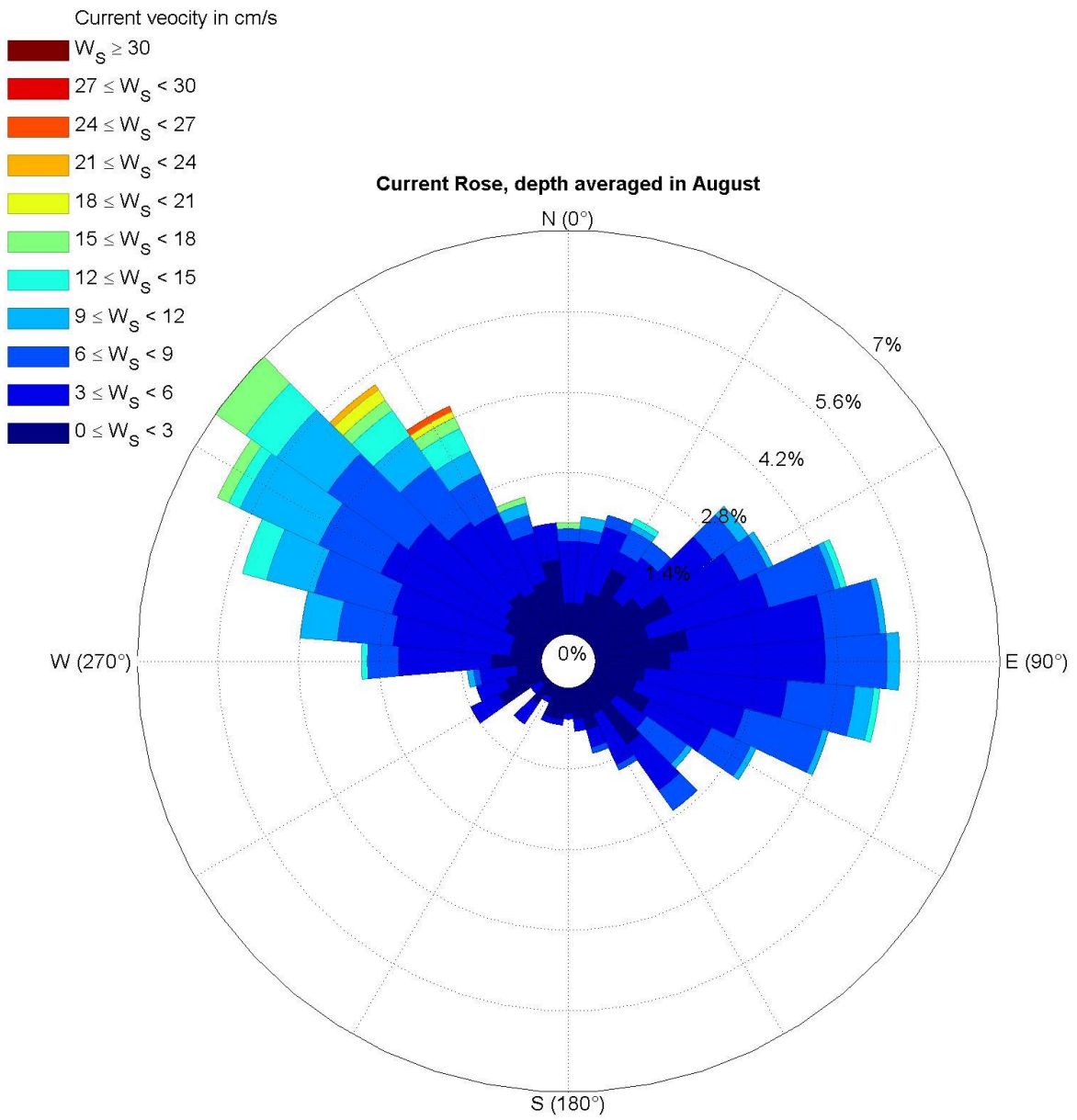


Fig. 3.3.1.32. Depth averaged current rose in August.

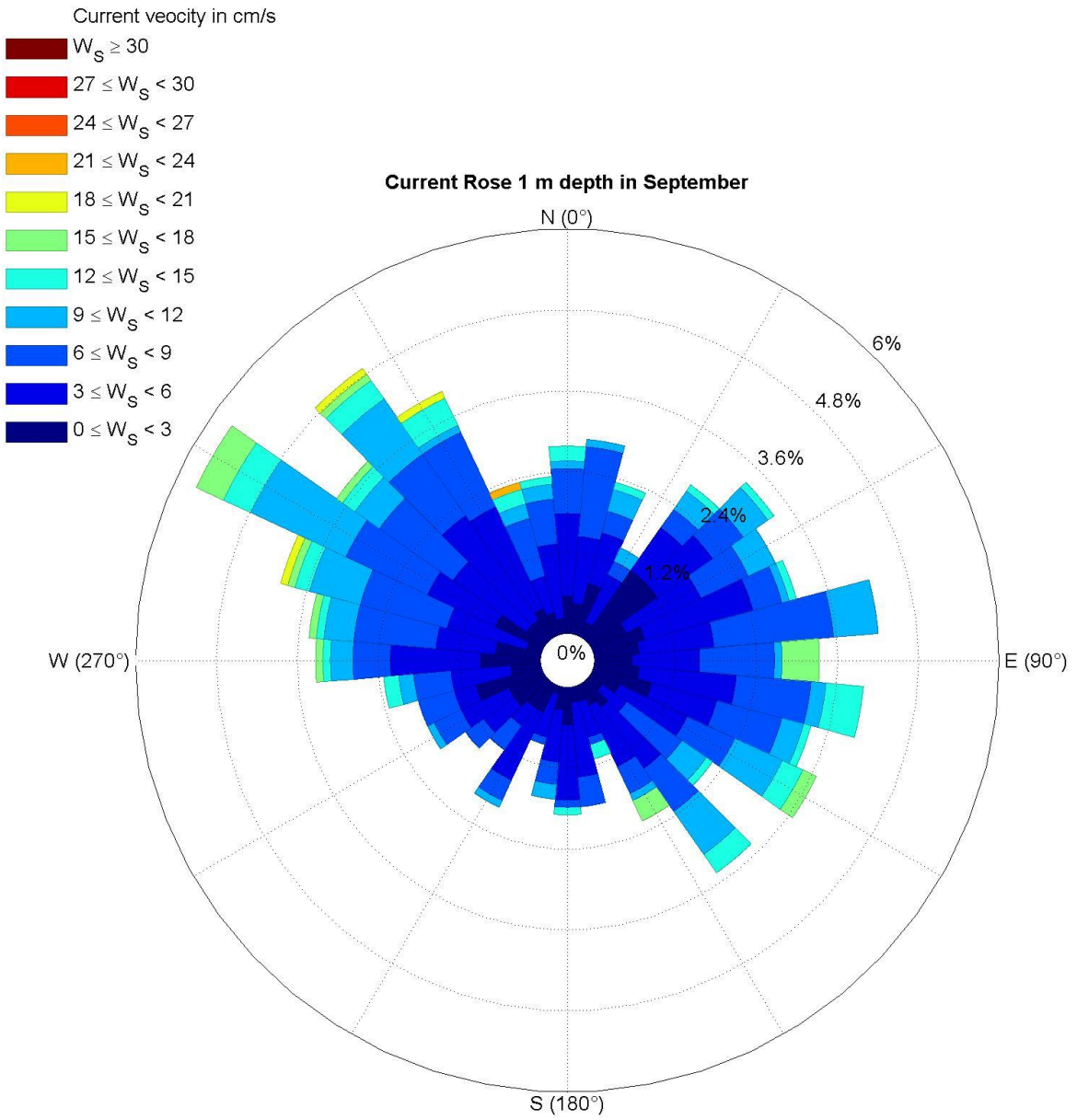


Fig. 3.3.1.33. Current rose at 1 m depth in September.

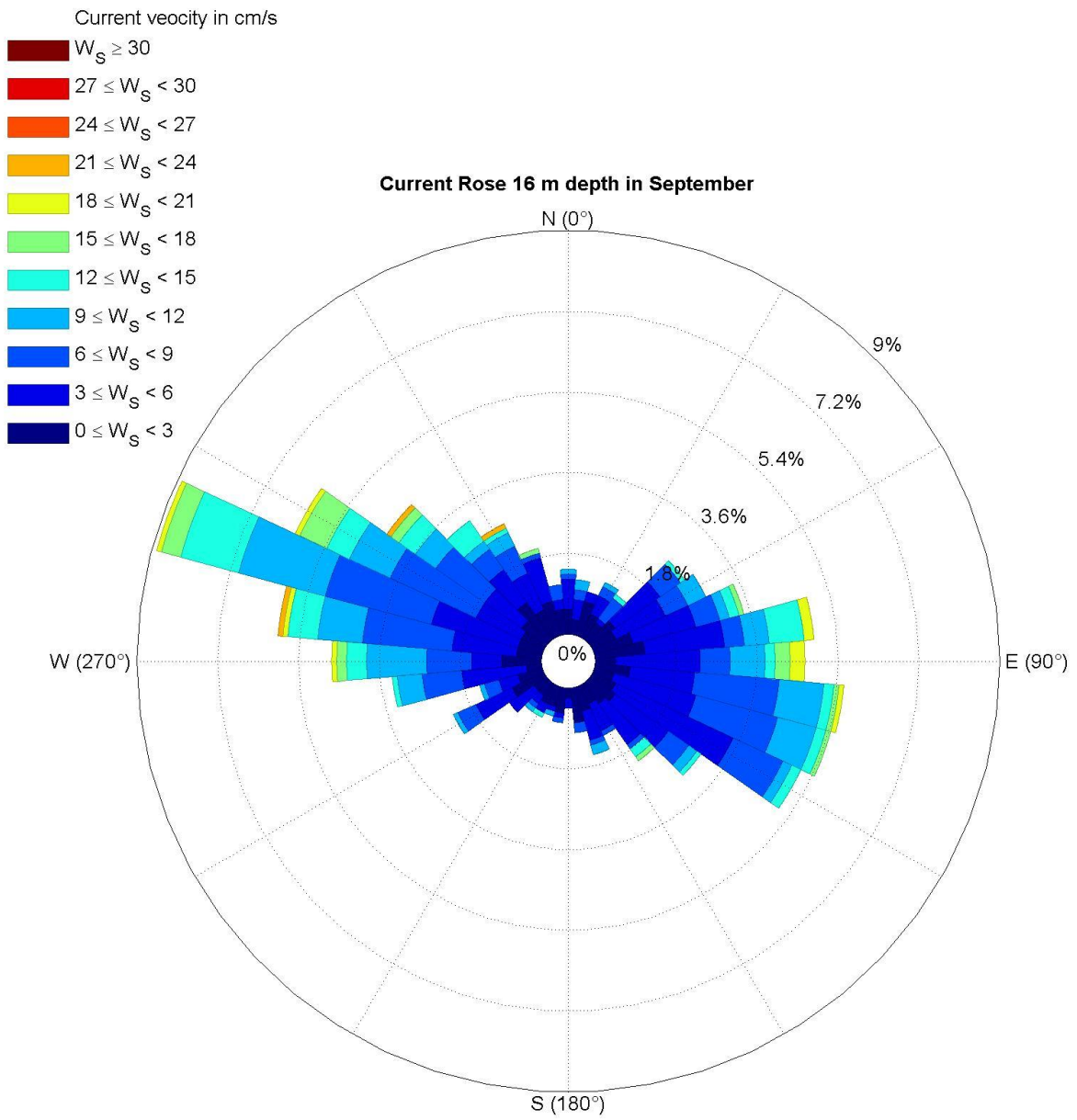


Fig. 3.3.1.34. Current rose at 16 m depth in September.

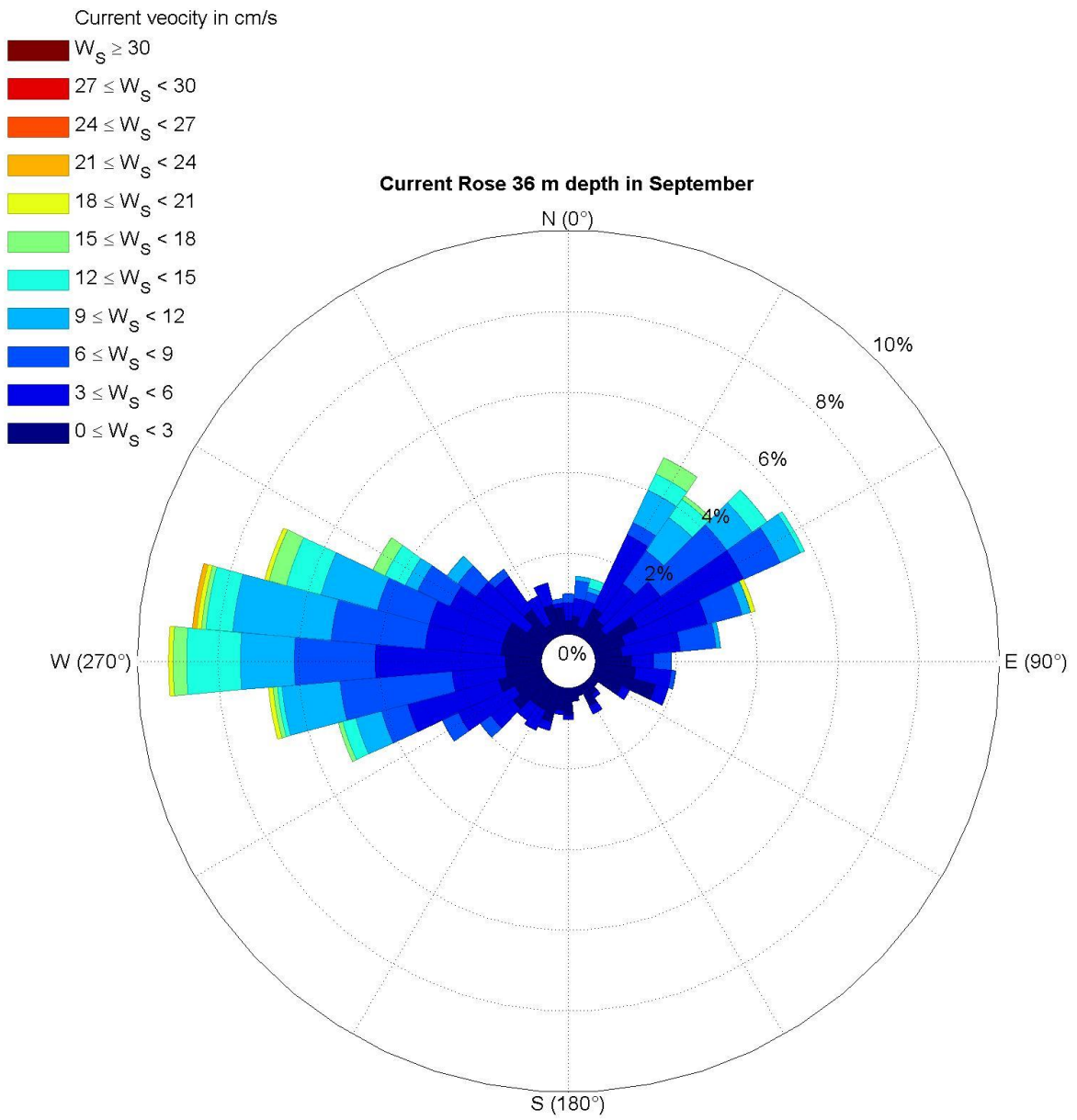


Fig. 3.3.1.35. Current rose at 36 m depth in September.

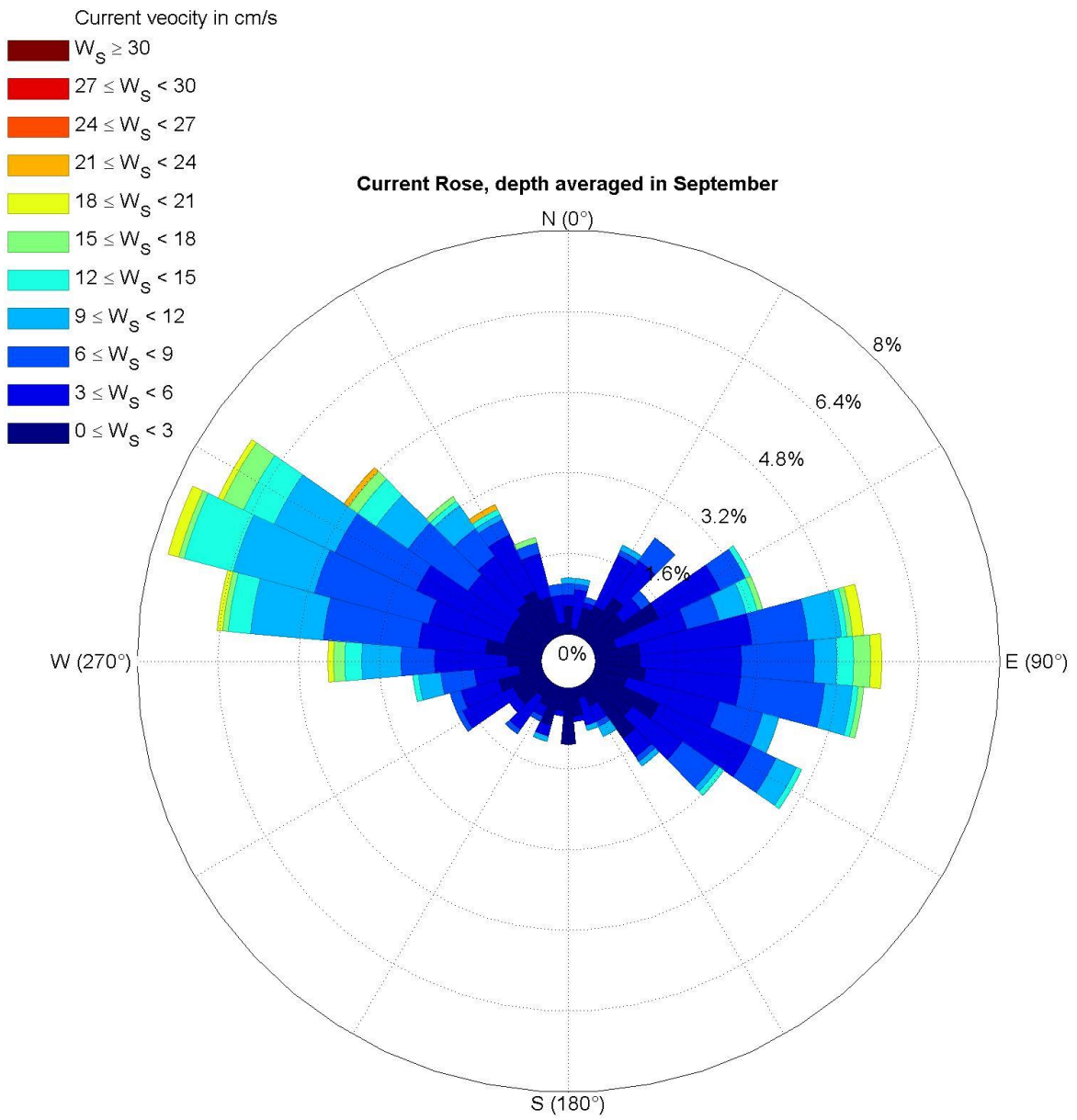


Fig. 3.3.1.36. Depth averaged current rose in September.

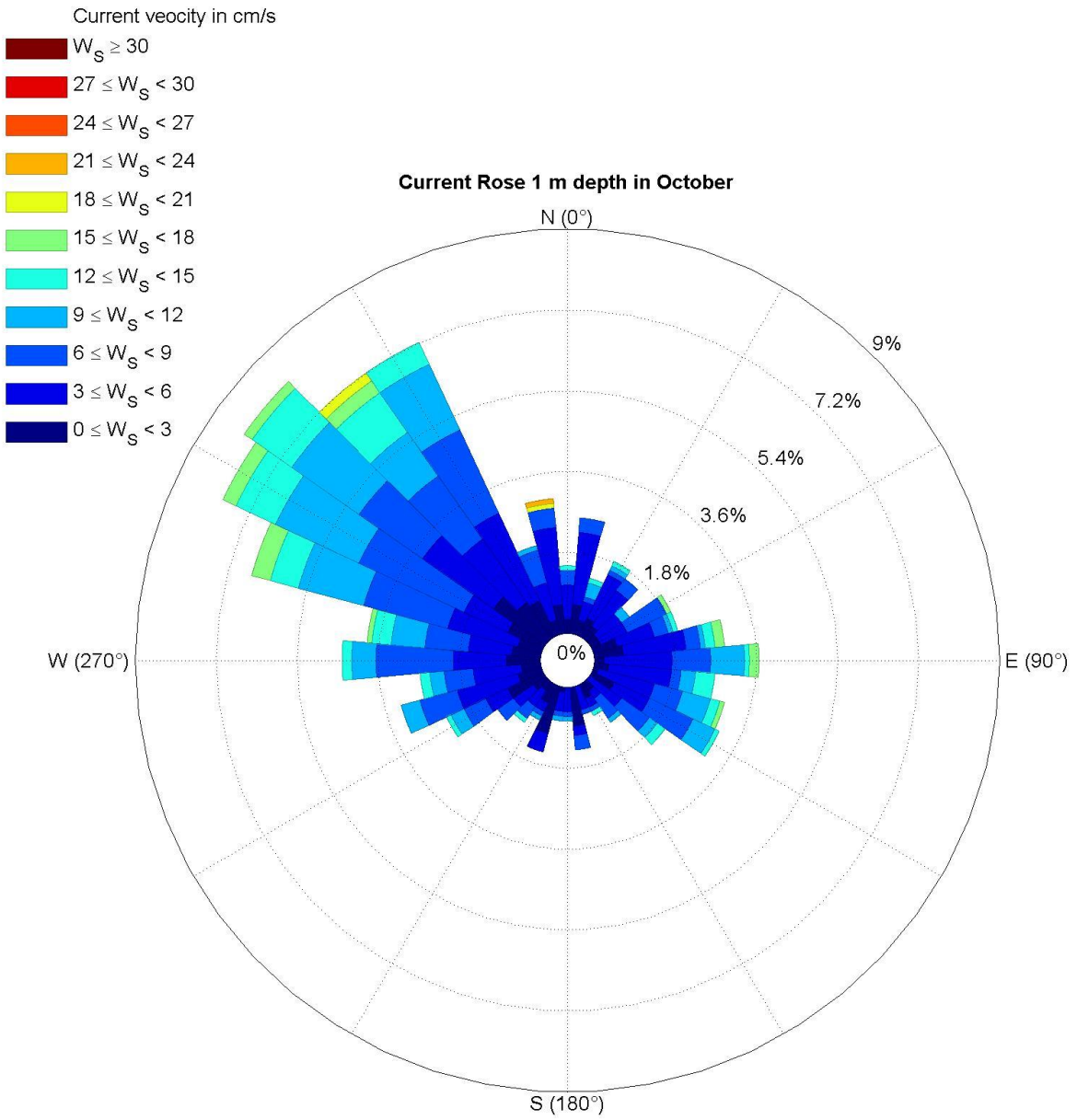


Fig. 3.3.1.37. Current rose at 1 m depth in October.

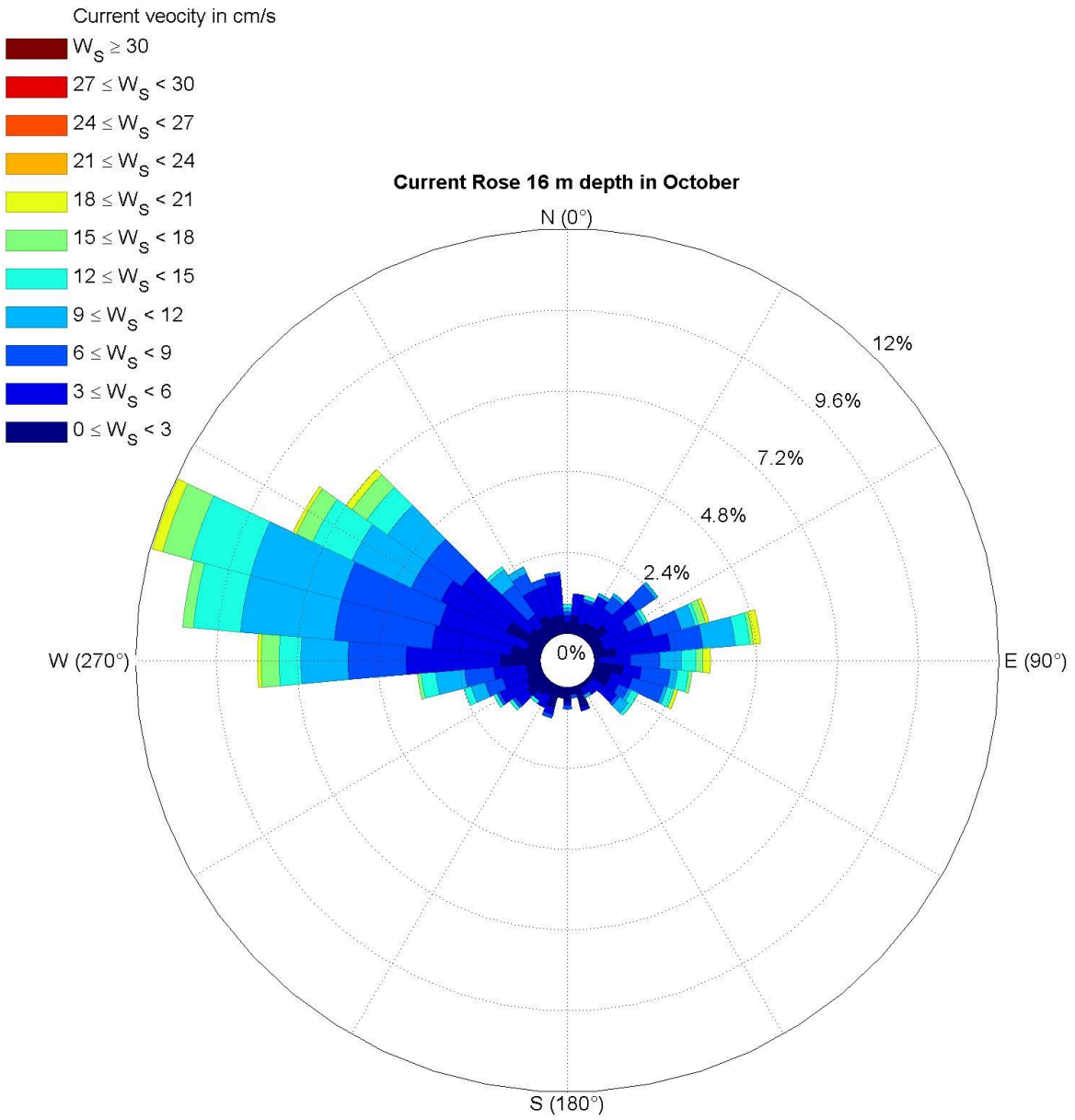


Fig. 3.3.1.38. Current rose at 16 m depth in October.

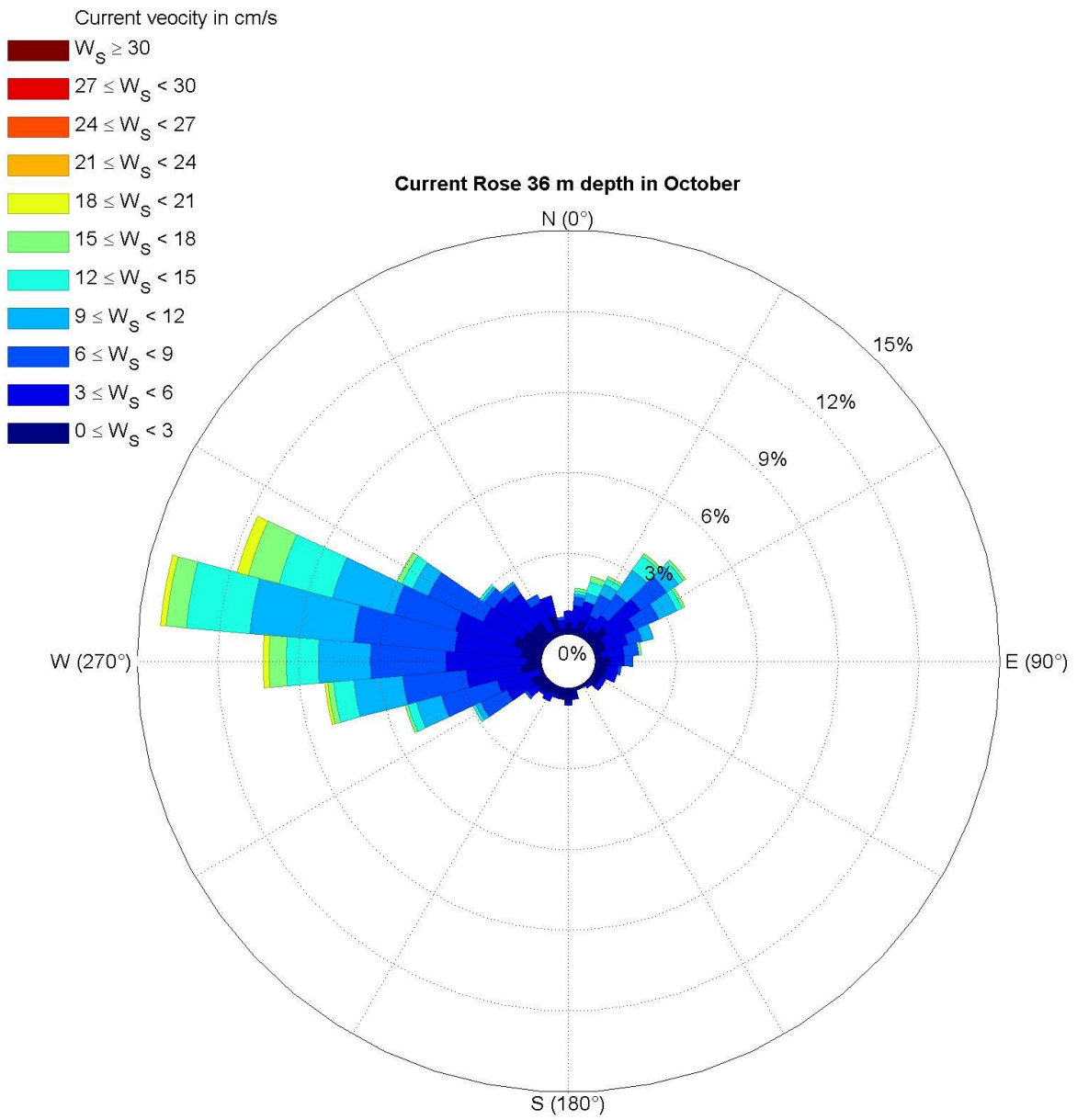


Fig. 3.3.1.39. Current rose at 36 m depth in October.

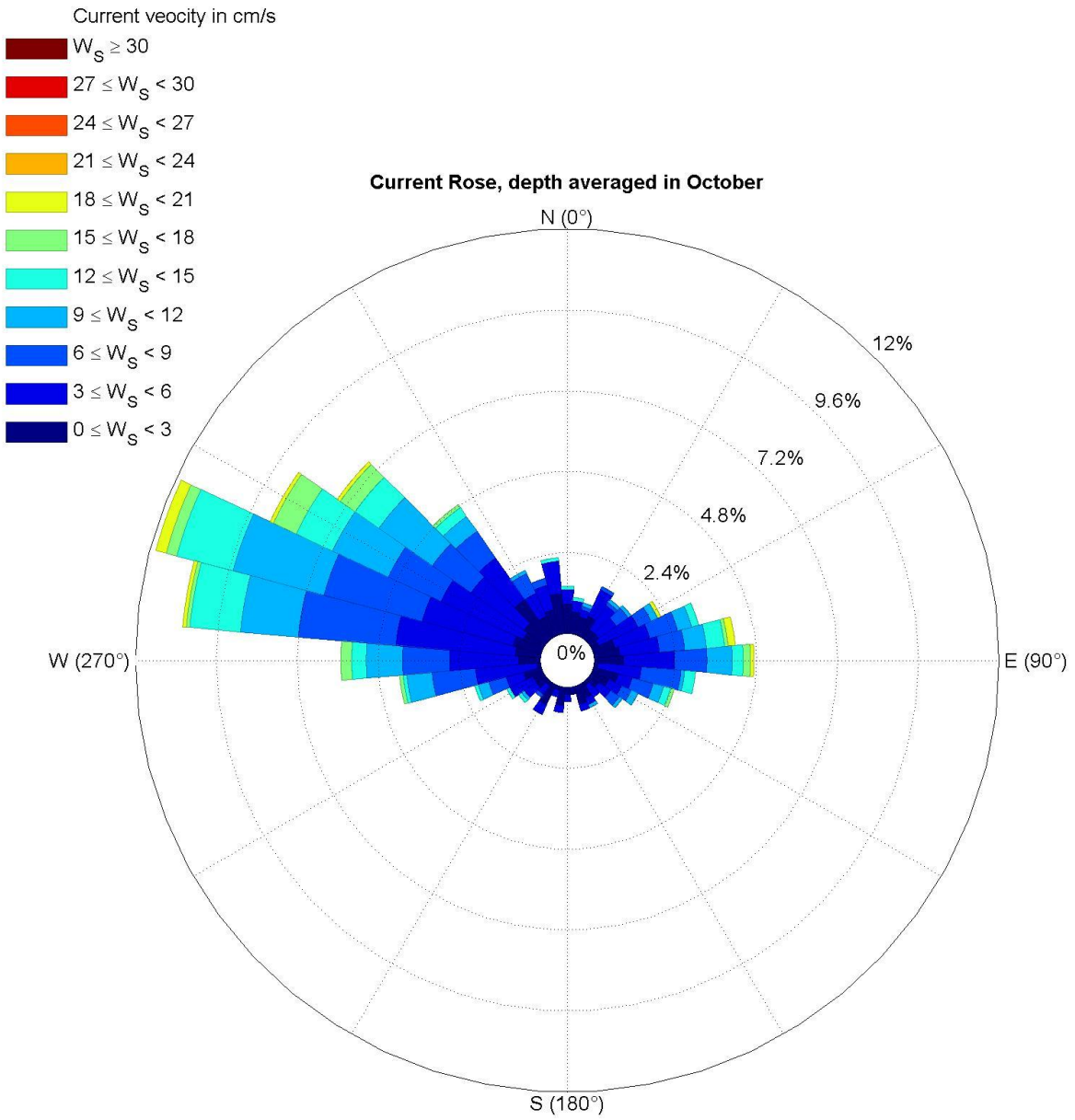


Fig. 3.3.1.40. Depth averaged current rose in October.

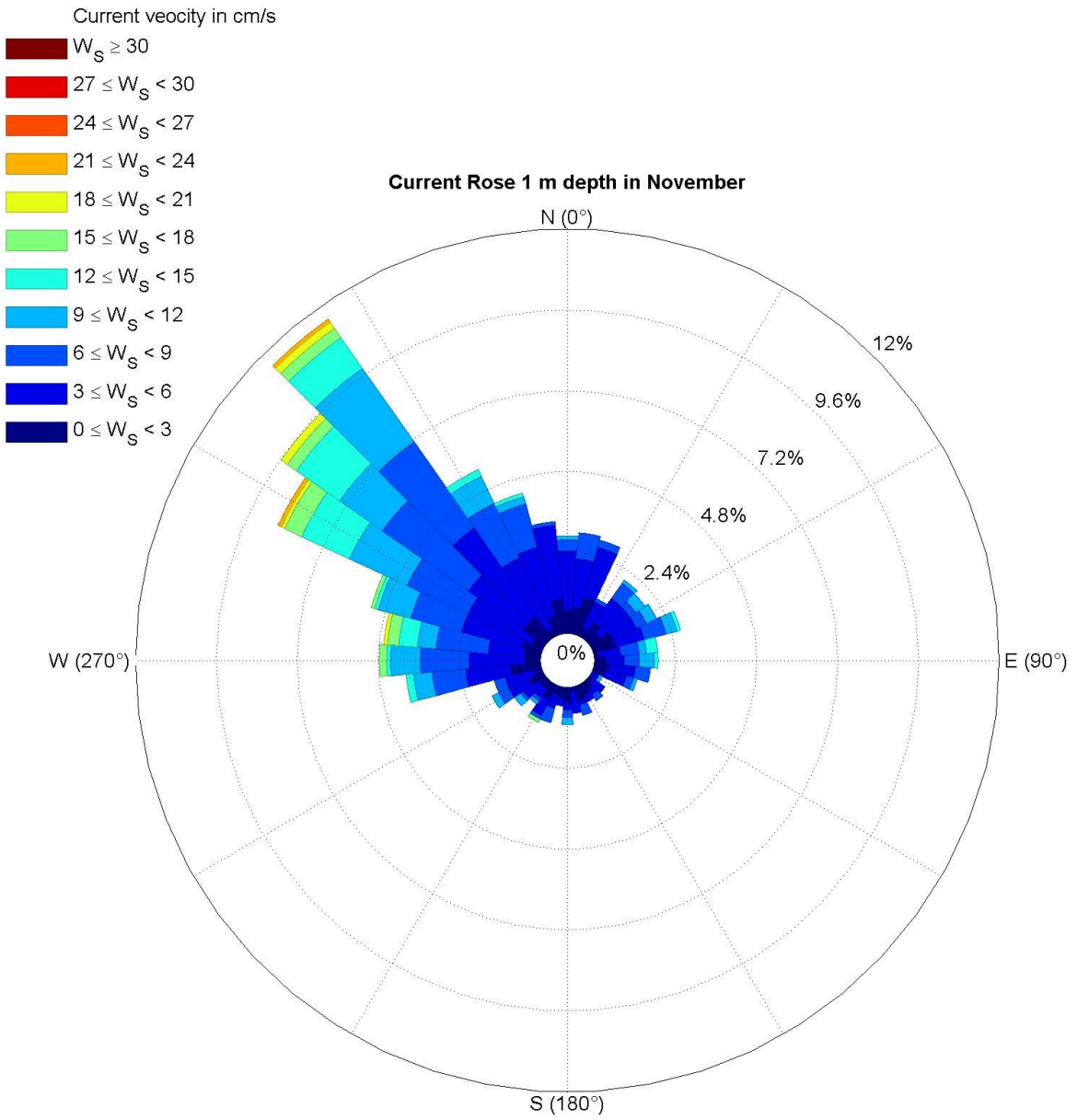


Fig. 3.3.1.41. Current rose at 1 m depth in November.

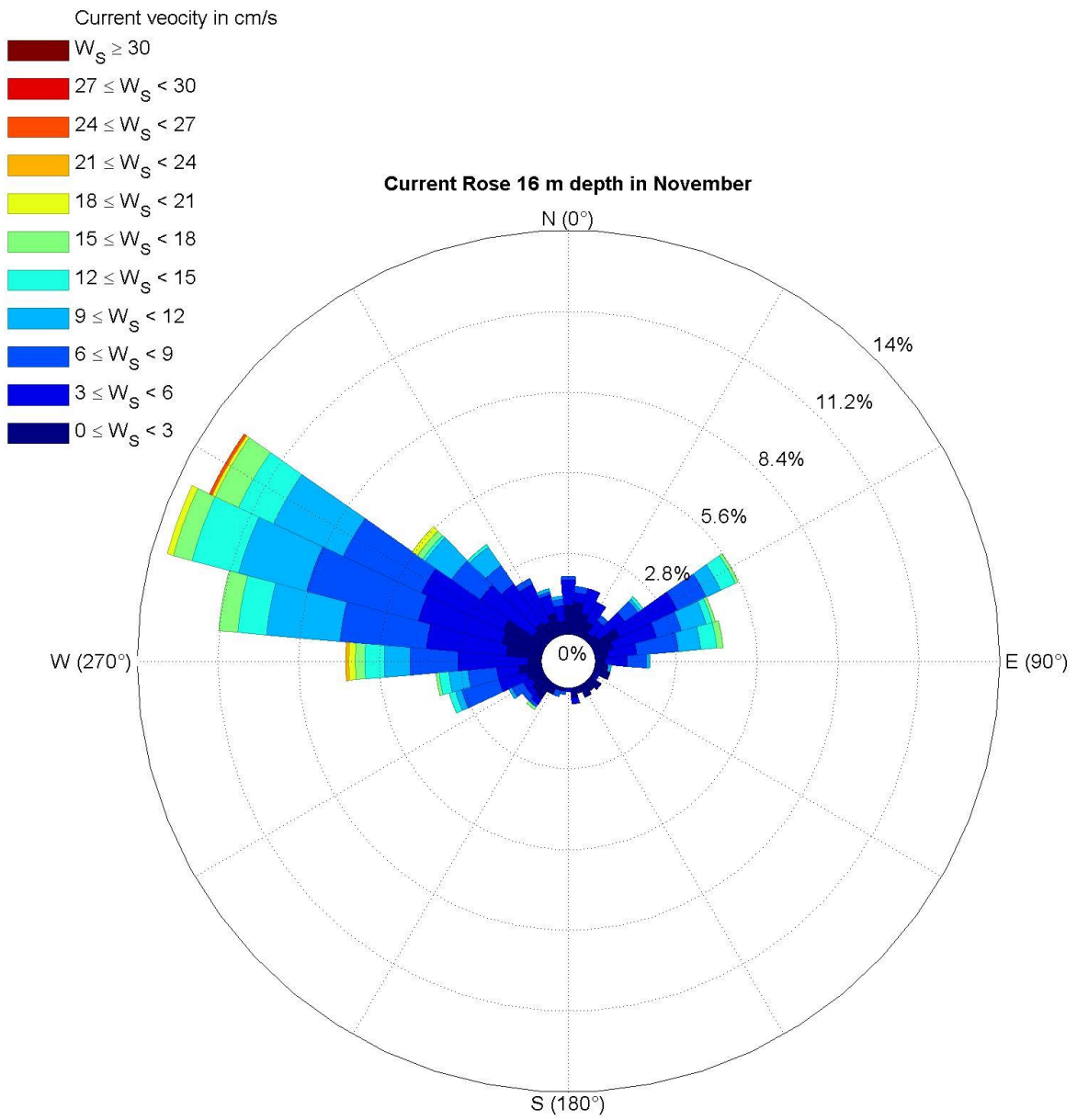


Fig. 3.3.1.42. Current rose at 16 m depth in November.

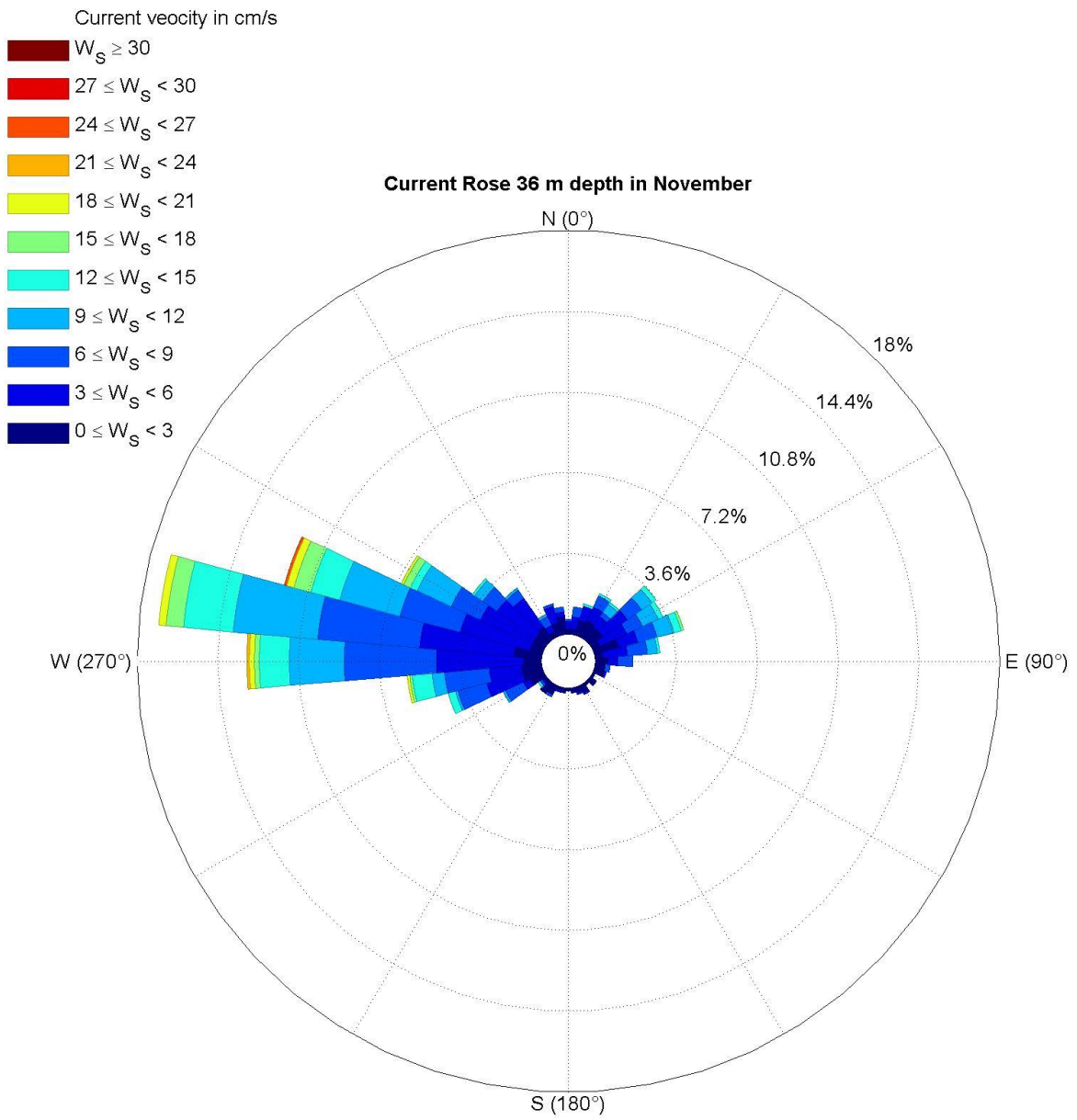


Fig. 3.3.1.43. Current rose at 36 m depth in November.

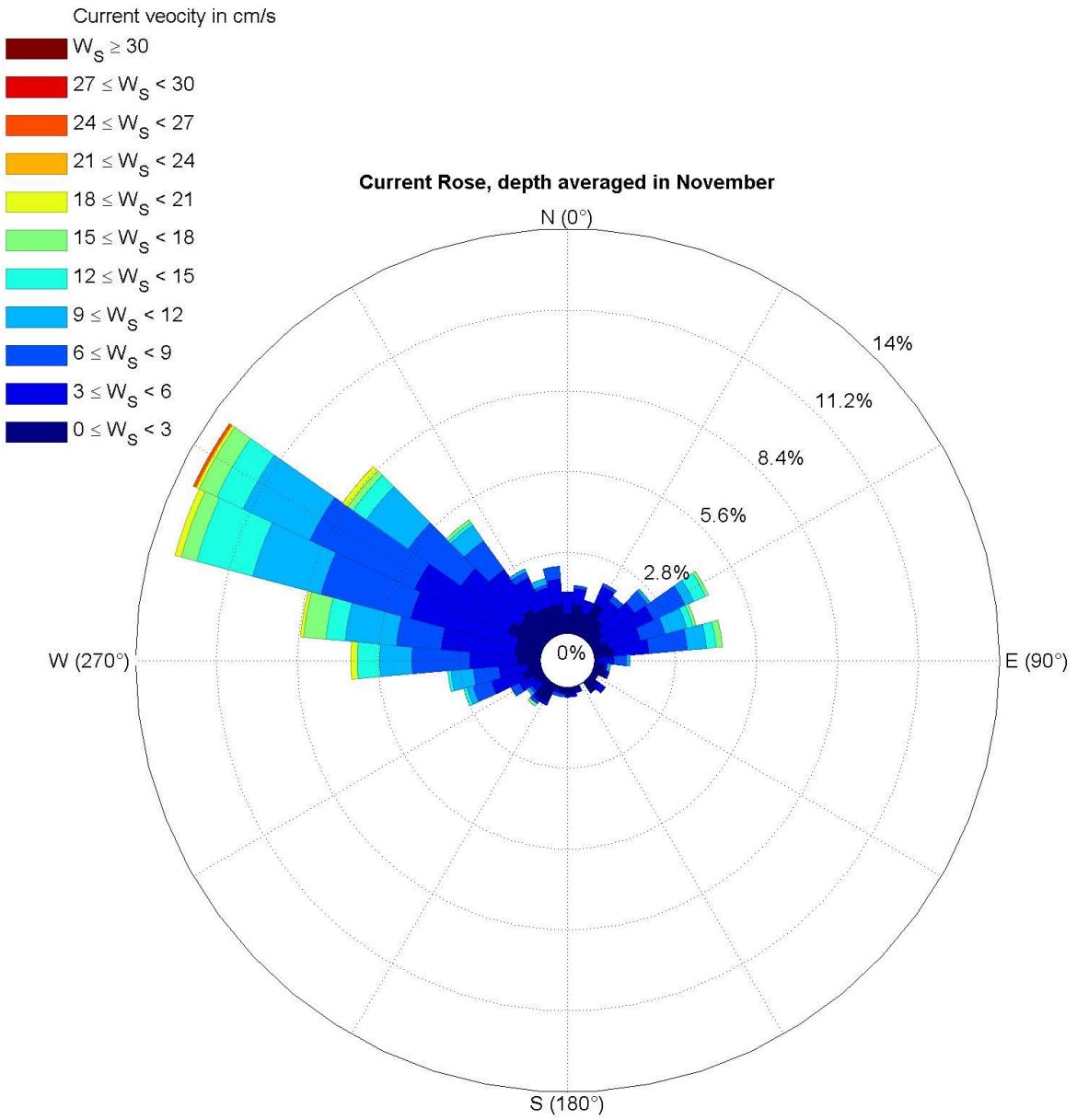


Fig. 3.3.1.44. Depth averaged current rose in November.

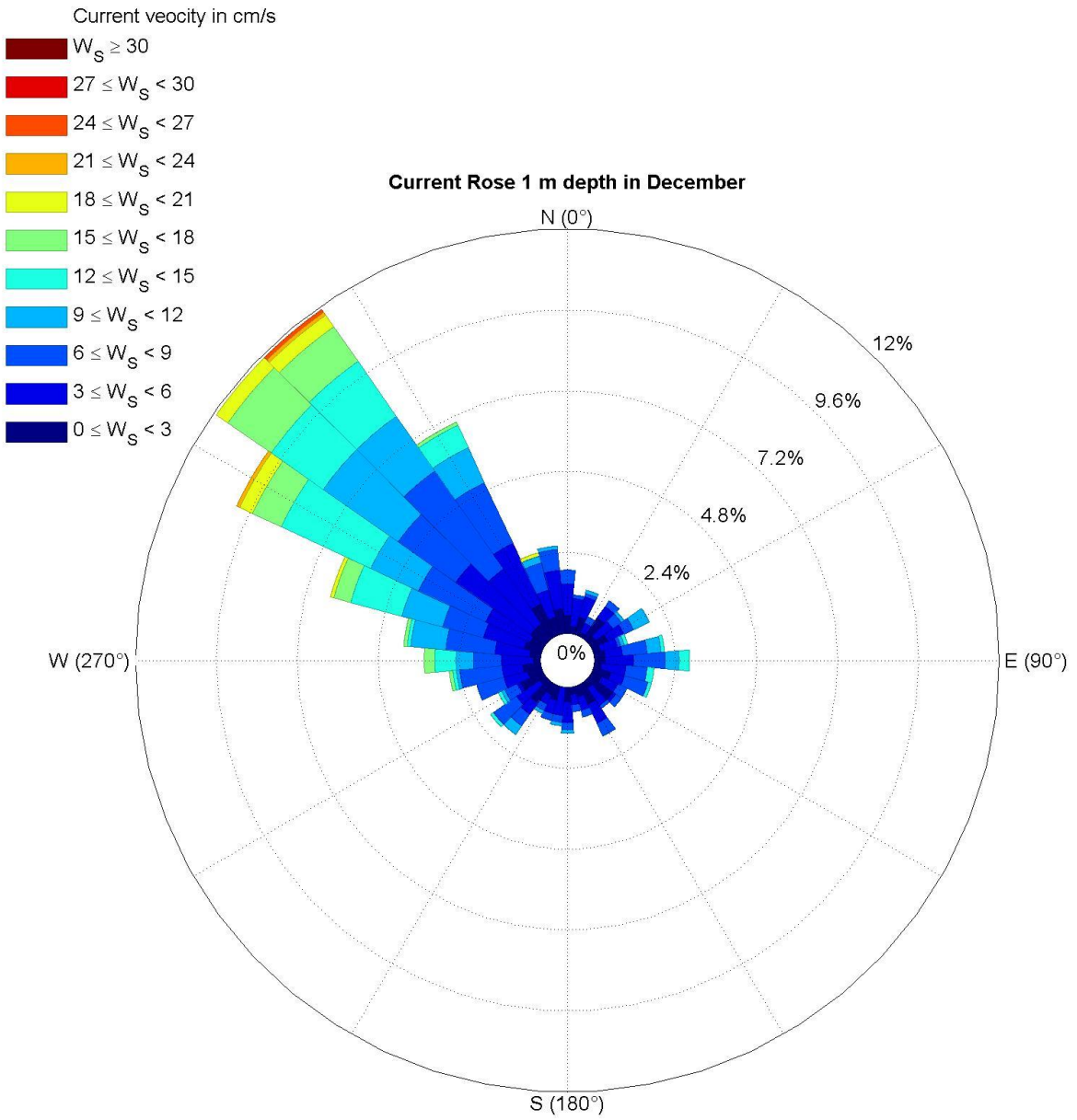


Fig. 3.3.1.45. Current rose at 1 m depth in December.

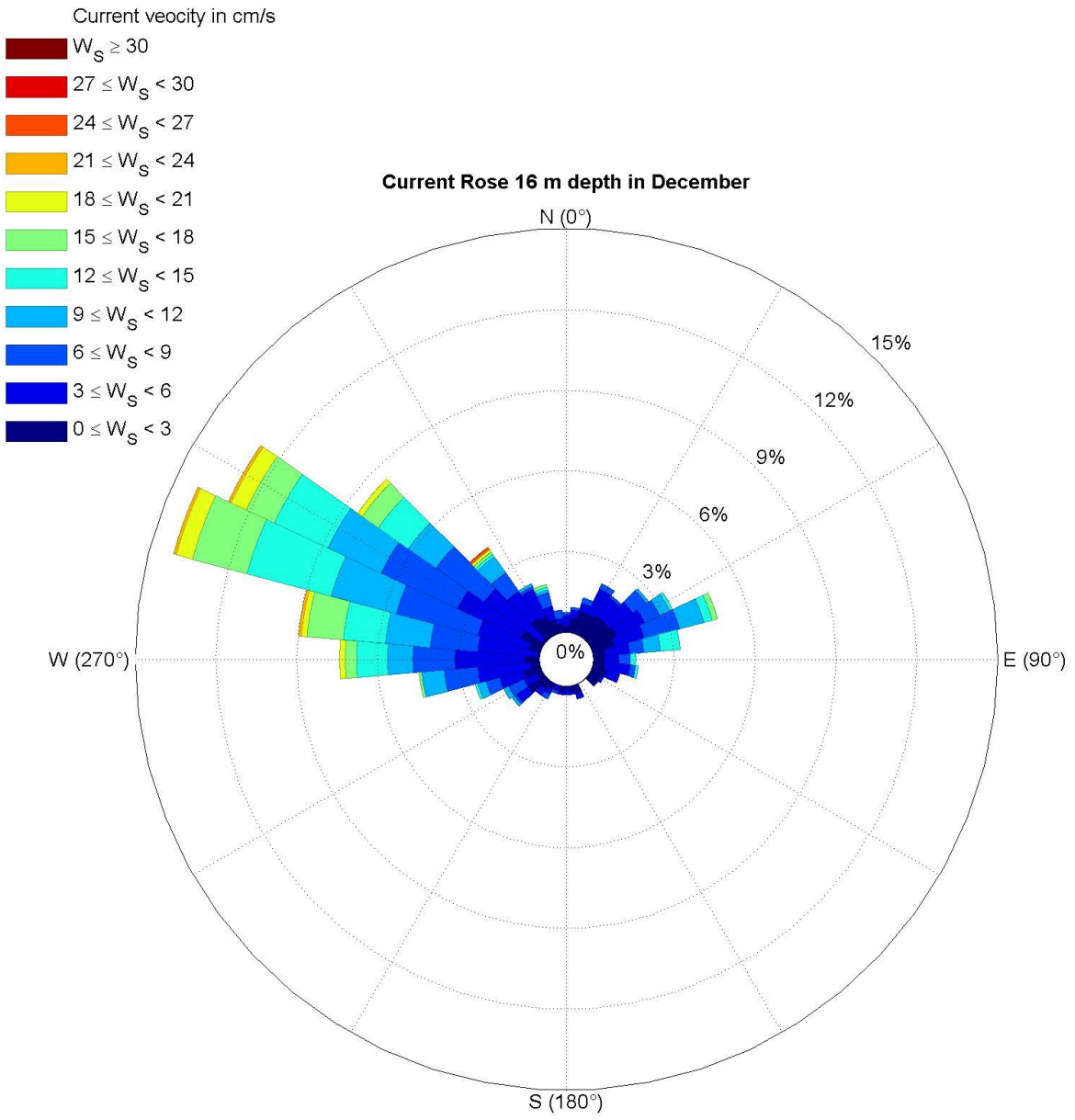


Fig. 3.3.1.46. Current rose at 16 m depth in December.

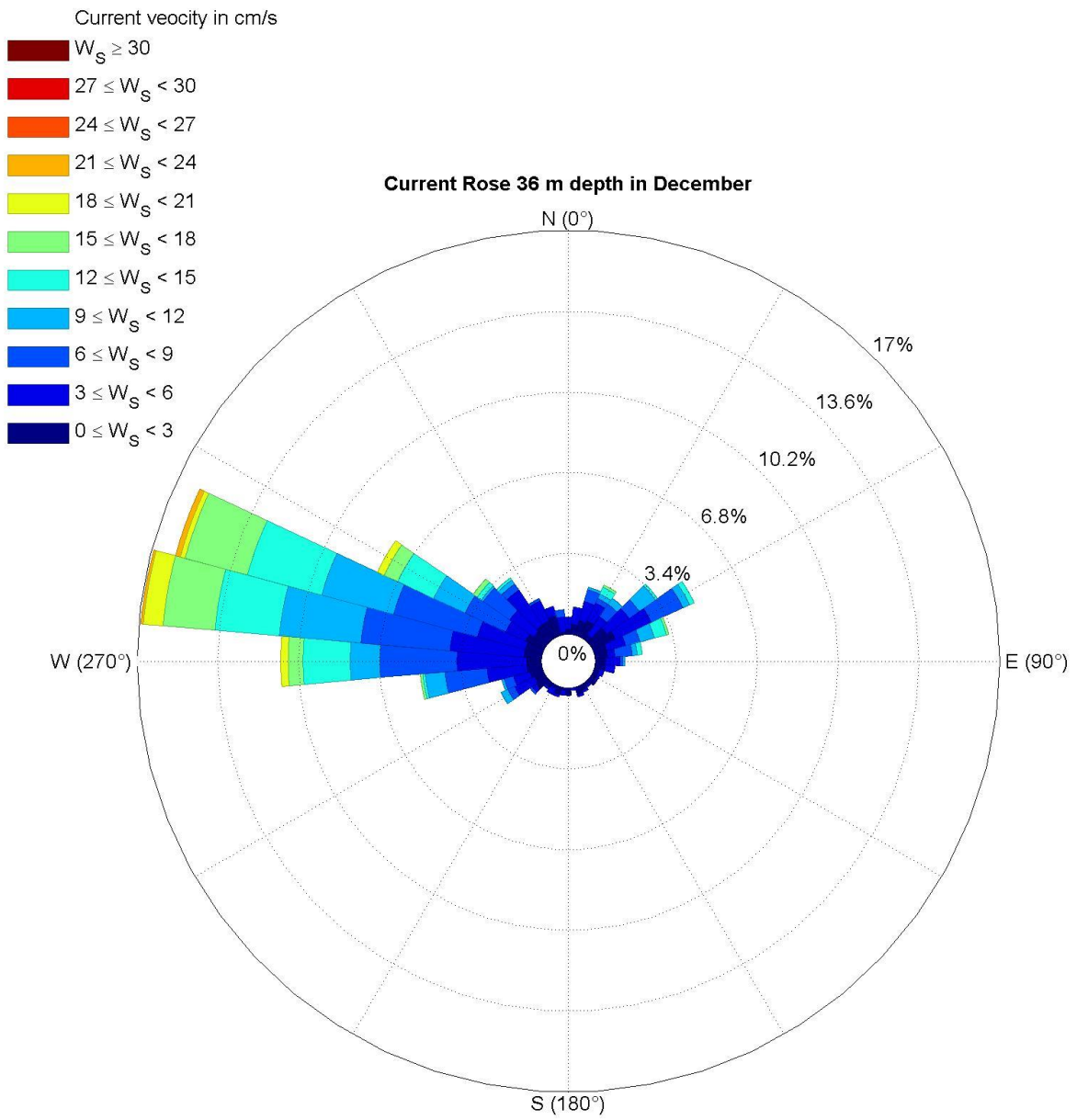


Fig. 3.3.1.47. Current rose at 36 m depth in December.

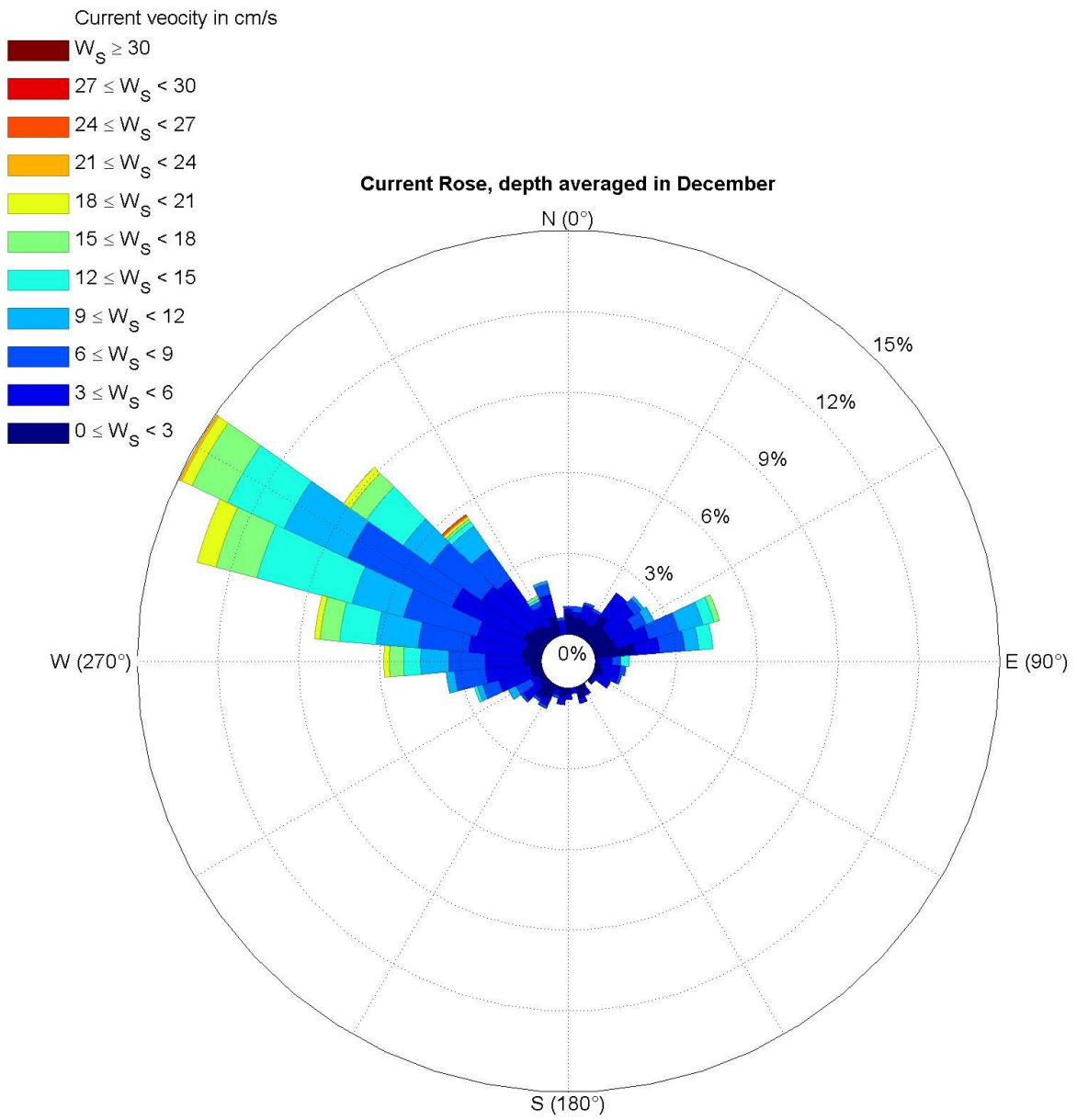


Fig. 3.3.1.48. Depth averaged current rose in December.

3.3.2. Extreme conditions

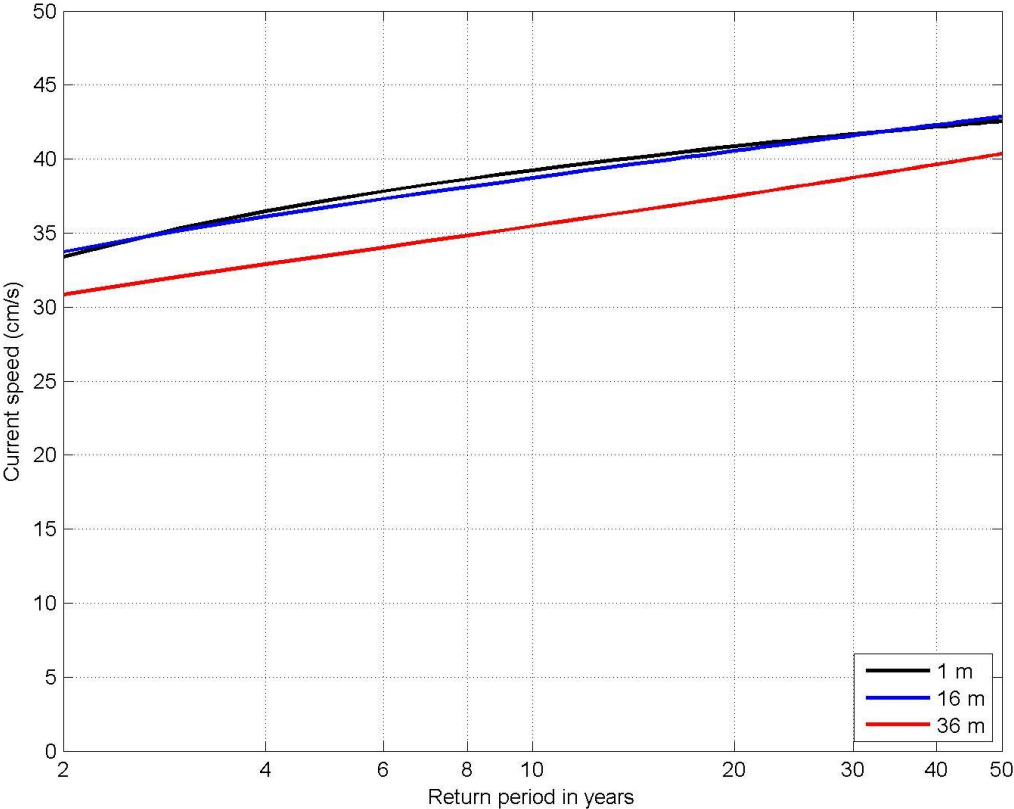


Fig 3.3.2.1. Return periods of current speed.

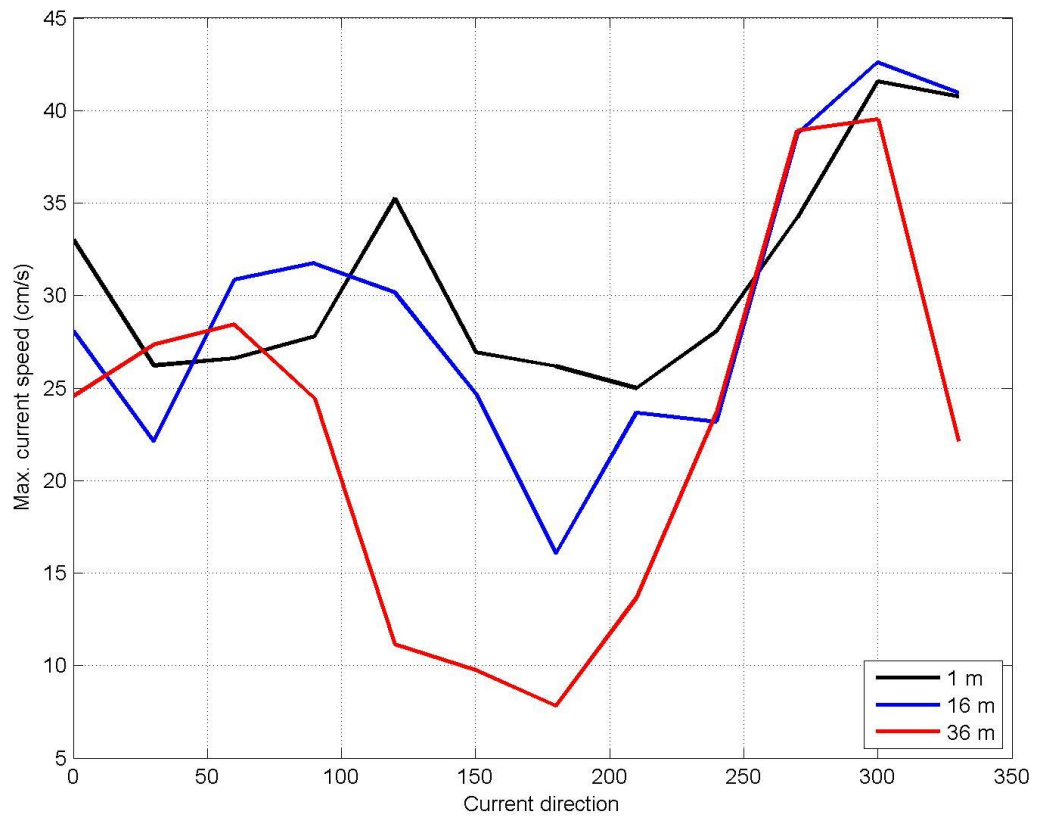


Fig 3.3.2.2. Maximum current speed in the case of current from different directions.

3.3.3. Spatial variations

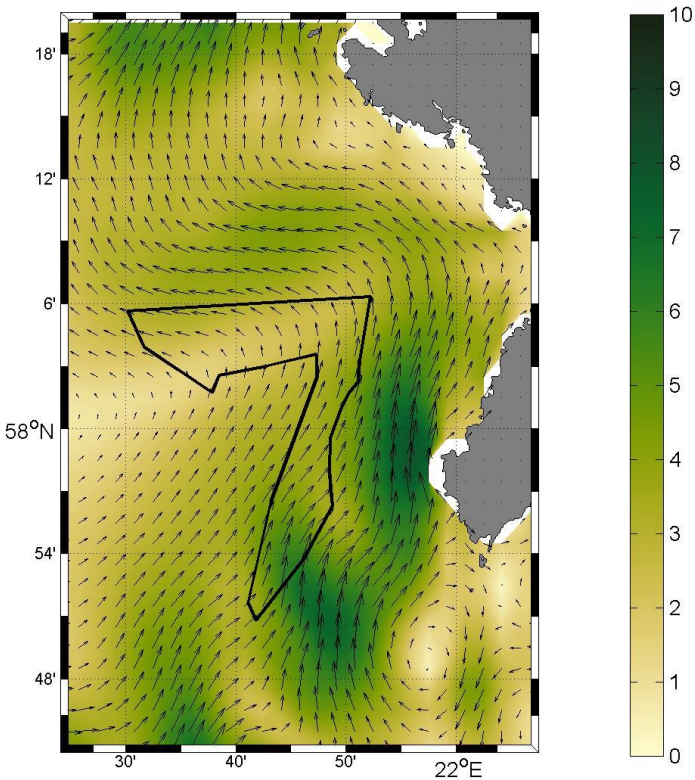


Fig. 3.3.3.1. Mean surface circulation. Colormap shows the mean current speed (m/s) while the vectors represent the mean current velocity components. The thick line represents the ELWIND area.

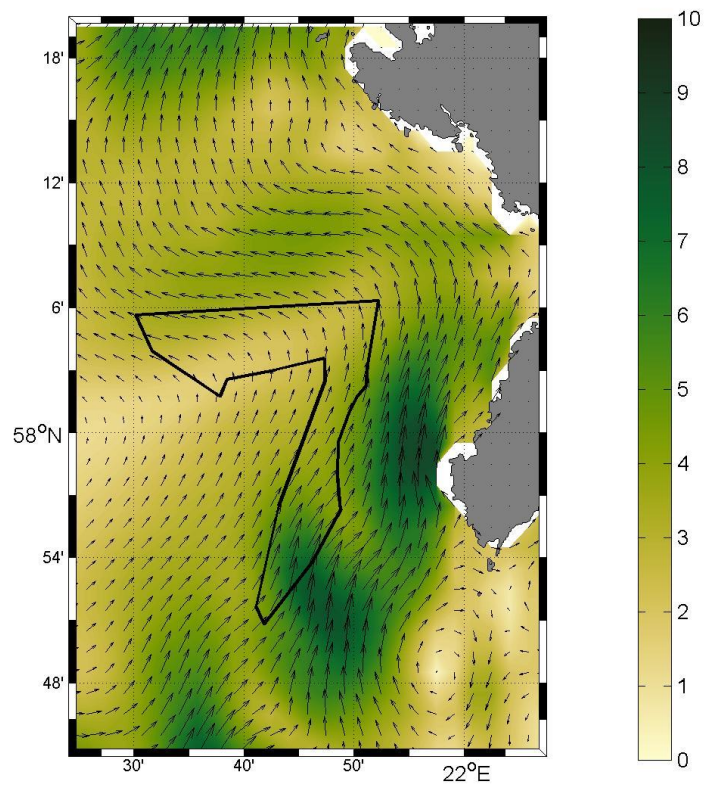


Fig. 3.3.3.2. Mean surface circulation in January. Colormap shows the mean current speed (m/s) while the vectors represent the mean current velocity components. The thick line represents the ELWIND area.

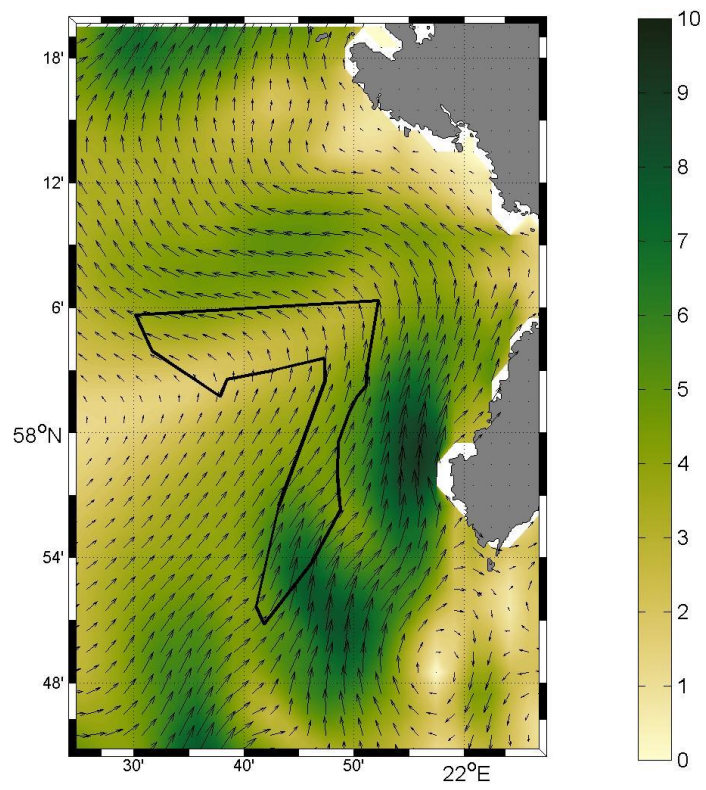


Fig. 3.3.3.3. Mean surface circulation in April. Colormap shows the mean current speed (m/s) while the vectors represent the mean current velocity components. The thick line represents the ELWIND area.

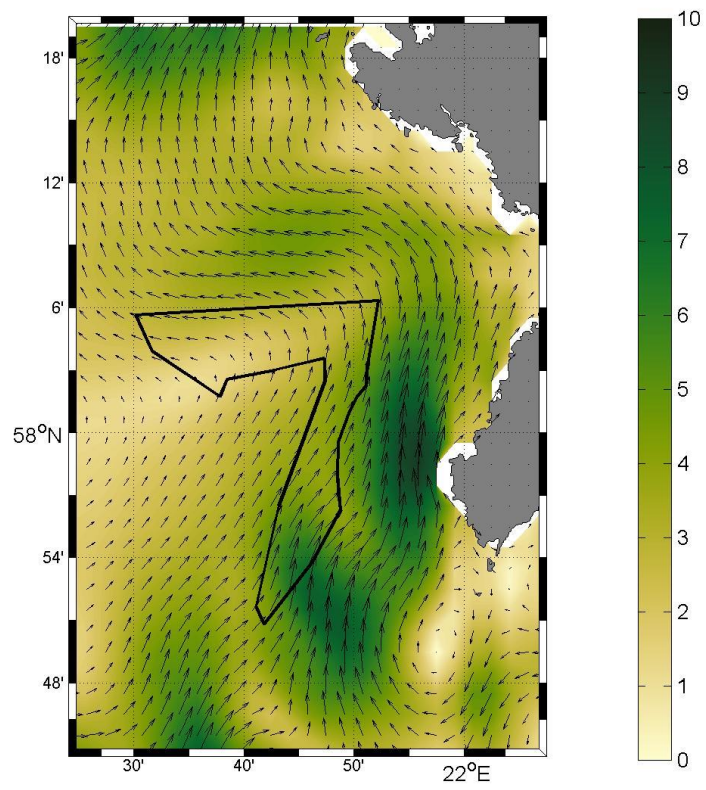


Fig. 3.3.3.4. Mean surface circulation in July. Colormap shows the mean current speed (m/s) while the vectors represent the mean current velocity components. The thick line represents the ELWIND area.

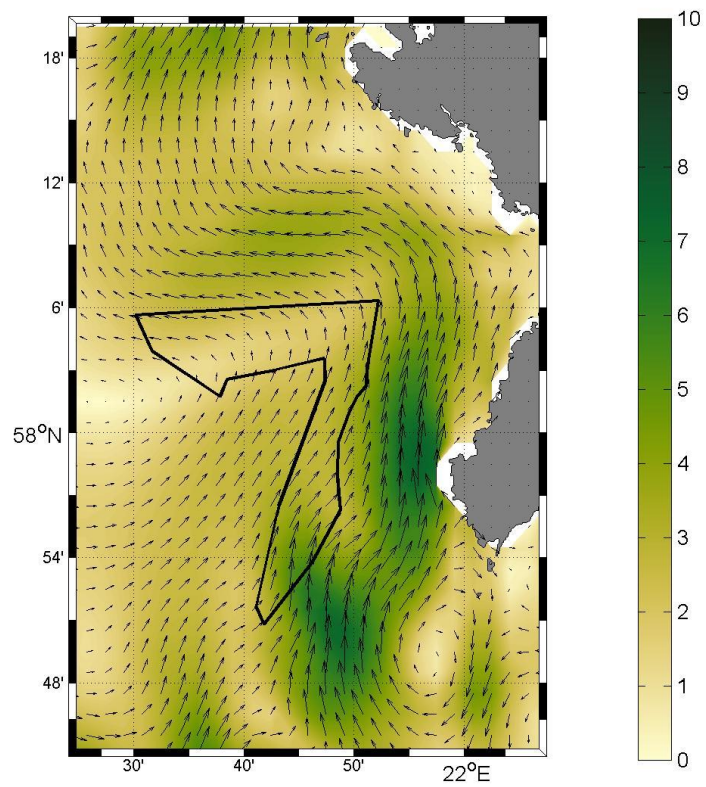


Fig. 3.3.3.5. Mean surface circulation in July. Colormap shows the mean current speed (m/s) while the vectors represent the mean current velocity components. The thick line represents the ELWIND area.

3.4. Sea level

Sea level variability is quite low in the area. The annual mean sea levels vary by about 25 cm and the climatological annual cycle has an amplitude of 20 cm (Fig. 3.4.2.1). The annual amplitude of daily sea level (maximum minus minimum of daily sea level on an annual basis) is rather less than 1.5 m. On a monthly basis, the highest and lowest sea levels occur in autumn and winter while the variability is lower in spring and summer (Fig. 3.4.2.2). The total amplitude of sea level variability is less than 2 m (Figs. 3.4.2.3). The spatial gradients of sea level are rather small (Figs. 3.4.2.1-3.4.2.5) compared to the temporal variability. The ELWIND area is not nearshore and the area is too small for a large sea level gradient formation.

3.4.1. Normal conditions

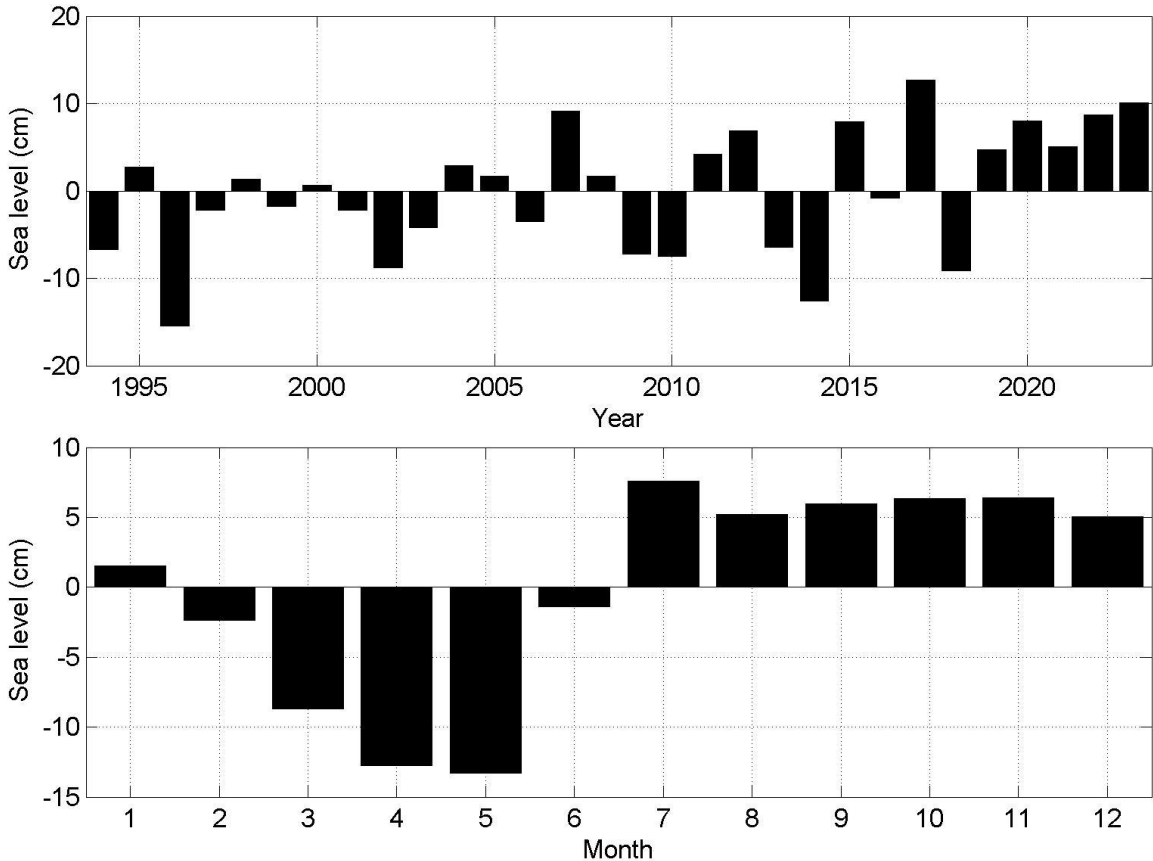


Fig 3.4.1.1. Annual and monthly mean sea levels.

3.4.2. Extreme conditions

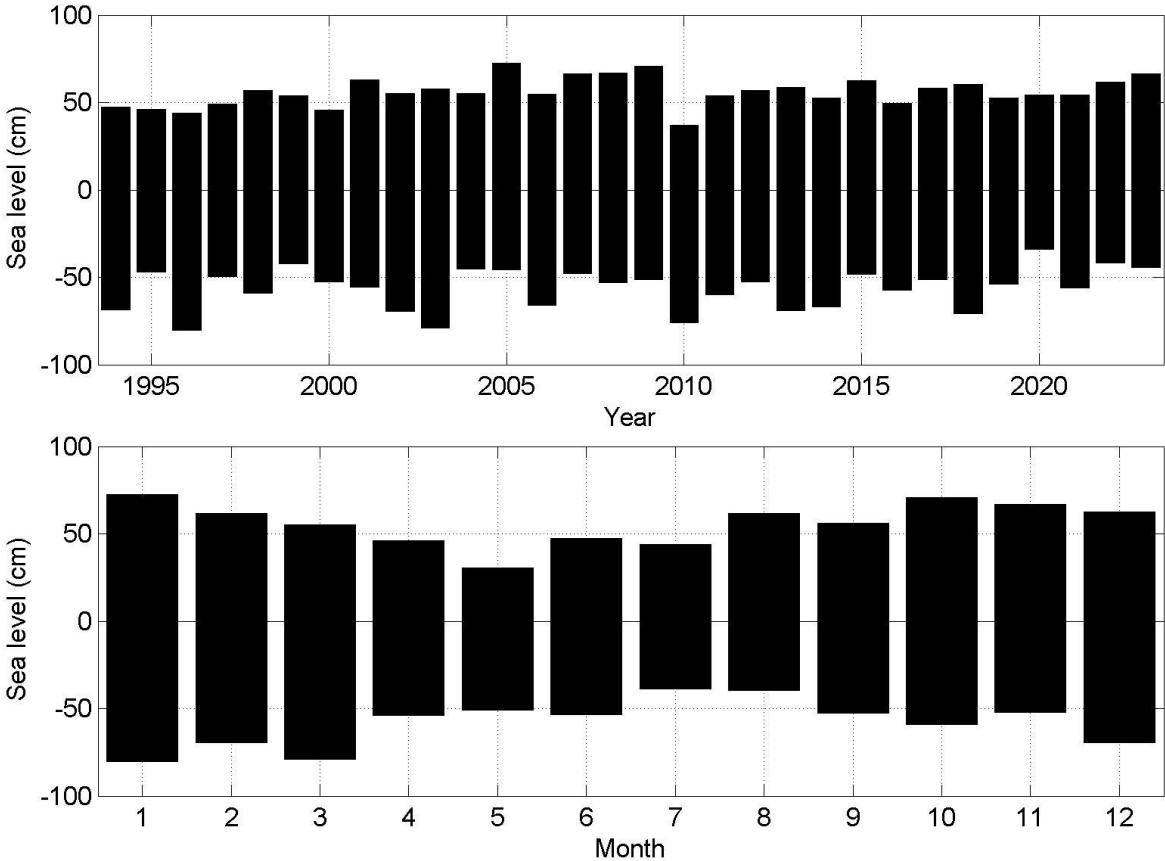


Fig 3.4.2.1. Annual and monthly maximum and minimum sea level.

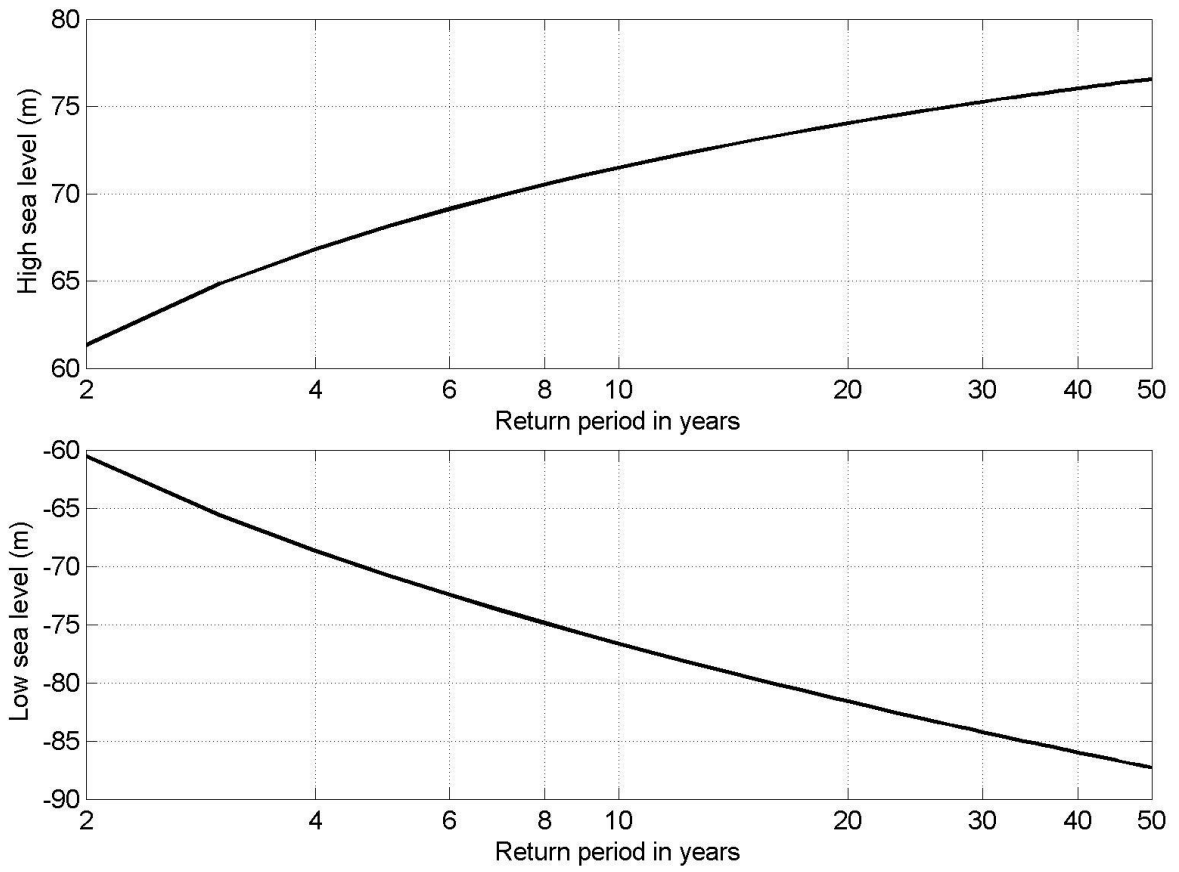


Fig 3.4.2.2. Return periods of high and low sea level.

3.4.3. Spatial variations

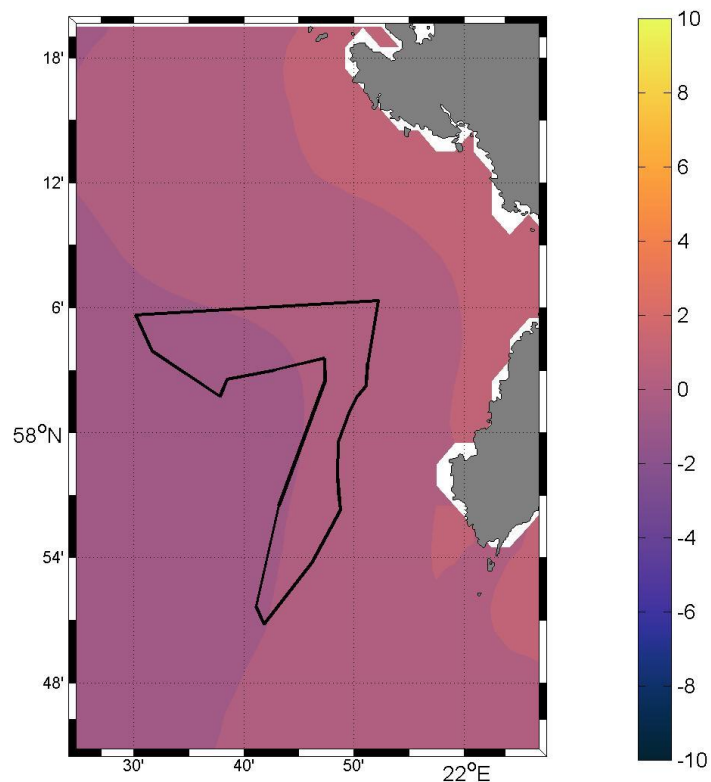


Fig 3.4.3.1. Mean spatial sea level distribution.

3.4.4. Assessment of long-term sea level rise

The absolute (referenced to geoid) sea level rise for the period of 1915-2014 has been about 2 mm y^{-1} in the ELWIND area (Madsen et al., 2019). The absolute sea level rise in 1993-2015 has been more rapid, $4\text{-}5 \text{ mm y}^{-1}$ (Madsen et al., 2019). The rise has been higher in winter than in summer (Passaro et al., 2021). The postglacial land uplift in the area is around $1\text{-}3 \text{ mm y}^{-1}$ (Kall et al., 2014; Vestøl et al., 2019). Thus, the absolute sea level rise has been greater than the compensating land uplift in recent decades. The absolute sea level rise for 2090–2099 relative to 1990–1999 has been estimated to be in the order of 0.6 m. In the case of a high-end scenario, the rise for the same period would be 1.1 m (Grinsted, 2015). If considering land uplift of 3 mm y^{-1} one would get the relative sea level rise (referenced to land) of 0.3 and 0.8 m, respectively (Grinsted, 2015) in the ELWIND area.

3.5. Ice conditions

3.5.1. Ice thickness for specified return periods

There is strong interannual variability of ice properties in the ELWIND area. Ice coverage does not occur every winter in the area (Fig. 3.5.1). The maximum spatially averaged daily ice thickness in the ELWIND area has been 15 cm in the period from 1994-2023 while the overall maximum thickness has been 40 cm in the same period. Due to very high inter-annual variability and changing climate, the return period of ice thickness is difficult to estimate. The 50-year (1980-2022) maximum drift ice thickness has been ca 50 cm in the area (Tikanmäki et al., 2025). The latter period included several very severe winters in the 1980s, when ice coverage of the Baltic exceeded 330 000 km² while more recently, since 2012 the ice coverage of the Baltic did not exceed 180 000 km². Wintertime ice coverage decreasing trend is expected to continue also in the future (Luomaranta et al., 2014), but occasionally winters with severe ice thickness, such as 50 cm still could occur in the ELWIND area.

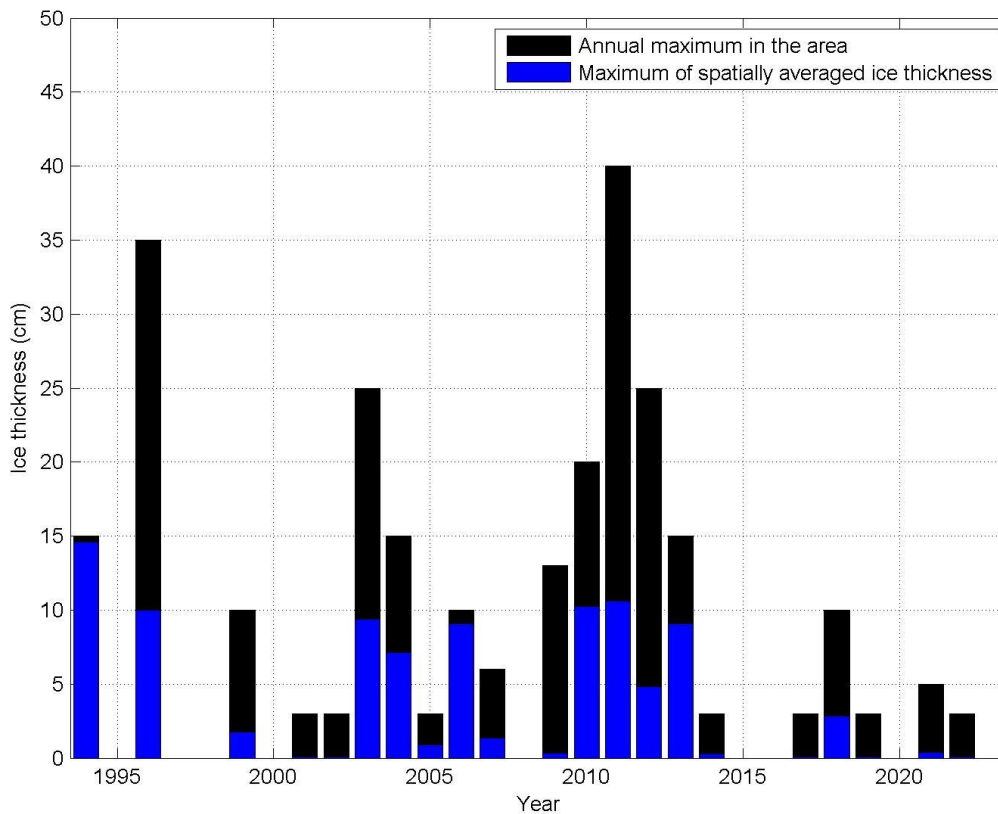


Fig. 3.5.1. Annual maximum of ice thickness in the ELWIND area and maximum of spatially averaged average ice thickness in the ELWIND area.

3.5.2. Risk of current or wind-induced ice floe

As shown in the recent comprehensive study (e.g. Tikanmäki et al., 2025) and the present document, ice is present in less than half of winters and ice concentration of over 50% occurs every third to fourth winter. The average length of ice cover is less than one month during ice season and most ice is in the form of drifting ice while fast ice is rather rare (e.g. Tikanmäki et al., 2025), but cannot be excluded, particularly in the eastern part of the ELWIND area. Thus, definitely, ice floe will occur in the ELWIND area, although it happens less than half of winters. The risk of ice floe is small during mild winters, which have been frequent in the recent decade. The trend toward milder winters has been observed in the Baltic Sea (Meier et al., 2022), and a decreasing trend in ice cover is expected to continue in the coming decades (Luomaranta et al., 2014). Although severe winters will be rarer, they still will occur (Luomaranta et al., 2014) and

thus, there will be wind and current-induced ice drift and it should be considered in the offshore installations in the ELWIND area.

3.5.3. Frequency of ice concentration

The spatially average ice concentration ≥ 0.9 in the ELWIND area occurred in three winters in the years 1994-2023. These winters occurred in a group: 2009/2010, 2010/2011, and 2011/2012 (Fig. 3.5.3.2). The duration of ≥ 0.9 concentration was on average one week in these three winters. The occurrence of winters when the spatial mean ice concentration was ≥ 0.5 and ≥ 0.1 was 28% and 42%, respectively, and the duration of respective conditions was approximately 10 days and 12 days on average (Fig. 3.5.3.3). However, in winter 2009/2010 ice with concentration of ≥ 0.1 was observed in the area about 2 months and ice concentration of ≥ 0.5 more than one month. There has not been considerable ice coverage after the 2017/2018 winter in the ELWIND area.

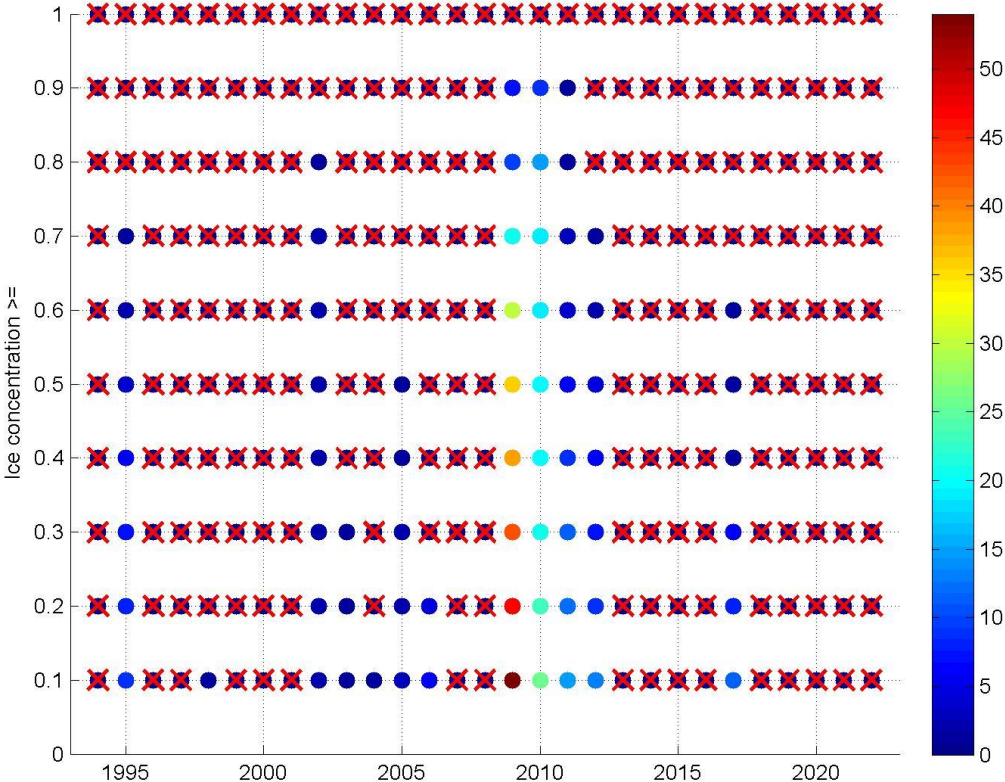


Fig 3.5.3.1. Number of days (color scale) in winter in certain ice concentration conditions. The mean ice concentration in the ELWIND area is considered. The red cross shows winters when respective ice concentration did not occur.

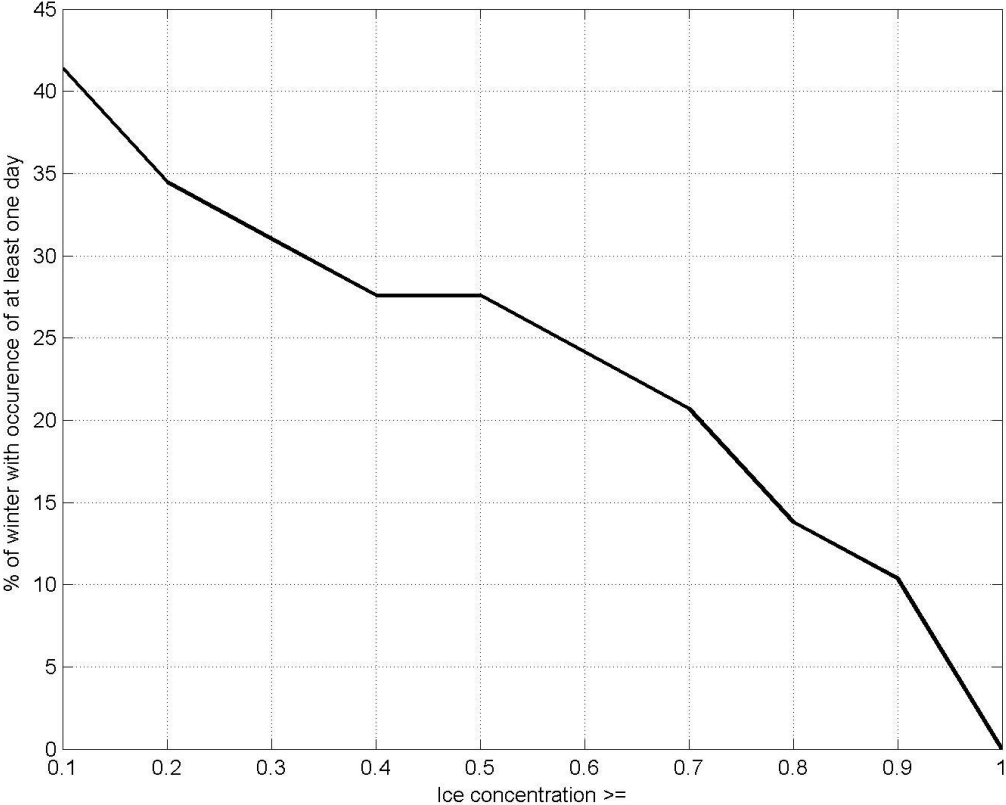


Fig 3.5.3.2. Share of winters with the occurrence of certain ice concentrations of at least one day. The mean ice concentration in the ELWIND area is considered.

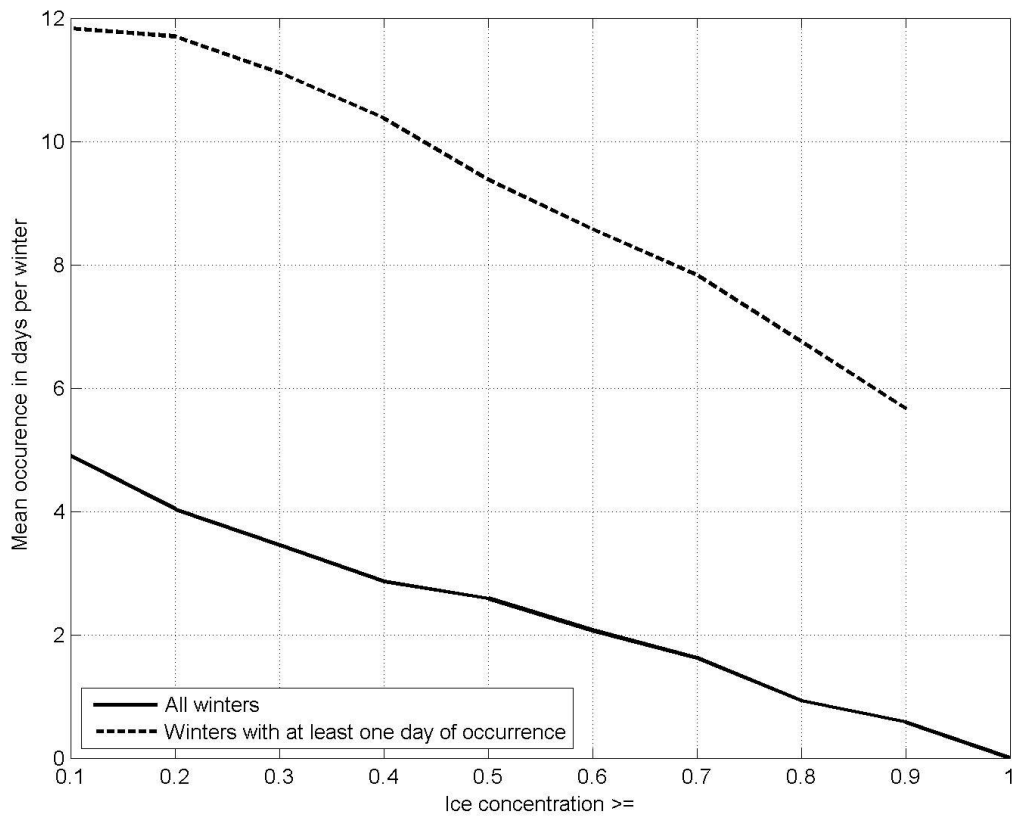


Fig 3.5.3.3. Mean occurrence in days of certain ice concentration in the case of all winters and winters with at least one day of occurrence. The mean ice concentration in the ELWIND area is considered.

3.5.4. Ridged ice

Ridged ice forms through the dynamic deformation of ice in the cases of interaction of sea ice floes, and ice floe with shoals, coast or offshore structures and is driven by wind and currents. The occurrence of deformed ice is rather low in the ELWIND due to the overall small presence of ice in the area (Tikanmäki et al., 2025). However, during severe winters considerable ridged ice could occur in the area. Although severe winters will be rarer, they still will occur (Luomaranta et al., 2014) and thus, there will be ridged ice in the area and it should be considered when designing offshore installations in the ELWIND area. Offshore structures could increase the amount of ridged ice as well in the area (Hendrikse, 2024).

3.5.5. Spatial variations

The spatial distributions show the coastal-offshore gradient in ice conditions (Fig. 3.5.4.1 and Fig. 3.5.4.3). The median annual maximum ice thickness map shows that there have been more winters when a considerable amount of ice was not present in the ELWIND area. However, in the coastal areas at Sörve peninsula and Vilsandi National Park, the ice coverage is more regular, and the median annual maximum ice thickness is up to 15 cm and there is some ice in the shallow coastal areas almost every year. The drifting ice that appears in the ELWIND area most likely originates from these areas. In severe winter, the ELWIND area is at least for some days fully covered with highly concentrated ice (Fig. 3.5.4.4). The greatest annual maximum ice thickness could be found in the eastern part of the ELWIND area while the western part experiences a bit easier conditions.

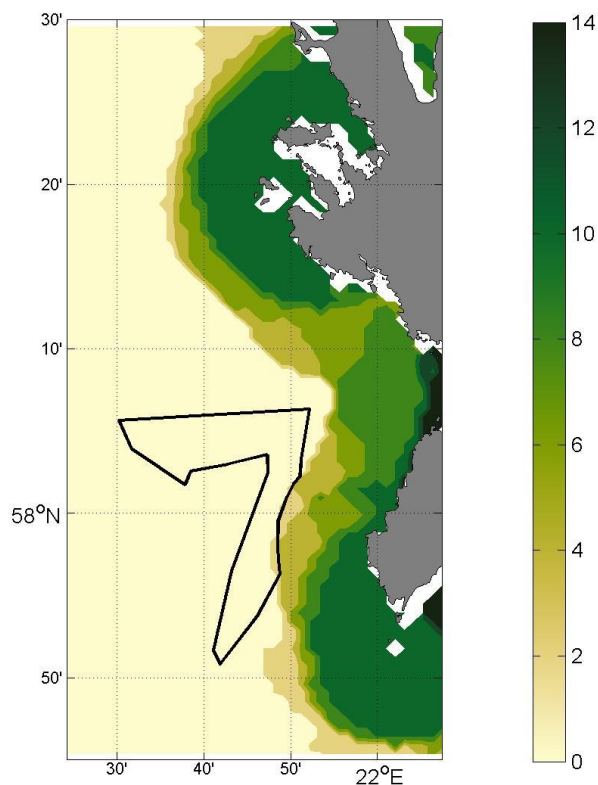


Fig 3.5.4.1. The median of annual maximum ice thickness in the area. The thick line represents the ELWIND area.

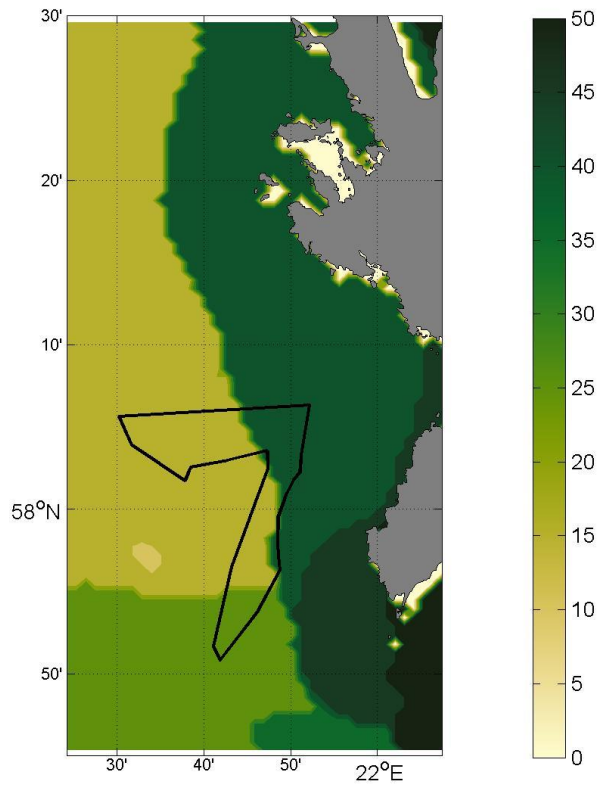


Fig 3.5.4.2. The maximum ice thickness in the area in 1994-2023. The thick line represents the ELWIND area.

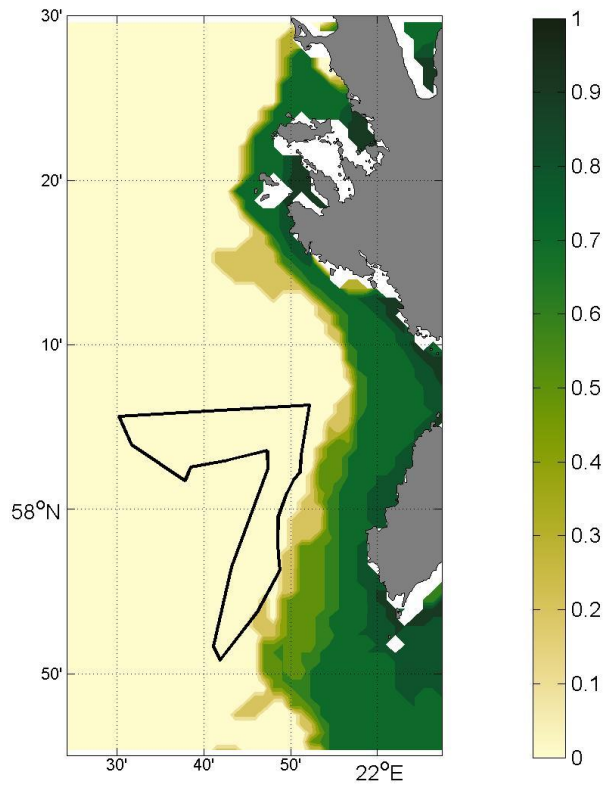


Fig 3.5.4.3. The median of annual maximum ice concentration in the area. The thick line represents the ELWIND area.

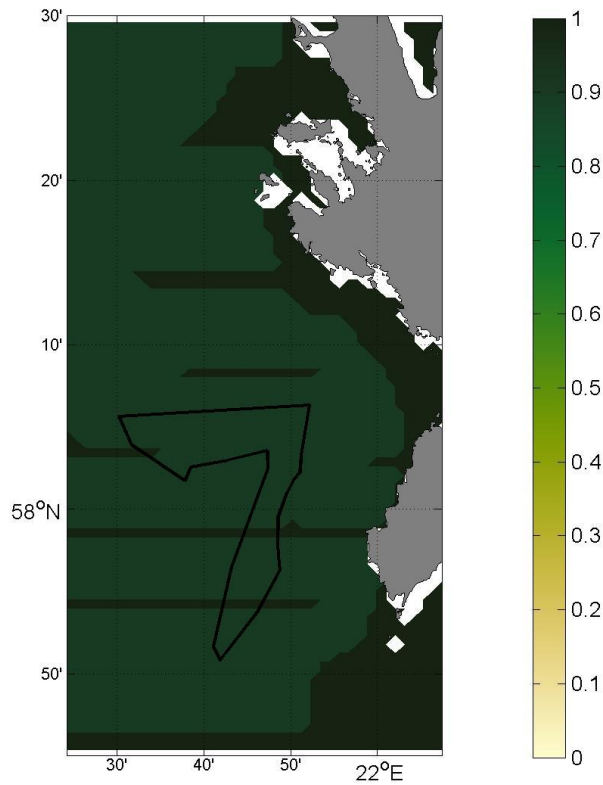


Fig 3.5.4.4. The maximum ice concentration in the area. The thick line represents the ELWIND area.

3.6. Other parameters

Next, we briefly describe selected other meteorological and oceanographic parameters. Relative humidity, air temperature, and air pressure and their variability have all considerable seasonality (Figs. 3.6.1-3.6.3). Spring and summer are characterized by lower humidity, and smaller air pressure variability while autumn and winter are characterized by high humidity and air pressure variability. The mean climatological air temperature amplitude between winter and summer is about 18-19 °C. Air temperature extremes could drop below -10 °C in winter and reach over 20 °C in summer.

The average density of ground flashes is approximately $0.3\text{-}0.5 \text{ km}^{-2} \text{ y}^{-1}$ in the ELWIND site according to the 2002- 2011 data (Mäkelä et al., 2014). If considering the area of ELWIND of 200 km^2 , the total number of annual ground flashes is in the order of 60-100. Most of the ground flashes occur from June to August in the Scandinavia–Baltic Sea area (Mäkelä et al., 2014). The occurrence of ground flashes has diurnal variation, the maximum is in the afternoon between 14 and 19 hours local time (Enno, 2014). There is a strong interannual variability in the occurrence of flashes. On average there have been approximately $27\,000 \text{ ground flashes y}^{-1}$ in Estonia during the period 2005-2023 (Keskkonnaagentuur, 2025). However, for instance, over 30 000 flashes were detected in 2024 while only approximately 10 000 flashes in 2015 (Keskkonnaagentuur, 2025). Approximately 10-15 thunderstorms a year occur in the ELWIND area (Enno, 2014; Mäkelä et al., 2014).

The water column is likely mixed down to the bottom in wintertime while in summertime primarily temperature contributes to the density stratification (Figs. 3.6.4 and 3.6.6). The role of salinity is smaller in density stratification (Fig. 3.6.5). The Baltic Sea is brackish and salinity is in the range of 6 to 8 g kg^{-1} in the ELWIND area. Temperature and salinity fields in the area are influenced by mesoscale processes, such as downwellings, upwellings, or eddies (Lehmann et al., 2012; Liblik et al., 2022; Väli et al., 2024). Thus, the time-series of water properties in synoptic timescale are much more variable than shown in Figs 3.6.4-3.6.6, which show the mean annual cycle.

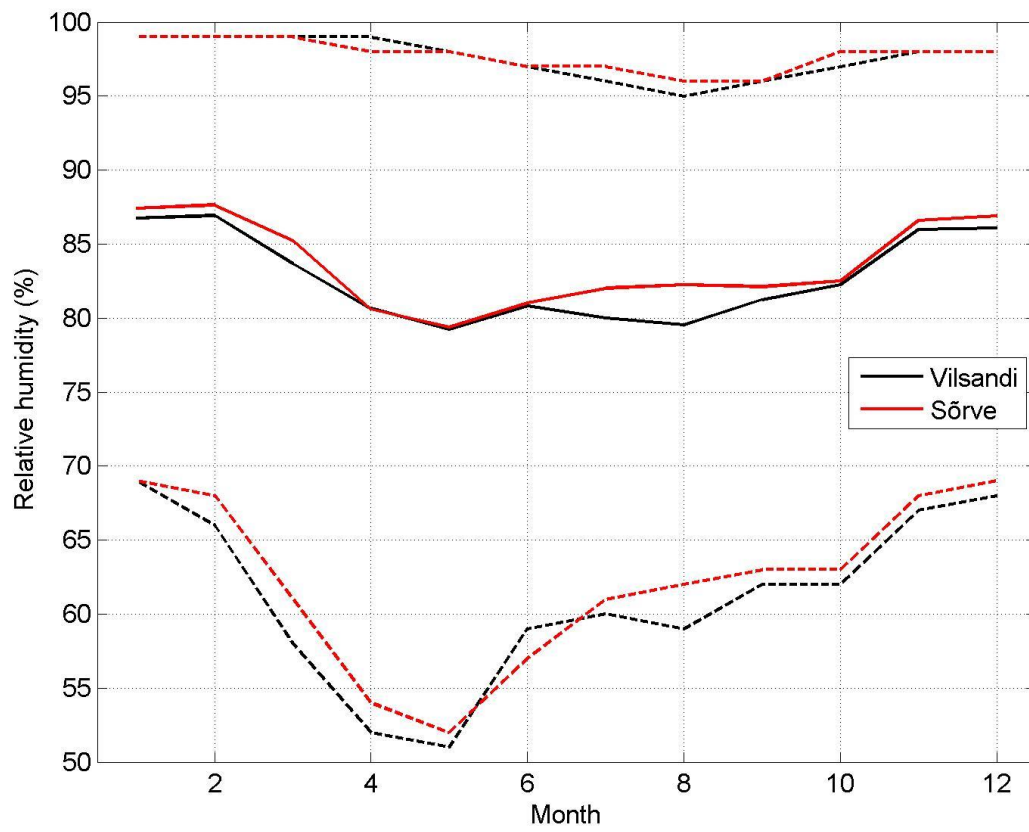


Fig 3.6.1. Monthly 95-percentile, average and 5-percentile of relative humidity (%) in Vilsandi and Sõrve meteorological stations.

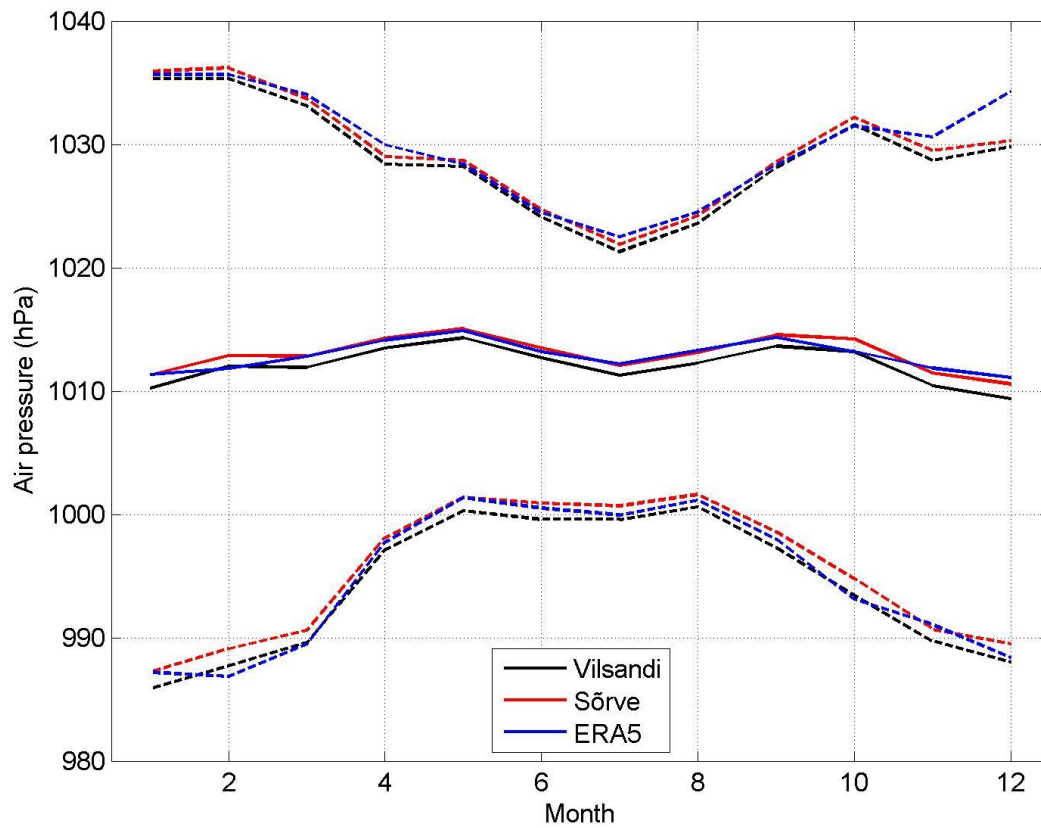


Fig 3.6.2. Monthly 95-percentile, average and 5-percentile of air pressure (hPa) in Vilsandi and Sörve meteostations, and in ERA5 reanalysis data.

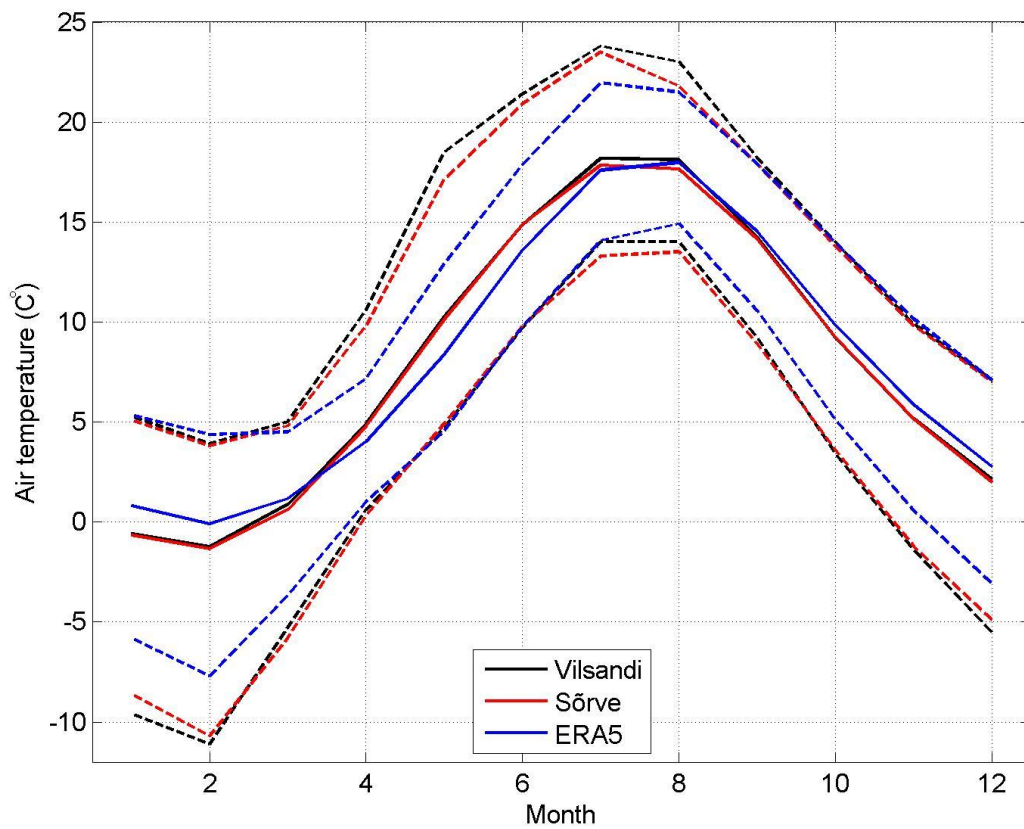


Fig 3.6.3. Monthly 95-percentile, average and 5-percentile of air temperature (°C) in Vilsandi and Sörve meteostation, and in ERA5 reanalysis data.

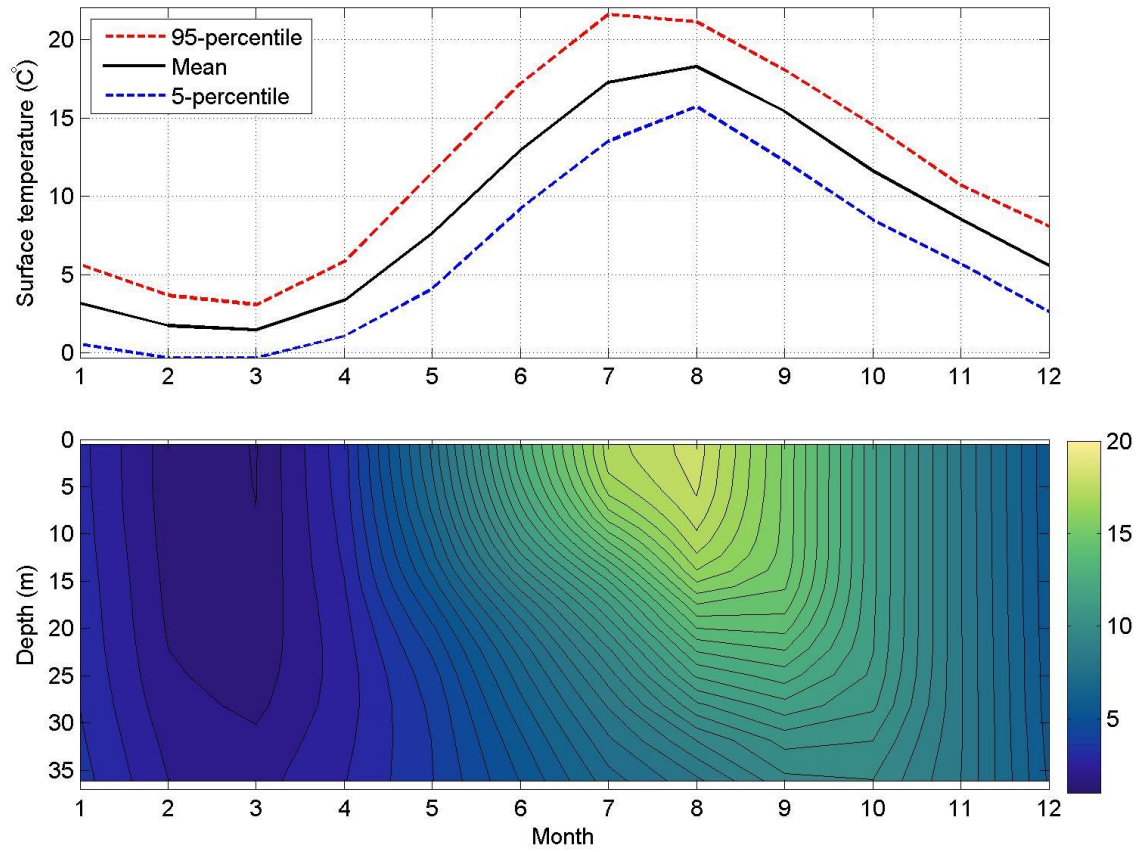


Fig 3.6.4. Monthly average sea surface (upper panel) and water column temperature (lower panel). 95-percentile and 5-percentile are shown for the sea surface as well.

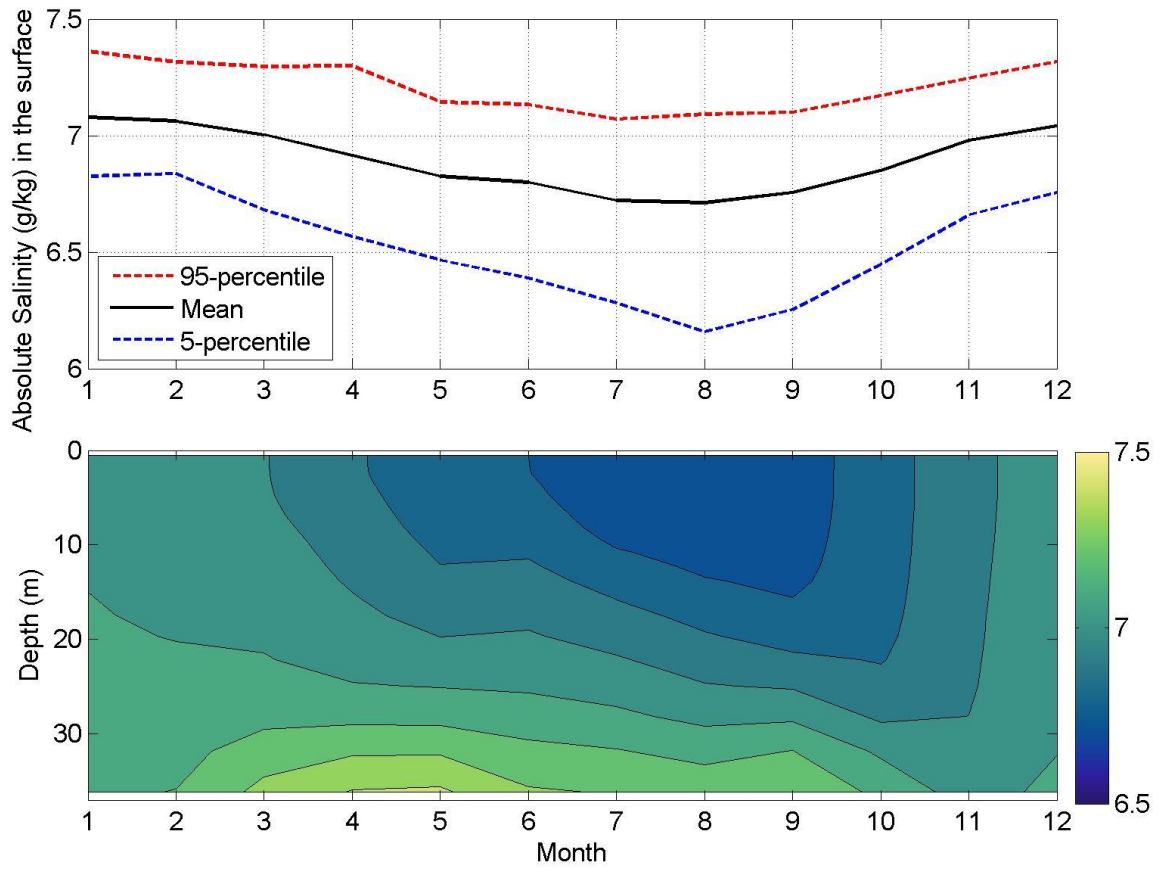


Fig 3.6.5. Monthly average sea surface (upper panel) and water column salinity (lower panel). 95-percentile and 5-percentile are shown for the sea surface as well.

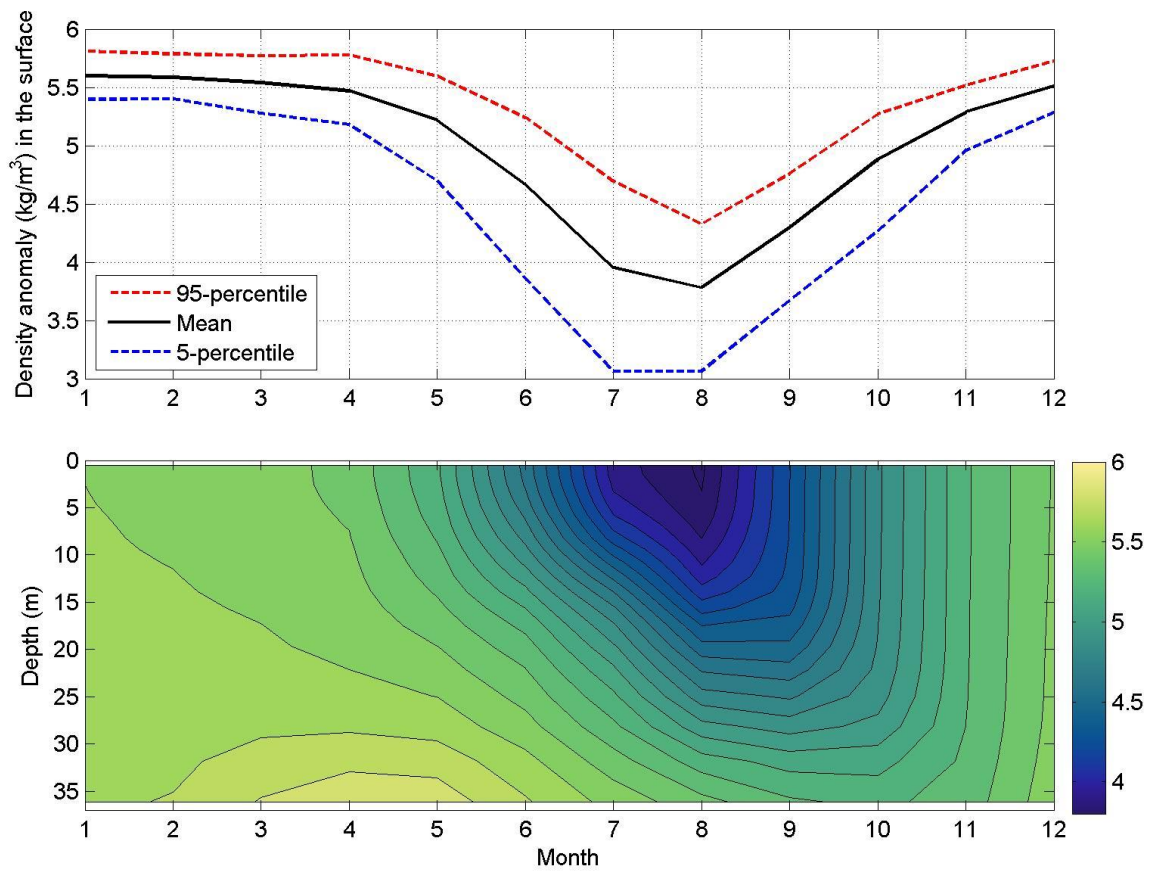


Fig 3.6.6. Monthly average sea surface (upper panel) and water column density anomaly (potential density minus 1000 kg/m³) (lower panel). 95-percentile and 5-percentile are shown for the sea surface as well.

4. Results of Joint Probability Analysis

The main force generating waves, currents, and sea level variations is coming from wind. Therefore, the correlation between wind and hydrodynamic processes is expected. Although other factors such as morphology, air pressure variability, thermohaline gradients, etc contribute to the variability as well. There is a clear tendency that higher significant wave height corresponds to higher wind speed during 12 hours before wave height observation (Fig. 4.1.1). The ratio of the standard deviation of wind speed in the corresponding range of wave height is higher in lower wind speeds, meaning that uncertainty of the relationship is higher at low wind speeds/wave height. The relationship is reflected also in the joint occurrence table (table 4.1.1): the highest waves occur only when wind speed is high. In figures 4.1.2-4.1.5 the distribution of wind speed and direction in the case of wave height ≥ 2 m, ≥ 3 m, ≥ 4 m, ≥ 5 m is shown. High waves occur primarily with wind from the southwest and also with northwesterly winds.

A similar relationship is between current speed and wave height (Fig. 4.2.1), and between wind and current (Fig. 4.3.1), although the relationships are not as strong as in the wind-wave case, and the latter is reflected also in the joint occurrence tables (tables 4.2.1 and 4.3.1).

There is a tendency that in the case of higher eastward wind velocity (i.e. winds from the west) sea level is higher (Fig. 4.4.1). This is expected as the ELWIND area is in the eastern side of the Baltic Proper and the wind stress causes the upper layer water mass transport and convergence in the eastern side of the basin. The standard deviation (Fig. 4.1.1) hints at the high variability between the wind components and sea level, which is also seen in the joint occurrence table (Table 4.1.1). Sea level height does not depend only on the wind forcing in the synoptic scale but also on longer periods.

There is also a tendency that in the case of higher water levels there is a stronger westward current (Fig. 4.5.1). This could be explained by the circulation regime in the area. Winds from the southwest cause the upper layer water transport to the eastern coast of the Baltic Proper and as a result sea level rises there and geostrophic current forms (Liblik et al., 2022). This current transports water along the coast towards the north. The current is modified by the morphology and as a result, the current turns west in the northern part of the ELWIND area (see Fig. 9 in Liblik et al., 2022), where is the time-series location of the study (see Fig. 2.1). Due to mesoscale and other variability relationships between absolute sea level and current is not strong.

4.1. Wind and waves

Table 4.1.1. Joint occurrence (%) of 1-h significant wave height (m) and 1-h wind speed (m/s). 1 m and 2 m/s step were used respectively for waves and wind, which corresponded to the classes of ≥ 0 m & < 1 m (0.5 m in table), ≥ 1 m & < 2 m (1.5 m in table) and so on for significant wave height, and ≥ 0 m/s & < 2 m/s (1 m/s in table), ≥ 2 m/s & < 4 m/s (3 m in table) and so on for wind speed.

		Significant wave height (m)								
		0.5	1.5	2.5	3.5	4.5	5.5	6.5	7.5	8.5
Wind speed (m/s)	1	3.46	0.09	0.00	0.00	0.00	0.00	0.00	0.00	0.00
	3	11.99	0.35	0.00	0.00	0.00	0.00	0.00	0.00	0.00
	5	18.41	1.58	0.02	0.00	0.00	0.00	0.00	0.00	0.00
	7	15.52	6.41	0.12	0.00	0.00	0.00	0.00	0.00	0.00
	9	5.34	12.72	0.78	0.01	0.00	0.00	0.00	0.00	0.00
	11	0.32	7.86	4.19	0.08	0.00	0.00	0.00	0.00	0.00
	13	0.00	1.24	3.95	1.00	0.01	0.00	0.00	0.00	0.00
	15	0.00	0.09	0.61	1.41	0.22	0.00	0.00	0.00	0.00
	17	0.00	0.00	0.04	0.18	0.33	0.05	0.00	0.00	0.00
	19	0.00	0.00	0.00	0.00	0.04	0.05	0.01	0.00	0.00
	21	0.00	0.00	0.00	0.00	0.00	0.01	0.01	0.00	0.00
	23	0.00	0.00	0.00	0.00	0.00	0.00	0.00	0.00	0.00
25	0.00	0.00	0.00	0.00	0.00	0.00	0.00	0.00	0.00	

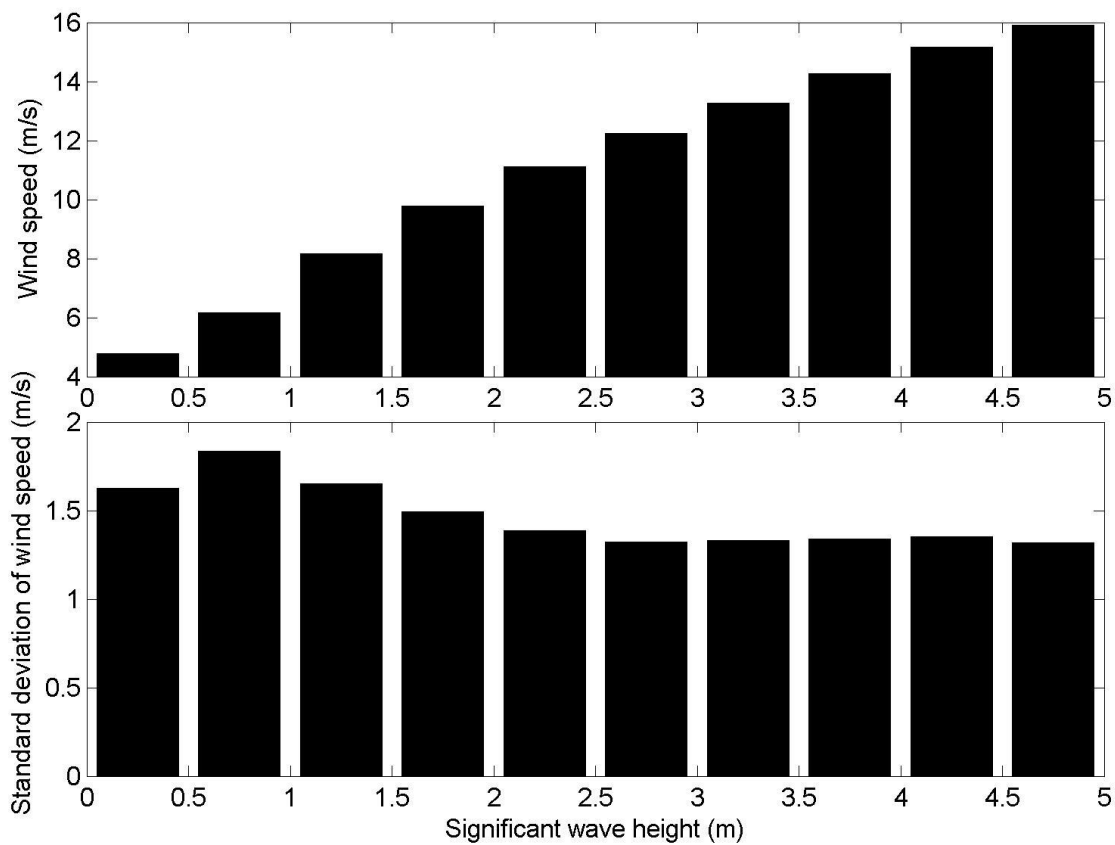


Fig 4.1.1. Wind speed to wave height. Wind speed data during 12 hours before a moment of wave height is considered. The mean wind speed according to the wave height classes is shown in the upper panel and standard deviation of wave height within the classes is shown in the lower panel.

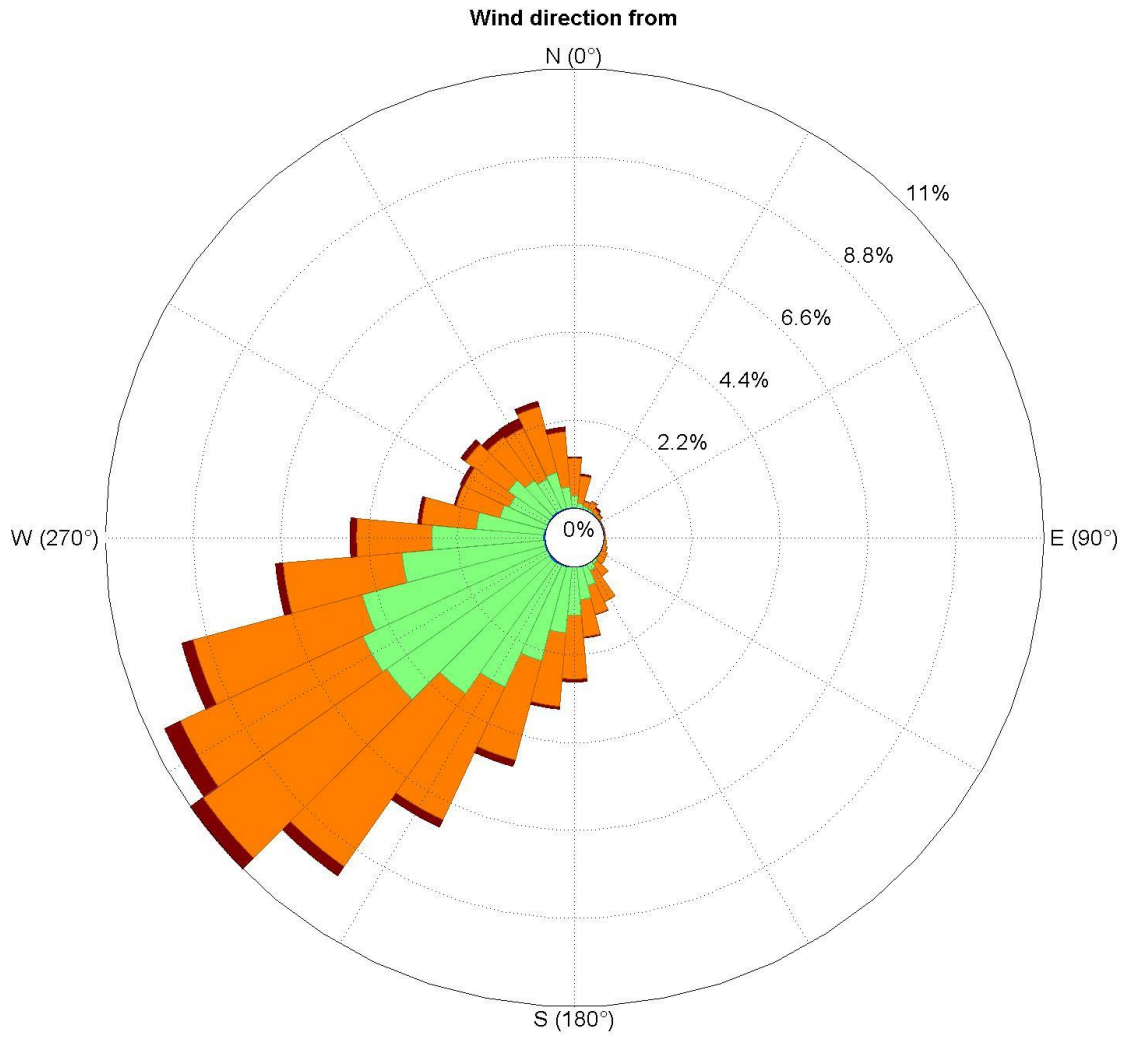


Fig 4.1.2. The wind rose for the occurrences of significant wave height above 2 m. Mean wind speed and direction during 12 hours before moments of wave height is considered.

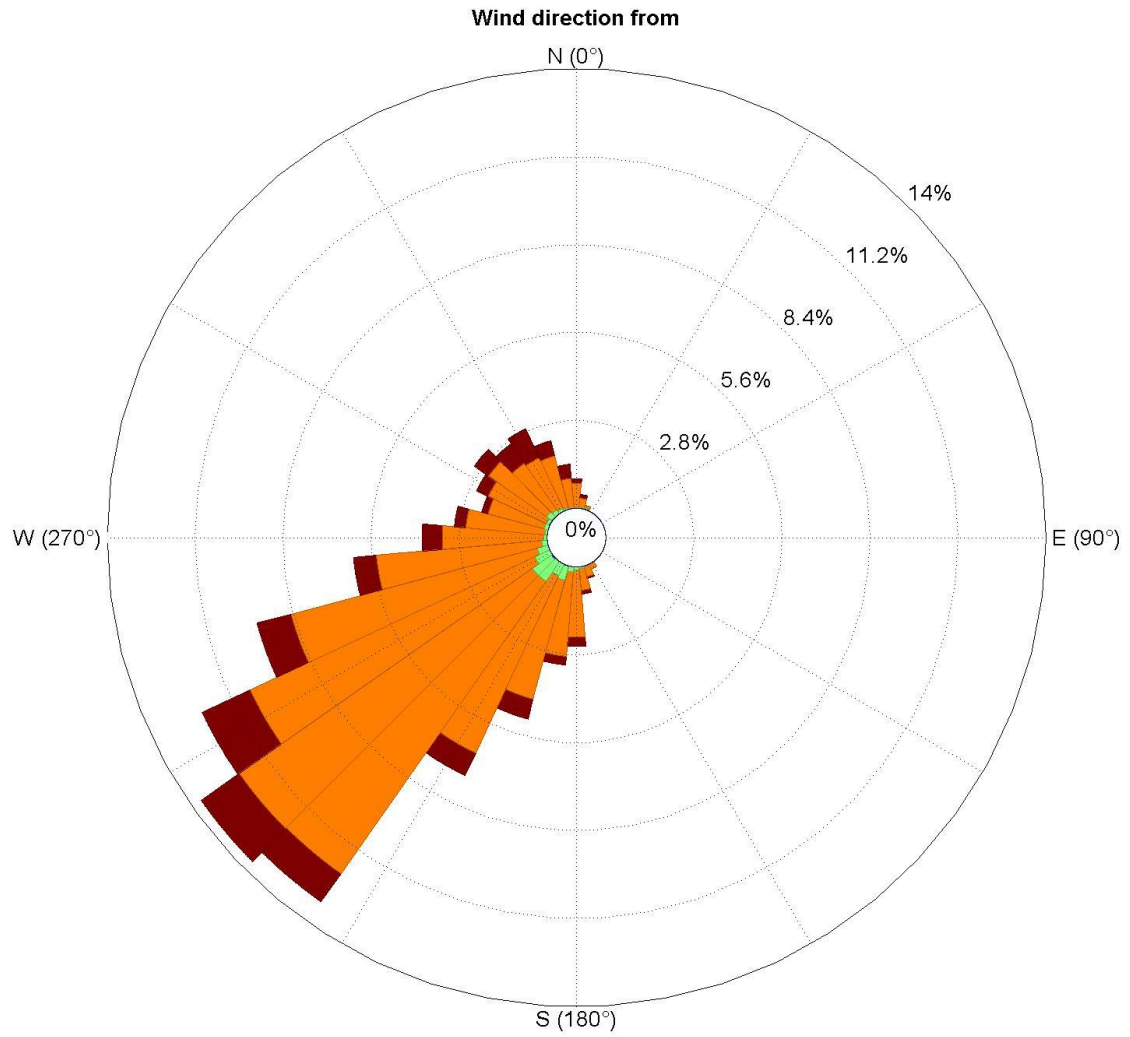


Fig 4.1.3. The wind rose for the occurrences of significant wave height above 3 m. Mean wind speed and direction during 12 hours before moments of wave height is considered.

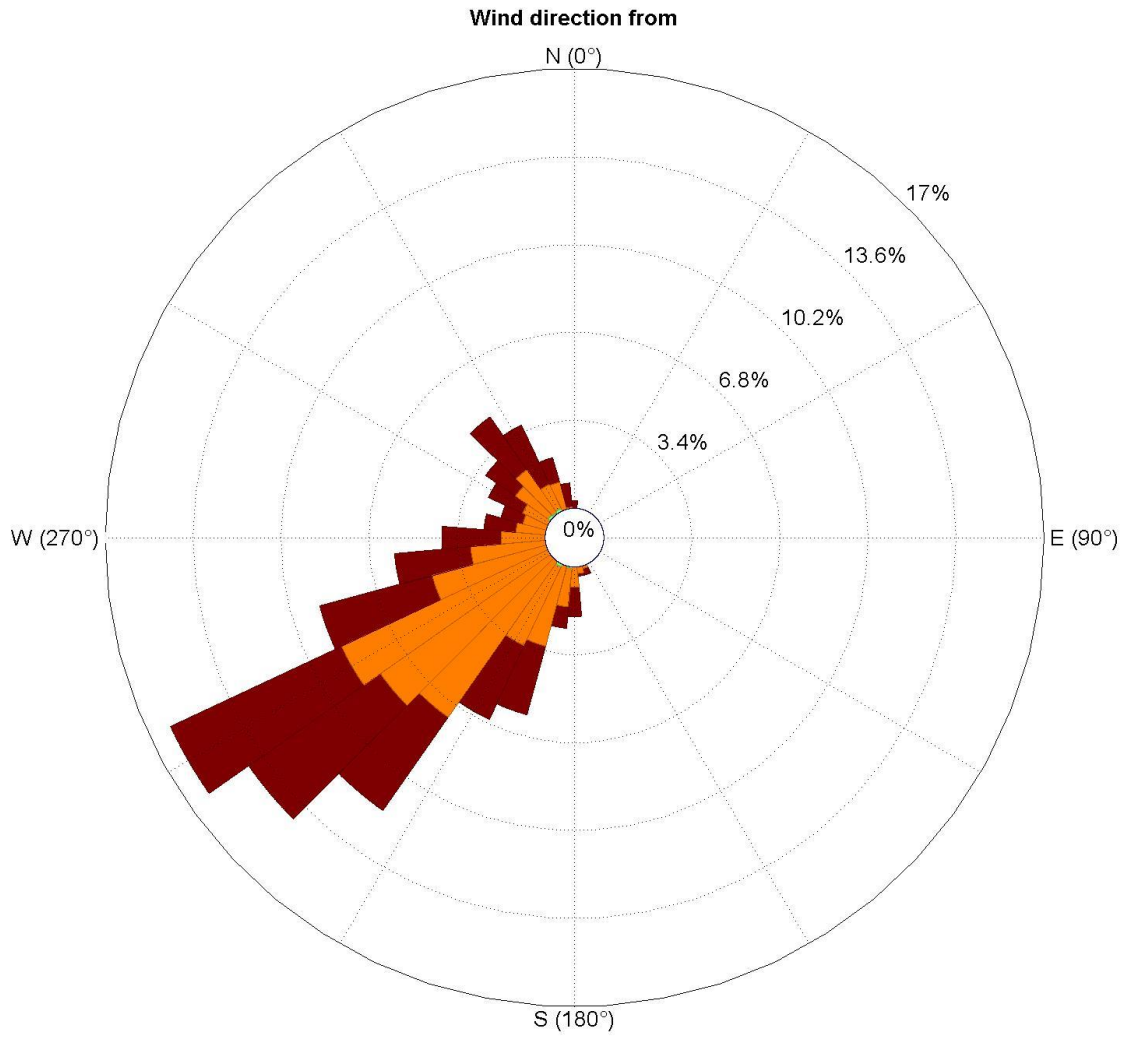


Fig 4.1.4. The wind rose for the occurrences of significant wave height above 4 m. Mean wind speed and direction during 12 hours before moments of wave height is considered.

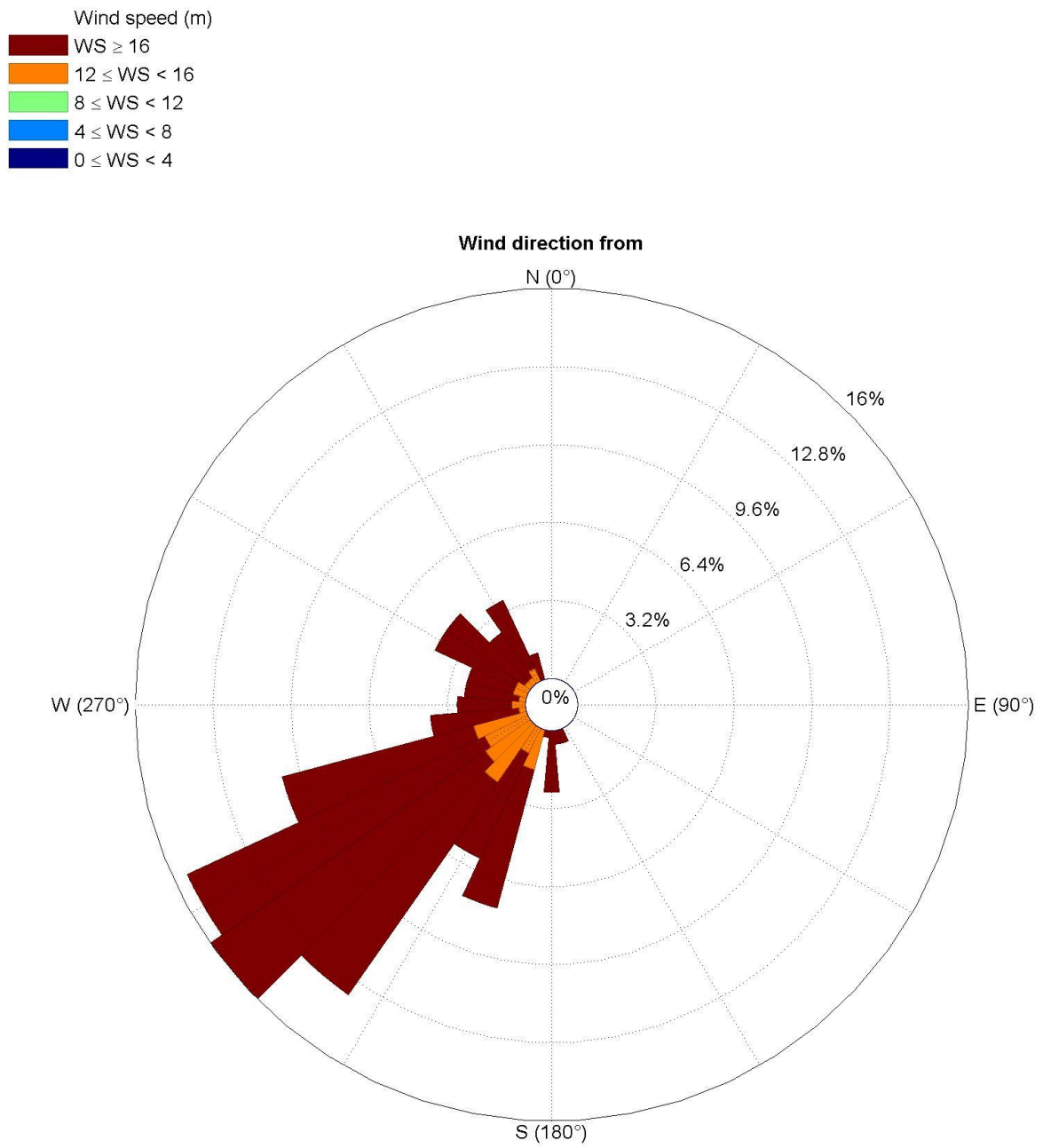


Fig 4.1.5. The wind rose for the occurrences of significant wave height above 5 m. Mean wind speed and direction during 12 hours before moments of wave height are considered.

4.2. Current and waves

Table 4.2.1. Joint occurrence (%) of 1-day mean significant wave height (m) and 1-day mean current speed (cm/s). 1 m and 4 cm/s step were used respectively for waves and current, which corresponded to the classes of ≥ 0 m & < 1 m (0.5 m in table), ≥ 1 m & < 2 m (1.5 m in table) and so on for significant wave height, and ≥ 0 cm/s & < 4 cm/s (2 cm/s in table), ≥ 4 cm/s & < 8 cm/s (6 cm/s in table) and so on for current speed.

		Significant wave height (m)							
		0.5	1.5	2.5	3.5	4.5	5.5	6.5	7.5
Current speed (cm/s)	2	19.02	8.29	0.95	0.09	0.01	0.00	0.00	0.00
	6	25.06	14.36	2.86	0.35	0.03	0.00	0.00	0.00
	10	7.85	7.12	3.25	0.60	0.05	0.00	0.00	0.00
	14	1.30	2.29	2.19	0.62	0.14	0.00	0.00	0.00
	18	0.13	0.37	0.49	0.42	0.11	0.02	0.00	0.00
	22	0.04	0.06	0.05	0.04	0.04	0.01	0.00	0.00
	26	0.00	0.03	0.02	0.02	0.00	0.00	0.00	0.00
	30	0.00	0.00	0.00	0.00	0.00	0.00	0.00	0.00

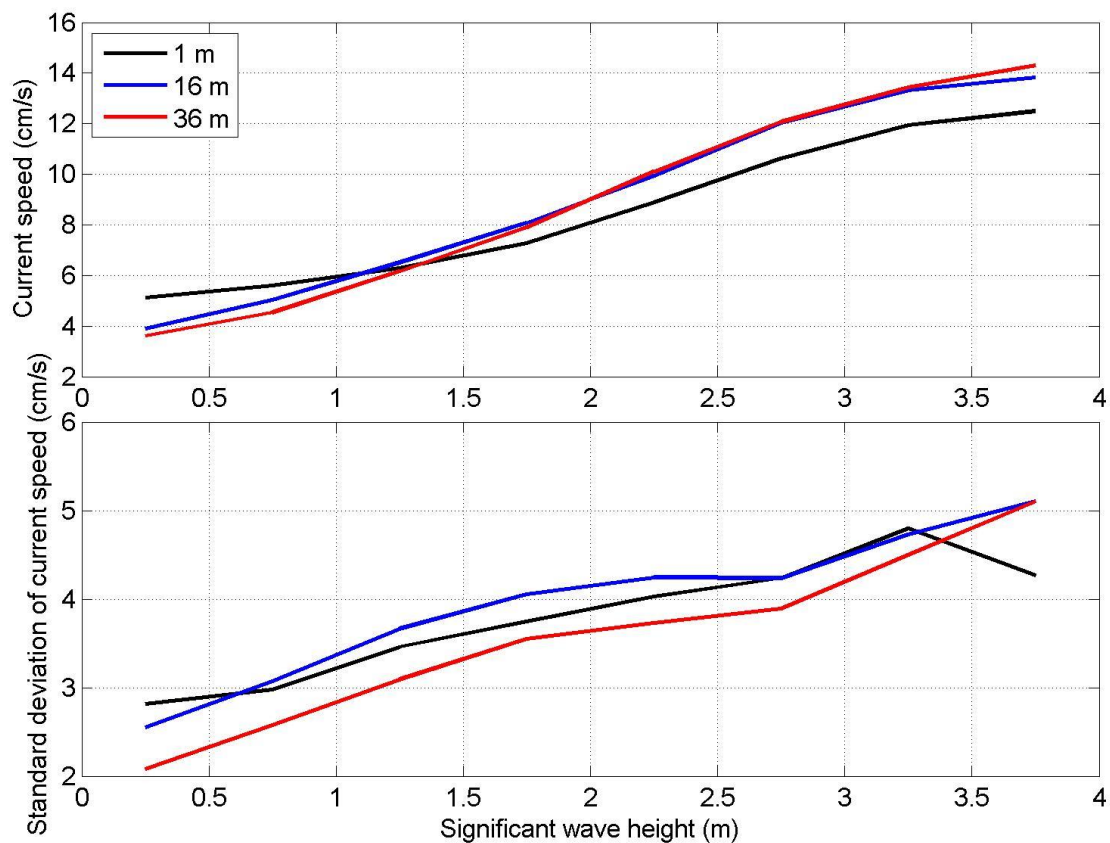


Fig 4.2.1. Daily mean current speed in three depths to daily mean significant wave height. The mean current speed according to the wave height classes is shown in the upper panel and the standard deviation of current speed within the classes is shown in the lower panel.

4.3. Current and wind

Table 4.3.1. Joint occurrence (%) of 1-day current speed (cm/s) and 1-day wind speed (m/s). 4 cm/s and 2 m/s step were used respectively for current and wind, which corresponded to the classes of ≥ 0 cm/s & < 4 cm/s (2 cm/s in table), ≥ 4 cm/s & < 8 cm/s (6 cm/s in table) and so on for current speed and ≥ 0 m/s & < 2 m/s (1 m/s in table), ≥ 2 m/s & < 4 m/s (3 m/s in table) and so on for wind speed.

		Current speed (cm/s)							
		2	6	10	14	18	22	26	30
Wind speed (m/s)	1	0.28	0.35	0.07	0.01	0.00	0.00	0.00	0.00
	3	5.07	4.68	1.15	0.19	0.03	0.00	0.00	0.00
	5	7.92	11.06	3.29	0.56	0.06	0.03	0.01	0.00
	7	7.83	11.88	4.43	1.08	0.08	0.05	0.01	0.00
	9	5.04	9.32	4.72	1.38	0.17	0.02	0.02	0.00
	11	2.18	4.59	3.42	1.84	0.43	0.03	0.01	0.00
	13	0.37	1.37	1.57	1.07	0.53	0.04	0.01	0.00
	15	0.05	0.27	0.45	0.39	0.23	0.05	0.01	0.00
	17	0.01	0.05	0.06	0.11	0.03	0.02	0.00	0.00
	19	0.00	0.00	0.00	0.00	0.01	0.00	0.00	0.00
21	0.00	0.00	0.00	0.00	0.00	0.00	0.00	0.00	

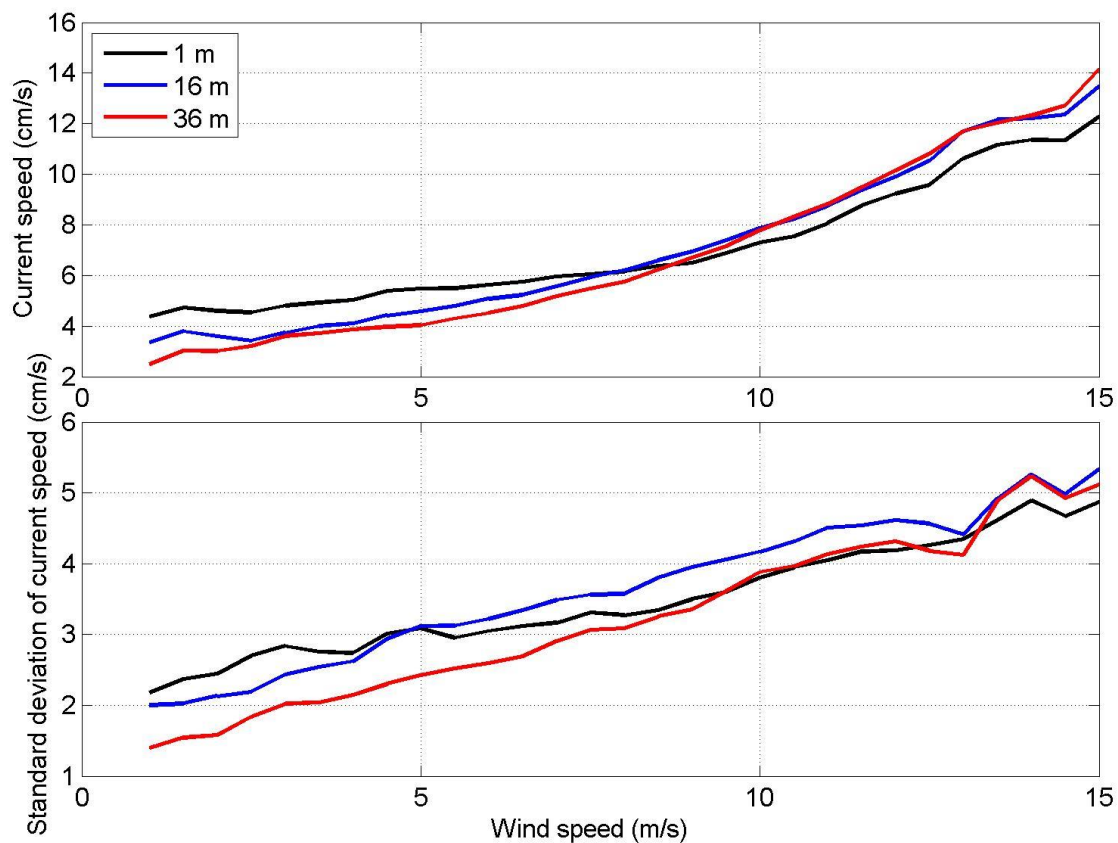


Fig 4.3.1. Daily mean current speed in three depths in relation to wind speed. The mean current speed according to the wind speed classes is shown in the upper panel and the standard deviation of current speed within the classes is shown in the lower panel.

4.4. Water level and wind

Table 4.4.1. Joint occurrence (%) of 1-day sea level (cm) and 1-day wind speed (m/s). 10 cm and 2 m/s step were used respectively for sea level and wind, which corresponded to the classes of ≥ -85 cm & < -75 cm (-80 cm in table), ≥ -75 cm & < -65 cm (-70 cm in table) and so on for sea level and ≥ 0 m/s & < 2 m/s (1 m/s in table), ≥ 2 m/s & < 4 m/s (3 m/s in table) and so on for wind speed.

		Sea level (cm)																		
		-80.00	-70.00	-60.00	-50.00	-40.00	-30.00	-20.00	-10.00	0.00	10.00	20.00	30.00	40.00	50.00	60.00	70.00	80.00	90.00	
Wind speed (m/s)	1	0.00	0.01	0.01	0.00	0.00	0.06	0.10	0.17	0.13	0.11	0.05	0.05	0.01	0.00	0.00	0.01	0.00	0.00	
	3	0.00	0.00	0.09	0.06	0.35	0.93	1.21	1.77	2.12	1.79	1.52	0.81	0.31	0.08	0.06	0.00	0.00	0.00	
	5	0.00	0.00	0.12	0.21	0.55	1.35	2.18	2.95	4.28	3.74	3.60	2.23	1.10	0.45	0.18	0.01	0.00	0.00	
	7	0.00	0.02	0.13	0.22	0.68	1.30	1.61	2.88	3.97	4.72	3.93	2.97	1.70	0.95	0.28	0.01	0.00	0.00	
	9	0.00	0.04	0.09	0.24	0.39	0.84	1.35	1.91	2.82	3.50	3.17	2.73	2.06	0.98	0.44	0.12	0.01	0.00	
	11	0.00	0.01	0.08	0.09	0.21	0.36	0.73	1.00	1.62	1.84	1.77	1.69	1.42	1.16	0.40	0.09	0.02	0.00	
	13	0.00	0.00	0.04	0.03	0.11	0.09	0.22	0.32	0.42	0.65	0.63	0.98	0.71	0.38	0.31	0.07	0.01	0.00	
	15	0.00	0.00	0.00	0.00	0.01	0.02	0.04	0.05	0.05	0.13	0.15	0.26	0.26	0.22	0.20	0.05	0.01	0.00	
	17	0.00	0.00	0.00	0.00	0.00	0.01	0.00	0.00	0.00	0.03	0.02	0.04	0.05	0.04	0.06	0.02	0.01	0.00	
	19	0.00	0.00	0.00	0.00	0.00	0.00	0.00	0.00	0.00	0.00	0.00	0.00	0.00	0.01	0.00	0.00	0.00	0.00	
	21	0.00	0.00	0.00	0.00	0.00	0.00	0.00	0.00	0.00	0.00	0.00	0.00	0.00	0.00	0.00	0.00	0.00	0.00	

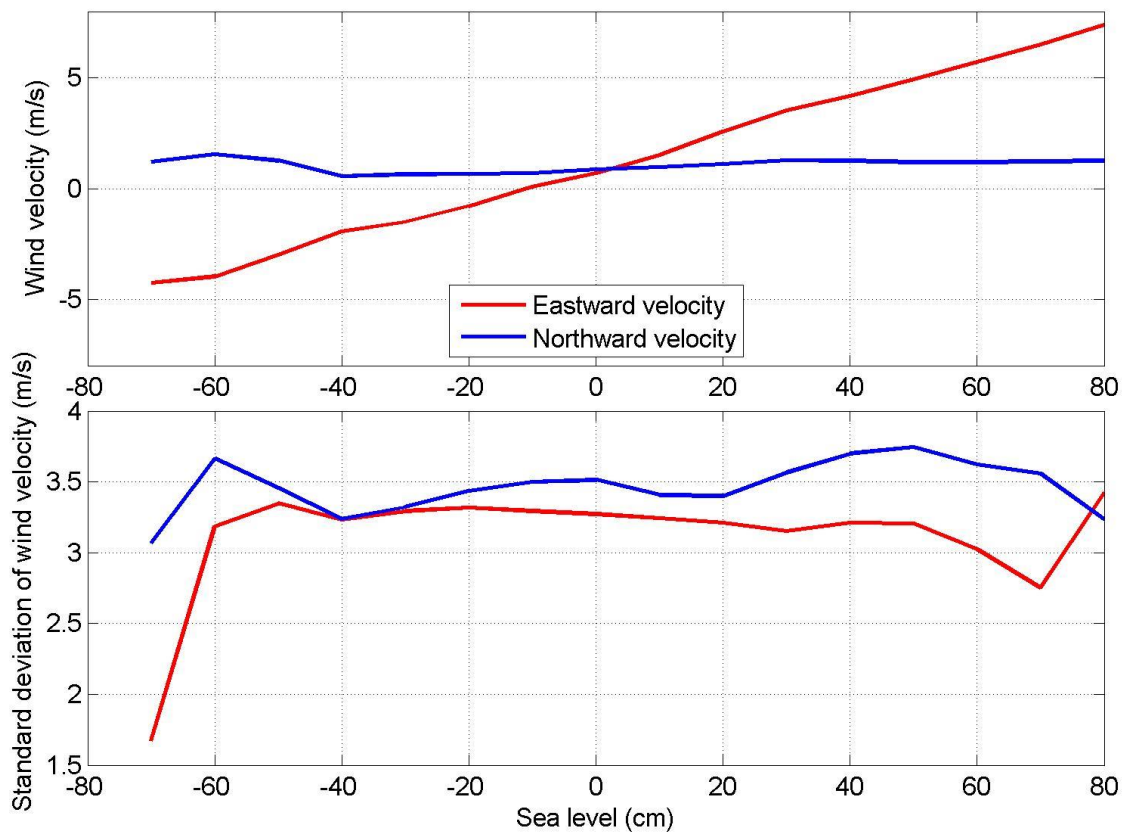


Fig 4.4.1. Daily mean wind velocities in relation to sea level. The mean eastward and northward wind velocities according to the sea level classes are shown in the upper panel and the standard deviation of wind velocities within the classes is shown in the lower panel. Mean wind components during four days before moments of sea level are considered.

4.5. Water level and current

Table 4.5.1. Joint occurrence of 1-day sea level (cm) and 1-day current speed (m/s). 10 cm and 4 cm/s step were used respectively for sea level and current, which corresponded to the classes of ≥ -85 cm & < -75 cm (-80 cm in table), ≥ -75 cm & < -65 cm (-70 cm in table) and so on for sea level and ≥ 0 cm/s & < 4 cm/s (2 cm/s in table), ≥ 4 cm/s & < 8 cm/s (6 cm/s in table) and so on for current speed.

		Sea level (cm)																	
		-80	-70	-60	-50	-40	-30	-20	-10	0	10	20	30	40	50	60	70	80	90
Current speed (m/s)	2	0.00	0.03	0.04	0.14	0.62	1.46	1.93	3.39	4.59	4.91	4.73	3.21	2.00	1.08	0.50	0.11	0.02	0
	6	0.00	0.02	0.31	0.50	1.06	2.24	3.58	4.99	7.02	7.26	6.15	4.85	3.09	1.60	0.74	0.14	0.02	0
	10	0.00	0.03	0.15	0.15	0.44	0.92	1.48	1.97	2.71	3.24	2.77	2.34	1.64	0.96	0.33	0.05	0.01	0
	14	0.00	0.00	0.05	0.06	0.13	0.29	0.37	0.58	0.92	0.84	0.95	1.05	0.66	0.45	0.28	0.01	0.00	0
	18	0.00	0.00	0.00	0.00	0.05	0.03	0.07	0.11	0.15	0.21	0.20	0.30	0.16	0.15	0.08	0.06	0.00	0
	22	0.00	0.00	0.00	0.00	0.02	0.02	0.00	0.01	0.02	0.02	0.04	0.01	0.07	0.02	0.01	0.00	0.01	0
	26	0.00	0.00	0.00	0.00	0.00	0.01	0.00	0.00	0.01	0.03	0.01	0.00	0.01	0.00	0.00	0.00	0.00	0
	30	0.00	0.00	0.00	0.00	0.00	0.00	0.00	0.00	0.00	0.00	0.00	0.00	0.00	0.00	0.00	0.00	0.00	0

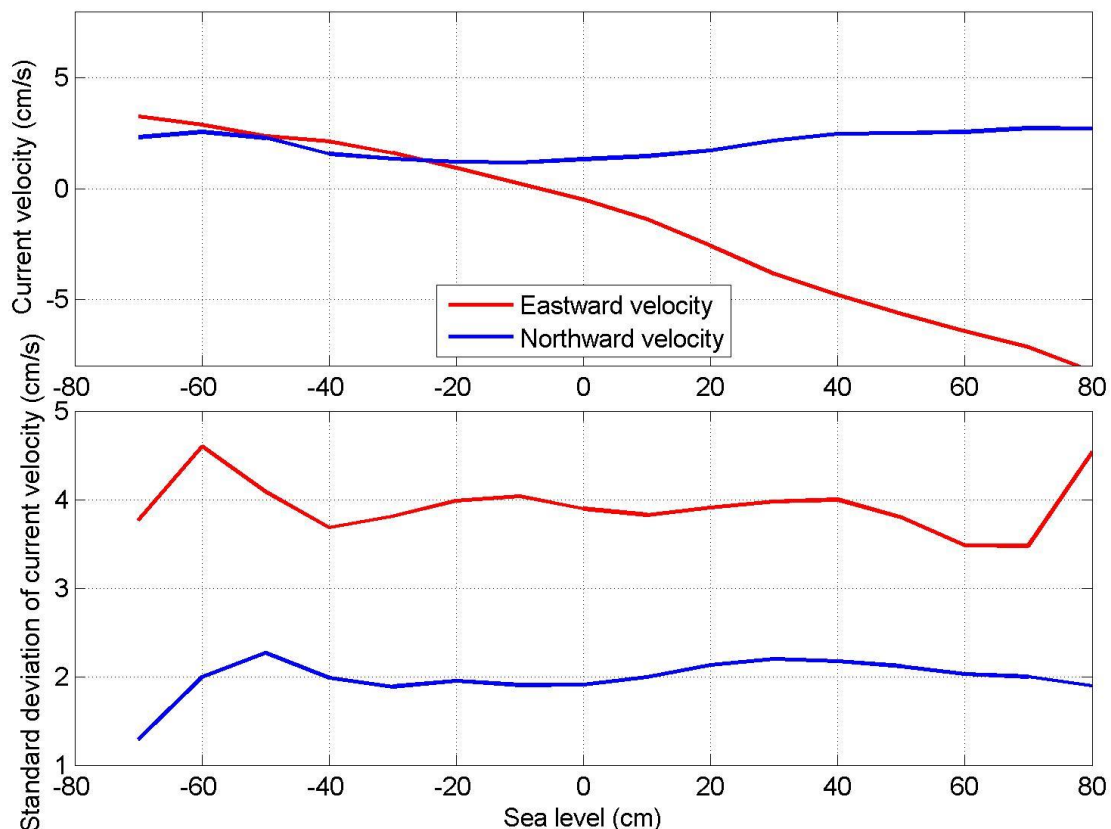


Fig 4.5.1. Daily mean depth-averaged current velocities to sea level. The mean current velocities according to the sea level classes are shown in the upper panel and the standard deviation of depth-averaged current velocities within the classes is shown in the lower panel. Mean current components during four days before moments of sea level are considered.

5. Identified uncertainties or knowledge gaps

ERA5 products perform reasonably well in offshore conditions (Cheynet et al., 2025) and is generally accepted for wind farm studies (Jourdier, 2020; Olauson, 2018), but as claimed earlier, it could underestimate strong wind events (Gandoin and Garza, 2024). Our results also indicate an underestimation of strong wind events. Higher maximum wind speeds have been registered in the meteostations, although spatial mean distribution shows higher wind speed offshore. There could be several reasons behind the underestimation, however, long temporal steps (1 hour) and large grid cells (0.25°) likely contribute to the issue. Sörve meteostation quite well represents marine wind conditions (Žukova, 2009), but still likely has some impact from land and does not 100% represent offshore conditions, including extreme wind events. The Weibull distribution parameters also point to the underestimation of extreme wind speed on the basis of ERA5. To fully understand the offshore conditions one should measure wind speed and direction in the ELWIND area and connect these with the modelled wind and/or meteostation measurements nearby (preferably Sörve station).

Another issue is with the vertical structure of the wind profile, which is described with very low resolution in the current study. The vertical profile is not measured in the nearby meteostations. Understanding of the wind profile is particularly important in coastal areas such as the ELWIND area, as the vertical structure of the wind profile could be more complicated, e.g. negative gradients under certain meteorological parameters might occur (Barthelmie et al., 2007). Partly negative shear in a wind speed profile can lead to a local wind maximum in the profile (low-level jet), or a local wind minimum in the profile (low-level minimum) (Hallgren et al., 2020). It has been shown that heterogeneity in land-surface roughness along the coastline could produce pronounced horizontal streaks of reduced wind speeds that under stable stratification are advected several tens of kilometers over the sea (Dörenkämper et al., 2015a). The vertical structure of the atmosphere also impacts the wakes of the offshore wind farm (Dörenkämper et al., 2015b; Lee et al., 2018; Peña and Rathmann, 2014). To understand the vertical structure in the ELWIND area lidar measurements should be conducted during one year to cover all four seasons.

The used wave product has been validated by earlier studies (Björkqvist et al., 2024; Björkqvist et al., 2020; Tallinna Tehnikaülikool, 2021) with in-situ measurements and it can be concluded the product performs well. Tallinna Tehnikaülikool (2021) compared the product about 45 km

north of the ELWIND area and concluded that the product well represents the wave conditions, although it slightly underestimated the highest waves in extreme storms. The current study did not describe the wave spectrum characteristics. To fill the latter gap and to capture the highest waves in extreme conditions wave measurements should be conducted in the ELWIND area.

The current velocities might be underestimated and there are likely uncertainties in resolving the vertical structure of currents in the present study. The time step (1 day) and horizontal resolution (1 Nm) are too large to describe the local circulation and current structure in the necessary detail. Targeted high-resolution modeling, which is validated with in-situ current profiling measurements should be conducted in the ELWIND area to gather the data with necessary detail. Understanding properly the current structure is likely more important for the studies related to the environmental impact assessment than engineering purposes as the current likely does not exceed 1 m/s in the area and hardly exceeds 0.5 m/s.

The sea level variability is probably well described in the current study. The only shortcoming is the long time step (1 day) of the used product. However, since the sea level amplitude is rather small, and the ELWIND site is an offshore area, sea level amplitude does not exceed 2 m.

The used sea ice product likely quite well represents the conditions as validation with observations has shown good results (<https://documentation.marine.copernicus.eu/QUID/CMEMS-SEAICE-QUID-011-004-011-019.pdf>, accessed 23.04.2025). Ice conditions could be challenging to predict as there is very high interannual variability. According to the product data, the maximum thickness of ice has been 10 cm in the whole ELWIND area during the recent decade. However, the historical data shows that ice thicknesses up to 50 cm could occur (Tikanmäki et al., 2025). Tikanmäki et al., (2025) analyzed the ice charts from winter 1980/81 to winter 2021/22 and studied the whole Baltic Sea. The used product in the present study is also for the whole Baltic Sea. One way to improve the knowledge of local ice conditions in the ELWIND area is to analyze ice charts and/or remote sensing data in higher spatial detail within the ELWIND area. Second way to improve the knowledge is to conduct in-situ observations, but for that winter with severe ice conditions must occur during the pre-construction period, which is not predictable.

Sea surface temperature and salinity are probably quite well described in the current study for engineering purposes. The presented vertical structure of the water column (temperature, salinity, density structure) gives an indication of the conditions in the area but for the

environmental impact assessment studies high-resolution modeling, which is validated by measurements in the ELWIND area, must be applied.

The annual cycles of air pressure, air temperature, and relative humidity are probably well described in the current document.

6. References

- Barthelmie, R.J., Badger, J., Pryor, S.C., Hasager, C.B., Christiansen, M.B., Jørgensen, B.H., 2007. Offshore coastal wind speed gradients: Issues for the design and development of large offshore windfarms. *Wind Eng.* 31. <https://doi.org/10.1260/030952407784079762>
- Barthelmie, R.J., Jensen, L.E., 2010. Evaluation of wind farm efficiency and wind turbine wakes at the Nysted offshore wind farm. *Wind Energy* 13, 573–586. <https://doi.org/10.1002/we.408>
- Björkqvist, J.-V., Kanarik, H., Tuomi, L., Niskanen, L., Kankainen, M., 2024. Event-based wave statistics for the Baltic Sea. SP 4-osr8. <https://doi.org/https://doi.org/10.5194/sp-4-osr8-10-2024>
- Bjorkqvist, J.V., Rikka, S., Alari, V., Männik, A., Tuomi, L., Pettersson, H., 2020. Wave height return periods from combined measurement-model data: A Baltic Sea case study. *Nat. Hazards Earth Syst. Sci.* 20, 3593–3609. <https://doi.org/10.5194/nhess-20-3593-2020>
- Cheyne, E., Diezel, J.M., Haakenstad, H., Breivik, O., Pena, A., 2025. Tall wind profile validation of ERA5, NORA3, and NEWA datasets using lidar observations. *WES* 10, 733–754. <https://doi.org/https://doi.org/10.5194/wes-10-733-2025>
- Dörenkämper, M., Optis, M., Monahan, A., Steinfeld, G., 2015a. On the Offshore Advection of Boundary-Layer Structures and the Influence on Offshore Wind Conditions. *Boundary-Layer Meteorol.* 155. <https://doi.org/10.1007/s10546-015-0008-x>
- Dörenkämper, M., Witha, B., Steinfeld, G., Heinemann, D., Kühn, M., 2015b. The impact of stable atmospheric boundary layers on wind-turbine wakes within offshore wind farms. *J. Wind Eng. Ind. Aerodyn.* 144, 146–153. <https://doi.org/10.1016/J.JWEIA.2014.12.011>
- Enno, S.E., 2014. Thunderstorm and lightning climatology in the Baltic countries and in northern Europe. University of Tartu.
- Gandoin, R., Garza, J., 2024. Underestimation of strong wind speeds offshore in ERA5: evidence, discussion and correction. *WES* 9, 1727–1745.
- Grinsted, A., 2015. Projected Change—Sea Level, in: BACC II Author Team, Springer International Publishing, C. (Ed.), *Second Assessment of Climate Change for the Baltic Sea Basin, Regional Climate Studies*. Springer, Cham, pp. 253–263. https://doi.org/10.1007/978-3-319-16006-1_14
- Hallgren, C., Arnqvist, J., Ivanell, S., Körnich, H., Vakkari, V., Sahlée, E., 2020. Looking for an offshore low-level jet champion among recent reanalyses: A tight race over the baltic sea. *Energies* 13. <https://doi.org/10.3390/en13143670>
- Hendrikse, H., 2024. Ice engineering challenges for offshore wind development in the Baltic Sea. *Proc. 27th IAHR Int. Symp. Ice*.
- Hersbach, H., Bell, B., Berrisford, P., Hirahara, S., Horányi, A., Muñoz-Sabater, J., Nicolas, J., Peubey, C., Radu, R., Schepers, D., Simmons, A., Soci, C., Abdalla, S., Abellan, X., Balsamo, G., Bechtold, P., Biavati, G., Bidlot, J., Bonavita, M., Chiara, G. De, Dahlgren, P., Dee, D., Diamantakis, M., Dragani, R., Flemming, J., Forbes, R., Fuentes, M., Geer,

- A., Haimberger, L., Healy, S., Hogan, R.J., Hólm, E., Janisková, M., Keeley, S., Laloyaux, P., Lopez, P., Lupu, C., Radnoti, G., Rosnay, P. de, Rozum, I., Vamborg, F., Villaume, S., Thépaut, J.-N., 2020. The ERA5 global reanalysis. *Q. J. R. Meteorol. Soc.* 146, 1999–2049. <https://doi.org/10.1002/QJ.3803>
- Jourdier, B., 2020. Evaluation of ERA5, MERRA-2, COSMO-REA6, NEWA and AROME to simulate wind power production over France, in: *Advances in Science and Research*. <https://doi.org/10.5194/asr-17-63-2020>
- Kall, T., Oja, T., Tänavsuu, K., 2014. Postglacial land uplift in Estonia based on four precise levelings. *Tectonophysics* 610. <https://doi.org/10.1016/j.tecto.2013.10.002>
- Keevallik, S., Soomere, T., Pärj, R., Žukova, V., 2007. Outlook for wind measurement at Estonian automatic weather stations. *Est. J. Eng.* 13. <https://doi.org/10.3176/eng.2007.3.05>
- Keskonnaagentuur, 2025. Äikeseanalüüs 2024.
- Lee, S., Vorobieff, P., Poroseva, S., 2018. Interaction of wind turbine wakes under various atmospheric conditions. *Energies* 11. <https://doi.org/10.3390/en11061442>
- Lehmann, A., Krauss, W., Hinrichsen, H.-H., 2002. Effects of remote and local atmospheric forcing on circulation and upwelling in the Baltic Sea. *Tellus A Dyn. Meteorol. Oceanogr.* 54, 299–316. <https://doi.org/10.3402/tellusa.v54i3.12138>
- Lehmann, A., Myrberg, K., Höflich, K., 2012. A statistical approach to coastal upwelling in the Baltic Sea based on the analysis of satellite data for 1990–2009. *Oceanologia* 54, 369–393. <https://doi.org/10.5697/OC.54-3.369>
- Leppäranta, M., Myrberg, K., 2009. Topography and hydrography of the Baltic Sea, in: Leppäranta, M., Myrberg, K. (Eds.), *Physical Oceanography of the Baltic Sea*. Springer Berlin Heidelberg, Berlin, Heidelberg, pp. 41–88. https://doi.org/10.1007/978-3-540-79703-6_3
- Liblik, T., Väli, G., Salm, K., Laanemets, J., Lilover, M.J., Lips, U., 2022. Quasi-steady circulation regimes in the Baltic Sea. *Ocean Sci.* 18, 857–879. <https://doi.org/10.5194/OS-18-857-2022>
- Luomaranta, A., Ruosteenoja, K., Jylhä, K., Gregow, H., Haapala, J., Laaksonen, A., 2014. Multimodel estimates of the changes in the Baltic Sea ice cover during the present century. *Tellus A Dyn. Meteorol. Oceanogr.* 66, 22617. <https://doi.org/10.3402/tellusa.v66.22617>
- Maas, O., Raasch, S., 2022. Wake properties and power output of very large wind farms for different meteorological conditions and turbine spacings: A large-eddy simulation case study for the German Bight. *Wind Energy Sci.* 7. <https://doi.org/10.5194/wes-7-715-2022>
- Madsen, K.S., Høyer, J.L., Suursaar, Ü., She, J., Knudsen, P., 2019. Sea Level Trends and Variability of the Baltic Sea From 2D Statistical Reconstruction and Altimetry. *Front. Earth Sci.* 7, 243. <https://doi.org/10.3389/FEART.2019.00243/BIBTEX>
- Mäkelä, A., Enno, S.E., Haapalainen, J., 2014. Nordic Lightning Information System: Thunderstorm climate of Northern Europe for the period 2002–2011. *Atmos. Res.* 139. <https://doi.org/10.1016/j.atmosres.2014.01.008>

- Meier, M.H.E., Kniebusch, M., Dieterich, C., Gröger, M., Zorita, E., Elmgren, R., Myrberg, K., Ahola, M.P., Bartosova, A., Bonsdorff, E., Börgel, F., Capell, R., Carlén, I., Carlund, T., Carstensen, J., Christensen, O.B., Dierschke, V., Frauen, C., Frederiksen, M., Gaget, E., Galatius, A., Haapala, J.J., Halkka, A., Hugelius, G., Hünicke, B., Jaagus, J., Jüssi, M., Käyhkö, J., Kirchner, N., Kjellström, E., Kulinski, K., Lehmann, A., Lindström, G., May, W., Miller, P.A., Mohrholz, V., Müller-Karulis, B., Pavón-Jordán, D., Quante, M., Reckermann, M., Rutgersson, A., Savchuk, O.P., Stendel, M., Tuomi, L., Viitasalo, M., Weisse, R., Zhang, W., 2022. Climate change in the Baltic Sea region: A summary. *Earth Syst. Dyn.* <https://doi.org/10.5194/esd-13-457-2022>
- Olauson, J., 2018. ERA5: The new champion of wind power modelling? *Renew. Energy* 126. <https://doi.org/10.1016/j.renene.2018.03.056>
- Passaro, M., Müller, F.L., Oelsmann, J., Rautiainen, L., Dettmering, D., Hart-Davis, M.G., Abulaitijiang, A., Andersen, O.B., Høyer, J.L., Madsen, K.S., Ringgaard, I.M., Särkkä, J., Scarrott, R., Schwatke, C., Seitz, F., Tuomi, L., Restano, M., Benveniste, J., 2021. Absolute Baltic Sea Level Trends in the Satellite Altimetry Era: A Revisit. *Front. Mar. Sci.* 8, 546. <https://doi.org/10.3389/FMARS.2021.647607/BIBTEX>
- Peña, A., Rathmann, O., 2014. Atmospheric stability-dependent infinite wind-farm models and the wake-decay coefficient. *Wind Energy* 17. <https://doi.org/10.1002/we.1632>
- Soomere, T., 2001. Extreme wind speeds and spatially uniform wind events in the Baltic Proper. *Proc. Est. Acad. Sci. Eng.* 7. <https://doi.org/10.3176/eng.2001.3.01>
- Soomere, T., Behrens, A., Tuomi, L., Nielsen, J.W., 2008. Wave conditions in the Baltic Proper and in the Gulf of Finland during windstorm Gudrun. *Nat. Hazards Earth Syst. Sci.* 8. <https://doi.org/10.5194/nhess-8-37-2008>
- Soomere, T., Keevallik, S., 2001. Anisotropy of moderate and strong winds in the Baltic Proper. *Proc. Estonian Acad. Sci. Eng.*
- Soomere, T., Pindsoo, K., Kudryavtseva, N., Eelsalu, M., 2020. Variability of distributions of wave set-up heights along a shoreline with complicated geometry. *Ocean Sci.* 16. <https://doi.org/10.5194/os-16-1047-2020>
- Suhhova, I., Liblik, T., Lilover, M.-J., Lips, U., 2018. A descriptive analysis of the linkage between the vertical stratification and current oscillations in the Gulf of Finland. *Boreal Environ. Res.* 23, 83–103.
- Suursaar, Ü., Jaagus, J., Kullas, T., 2007. Recent tendencies in wind storm climatology with implications to storm surge statistics in Estonia, in: *WIT Transactions on Engineering Sciences*. <https://doi.org/10.2495/EN070051>
- Suursaar, Ü., Kullas, T., Otsmann, M., 2001. The influence of currents and waves on ecological conditions of the Väinameri. *Proc. Est. Acad. Sci. Biol. Ecol.*, 50, 231–247.
- Suursaar, Ü., Kullas, T., Otsmann, M., Saaremäe, I., Kuik, J., Merilain, M., 2006. Cyclone Gudrun in January 2005 and modelling its hydrodynamic consequences in the Estonian coastal waters. *Boreal Environ. Res.* 11.
- Tallinna Tehnikaülikool, 2021. Mere elupaikade kirjeldamise parandamise võimalused kasutades autonoomseid mõõtmisi ja andmeprodukte (Deliverable 2.1.1. Methodology for spatial characterization of habitats using autonomous high-frequency in situ observations in combination with conventi.

- Tikanmäki, M., Heinonen, J., Jokiniemi, A., Eriksson, P., 2025. Design sea ice conditions for offshore wind power in the Baltic Sea. *Cold Reg. Sci. Technol.* 234. <https://doi.org/https://doi.org/10.1016/j.coldregions.2025.104463>
- Väli, G., Meier, H.E.M., Liblik, T., Radtke, H., Klingbeil, K., Gräwe, U., Lips, U., 2024. Submesoscale processes in the surface layer of the central Baltic Sea: A high-resolution modelling study. *Oceanologia* 66. <https://doi.org/10.1016/j.oceano.2023.11.002>
- Vestøl, O., Ågren, J., Steffen, H., Kierulf, H., Tarasov, L., 2019. NKG2016LU: a new land uplift model for Fennoscandia and the Baltic Region. *J. Geod.* 93. <https://doi.org/10.1007/s00190-019-01280-8>
- Westerhellweg, A., Cañadillas, B., Kinder, F., Neumann, T., 2014. Wake measurements at alpha ventus - Dependency on stability and turbulence intensity, in: *Journal of Physics: Conference Series*. <https://doi.org/10.1088/1742-6596/555/1/012106>
- Žukova, V., 2009. Eesti rannikujaamade võimalused meretuule hindamisel. Magistritöö. Tallinna Tehnikaülikool.